DUBLIN CITY UNIVERSITY

PLASMA NITRIDING AND DUPLEX COATING OF BIOCOMPATIBLE SURFACES FOR LOW FRICTION AND WEAR RESISTANT APPLICATIONS

A thesis submitted for the degree of Doctor of Philosophy (Ph.D.) to the School of Mechanical and Manufacturing Engineering under the faculty of Engineering and Computing, Dublin City University

By

Md. Mahfujur Rahman, B.Sc. Eng.

School of Mechanical and Manufacturing Engineering,

National Centre of Plasma Research (NCPST) and

Material Processing Research Centre (MPRC)

Dublin City University (DCU), Dublin 9, Ireland

Research Supervisor

Professor M. S. J. Hashmi
(D.Sc., Ph.D., C.Eng, FIMechE., FIEI, MASME, M.Sc., B.Sc.)

July, 2006

DECLARATION

I hereby certify this material, which I now submit for assessment on the programme of study leading to the award of Ph.D. is my own work and has not been taken from the work of others save and to the extent that such work has been cited and acknowledged within the text of my work.

Signed: MD. MAHFUJUR RAHMAN ID No. 52141110

Dated: 06/07/06

ACKNOWLEDGMENT

Firstly, I would like to take the privilege to express my respect and gratitude to my academic supervisor Professor M. S. J Hashmi, School of MME, DCU, for his constant guidance, enormous support and valuable advice throughout my work. I will be forever indebted to him for acting not only as academic supervisor but also giving valuable suggestions, guidelines and help in practical life during the last three and half years. I also sincerely thank him for facilitating my entrance to the field of surface engineering and providing me with resources and funding throughout this PhD work.

Many thanks specially to Mr. Liam Domican and Mr. Michael Tyrrell, the technical staff in the school of MME, who devoted much time to assisting with the PVD and PECVD rig respectively. Thanks also to Mr. Michael May and Mr. Christopher Crouch, school of MME, DCU and Mr. Billy Roarty, school of EE, DCU for assisting with materials characterization.

I would like to thanks Prof. David Cameron and Dr. Stephen Daniels, in the school of EE, DCU, for giving me authorization to use the AFM and FTIR facilities and also their valuable comments and suggestions on the operation and upgrading of the existing PVD and PECVD machines. Thanks are also due to Mr. Lu Xu and Prof. Patrick J. McNally of Microelectronics Research Lab, DCU for providing the Micro Raman Spectrometry facilities.

I should also acknowledge all the help from our collaborators. Specially, my sincere thanks to Dr. Paul Duggan and Dr. Denis Dowling, Manufacturing Engineering Department, University College Dublin, for their help, support and suggestions on Pin-on-disk wear test work. Thanks to Mr. Ian Reid and Dr. Greg Hughes of the School of Physical sciences, DCU for assisting with XPS analysis.

It will be a pleasure to give very special thanks and acknowledgment to Dr. Julfikar Haider, my previous co-worker in PVD lab for his valuable comments and suggestions for the first two years of my research work.

I am grateful to Dr Tim Prescott for helping me writing the journal paper and many thanks to Dr. Brian Corcoran for his constructive suggestion regarding simulation work.

I had the opportunities to attend and present my work in several international conferences, including ICM04, PSE04, ICMCTF05, AEPSE05, nanoSmarts05. Thanks to the American Vacuum Society, the NanoSmarts05 conference committee, the National Centre of Plasma Science and Technology and School of MME, DCU, Ireland for providing me with the funds to make this possible.

Next I am very grateful to all the friends (Irish, Bangladeshi, and from other countries) that I have made (the list is too long to mention) and my house mates for their encouragement and help in real life.

I also give my sincere thanks to my family members, especially my father Mr. Elius Hossain and mother Mrs. Zinatun Nesa, without whose support and encouragement, it would have been impossible for me to come this far. Thanks are also due to my brothers, sisters, mother-in-law, nieces, nephews, and uncles, who always wished me every success in life.

Finally, many thanks and regards go to my dearest wife, Mrs. Taslima Akter, for her continuous moral support, patience and good humor in every part of my life. Without her support this works would not have been completed in time.

PLASMA NITRIDING AND DUPLEX COATING OF BIOCOMPATIBLE SURFACES FOR LOW FRICTION AND WEAR RESISTANT APPLICATIONS

ABSTRACT

Md. Mahfujur Rahman, B.Sc. Eng.

The 316L austenitic stainless steels, Ti-6Al-4V and Ultrahigh molecular weight polyethylene (UHMWP) are very attractive and well known materials for diverse engineering applications due to their many superior properties. More specifically, these materials have acquired much attention in biomedical applications due to their excellent biocompatibility. However, the practical use of these materials are limited in many cases by the need to attain specific tribological (that means, low friction and wear rate) and mechanical (that means, high hardness, high load-bearing capacity) properties. The long-term outcome of the total joint replacement is currently limited by the breakdown of the implant by wear processes. Therefore, much research has been carried out in this area to reduce the incidence of wear. The goal of this project was to enhance the mechanical and tribological properties of the biocompatible surface by the plasma nitriding and duplex coating process.

The works consisted of three phases. In the first phase, in order to acquire a preliminary approximation of the different process parameters, finite volume and finite element methods have been employed to determine (i) the gas mixture pattern inside the sputtering chamber and (ii) the thermal stress inside the coating, with and without considering graded interlayer respectively.

In the second phase of the work, a new plasma nitriding process has been used using an existing carbon based coating system. Plasma nitriding was performed on biomaterials substrates where a Saddle field neutral fast atom beam source and an auxiliary heater was used for substrate heating. It has been observed that low temperature plasma nitriding of the stainless steel samples produced a precipitation and black layer free, hard, thick and load supporting nitrided layer within a short processing time which was suitable for subsequent coating deposition as well. Plasma nitriding has also been carried out on Ti-6Al-4V and non-conductive UHMWP biomaterials. In both cases plasma nitriding treatment increased the untreated substrate hardness and wear properties substantially.

In the third phase of the work, the additional improvement of mechanical and tribological properties of the solid lubricant based coatings (MoS_2 and DLC), a continuous and discontinuous duplex coating system has been investigated. The main focus has been on the improvement of the load bearing capacity of the coating-substrate system. For the first time a continuous duplex process is being introduced consisting of the plasma nitriding followed by in situ deposition of the DLC biomedical coating. The process has been successfully carried out in a single process chamber (PECVD based Saddle field neutral fast atom beam source) without any interlayer or post nitriding treatment. Rockwell C indention results confirmed the improvement of the adhesion in the duplex treated coating samples compared to the non-duplex treated sample. Duplex treatment significantly increased the composite hardness and reduced the plastic deformation of the substrate. The Pin on disk tests showed that the duplex treatment increase the overall wear properties of the coating compared to the non-duplex coating. In addition, a discontinuous duplex treatment consisting of plasma nitriding and TiN+MoS, coatings with and without a graded interlayer on the stainless steel substrate were investigated. Low-temperature plasma nitriding was performed with the newly developed process (Saddle field fast atom beam source) and coatings were deposited by closed-field unbalanced magnetron sputtering. Results showed that the graded interlayer and plasma nitriding had a great influence on the load bearing and overall tribological properties of the coating-substrate system.

DEDICATION

This thesis is dedicated to my parents who always wished me success with my research.

TABLE OF CONTENTS

3. SIMULATION WORK DESIGN, EXPERIMENTAL WORK AND CHARACTERIZATION TECHNIQUES

4. RESULTS AND DISCUSSION

LIST OF ABBREVIATIONS

A	Ampere
AC	Alternative Current
AFM	Atomic Force Microscopy
Ar	Argon
ASTM	American Society for Testing and Materials
Atm	Atmospheric
CFD	Computational Fluid Dynamics
CFUBMS	Closed-field Unbalanced Magnetron Sputtering
CrN	Chromium Nitride
CTE	Coefficient of Thermal Expansion
CVD	Chemical Vapor Deposition
DC	Direct Current
DCU	Dublin City University
DLC	Diamond-like Carbon
E	Young's modulus of Elasticity
ECR	Electron Cyclotron Resonance
EE	Electronic Engineering
EDX	Energy Dispersive X-ray
FAB	Fast Atom Beam
FCC	Face Centred Cubic
FCT	Face Centred Tetragonal
FEA	Finite Element Analysis
FTIR	Fourier Transmitted Infrared Spectroscopy
GPa	Giga-Pascal
KV	Kilo Volt
h	Hour
He	Helium
HV	Vicker's Hardness
IR	Infrared
K	Kelvin
KeV	Kilo-electron-Volt
mA	Milli-Ampere
MFC	Mass Flow Controller
MHz	Mega-Hertz
MME	Mechanical and Manufacturing Engineering
MoS_2	Molybdenum Disulphide
N_2	Nitrogen
Pa	Pascal
PACVD	Plasma Assisted Chemical Vapor Deposition
PAN	Plasma Assisted Nitriding
PECVD	Plasma Enhanced Chemical Vapor Deposition
PIII or PI^3	Plasma Immersion Ion Implantation
PTEF	Poly Tetra Fluoro Ethylene
PSII	Plasma Source Ion Implantation
PVD	Physical Vapor Deposition
RF	Radio Frequency
RPM	Rotation Per Minute
SE	Secondary Electrons
SEM	Scanning Electron Microscopy
SCCM	Standard Cubic Centimetre per Minute
TAD	Thermionic Arc Discharge
TAT	Thermionically Assisted Triode
TiN	Titanium Nitride
XPS	X-ray Photoelectron Spectroscopy
XRD	X-Ray Diffraction
UHMWPE	Ultra High Molecular Weight Ploy Ethylene
USA	United State of America

LIST OF FIGURES

LIST OF TABLES

CHAPTER 1: INTRODUCTION

1.1. INTRODUCTION

Engineering materials, which are used in different applications, in certain cases need to amend their surface properties in order to extend their service lives and improve their reliability. Surface Engineering is the process of enhancing the subsurface properties of a material, while in general maintaining the bulk properties of the treated substrate. This process reduces the cost in the service arising due to the early declination of the engineering components. In service modification of the existing surface of the bulk materials without adding any layer (heat treatment, nitriding and so on) and the deposition of a film layer on the bulk material are the common techniques to achieve this goal. These two techniques are the most important and versatile means of improving component performance.

Surface engineering techniques are used in a diverse field of applications such as Biomedical (details in appendix), Cutting tool, Electronic, Aerospace, Optical and so on. In each application, materials need to be modified according to the physical, chemical, mechanical and biological characteristics of the particular applications environment. For example, in the orthopaedic application (biomedical), the first criterion is that the surface has to be biocompatible. The surface also has to exhibit good wear resistance properties as currently wear is the most important limiting factor for using such materials in orthopedics application. Materials used in tribological applications, low wear and low friction are mainly controlled by their surface properties. Various surface properties (such as hardness, surface energy, roughness, work hardening, cleanliness, contamination, imperfection and so on) and also bulk properties (such as metallurgical, mechanical, thermal) of a material play a key role in determining its tribological behaviour. A major area of tribology is to design surfaces so when they slide and roll against each other friction and wear is minimised. By reducing friction and wear many benefits, both economical and environmental, can be achieved in several technological fields of applications. Low wear means that the interval between maintaining and replacing expensive machines will be shortened. Low friction between the contacting surfaces in a machine results in less energy losses and thereby lowers fuel consumption. One way to achieve this is to use a material with poor tribological performance but otherwise optimal properties, that means high toughness, or low price, as a base material and modifying its surface with a surface treatment method (for example nitriding) or coating it with a thin layer of a wear resistant material with a low friction coefficient.

A large number of techniques, materials and design criteria have been used for surface treatment and deposition of the thin film coating for several years. Development of all these techniques have been made gradually to overcome the problems (physical, mechanical and structural properties of the deposited material) associated with the previous one. Many methods have been developed for surface treatment and deposition of thin film coating such as welding, thermal spraying, physical vapour deposition (PVD), chemical vapour deposition (CVD), and plasma and ion based methods and so on. Selections of a method depends on a number of factors, such as (a) structure and property required for the modified surface, (b) maximum temperature can be used for particular samples to maintain its structural integrity, (c) thickness requirement, (d) conductivity and non-conductivity of the samples, (e) area of applications and (f) deposition or treatment rates. Among all the techniques, PVD and CVD based methods are commonly used to deposit wear resistance coating [1]. There are also numerous variations of both these techniques. Many scientists, for their required film deposition or surface modification, follow different processes under PVD and CVD. But yet, most of these techniques present a number of problems in relation to coating/treated sample properties such as adhesion, stress development, uniformity, line of sight or limitations regarding the wide range of materials that can be used, the thickness of the treated layer and so on. The problem with the selection of appropriate methods is mainly due to difficulties in obtaining all the desired properties simultaneously. Again, there are a number of coatings, such as TiN, CrN, TiCN, TiAlN, MoS_x, diamond like carbon (DLC), CN_x coating and so on, which are developed for use in different applications. For example in certain tribological applications, there is a significant interest in solid lubricant based coating such as metal/compound-MoS_2 and diamond like coatings because of their unique combination of desirable properties like high hardness and the ability to form transfer layers which reduce wear [2-10]. These coatings are beginning to replace conventional liquid lubricants as they perform efficiently and are environmental friendly.

It is important to have criteria for the selection of the most suitable coating materials for specific needs. This is not easy because the requirements for the composite substrate and overlayer are often very complex and many compromises must be accepted. Complex requirements for surface engineering cannot be realized in a single homogeneous coating or a single surface treatment process. A combination of more than one method is used to attain the desired requirement. Several new generation coatings such as multicomponent, graded, hybrid, duplex, superlatice and so on, have recently drawn the attention of the tribologists with the intention of achieving further improvement of

properties over the traditional single layer homogeneous coating [11,12]. Another very important issue in surface engineering is characterization of the process and treated samples by using different methods to evaluate the ability and performance of the new process, material or design. Selection of the method of characterization depends on a number of factors, such as the property that needs to be characterized, the material used, the level of precision required and so on.

A significant amount of research and development is continuing in all areas of surface engineering (material, technique, design and characterization) to develop this field to a mature level. This work aims to Plasma nitriding of both metallic and non-metallic material (i.e., Stainless steel, Ti-alloy and Polymer), in a new low temperature and low pressure chamber with an engineering application where a surface is in contact motion with another surface. Secondly, to meet the increasing demands for combined properties under severe contact conditions, there is a new surface engineering approach: hard-solid lubricant based coatings (DLC and TiN+MoS_x) on plasma-nitrided substrate (Duplex coating) have been investigated with application in low friction and wear resistance. The configuration for duplex system is shown in figure 1.1. The focus is on a thorough characterization of the microstructure and tribological properties of the nitrided and coated samples. The detailed objective of this work has been finalized and presented after the literature review in chapter 2.

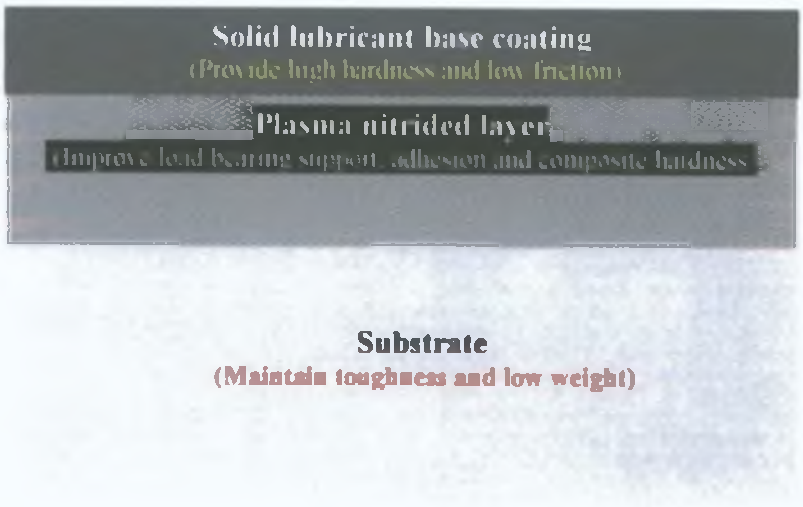

Figure 1.1: Duplex, solid lubricant based coating on plasma nitrided sample

The thesis is arranged as follows: Chapter 2 (Literature review) provides information and theory regarding the surface engineering techniques, materials, methods, design and application, considering their present capabilities and limitations. In the first section of Chapter 3 (simulation work design, experimental work and characterization techniques), in order to acquire a preliminary approximation of the different process parameters, simulation work has been presented. The next section of this chapter describes the process and techniques employed for the plasma nitriding and coating deposition process in the present work. The experimental procedure and design-methods used are also presented. In the last section of Chapter 3, the different characterization techniques used to determine the physical, structural, mechanical and tribological properties of the resultant surfaces have been discussed. In Chapter 4 (Results and Discussion), the results of all experiments have been presented and discussed and Chapter 5 provides concluding remarks, and an outline of the direction of further research.

CHAPTER 2: LITERATURE REVIEW

2.1. INTRODUCTION

The control of friction and wear properties of materials in different tribological applications (such as biomedical, electronics, mechanical, and so on) are vital. Materials in these applications need high hardness, wear resistance, chemical stability and high toughness. They must be cable of forming a stable compound at the contact interface in order to control the friction and wear behaviour [13]. The use of surface engineering to develop a specific tailor made surface that responds effectively and efficiently to generate satisfactory design life serviceability in engineering artifacts is not new. Indeed, it is possible to recognise a whole historical perspective to surface engineering practices such as the ancient pre-Christ art of carburizing to generate sharp and enduring cutting edges in the weapons and tools [14]. Surface engineering either by (a) surface treatment or (b) surface coating has become a well-established technology and is an extremely versatile means of improving component performance in different science and engineering applications.

2.2. SURFACE ENGINEERING METHODS

Various methods are used to perform surface treatment and surface coating. A classification of surface engineering methods is given in figure 2.1. The major developments in the early and mid-nineteenth century in Europe in processes such as electroplating and galvanising, to the very recent development of plasma surface engineering, led to the development of interdisciplinary subject of surface engineering. Among all the methods physical vapor deposition (PVD) and chemical vapor deposition (CVD) based methods are the most versatile and widely used [15]. Figure 2.1 shows, in detail the classification of CVD and PVD methods. Both CVD and PVD process followed mainly three principles steps in the formation of a thin film or modification of a surface [16]: (1) decomposition of starting material into various fragments of neutrals or ions in the form of atoms, molecules and clusters, (2) transportation of decomposition materials through the medium of gas or liquid towards the substrate, and (3) nucleation and growth of these materials on the substrate surface, as described in figure 2.2.

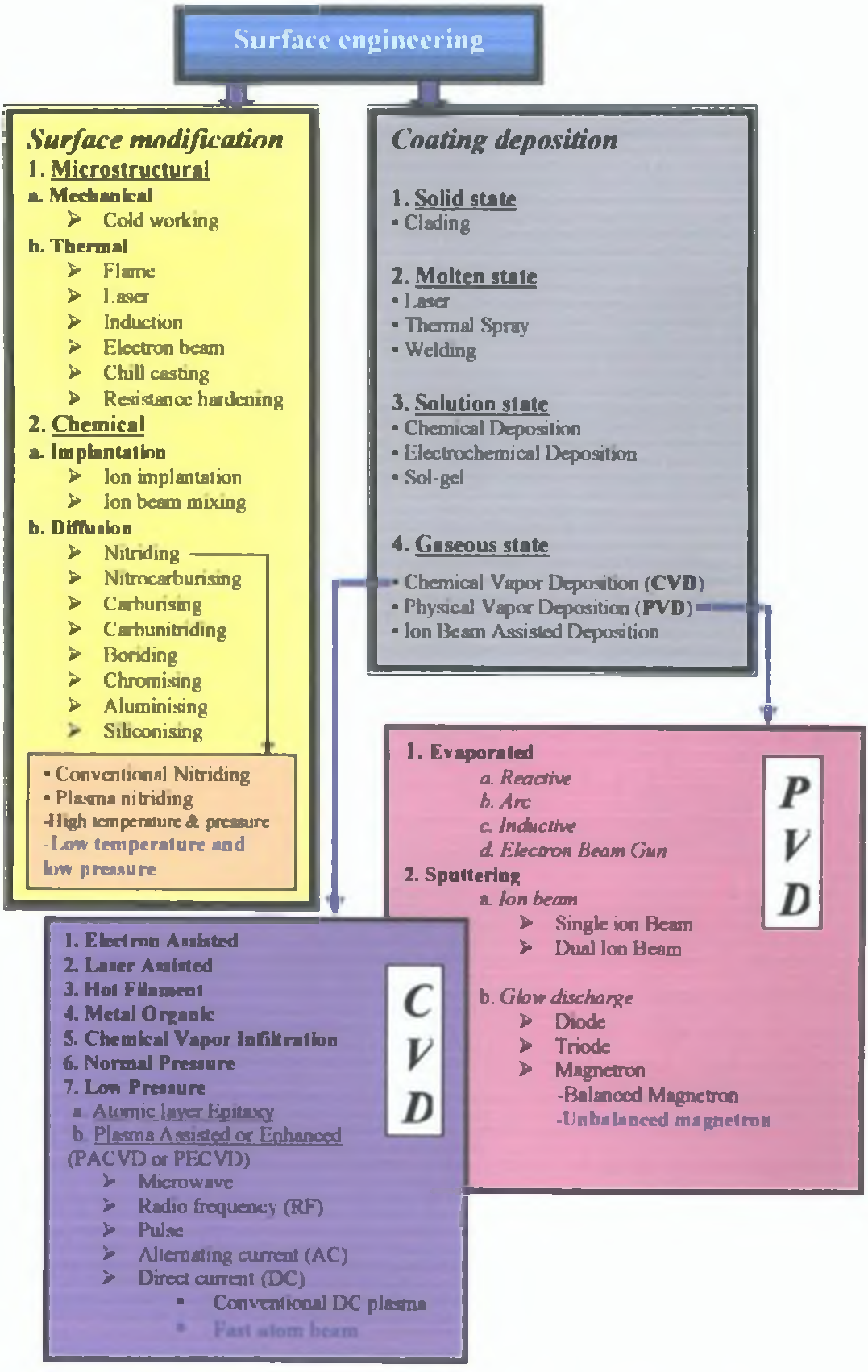

Figure 2.1: Classification of surface engineering methods [17, 18].

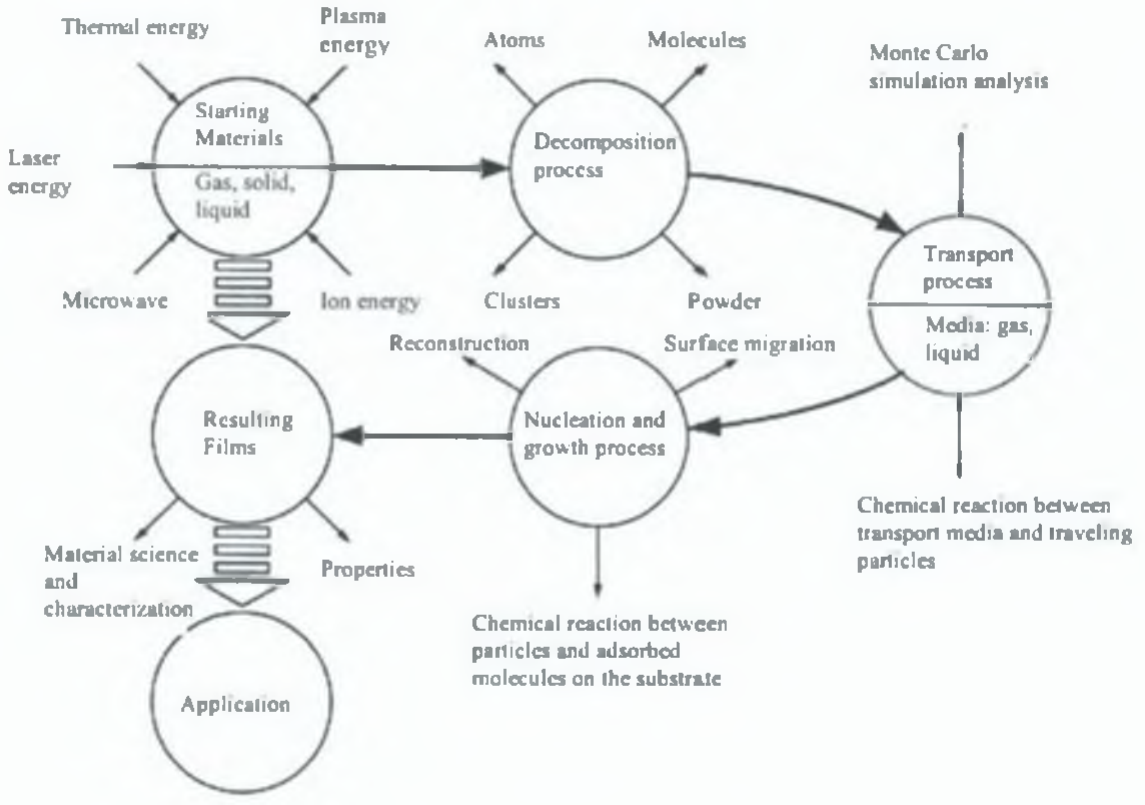

Figure 2.2: Principle steps for PVD and CVD process [16]

The properties of the thin film or modifying surface strongly depend on steps (3) of the process because the energy of the decomposed species is dissipated in the very shallow surface region of the substrate. The surface migration of the absorbed species, chemical reaction between landing species and finally reconstruction into the structures of the resulting films are greatly influenced by the dissipation of the energy of the decomposed species. In the next two sections of this chapter, brief descriptions of both CVD and PVD methods have been discussed.

2.2.1. CHEMICAL VAPOR DEPOSITION (CVD)

Chemical vapor deposition (CVD) [19] is a material synthesis process whereby constituents of the vapor phase react chemically near or on a substrate surface to form a solid product. It belongs to the class of vapor-transfer processes which is atomistic in nature, that means, the deposition species are atoms or molecules or a combination of these. This deposition technology has become one of the most important means for creating thin films of a very large variety of materials.

The main feature of CVD is its versatility for synthesizing both simple and complex compounds. Both chemical composition and physical structure can be tailored by control of the reaction chemistry and deposition conditions. The fundamental principles of CVD encompass an interdisciplinary range of thermo-dynamics, kinetics, gas-phase reaction chemistry, transport mechanisms, film growth phenomena, and reactor engineering [19]. A CVD reaction is governed by thermodynamics [17,19,20] that is the driving force, which indicates the direction the reaction, is going to proceed. Chemical thermodynamics is concerned with the interrelation of various forms of energy and the transfer of energy from one chemical system to another in accordance with the first and second laws of thermodynamics. This reaction is also regulated by kinetics, which defines the transport process and determines the rate-control mechanism (the rate of reactions). Kinetics controls depend on temperature and factors such as substrate orientation [17]. Considerations relating to heat, mass, and momentum transport phenomena are especially important in designing CVD reactors of maximum efficiency [17,20]. In the case of CVD, this transfer occurs when the gaseous compounds, introduced in the deposition chamber, react to form the solid deposit and by-product gases. In general, the transport of the gases is determined by the process pressure and the gas flow rates. Diffusion of source gases to substrate surface and by-product gases away from the deposition surface is enhanced at low pressures. Since important physical properties of a given film material are critically influenced by the structure (such as crystallinity), control of the factors governing the nucleation and structure of a growing film is necessary [17].

Deposition variables such as temperature, pressure, gas flow rates, reactor geometry and operating principle determine the deposition rate and the properties of the film deposit. Thin-film materials that can be prepared by CVD cover a tremendous range of elements and compounds. Inorganic, organo-metallic, and organic reactants are used as starting materials. Gases are preferred because they can be readily controlled and distributed to the reactor by means of pressure controllers, gauges, flow meters, and mass-flow controllers. [20-22]. Liquid and solid reactants must be vaporized without decomposition at suitable temperatures and transported [20] with a carrier gas through heated tubes to the reaction chamber which complicates processing, especially in the case of reduced-pressure systems. CVD has become an important process technology in several industrial fields. For example, hard, wear and corrosion resistant coatings of materials such oxide, carbides and nitrides are used in tribological application [19].

2.2.1.1. PLASMA ENHANCED OR ASSISTED CVD

The main difference between the various CVD processes, such as thermal CVD, laser and photo CVD, and plasma CVD, is the method of applying the energy required for the CVD reaction to take place [17,19,20]. Figure 2.1 showed, the many derivatives of the original thermal CVD process. These have arisen in response to energy required for the CVD reaction, to a need to achieve specific coating characteristics, such as deposition at lower temperatures (less than 300 ^{0}C) and pressures (~ 67 Pascal) [23]. Furthermore, certain coating types, such as diamond [24-27], are only achievable using particular process technologies and parameters. Thermal CVD relies on thermal energy to activate the reaction, and deposition temperatures are usually high. In plasma CVD, also known as plasma-enhanced CVD (PECV) or plasma-assisted CVD (PACVD), the reaction is activated by plasma and the deposition temperature is substantially lower (less than 300 ^{0}C) [19,23]. In thermally driven CVD process, ground state species containing the elements to be deposited are transported to the vicinity of the substrate surface where they diffuse to the surface, adsorb on the surface, undergo chemical reactions and surface migration, and eventually yield a solid film. Reaction by products also form, and they desorbs, diffuse away into the main gas stream, and are transported out of the chamber. This sequence of steps is summarized as follows [28]: transport of reactants to the growth region, mass transport of reactants to the substrate surface, adsorption of reactants, physical-chemical reactions yielding the solid film and reaction byproducts, desorption of byproducts, mass transport of by products to the main gas stream and transport of by products away from the growth region. When plasma is generated in a CVD environment, a fraction of the ground-state parent species in the gas phase undergoes electron impact dissociation and excitation, and highly reactive species are consequently generated [19, 28]. As a result, in addition to the ground state species, these highly reactive species also diffuse to the surface, and undergo similar processes of adsorption, chemical reactions, surface migration, and so on.

Principle of PECVD

If a gas (H_2, Ar, He and so on) is heated above a given temperature, eventually most (not all) of these atoms become ionized, and plasma is formed which consists of ions (with positive charge), electrons (with negative charge), and atoms that have not been ionized (neutral) [20]. In such plasma, the following events occur:

- In an electric field, the gases are ionized into electrons and ions. The electrons, with their extremely small mass, are quickly accelerated to high-energy levels.
- The heavier ions with their much greater inertia cannot respond to the rapid changes in field direction. As a result, their temperature and that of the plasma remain low, as opposed to the electron temperature (hence it's called non-isothermal plasma).
- The high-energy electrons collide with the gas molecules with resulting dissociation and generation of reactive chemical species and the initiation of the chemical reaction.

However in plasma process, since ionization temperatures are usually extremely high (>5000K) [20], a large amount of thermal energy is required. A convenient way to achieve plasma is with electrical energy. By increasing the electrical energy in a fixed amount of gas, all molecules are eventually dissociated and complete ionization is achieved. Mainly two types of plasma are currently used in CVD: glow-discharge plasma (non-isothermal) and arc plasma (isothermal). A glow discharge can be defined as a partially ionized gas containing equal volume concentrations of positive and negative charged species (mostly ions and electrons, respectively) and different concentrations of ground-state and excited species [29,30]. The glow discharge owes its name to the fact that plasma is luminous. The glow can be produced by applying a potential difference between two electrodes in a gas. The potential drops rapidly close to the cathode, vary slowly in the plasma, and change again close to the anode. The electric fields in the system are restricted to sheaths at each of the electrodes. The sheath fields are such as to repel electrons trying to reach either electrode (Figure 2.3). Electrons originating at the cathode will be accelerated, collide, transfer energy, leave by diffusion and recombination, slow by the anode and get transferred into the outside circuit.

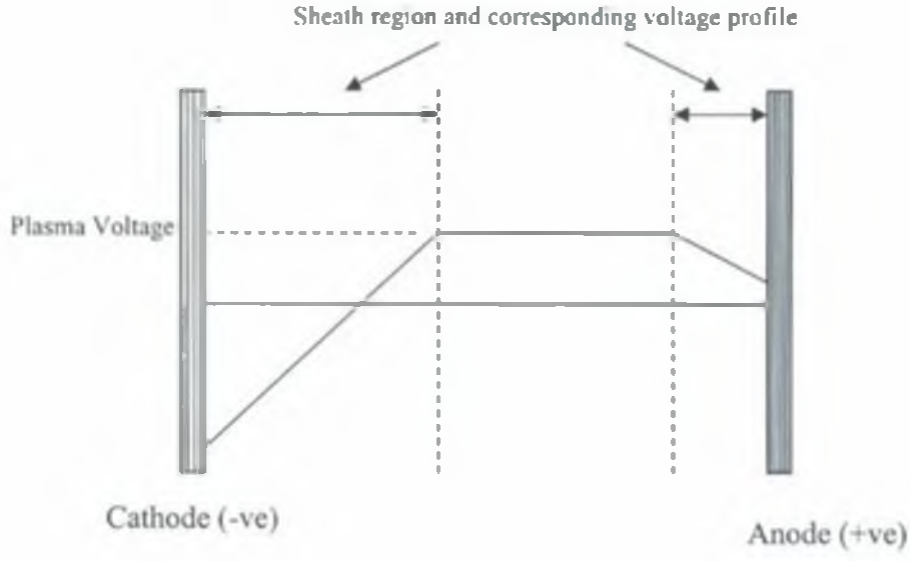

Figure 2.3: Voltage distribution in a Direct current glow discharge process.

The luminous glow is produced because the electrons have enough energy to generate visible light by excitation collisions. Since there is a continuous loss of electrons, there must be an equal degree of ionization going on to maintain the steady state. The energy is being continuously transferred out of the discharge and hence the energy balance must be satisfied. This partially ionized gas can be generated by subjecting the gas to very high temperatures or to strong electric or magnetic fields. In thermal plasmas, the electrons, ions, and neutral species are in local thermodynamic equilibrium. In non equilibrium or "cold" plasmas, the electrons and ions are more energetic than the neutral species. The reactive species produced in the plasma have lower energy barriers to physical and chemical reactions than the parent species and, consequently, can react at lower temperatures. PECVD uses these reactive species to deposit thin films at temperatures lower than those possible with thermally driven CVD. The charged species in the glow discharge may also affect the properties of the deposited films [31]. Glow-discharge (non-isothermal) plasma is generated in a gas by direct current (DC), alternative current and a high-frequency electric field, such as microwave (2.45 GHz), at relatively low pressure [20]. Conventional direct plasma process have some problems such as a higher sample temperature, which is set by the discharge parameters and cannot be controlled independently, and a comparatively

higher operating pressure increases the possibility of surface contamination, which retards the diffusion of nitrogen [32] . In contray to this, remote plasma CVD is a technique which provides independent control of the generation of plasma [33-35] and is designed in such a way that the plasma source is separated from substrate material. In this technique, only certain desired species are excited by the glow discharge. These are then transported to the vicinity of the substrate where the desired deposition reactions take place. The remote plasma CVD technique does not require the substrate to be exposed to the plasma discharge environment. Furthermore, it allows independent optimization of plasma parameters. Microwave plasma can be produced by electron cyclotron resonance (ECR), through the proper combination of electric and magnetic fields [33,36]. Cyclotron resonance is achieved when the frequency of the alternating electric field is made to match the natural frequency of the electrons orbiting the lines of force of the magnetic field. This occurs at the standard microwave frequency of 2.45 GHz when it is coupled with a magnetic field of 875 Gauss Capacitive and inductive radio-frequency (RF) coupling plasma is generated at a frequency of 13.56 MHz [37].

2.2.2. PHYSICAL VAPOR DEPOSITION (PVD)

Physical Vapour Deposition (PVD) is becoming increasingly important for small engineering components. This is a deposition processes in which atoms or molecules of a material are taken from a solid or liquid source, transported in the form of a vapor through a vacuum and condensed on a substrate. PVD processes can be used to deposit films of elemental, alloy, compound as well as some polymeric materials. PVD embraces mainly evaporative deposition and sputtering in reactive or inert environments (Figure 2.1). Process temperatures are relatively low, 400 to 600 ^{0}C [38], thus minimising distortion and preserving the heat-treated state of the substrate. PVD processes have the advantage that almost any inorganic material and many organic materials can be deposited using pollution-free deposition processes. The deposits can be of single materials, layers with a graded composition, multi layer coatings, or very thick deposits. PVD processes are used to deposit films with a thickness range from a few angstroms to thousands of angstroms. Although one of the oldest techniques used for depositing thin films, thermal evaporation or vacuum evaporation, is still widely used in the laboratory and in industry for depositing metal and metal alloys. The following sequential basic steps take place: (i) a vapor is generated by boiling or subliming a source material, (ii) the vapor is transported from the source to the substrate, and (iii) the vapor is condensed to a solid film on the substrate

surface Evaporants cover an extraordinary range of varying chemical reactivity and vapor pressures [39] This variety leads to a large diversity of source including resistance-heated filaments, electron beams, conduction, radiation, or RF induction, arcs, exploding wires, and lasers Additional complications include source-container interactions, requirements for high vacuum, precise substrate motion (to ensure uniformity) and the need for process monitoring and control

Sputter techniques are used to deposit a wide range of materials [40] Peculiar features of the sputter deposition technique are generally explained in terms of the energy of the sputtered particles which are decomposed and emitted as a result of high energy ion bombardment in the plasma A complex variety of processes simultaneously occur whenever energetic particles interact with a substrate or growing films

Reactive coating deposition takes place in an inert gas A partial pressure of reactive gas supplies the carbon or nitrogen, and the metallic species is added to the system by resistance heating, arc or electron beam evaporation, or sputtering from a solid target Nitrides, carbides, oxides and so on, of metals have been deposited onto metallic components to provide thin, hard layers of inert, low friction coefficient compounds Ceramic coating enhances the performance of cutting tools and has considerable potential for many applications [41]

2 2 2 1 SPUTTERING A THIN FILM DEPOSITION TECHNIQUE

Sputtering is a glow discharge process (details about glow discharge have been described in section 2 2 1 1) Basically, sputtering device is divided into (i) conventional sputtering (DC Current, RF Current and so on) and (ii) magnetron sputtering The DC sputtering technique is the oldest construction with simply a target held at a negative potential, this construction ,is however, not very efficient and need to be operated at a high pressure and at a high target potential (2-3 KV) in order to sustain the discharge [42]

(a) Basic sputtering

In the basic sputtering process, a target or cathode plate, composed of the materials to be deposited on samples, is bombarded by energetic ions These ions are generated in a glow discharge plasma situated in front of the target The bombardment process causes the removal or sputtering', of target atoms, which may then condense on a substrate as a thin film [43] Secondary electrons are also emitted from the target surface as a result of the ion bombardment, and these electrons play an important role in maintaining the plasma The

basic sputtering process has been known for many years and many materials have been successfully deposited using this technique [44]. However, the process is limited by low deposition rates, low ionisation efficiencies in the plasma, and high substrate heating effects [42]. These limitations have been overcome by the development of a process called magnetron sputtering.

(b) Magnetron sputtering

Magnetron sputtering utilises a magnetic field parallel to the target surface, which in combination with the electrical field causes the secondary electrons to orbit in a closed circuit in front of the target surface. The force involved is termed the Lorentz force. This arrangement traps the electron and also creates a long electron path near the target surface. This process increased ionisation efficiency, compared with the DC sputtering technique. This is because each electron is able to ionise more working gas atoms close to the target surface, which in turn results in increased ion bombardment of the target and, therefore, a higher evaporation rate. Due to the increased ionisation achieved using magnetron sputtering, the glow discharge will be maintained at lower operating pressures (0.1 Pascal) and at lower operating voltage (500 V) than that used during DC sputtering (operating pressure ~ 1 Pascal and voltage 2-3 KV) [42,45]. A low working pressure will increase the deposition rate due to reduced scattering of the evaporated atoms. In addition, the trapping of the electrons by electric and magnetic fields near the target, results in lowered electron bombardment of the substrate and hence lower temperatures at the substrate surface. Ions are not trapped and therefore beneficial ion bombardment of the film continues. During the sputtering process it is also possible to use a reactive gas. The process is then referred to as reactive sputtering. During reactive sputtering the partial pressure of the reactive gas is carefully regulated, to keep a wanted covering of the target by reactive compound and get the correct stoichiometry of the coating.

(c) Development of Magnetron sputtering

Step by step modifications of the magnetron sputtering system have occurred over last few years in research. One such modification is the RF power supply (RF diode), enabling sputtering of dielectric compounds which is not possible using the normal DC process (DC diode) due to the charging effect. This technique avoids charge built up on the target surface by switching the polarity of target. By doing this, arc discharges on the target surface that may occur when sputtering low conductivity materials, are minimised. A balanced or conventional magnetron is configured in such a way that the magnetic fluxes of

the opposing magnetic poles are equal (Figure 2.4 (a)), that means, the surface of both the north and south poles of the magnetron are equal. In this magnetron the plasma is strongly confined near to the target region.

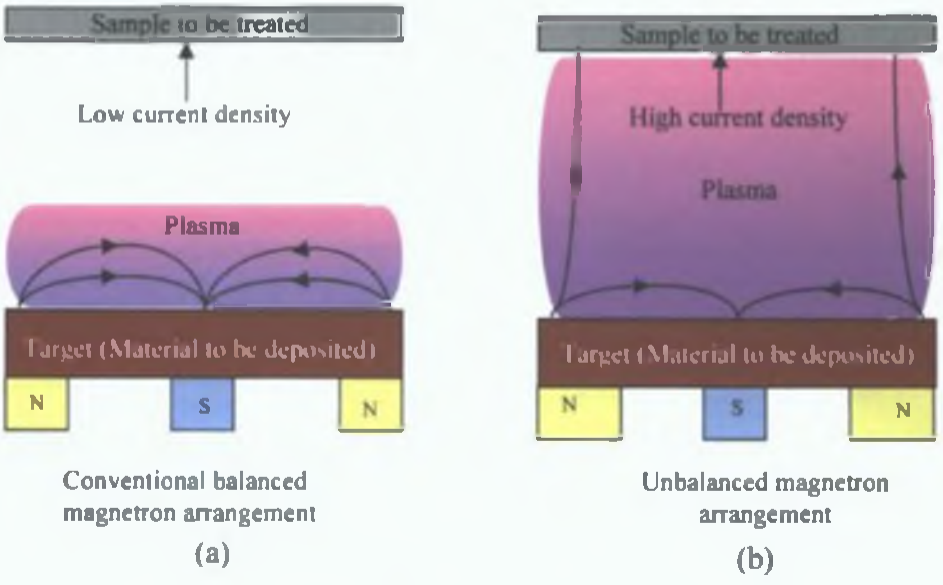

Figure 2.4: Schematic diagram of conventional and unbalanced magnetrons configuration.

Films grown on substrates positioned near to the target region will be subjected to concurrent ion bombardment which can strongly influence the structure and properties of the growing film. Substrates placed outside this region, however, will lie in an area of low plasma density. The ion current drawn at the substrate is generally insufficient to modify the structure of the film. The energy of the bombarding ions can be increased by increasing the negative bias applied to the substrate. However, this can lead to defects in the film and increased film stress and therefore be detrimental to the overall film properties. Thus, it is difficult to deposit fully dense films on large or complex components using the conventional magnetrons [46]. However, these problems can be solved by using the unbalanced magnetrons arrangement.

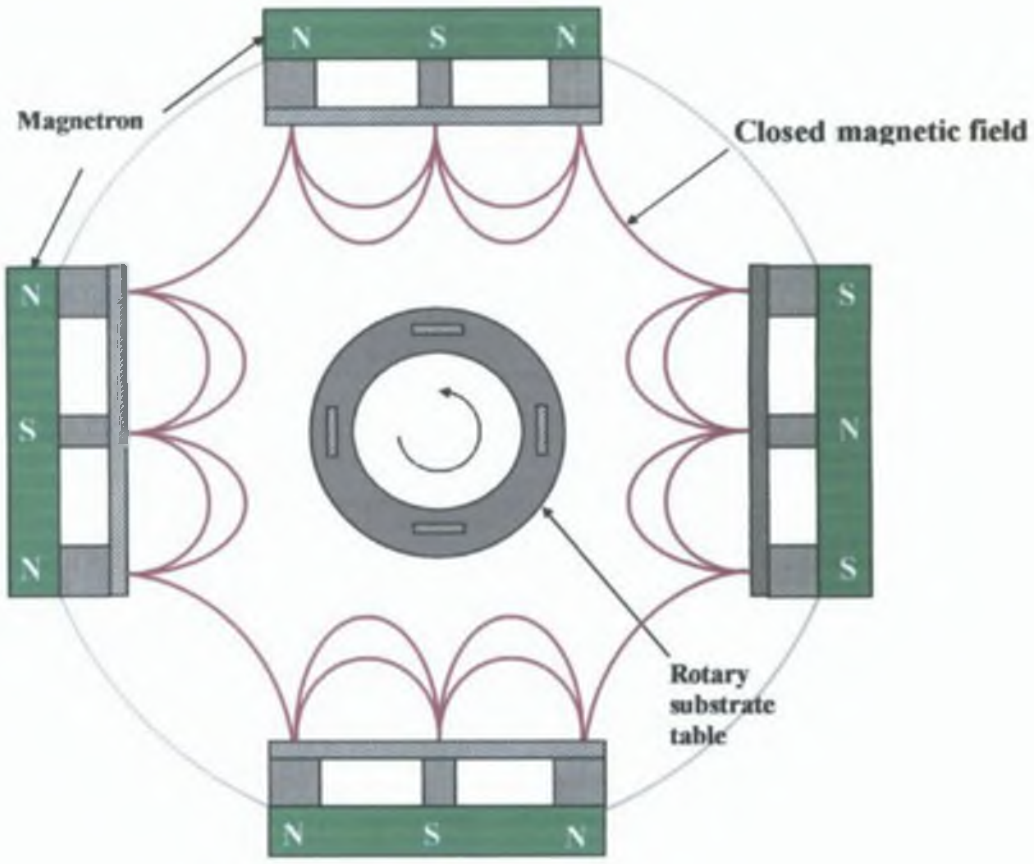

Figure 2.5: Closed field unbalanced magnetron sputtering (CFUBMS) configurations. (Where "N" and "S" indicate the north and south pole respectively) [47]

In an unbalanced magnetron the outer ring of magnets is strengthened relative to the central pole. A schematic diagram of the unbalanced magnetron configuration is shown in figure 2.4 (b). In an unbalanced magnetron, not all the field lines are closed between the central and outer poles in the magnetron, but some are directed towards the substrate, and some secondary electrons are able to follow these field lines. Consequently, the plasma is no longer strongly confined to the target region, but is also allowed to flow out towards the substrate. Therefore, high ion currents can be extracted from the plasma without the need to externally bias the substrate. Although unbalanced magnetrons proved some good advantage, it is still difficult to uniformly coat complex components at acceptable rates from a single source. Multiple magnetron systems have been introduced to overcome this drawback. In a multiple magnetron system, the magnetic arrays in adjacent magnetrons can be configured with opposite magnetic polarities (north and south) to create a 'closed field arrangement'. The configuration of magnetron and target is shown in figure 2.5. In the

closed field configuration, the field lines are linked between the magnetrons Losses of electron to the chamber walls are low and the substrate lies in a high density plasma region Operating in the closed field mode results in an ion-to-atom ratio incident at the substrate some two to three times greater than that obtained under single unbalanced magnetron configurations [48] The influence of the closed magnetic field on the ion-to-atom ratio becomes more significant as the distance from the target increases Moreover, due to recent development in magnetron design and the introduction of rare earth magnets, very high magnetic field strengths at the target surface are obtainable [49-51] The increased field strength increases the ionisation efficiency in the plasma, which in turn, results in a good quality coating In general, the most commercially useful coatings tend to be ceramic materials, including oxides, nitrides and carbides These materials can be deposited by sputtering a metallic target in the presence of the appropriate reactive gas Single element nitrides, most commonly titanium nitride, are now routinely produced by magnetron sputtering However, the multiple magnetron CFUBMS systems are ideally suited to the deposition of multi-component, or alloy nitrides, as each of the magnetron targets can, in principle, be of a different material By sputtering the targets at different rates, any desired alloy composition can be attained Moreover, by varying either the sputtering rates or the flow of reactive gas during deposition, composition, and, therefore, properties can be graded through the thickness of the coating In this manner, properties can be optimised, both at the coating and substrate interface for adhesion, and at the coating surface for the desired functionality

2.2.3. COMPARISON BETWEEN CVD AND PVD PROCESSES

The main difference between CVD and PVD is how the coating materials are evaporated and the process temperature Typical deposition temperatures in PVD processes are 200-500 °C but recently also processes running at lower temperatures have been developed [52] Traditionally, the temperature is in the range 600-1100 °C for thermally activated CVD processes Today, as a result of extensive research, CVD processes where the reaction is activated by for example plasma or laser at significantly lower temperatures are available [52] Plasma CVD combines a chemical and a physical process to bridge the gap between CVD and PVD In this respect, it is similar to PVD processes operating in a chemical environment, such as reactive sputtering A general comparison between PVD, Thermal CVD and PECVD processes has been given in table 2 1

Table 2 1 General comparison between PVD, Thermal CVD and PECVD processes [23, 52-54],

	PVD (Sputtering)	**Thermal CVD**	**PECVD**
Mechanism of production of depositing species	momentum transfer	chemical reaction	chemical reaction
Deposition temperature	200-500 ^{0}C	600-1100 °C	below 300 °C
Depositing rate	low except for pure metal	moderate	moderate
Energy of deposited species	can be high (1-100 ev)	low	can be high
Throwing power	good, But non-uniform thickness distribution	good	good
Operating pressure	carried out under low-medium vacuum (below ~1 3 Pascal)	ambient pressure	a moderate vacuum (~0 133 – 13 3 Pascal)
Source materials	solid	volatile liquid / gases	volatile liquid / gases
Source of Energy	plasma	heat	plasma
Impurity incorporation (such as organic groups etc)	low	high	low
Step Coverage	moderate	good	good
Density	high	moderate	high
Range of Material can deposited	high	medium	medium

2.3. SURFACE MODIFICATION

Surface treatment is a process through which properties of the surface tailored without adding any layer on top substrate surface Surface treatment such as, surface hardening of steels by carburising to sharpen the cutting edges of tools and weapons has been practised since the passing of the Bronze age [55] However the new technology of plasma-assisted carburising (and nitriding) is greatly improved variant of this old process, offering a higher degree of control and sophistication with economy and much enhanced properties and improved quality in turn With the progress of technology, further improvement of the plasma-assisted process like pulsed plasma mtriding or laser treatment processes like laser nitriding or laser carburismg are also continuing Details classification of surface modification methods is shown in figure 2 1 Surface modification usually can be divided into two groups (a) By microstructural modification modifying the surface without altering the substrate's chemical constitution, (b) By chemical modification changing the surface layers by altering the alloy chemistry

2.3.1. MICROSTRUCTURAL MODIFICATION

In this case the surface microstructure is modified without altering the substrate's chemical constitution and without or little change of the core This treatment is mostly used for ferrous materials There are two alternative methods for modifying the surface

(a) Microstructural modification by heating

In this case, instead of heating the whole component (as in through hardening), only the surface is affected, so that the bulk properties, specifically the toughness, remain unaffected, and component distortion is minimized In most treatments, a thin surface shell of ferrous material is rapidly heated to a temperature above the critical point so that steel changes the microstructure from a bcc lattice, ferrite, to an fcc lattice, austenite The quick quenching of the steel transforms austenite to body centered tetragonal structure, martensite (a phase with high hardness) Two treatments are being widely used, induction and flame hardening while electron beam and laser hardening have also become popular [56] As close control cannot be maintained by flame hardening, it is usually for large parts Such

processes produce parts which must be post ground in order to achieve the correct size and to provide a good surface finish As the build-up of energy in laser and electron beam hardening is rapid and well controlled, post heat treatment operations are not necessary in many cases Very thin surface layers (0 2 [57] - 0 6 [58] mm) can be hardened by laser hardening They produce almost no features that would be detrimental to opposing surface, but the processes are unlikely to be applied to lightweight alloys of titanium or aluminum

(b) Microstructural modification by mechanical working

While a ductile metal is deformed plastically below the recrystallization temperature, dislocations are produced in numbers proportionate to the degree of deformation A complicated network of interlocking dislocation is produced which impedes the dislocation movement and the metal is strengthened or work-hardened Cold working the surface by metal working, shot peening, shot blasting or other specialized machining processes to produce deformed layers increases the stored energy and compressive stress, thereby increasing the hardness, fatigue and stress corrosion resistance The process is highly controlled and leaves no residues or inclusions in the surface Shot peening can be applied to lightweight alloys to provide a controlled surface texture For example, it can be used to influence friction or prior to the deposition of a solid lubricant coating

2.3.2. CHEMICAL MODIFICATION

In this category, both surface microstructure and composition is changed either by the incorporation of carbon, nitrogen, boron, or occasionally other elements through diffusion or implantation into the material It can be divided into two categories

2 3 2 1 THERMOCHEMICAL DIFFUSION TREATMENT

Thermochemical diffusion treatment is a combination of heat treatment and chemical processes in which the chemical composition of the surface layers of a component is modified at elevated temperatures through diffusion The typical elements diffused into the surface include nonmetallic elements (C, N) metalloids (B, Si) and metals (Cr, Al) [59-61] Depending on to the elements to be incorporated into the material, thermochemical diffusion process can be divided into interstitial diffusion or metallic substitution by elements or metalloids In the case of interstitial diffusion, the diffusion element or

elements enter into the solution at the metal surface With increasing concentration of the diffused elements, the solubility limits are exceeded and the second phase may be precipitated Any further increase in concentration forms a continuous layer on the outer exposed surface The most common interstitial diffusion processes are nitriding, carburizing, nitrocarburizing, carbonitriding, surface alloying and boronising [59,60,62] Interstitial element diffusion into steels falls into two categories those carried out at low a temperature, within the ferritic range, or high temperature treatments in the austenitic range Ferritic processes involve the introduction of element (s) into the ferrite phase

Ferritic processes include gas nitriding plasma nitriding and nitrocarburising processes They are used to increase the hardness and wear resistance of a steel surface Nitriding of low alloy steels for gears is ideal, but if a lightweight material (titanium) is required, only the technique of plasma nitriding can be applied Austenitic processes involve the introduction of element (s) into the austenite phase The austenitic treatments broadly include carburising employing solid (pack), liquid (salt bath) or gaseous media, carbonitriding and boronising They are performed at temperatures near 900 ^{0}C [61] and produce much greater case depths (up to several mm) than the ferritic treatments Thermochemical diffusion processes can be divided into five categories according to the treatment media used [59-61]

1) Pack process (such as pack carburising, and boriding)
2) Salt bath process (salt-bath carburising, carbonitriding, and boriding)
3) Gaseous process (gas carburising, carbonitriding, nitriding, and boriding)
4) Vacuum and plasma process (vacuum carburising, plasma carburising and nitriding)
5) Laser process (laser carburising and nitriding)

Gas and vacuum processes produce better quality cases with more precise control of the diffused element profile than the pack and salt bath processes Later processes are very cheap and simpler to use Plasma processes produce better quality cases in a considerably reduced treatment time or temperature

2 3 2 2 ION IMPLANTATION

Ion implantation is not a coating process It bears a great resemblance to nitriding and shot peening rather than to coatings The essential feature of ion implantation generally involves positive ion production, acceleration and delivery to the surface of a base material If the energy of the ions is high enough, they will go into the surface and change the surface

composition. If this material is an electrical conductor, acceleration to the desired energy can be accomplished near the surface [63]. If the material is not conductive then acceleration must take place remotely, either near the positive ion production source or near electrodes that possess the contour of the surface and can be placed adjacent to it. If the material is an electrical insulator, or if the ion energies are low, electrons or negative ions may have to be injected with positive ions to prevent surface charging, which leads, in turn, to deflection of ions away from the surface [63]. Three different ion implantation processes are identified, namely, beam line ion implantation, direct ion implantation and plasma immersion or plasma source ion implantation (PIII/PI^3 or PSII) [43].

The implanted species occupy interstitial sites and distort the lattice. It is a low temperature process, typically 150 ^{0}C for small items and less for larger components [61]. The ions become embedded into the substrate lattice to a depth of 0.01 to1 μm, controlled by the incident ion energy in the range of 50-500 keV. The implantation parameters that are controlled directly to establish the thermal power, radiation damage and concentration of incident atoms in the treated surface layer are the ion energy, ion current density, the implantation time and the particular species implanted. By establishing the correct balance between the thermal input power from the ions and heat removal rate via radiation and/or conduction to some heat sink, very precise control of the surface temperature can also be achieved. The usefulness and breadth of applicability of the process lies in the fact that these five parameters (energy, current density, species, time and temperature) can be controlled independently and with great precision to achieve a desired microstructure, composition and thickness of engineered surface layers. When it is possible to implant any ionic species to engineer desired surface properties, it is generally easier to implant species that are gaseous either at room temperature or have a relatively modest vaporization temperature. The general shortcomings of ion implantation are high cost, inability to produce thick layers and inability to treat geometrically complex surfaces, have largely been overcome in recent years. This has been accomplished by processing at high current densities and elevated target surface temperatures [64,65], and by using Plasma source ion implantation [66] or Plasma immersion ion implantation [67] techniques.

2.3.3. PLASMA NITRIDING: AN IMPROVED METHOD FOR SURFACE TREATMENT

Nitriding is a thermochemical surface treatment process for ferrous/austenitic alloys involving the introduction of atomic nitrogen into the ferrite phase at a wide range of temperature (590-340 ^{0}C) [60]. The nitrogen then reacts with steel and produces hard, wear resistance iron-alloy nitrogen compounds. Various nitriding methods, such as, gas nitriding, liquid nitriding and carbonitriding, have been applied to various ferrous alloys to achieve superior surface hardness. Plasma nitriding, also called Ion nitriding or Glow discharge nitriding or Plasma assisted nitriding, is now widely used for surface hardening of ferrous (steel) and non-ferrous materials (Ti and Al) in the manufacturing industry for surface modifications, such as improving hardness, fatigue and wear resistance [68-70].

2.3.3.1. METHODS OF PLASMA NITRIDING

Broadly, plasma nitriding can be classified into two categories according to the method of sustaining the plasma during nitriding: conventional DC or DC diode and enhanced or intensified plasma nitriding.

(a) Conventional or DC diode plasma nitriding

Plasma nitriding by a DC glow discharge is generally efficient for numerous materials such as low-alloyed steels and tool steels. It is usually carried out under a near vacuum (100-1000 Pa) and with a moderate substrate voltage (0.3-0.8 kV) [70]. Glow discharge plasma is set up in a vacuum chamber by introducing nitrogen gas and applying a DC potential where the workpieces form the cathode with respect to the vacuum vessel. In this configuration, a large cathode sheath (a few centimetres) surrounds the nitriding substrates. The nitrogen and hydrogen ions and neutral atoms accelerate towards the workpiece and heat it via the transfer of kinetic energy. The nitrogen and hydrogen ions bombard the cathode surface and remove oxide and other contaminants providing a sputtering effect. In case of small samples ion bombardment can heat the sample to the nitriding temperature, whereas for large samples auxiliary resistive heating is necessary. Parts are held for a period of time to allow nitrogen atoms diffuse into the substrate and react with the alloy constituent of ferrous material or with the bulk material (Ti or Al) to form the nitride compound.

Depending on the process parameters and the steel compositions, like other conventional nitriding, two zones are formed: a diffusion zone and a compound zone on top of the diffusion zone, consisting of a solid solution of N in Fe and precipitates of the nitrided alloying elements dispersed on the microstructure. In the compound zone, γ'-(Fe_4N) and ε-($Fe_{2-3}N$) intermetallics as well as nitrides with alloying elements are formed. These compound layers are called white layers because they appear white on polished and etched surfaces [71]. This method is also called cathode nitriding as the substrates become the cathode. However, it has also been reported that nitriding of a substrate surface can be achieved by RF nitriding [72] or by anodic plasma nitriding [73]. In RF nitriding the substrate is held at a negative potential (about-100 V [72]), which means that it can be considered as a modification of the cathodic process. In anodic plasma nitriding, the discharge anode is nitrided and so the nitrided parts are at the positive potential [73]. In this case, surfaces of treated parts are, however, not only nitrided but also enriched by material from the cathode, which is sputtered in the nitriding discharge. As the material of the cathode can be different from that of samples to be nitrided, the surfaces of nitrided substrates can be modified by the addition of selected materials, such as Mo, Cr, Ti, V, C, and so on. The sputtered material transferred onto the surface of a treated sample forms a surface layer of nitrides from the deposited material.

Czerwiec et al. [32] identified some problems with the conventional plasma nitriding. In this process, the substrate temperature is dominated by the discharge parameters and cannot be set independently from the plasma reactivity. The minimum current density necessary to maintain an abnormal glow discharge can be high, leading thus to workpiece overtempering. The substrate voltage can also entail surface finish degradation and distortion for a large number of materials of practical interest. Also, at rather high operating pressures (about 1000 Pa) used in conventional nitriding, the surface of the substrates is sensitive to impurity contamination, which can block nitrogen uptake. The sputtering of the cathode in anodic nitriding plasma nitriding discharge is, however, too slow due to high-pressure (about 1000 Pa). Instead of using the DC power supply; pulsed power supply has significantly improved the performance of the conventional plasma nitriding process [34].

(b) Enhanced /intensified plasma nitriding: Toward low temperature and low-pressure nitriding

To overcome some of these problems the introduction of new generation low-pressure low temperature, and high-density plasma sources has led to the development of an enhanced or intensified Plasma Assisted Nitriding (PAN) concept [34]. They can provide low-pressure low temperature treatment along with are deduction in nitriding time. Because of the reduced collisionality at the lower pressure, the plasma contains a large number of active species, which increases the nitriding efficiency. Lower temperature means lower cost, less distortion and less surface roughening. Perhaps more importantly, certain alloys suffer degradation of their properties at the temperatures normally associated with conventional processes. For example, Plasma nitriding at temperatures above 480 ^{0}C, while giving significant improvement in wear resistance, tends to affect adversely the corrosion performance of stainless steels owing to the precipitation of CrN, which removes Cr from solid solution [74-76]. Lowering the process temperature widens the range of alloys and components that can be treated. Plasma nitriding at low temperature also allows the development of duplex plasma treatments where the nitrided surfaces are subsequently coated by PVD or CVD techniques [77]. Recently, Mandl et al. [78] used plasma-immersion ion implantation and found a very small fraction of chromium nitride on the surface. The concentration of the CrN precipitates depends upon the nitriding temperature and on the concentrations of chromium and carbon in the steel, as well as on the nitriding potential [79]. The currently used plasma-assisted techniques for low-pressure nitriding (0.1-10 Pa) can be classified under the following four categories (Figure 2.6): (1) thermionically assisted d. c. triode (TAT); (2) plasma immersion ion implantation (PIII) or plasma source ion implantation (PSII); (3) electron cyclotron resonance (ECR) systems; (4) thermionic arc discharge (TAD) [34]

(i) Thermionically assisted d. c. triode (TAT)

The triode arrangement is generally composed of a positive electrode and a thermionic electron source in addition to the conventional diode system. The additional electrons produced by thermionic source are then attracted by positive electrode and increase the ionisation of the plasma, which in turn reduces the pressure. One of the earliest successful applications of this process was reported by Korhonen et al. [80,81].

The advantage of the thermionically assisted triode system relates to the ability to adjust the current density (2-4 $mAcm^{-2}$) independently from the substrate potential, by changing the diode parameters of the electron emitter. This discharge can be operated at low pressures (1-10 Pa in N_2 or Ar-N_2 gas mixtures), because the supply of electrons is no longer dependent on the rate of ionic bombardment of the cathode [82,83].

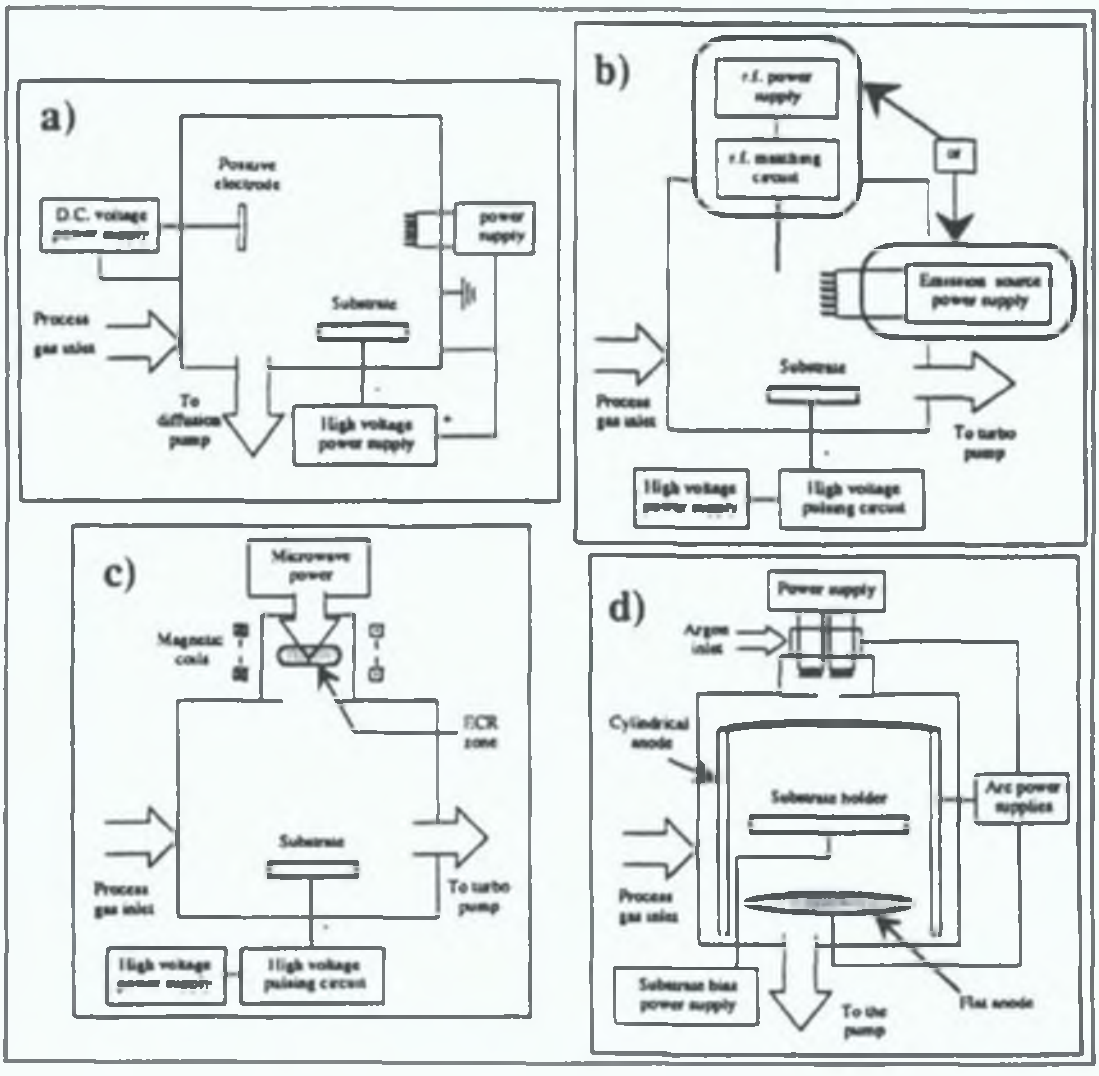

Figure 2.6: Schematic view of a thermionically assisted d. c. triode (a), plasma immersion ion implantation or plasma source implantation (b), electron cyclotron resonance (c) and thermionic arc discharge (d) for plasma-assisted nitriding (adapted from [34]).

Owing to the higher current densities triode nitriding can be performed at lower voltage than those used in diode nitriding [84, 85]. Most of the work on triode nitriding was performed by two groups: Matthews et al. [84-88] and Meletis and et al. [89].

(ii) Plasma immersion ion implantation (PIII) or plasma source ion implantation (PSII)

Plasma immersion ion implantation (PIII or PI^3) or Plasma source ion implantation (PSII) are new hybrid technologies combining elements from ion implantation with elements from conventional ion nitriding for the surface modification of materials. Both designations are currently used in the literature to designate similar processes, PI^3 is generally used in Australia [75,90-92] and PSII in the USA [93]. Generally both systems can be called Plasma Implantation (PI). In PI, the substrate to be nitrided is immersed in plasma, and ions are extracted directly from the plasma and accelerated by applying a series of negative high-voltage triode pulses (10-50 kV; pulse length, 2-100 s; repetition rate, 100-200 Hz) [34,94,95] to the substrate, thus eliminating the line-of-sight restrictions of conventional ion implantation. The accelerated nitrogen ions are implanted into the samples. The ion bombardment causes significant heating from 200 ^{n}C to temperatures typical of conventional plasma nitriding and this can result in the diffusion of nitrogen well beyond the implantation range [94-96]. This allows the extremely shallow implanted depth limitation to be overcome and brings about large increases in surface hardness and improvements in the wear resistance. Another advantage of the process is the formation of a plasma sheath around the target which causes ions to bombard the target normal to the surface, thus minimising material sputtering caused by the oblique incidence in diode nitriding. The pulsing of the voltage is essential to achieve spatial uniformity and a uniform implantation depth. In PSII, the plasma is generated by a conventional filament discharge whereas it is created by an inductively coupled radio-frequency discharge in PIII.

(iii) Electron cyclotron resonance (ECR) systems

In this system, the workpiece is placed in electron cyclotron resonance (ECR) microwave plasma and biased to a low-pulsed negative potential of - 0.4 to - 3 kV [96], which is much lower than the potential used for the PI process. The process temperature is 150 – 480 °C [96] and this is regulated by an auxiliary heater. Efficient nitriding can be achieved at a low pressure (0.1-1Pa) using this process. This new low-temperature, low-pressure nitriding approach is called "plasma source ion nitriding" [96,97]. ECR nitriding has several advantageous over other processes [98,99]. This included (i) high plasma

reactivity induced by effective production of active species at elevated electron temperatures and densities, (ii) a high degree of plasma uniformity over large areas, (iii) no contamination of substrate surfaces from additional electrodes and (iv) effective plasma nitriding can be achieved even outside the discharge (the substrate to ECR plasma distance can be up to 750 mm, whereas the standard distance is 250 mm) [98]. Plasma source ion nitriding has been demonstrated as a new low-temperature, low-pressure nitriding approach, which provides great experimental flexibility, low unit cost, and technologically simple apparatus design. The latter enables easy scaling to industrial applications.

(iv) Thermionic arc discharge (TAD)

D'Haen et al. [100] developed an arc-assisted nitriding process, where they have used a thermionic arc of the type widely used in activated reactive ion plating processes (ARIP). A high-current (100-300 A), low-voltage (25-40 V) TAD is generated in argon in an ionization chamber mounted on the top of the nitriding reactor itself. Unlike the ARIP process, where the arc plasma is more or less confined to an anodic crucible, the PAN reactor attempts to spread the plasma emanating from the ionisation chamber uniformly over the nitriding chamber. This is achieved by suitable magnetic field configurations and segmented anodes lining the reactor wall. Substrates are loaded freely between anodes and the ionisation chamber(s). These segmented anodes and the hot filaments in the ionisation chamber create uniform low-pressure plasma in the reactor (0.4-0.8 Pa) [34]. In the PAN reactor, an additional resistive heater produces a uniform temperature over a large payload. This technique has been called the 'arc-assisted nitriding' process. The fact that nitriding in this process is caused by nitrogen atoms, rather than nitrogen ions, is confirmed by the observation that the substrate bias potential has either an insignificant influence or no influence at all on the nitriding rate. Therefore the substrates can be left floating. The low plasma potential of this discharge (-5 to 15 V) ensures that sputtering is negligible on the substrate surface [34]. This feature allows, for the first time, nitriding without degradation of the surface finish and is the key to integrated duplex processes.

2.3.3.2. MODEL FOR PLASMA NITRIDING

Czerwiec et al. [32,34] proposed a plasma nitriding model identifying four different nitriding routes for plasma assisted nitriding as shown in figure 2.7: (1) physisorption route; (2) direct chemisorption route; (3) bulk phase dissociation route; (4) ion implantation route. Nitrogen molecules will be adsorbed by the surface to form a physisorbed layer.

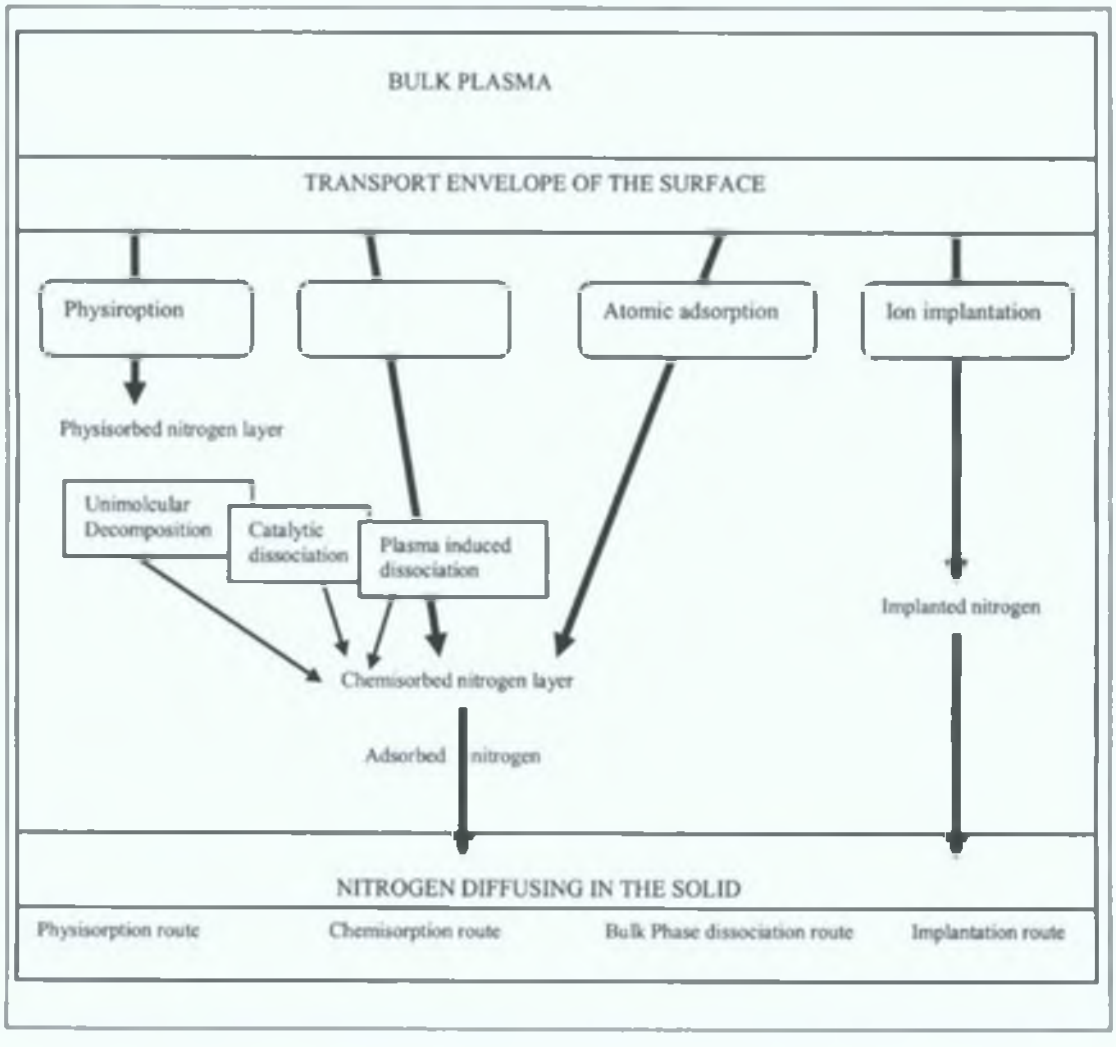

Figure 2.7: Schematic representation of the model proposed for plasma-assisted nitriding (adapted from [34]).

Nitrogen molecule diffusion in the metal can be neglected. Different reaction paths link this physisorbed nitrogen to a layer of chemisorbed nitrogen: unimolecular decomposition, catalytic decomposition, and plasma-induced dissociation. Direct chemisorption and atomic adsorption produce chemisorbed nitrogen directly. Ion implantation produces absorbed nitrogen directly. It was assumed that the absorbed nitrogen was the starting point for the nitrogen diffusion. In view of the material published on the different processes, the following conclusions were proposed: gas nitriding proceeds exclusively via the physisorption route. Diode nitriding may combine contributions from all four routes. TAD, ECR and post-discharge nitriding proceed probably mainly via the bulk phase dissociation route. PI has certainly a large contribution from the implantation route. The following ranking with respect to the rate for the different routes was also proposed: implantation > bulk phase dissociation > chemisorption > physisorption [34].

2.3.3.3. ROLE OF PROCESS GAS DURING PLASMA NITRIDING

There is lot of controversy over the addition of adding gases other than nitrogen during the plasma nitriding process. The addition of argon in diode nitriding is reported to give no improvement in nitriding effects [101]. But the presence of argon in low-pressure nitriding has, however, been reported to increase hardness and it may be beneficial (either alone or in combination with hydrogen) in controlling white layer effects and/or modifying surface layer morphology [70]. The addition of neon in a low-pressure plasma nitriding effectively increased the nitrogen ion flux with maximum energy to the substrate due to the penning ionization of nitrogen by neon [87]. It is known that nitriding of steels is greatly affected by the presence of hydrogen [69]. It was related to the fact that H^+ ions, which have lower mass and higher kinetic energy than N^+ ions under the same conditions of pressures, voltage, and temperature, can dissociate N_2 molecules into NH_x species through collision at lower energy [102]. NH_x species seem to dissociate prior to reaching the surface of the cathode to produce active nitrogen atoms [101,103]. Recently, it was observed that the introduction of highly energetic hydrogen species during the plasma nitriding process would remove the chromium on the surface by chemical reactions. An increase of the hydrogen concentration decreased the CrN concentration on the surface. This suggests that hydrogen should play an important role during the nitriding process [79].

2.3.3.4. FUTURE DIRECTION

In most surface-hardening applications, enhanced plasma nitriding is expected ultimately to replace conventional nitriding. It is more economical because it introduces faster nitrogen diffusion, which in turn allows for lower nitriding temperatures or shorter treatment times. It has other advantages, such as, it result in improved corrosion resistance, it is an environmentally friendly process, and almost no distortion of the treated parts results. Although the companies are increasingly inclined towards the use of this process, it still hasn't reached full industrial market maturity due to the more costly and time-consuming vacuum environment required.

Plasma nitriding is a "surface hardening heat treatment that introduces nitrogen into the surface" of a material. As such it does not affect the properties of the rest of the material. This relatively new process has many advantages over traditional nitriding process, such as Salt Bath Nitriding and Gas Nitriding, including cost, consistency of hardness, increased environment protection and it does not cause roughening of the surface. The hardness is increased due to the formation of nitrides combined with other elements in the material such as chromium nitrides, iron nitrides and carbon nitrides the amount, type and distribution of which determines the hardness level. Compressive residual stresses are set up in the nitrided layers of the material and are beneficial as regards wear. This process does not add extra weight to the material and so can be used for orthopaedic applications. At its optimal this process provides a surface which has an improved wear resistance, fatigue strength and corrosion resistance.

2.4. SURFACE COATING

The modification of the surface properties of a material by using a surface engineering process to apply a thin hard coating has long been proven to be a hugely successful way of improving tribological properties. As nitrided layers produced by different nitriding process may not be sufficient enough to combat severe wear and corrosion conditions, a significant number of hard coatings such as TiN, TiCN, and TiAlN and so on, have been used to improve the performance and extend the life of a component. But yet, all these coating face a number of problems such as insufficient load bearing capacity, poor adhesion strength, stress development, poor tribological properties (hardness, friction and wear properties) and so on. Among all this properties, load-bearing capacity and adhesion strength of deposit are very important as they largely control the final performance of the deposited coating.

2.4.1. LOAD BEARING CAPACITY AND ADHESION

The ability of coated component to withstand loads and stresses without large deformation or coating failure is called the load-bearing capacity [104]. Failure of thin hard coatings may occur due to the plastic deformation of a substrate with insufficient strength (that means, low load bearing capacity) [105]. Whereas, the word adhesion is frequently used in a broad sense to describe the sticking together of two materials with or without an intermediate layer, and terms autohesion (or homohesion) and heterohesion have been introduced to describe situations where the two materials are either identical or dissimilar, respectively. These words are used rather loosely to describe complex situations since the average adhesive joint has two interfaces at which adhesive failure can occur and three regions of possible cohesive failure. The term adhesion should be strictly reserved for the bonding at an interface between two different materials and carries the implication of intimate contact at the interface. The closest approach to perfect contact is obtained by condensing vapor atoms directly on a solid surface to form a thin film, as in the various methods of vacuum deposition [106]. Load bearing capacity and or adhesion can be increased in the following way.

(i) By using a high hardness, high stiffness substrate, that means, tool steel, cementite carbide and so on.

(ii) In case a of low hardness substrate a) adding a layer of a new material or (b) modification of the existing surface by case hardening, nitriding or ion implanting

(a) Adding a layer of a new material

The purpose of the intermediate layer is to increase the adhesion and in some cases also to protect the substrate from plastic deformation. In order to protect the substrate from plastic deformation, the layer must provide good load-carrying support to the brittle ceramic coatings, that means hinder cracking and premature coating failure. In order to meet these demands, the load-carrying layer has to be considerably thicker and tougher than the thin brittle coating but at the same time harder and stiffer than the base material. In generally, a ceramic interlayer is used to improve the load-bearing capacity of the substrate [107]. Again, in hard coating applications, adhesion of coating materials to substrate materials is one of the most important. Generally, nitrides of transition metals, such as TiN, WN and ZrN deposited by a PVD process exhibit a poor adhesion to substrate materials [108]. In spite of few disadvantages, PVD processes are convenient and extremely industrialized coating technique for refractory materials [108]. The use of an interface layer with the correct materials combination has been found to enhance the adhesion of coatings deposited by a PVD process [1]. This techniques shows promise for future development. For example, a pure Ti or a sub-stoichiometric TiN interface interlayer has been used to improve the adhesion of TiN coatings [108-110]. The increase in adhesion brought about by the interface layer is thought to be due to mixing of the transition layer which results in improved bonding at the TiN- substrate interface [109-110]. The interdiffusion zone broadens with the Ti interlayer, to some extent, overlaps the Ti interlayer; it helps to increase the adhesion of TiN. On the basis of this hypothesis, by making a composition change in the interface transition region gradient, both chemical and mechanical bondings are expected to be improved. In addition interface layers are thought to prevent the growth of a fatigue crack during loading of the surface, possibly resulting in an increase in micro hardness. It is also believed that the improvement of adhesion with precoating is closely related to a plastic deformation of the interlayer, which could reduce the stress concentration which causes the failure of the compound film.

One of the major factors causing film failure during deposition processes or application of coatings is the stress discontinuity at the interface between the deposited film and substrate [111]. This stress discontinuity at the interface is generated by the differences between their elastic modulii and thermal expansion coefficient and results in either compressive or tensile residual stresses in the coating. Therefore it is of critical importance

to reduce these residual stresses as small as possible in hard coatings. Traditionally, a metal interlayer is used to improve adhesion as described above. However, it has recently been reported that a graded interlayer formation with a gradual change of composition between the top hard coating and the soft substrate can be achieved by depositing an intermediate layer [112-114]. This reduces the abrupt discontinuity and improves the mechanical and tribological properties considerably [112,113,115-117]. For example, a greater improvement in adhesion, can be attained using a gradient Ti-TiN_x interlayer than using a single Ti intermediate layer. The deposition of this Ti-TiN_x intermediate layer reduces the hardness gradient and residual stress gradient between the substrate and the stoichiometric TiN [118].

(b) Modification of existing surface

Thin hard coatings can provide a surface with dramatically improved properties in terms of low friction and high resistance to wear and corrosion, but catastrophic premature failure will occur if the substrate plastically deforms under a high load [107,119-121]. An innovative approach to solve this problem is to design and develop duplex diffusion/coating treatments [122,123]. A details description of duplex and graded coatings/interlayers have is presented in the next section.

2.4.2. COATING WITH ADVANCED DESIGN

Several new generation coatings have recently drawn the attention of the tribologists with the intention of achieving further improvement of properties over the traditional single layer homogeneous coating [11,12] (Figure 2.8).

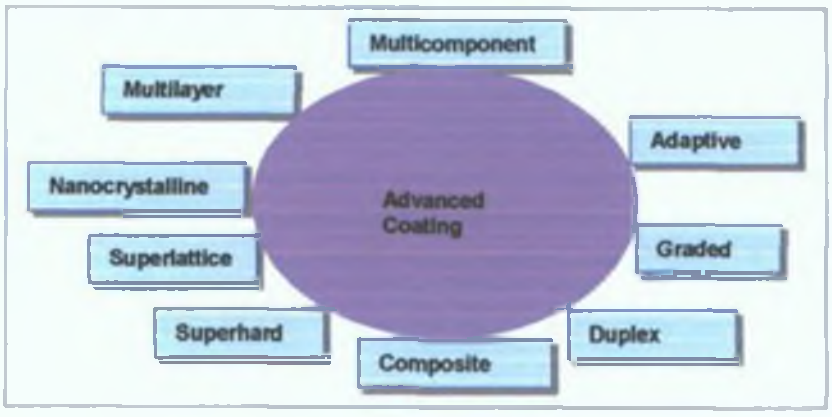

Figure 2.8: Advanced coating for future application.

Possible structures of some of these coatings are shown in the figure 2.9. In the following sections the potential of these coatings will be discussed briefly.

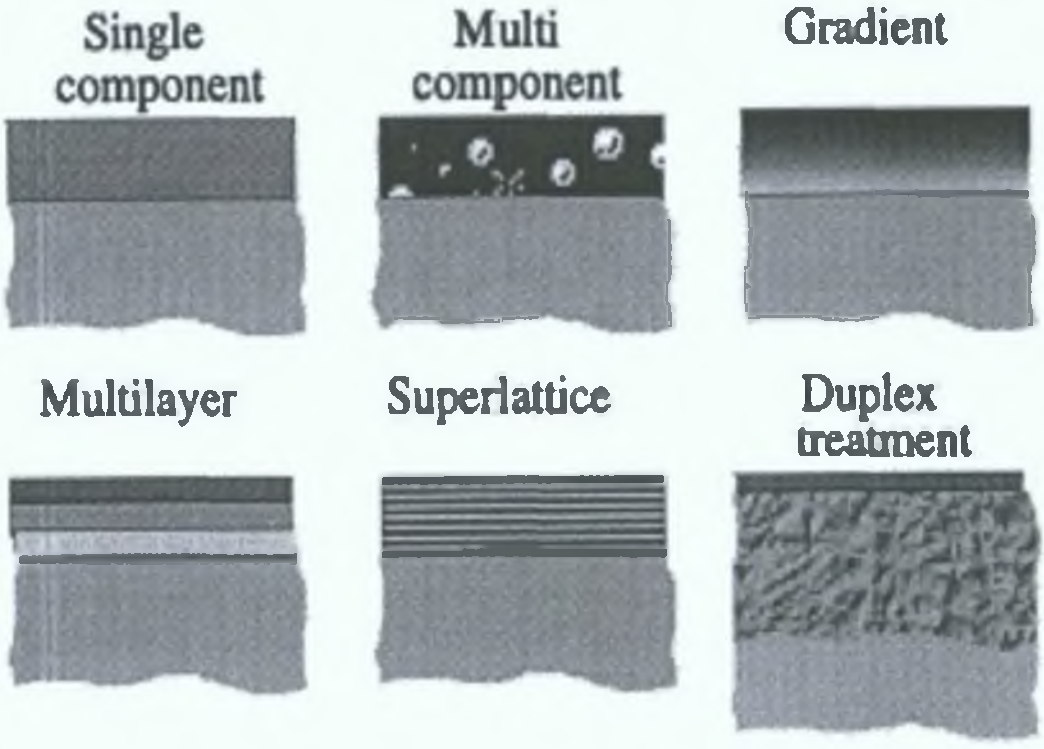

Figure 2.9: Possible architecture of some selected advanced coating [124].

2.4.2.1. GRADIENT COATING

(a) Compositionally graded coating

Multicomponent coatings can readily improve the coating hardness via alloying. However, coating alloyed nitrides directly on substrate surfaces usually reduces the adhesion strength due to higher brittleness and residual stress. Gradient coatings are a type of multicomponent coating in which the compositions continuously change when moving from the substrate to the coating surface. This allows the properties of the coating at different depths from the surface to be varied with no visible interface [13]. One advantage of such coatings is that problems associated with interfaces in conventional multi-layered coatings are eliminated [125]. A graded coating composition or structure improves the load

carrying capacity by offering smoother transitions in mechanical properties from those of the hard and stiff coating to those of the softer and more flexible substrate.

Compositionally graded films are mainly applied for thermal barrier coatings and wear resistance coatings [126]. Instead of homogeneous multicomponent coatings with discontinuous phases, graded coatings are expected to be more effective in terms of adhesion, wear, thermal shock and corrosion resistance [126,127]. The most frequently reported compositionally gradient coating is TiAlN [112,127-129]. Composition of the film is controlled in such a way that the Ti-rich composition is formed near the substrate layer and the Al-rich composition near the surface layer, which would improve the adhesive strength while maintaining the hardness, oxidation and wear resistance properties. Experimental results have shown that the adhesion strength and thermal shock resistance is better than that of (Ti, Al) N homogeneous coatings and increases with decreasing composition gradient [127]. With decreasing composition gradient, the zone of gradient between the substrate and (Ti, Al) N coating increases and the stress cannot concentrate any longer in the boundary but distributes in a gradient zone during deformation, which causes the increase in adhesive strength [127]. Raveh et al. [130] mentioned several advantages of graded and multi component films such as (TiAl) (N, C) over uniform TiC, AlN, and TiN coatings. The main advantages are better adhesion due to the absence of a discrete interphase, lower internal stresses, and a higher corrosion resistance. Under optimised deposition conditions, graded Cr-Ti-N coatings showed very high elasticity, (an elastic recovery of 80% was observed) hardness and adhesive strength. It was believed that the hardness enhancement results from the alloy-hardening mechanism. The adhesion improvement is attributed to the grading effect through an intermediate compound [112]. Ti-Al-N gradient coatings are similar to multilayers in which the composition, microstructure and property, especially the coefficient of linear thermal expansion of each layer, is approximate to that of the nearby layer. Therefore, the difference in thermal strain and thermal stress between any two conterminous layers is smaller than that of homogeneous (Ti, Al) N coatings. However, there is soft phase (metal) in gradient coatings, which can deform easily to relax part of the thermal stress and to prevent the crack formation and propagation. All those factors are beneficial to the thermal shock resistance of Ti-Al-N functional gradient coating [112]. Inoue et al. [131] suggested that aluminium nitride coatings made of a compositional gradient (from Al to AlN) may have a greater thermal conductivity and resistivity compared with those of a uniform layer and are subjected to lower thermal stresses.

(b) Functionally gradient (FG) coatings

Instead of using alternating layers of two different coatings, recently, a functionally gradient multilayer approach has been introduced, where each layer is designed to meet specific purposes. The layers are deposited in such a way that there must be a smooth transition of microstructural, mechanical and chemical properties among each successive layer. Different layer properties are required in different tribological systems. Among the most important are adhesion layers, load support layers, hard and wear resistant layers, low friction layers and corrosion resistant layers. Depending on the specific requirement in a tribological system, layers are arranged accordingly. Voevodin et al. [132] designed a wear resistant Ti/TiC/DLC functional gradient multilayer coating with an adhesion layer-load supporting layer-superhard self-lubricating layer structure. In this design there is a smooth transition of hardness and elastic modulus from the substrate to coating surface. This results in a superhard (60-70 GPa) coating with low friction surface, improved adhesion to the substrate, and no brittle failure with high contact load. Similar Ti-TiN-TiCN-[TiC-(Ti_x%-DLC)] multilayer coatings have been reported, where the metal-ceramic Ti-TiN-TiCN formed the supporting interlayer. Several coatings have been prepared with the same supporting interlayer and variations in the preparation of the Ti_x%-DLC layer. Low friction coefficients (below 0.2 at an air humidity of 50% RH) in combination with low normalized wear rates were found for multilayer coatings with upper $Ti_{20\%}$-DLC and $Ti_{35\%}$-DLC layers [133].

2.4.2.2. DUPLEX SURFACE ENGINEERING

Surface engineering, either by surface treatment or surface coating, has become a well-established technology and is extremely versatile means of improving component performance in mechanical and tribological applications. Thermochemical diffusion processes, such as plasma nitriding, produce an enhanced surface layer, which improves fatigue and corrosion resistance as well as load-bearing capacity of workpiece. But this layer may not be sufficient in severe wear conditions. On the contrary, thin hard coatings have been widely used due to their high hardness and wear resistance.

However, failure of thin hard coatings occurs due to excessive plastic deformation of the substrate having insufficient strength [105]. A thin coating alone cannot provide improvements over uncoated parts in the following cases [134]:

- The corrosion properties required cannot be met by any material with appropriate mechanical properties,
- The fatigue strength of the steels that have suitable core stiffness is not sufficient and
- The occurrence of three body abrasion with grain sizes exceeding several microns in a closed tribological system [120,135].

Thus, the complex requirements for surface engineering cannot be realized in a single homogeneous coating or a single surface treatment. Combining successful single processes into one treatment can result in the increased resistance of metals to complex loads. The wear, fatigue and corrosion properties are improved by combing the advantages from various processes and eliminating the disadvantages single process [136]. Processes combined in this way, sometimes called duplex, hybrid, or combined process, offer a novel approach in surface engineering. Duplex coating systems (that means, coating deposition on plasma nitrided substrate) therefore seem to be the best compromise [105,121,137-138]. This type of duplex coating system was proposed in the early 1990's by Bell and co-workers [139] and independently by Zlatanovic and Munz [140]. Duplex surface engineering, as the name implies, involves the sequential application of two (or more) established surface technologies to engineer the surface of the components in order to produce a surface composite with combined mechanical, metallurgical, and chemical properties, which are unobtainable through any individual surface technology (Figure 2.10) [121]. Better adhesion can be expected due to the interdiffusion of the coating material with the substrate material in the reverse duplex coating (nitriding and/ or vacuum heat treatment of the coating/substrate couple) [141].

In addition, plasma nitriding followed by in situ coating deposition in the same process chamber (continuous process) is considered to be advantageous over the discontinuous process have been reported by others researchers [135,142-145]. This area is still under investigation and no industrial applications of the duplex process have yet been established and extensive research still needs to be carried out in this area.

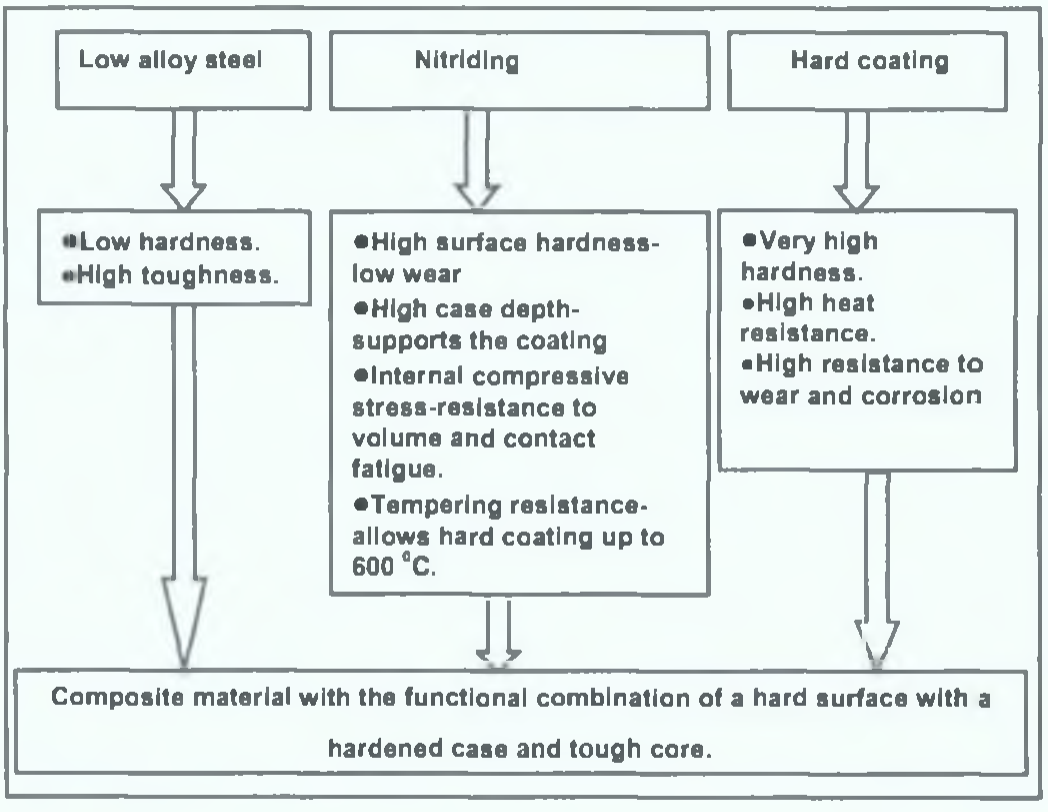

Figure 2.10. Properties of composite components produced by duplex surface engineering (adapted from [146]).

Of all the possible duplex coating systems, thermochemical treatment (nitriding, carburizing, nitrocarburizing and so on) and coating processes (PVD, CVD) are the promising. Numerous researchers have reported the use of nitriding (gas nitriding, plasma nitriding) plus PVD (ion plating [118,139], electron beam evaporation [147,148], cathodic arc plating [149], magnetron sputtering [150,151], and reactive arc evaporation [152], for the deposition for common materials like TiN and TiAlN on steel substrates. Other combinations of duplex coatings that have been reported so far included high temperature-CVD TiN coating on low-pressure carburised steel [136], DLC (Diamond-Like Carbon) coating on plasma nitrided soft substrate Ti-6Al-4V [153], TiC coating on plasma nitrided, carburised and nitrocarburised TiAl6V4 substrate [154], pulsed plasma nitriding and DLC coating on a high-speed steel substrate [155] and PVD TiN coating on laser nitrided Ti alloy [156]. Conventional nitriding causes the formation of two zones: a relatively thick diffusion zone (~500μm) of hard (900-1000 HV) subsurface and internal compressive stress (600-1000Mpa [144]) with a fine dispersion of alloy nitrides and a thin compound or white layer on the component surface. The compound layer consists of a heterogeneous mixture of two different iron nitride phases: γ'-(Fe_4N) and ε-($Fe_{2-3}N$).

This will sufficiently support the hard coating and reduce the hardness and stress gradient between the substrate and the hard coating, which improves the adhesion and avoids any "egg-shell cracking". The main improvement of the duplex treatment is dependent on the nitriding process [157]. Incorrect process control during nitriding leads to the formation of a porous "white layer", which has lower hardness and cannot support the hard coating.

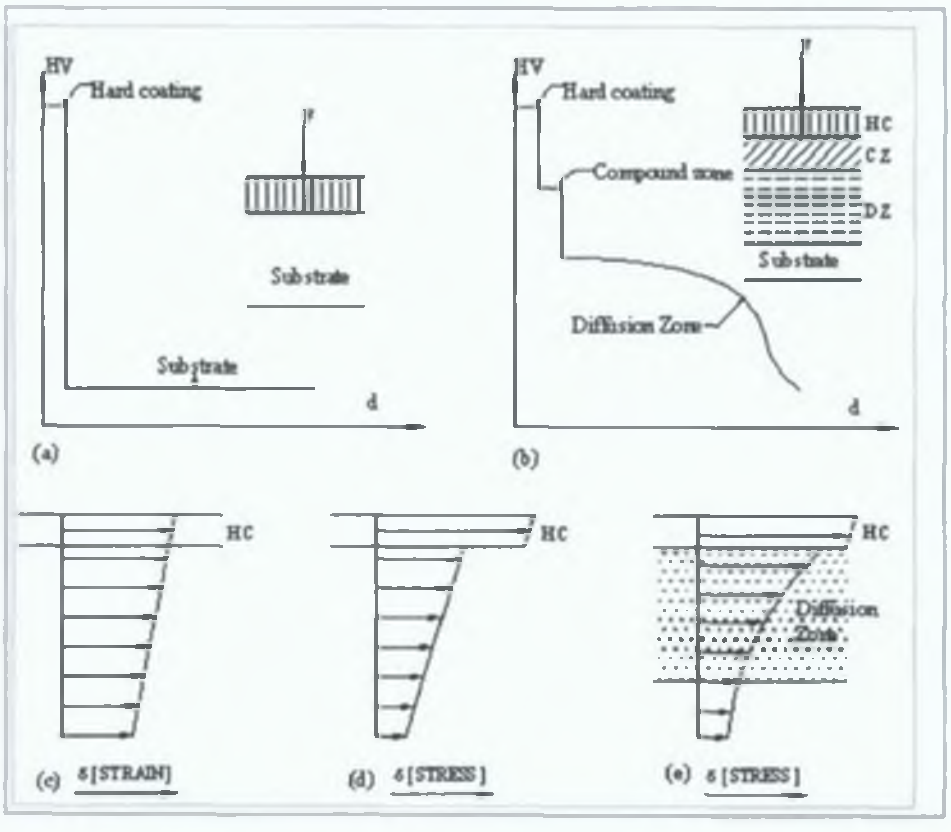

Figure 2.11. Microhardness distribution of (a) the coated substrate and (b) the plasma nitrided and coated substrate, (c) strain distribution of the coated substrate, stress distribution of (d) the coated substrate, and (e) the plasma nitrided and coated substrate [157].

During coating deposition on the nitrided samples, high temperature and extended ion bombardment cause thermo-chemical decomposition of the white layer and lead to the formation of a soft and porous "black" layer [139,158,159], which severely deteriorates corrosion resistance and the load bearing capacity of the composite. Adhesion and load

bearing capacity of the coating on nitride substrate depend on type of nitride layer formed [157]. Recently more attention has been given to low temperature plasma nitriding (below 500 °C) of substrate to acquire more enhanced surface properties and to control nitride layer formation in comparison to conventional high temperature nitriding/plasma nitriding [32,35,160]. With respect to non-nitrided substrates, plasma nitrided steels are, in theory, more suitable substrates for hard coating deposition, as shown in figure 2.11. The resistance to plastic deformation of the surface layer is enhanced as a result of the improved load support provided by the plasma nitrided layer [157]. The hardness of the composite (coating-substrate system) is influenced by the hardness of the nitrided substrate and by the hard coating structure. Usually, the structure of the coating is denser on nitrided samples provided that the porous outer zone is removed and the hardness is increased. Results from the current researchers [139,148,161,162] indicate that the tribological performances of the coating produced by the duplex treatment method are much better than when the individual processes in the duplex treatment are used separately. Compared with coated hardened substrates, the nitrided and coated specimens show a much lower level of wear mainly because of their superior load-carrying capacity, which is due to the higher substrate hardness [163,164].

Duplex treatment has been shown to result in improved adhesion in several studies [118,146]. Nitriding lessens the differences between the stress environments in the coating and substrate by promoting the development of compressive stress in the surface of the substrate, provided that the porous compound layer is removed. Adhesion can be further improved by inserting an interlayer before depositing the coating [142,162]. Duplex treatment also improves the fatigue resistance due to the compressive stress induced in the substrate [147,151]. Several researchers [120,149,165,166] have reported that thermochemical treatment (plasma nitriding) followed by a hard coating could effectively solve the corrosion problem. The better corrosion resistance in the duplex coating is related to the passivation power of the iron nitride compound layer formed during the plasma nitriding process. The performance of the duplex coating is further improved by the deposition of a multilayer coating instead of single layer on the plasma nitrided substrate [147,167]. Navinek et al. reported that the duplex coating consisted of a multilayer TiN/TiAlN coating and low pressure plasma nitriding would improve the tool life of hot forging dies and result in reproducible quality of forged parts, in comparison to the use of dies with a traditional coating only [167].

2.4.2.3. MULTICOMPONENT COATINGS

Multicomponent coatings are composed of two or more constituents in the form of grains, particles or fibres. Depending on the non-metallic components, multicomponent coatings found are nitride, carbide, boride and oxide coatings. The multicomponent coatings can be classified into the following three categories: binary, ternary, and quartnary and higher component coatings. Multicomponent coatings are mainly deposited as a compound of metal(s) (Ti, Cr) and non-metal (N, O, C, B) or non-metal and non-metal (SiC, SiN, CN). Most of the developed coatings are Ti-based and to some extent Cr-based. There are very few reports of Al and C based coatings. The most common binary coatings, TiN [168], TiC [169,170], and CrN [171,172], deposited by PVD and CVD methods, have gained increasing importance in several industrial sectors, including cutting tool industries, because of their outstanding tribological properties. Research on improving the performance of binary coating by adding another element or elements to form ternary, quartnary or higher constituent elements is increasingly reported. These higher constituent compounds change the properties of the coatings in such a way that they can possess better performance than the binary coatings in terms of wear, corrosion and oxidation resistance. This superiority is due to several effects that may become dominant in multicomponent systems. These effects included the formation of multi-phase structures (causing a better mechanical and thermal stability) [173], solid solution strengthening, and formation of an external layer as a result of a partial reaction (the latter two effects promoting wear resistance) [174]. The alloying in multicomponent coatings imparts higher chemical stability and improved oxidation resistance. The increase in the number of elements of the coating renders a finer microstructure and a small grain size, leading to an increase in strength and elasticity in thin hard films. Metallic and non-metallic element/elements are added to the binary coating to form ternary quartnary and higher component coatings. At present (TiAl) N and (TiC) N are accepted as standard ternary coatings in industry. There is also much interest recently in superlattice, nanostructure and adaptive and so on coatings, for different applications.

2.4.3. NEW GENERATION COATINGS WITH SELF-LUBRICATION

Several new generation coatings, that are attempting to achieve further improvements in properties over the traditional single layer homogeneous coatings, have recently drawn the attention of the tribologists [11,12]. But many of these coatings are very hard and they can form hard particles which act like grit when the coatings are worn and have a higher co-efficient of friction.

Solid lubricants are often used in industrial applications to reduce friction between two metallic surfaces in contact [175]. Solid lubricants are also an appealing choice in promoting dry machining to avoid environmentally harmful liquid lubricants either fully or partially. There has been considerable interest in identifying and developing solid lubricant system, which offers higher operation temperatures and greater load bearing capacities than liquid lubricants. Solid lubricants films, however, wear away rapidly and thus require some mechanical means for replenishment. This is impractical for many hard-to-reach surfaces in motion and has prompted recent attempts at extending the sliding life of solid lubricant films [176]. Ideal solid lubricant should have the properties of a hard surface while providing lubrication. In most cases, solid lubricant has provided good lubrication but they are not very effective during sliding as the surface hardness is not high. Another problem with the solid lubricant is that some solid lubricants, such as MoS_2, can provide good lubrication in a vacuum or inert gas environment but they loose their lubrication property in humid weather. Several approaches have been tried to improve their sliding characteristics in normal or humid environment. Soft metal coatings [177] have been used as solid lubricants for space and other specialised applications but, these have poor wear properties and cannot be considered for general wear protection. Diamond-like carbon (DLC) coatings [178] are hard and have lower friction than the hard nitride coatings and are starting to be used to protect some relatively lightly loaded mechanical components, but the true DLC coatings are very hard with high internal stresses, tend to be brittle, and have poor adhesion and therefore are unsuitable for highly loaded applications.

2.4.3.1. MoS_2 BASED SOLID LUBRICANT COATING

Soft coatings like MoS_2 coating have been used as a solid lubricant for a long time due to its low friction [179-181]. It has a layered molecular structure with individual sheets of molybdenum (Mo) and sulphur (S) atoms. The low shear strength is explained by its anisotropy. The material is comprised of hexagonally packed planes consisting of a layer of Mo bonded on each side by a layer of S and each Mo atom is surrounded at equal distance by six sulphur atoms placed at the corners of a triangular prism, as shown in the figure 2.12. The forces holding the atoms together in each group of S: Mo: S layers are covalent bonds whereas the forces between the adjacent planes of sulphur atoms are weak Van der Waals type bonds. All effective strong bonding is within the resulting sandwich planes. The bond strength between the neighbouring sandwiches is very weak. Thus MoS_2 has a strong structure in two dimensions and weak in the third [175]. Because the adhesion is poor and the films are soft resulting in low wear resistance, MoS_2 coatings are not suitable for highly loaded application. They tend to be worn away rapidly and thus require some mechanical means for replenishment. Also their good lubricant property can be obtained only in a vacuum or dry atmosphere [182]. Several attempts have been made to improve the strength of the soft solid lubricant coating. These problems have been addressed using three different approaches as follows:

- Inclusion of metal doping (for example Ti, Cr and so on) in solid lubricant (MoS_2) coating [2-3]. By alloying with selected metals, MoS_2 coating becomes applicable to terrestrial, humid environments [183]. The co-deposition of metals with MoS_2 during sputtering was found to result in reduced friction and high wear resistance in humid atmosphere.

- The application of a solid lubricant coating layer on top of a hard coating layer (for example on TiN layer) in the form of multilayer [4].

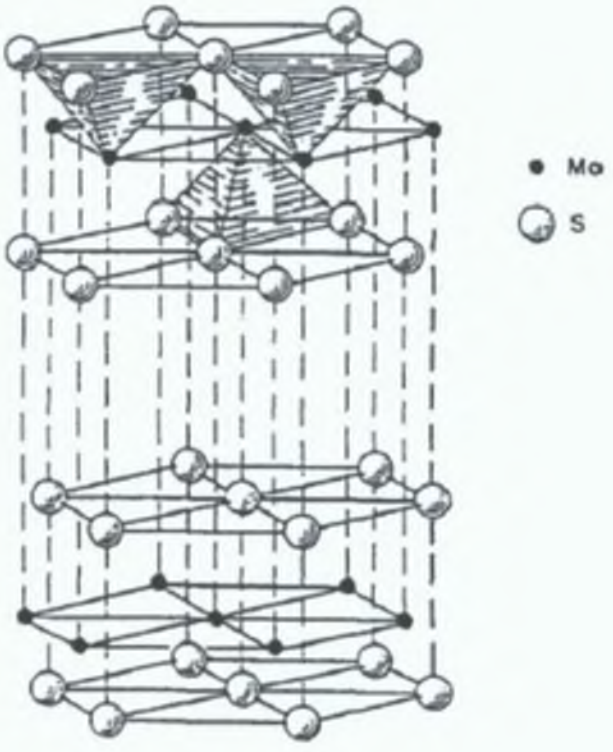

Figure 2.12: Crystal structure of MoS_2 [184]

- The inclusion of solid lubricant in a hard matrix (for example in TiN) [5,185-188]. The hard phase should provide wear, scratch and abrasion resistance for the coated surface. The soft phase should lower the friction coefficient between the coated and counterpart surface [189]. TiN and MoS_2 composite coating have been produced using CVD [187], a hybrid reactive arc (TiN) and magnetron sputter (MoS_x) deposition process [185] and a single unbalanced magnetron target composed of TiN and MoS_2 halves [5], that have low friction, high endurance and good wear resistance.

By combining materials having quite different properties, it is hoped to tailor the functional characteristics of the coating to the needs of a particular application and tribological environment. Again, the performance of this hard and/or solid lubricant coating can be limited by poor load bearing capacity and adhesion resulting from the sharp interface

between the coating and substrate when the coatings are directly applied on the substrate. Traditionally, a metal interlayer (such as Ti) is used to improve adhesion and a ceramic interlayer to improved load bearing capacity [107]. However, recently it has been demonstrated that a considerable improvement in the mechanical and tribological properties can be achieved through the use of graded interlayers with a gradual change in composition from the substrate to top coating [112,117] and also by depositing the coating on hard substrate as described above. However, few works have reported [5,185] on the mechanical and tribological properties of hard-solid lubricant ($TiN+MoS_x$) based coatings, in particular inadequate attention has been paid on the interlayer effect to this type of coating.

2.4.3.2. CARBON BASED HARD AND SOLID LUBRICANT COATING

Diamond like carbon (DLC) is metastable and amorphous carbon material, which can be produced as a thin coating. A number of important applications with promising futures have been developed. DLC films are characterized by high hardness (up to about 50 GPa) and high compressive stress (up to several GPa range). DLC films on smooth metal substrates have a shiny appearance with a charcoal-black coloration. They are hard, do not scratch, and are chemically resistant. They are being tested for use in decorative and protective applications, such as jewellery and watch parts. Deposition of very smooth films can be achieved from gaseous or solid precursors, at low substrate temperatures through a variety of methods, including direct Current (DC) or radio frequency (RF) based plasma-assisted chemical vapor deposition (PACVD), sputtering and ion beam deposition methods. All methods for the deposition of DLC films are nonequilibrium processes characterized by the interaction of energetic ions with the surface of the growing film. As is well known, carbon–carbon interatomic bonds can be of two types: the near-planar trigonal form of sp^2 found in graphite, or the tetragonal form of sp^3 that occurs in diamond. It is the three-dimensional character of sp^3 bonding, together with the strength of the short C–C covalent bond that gives diamond its great strength. DLC is intermediate in that it contains both types of bonding and clearly it is harder and more brittle if the sp^3: sp^2 ratio is high. DLC is composed of small crystallites, which have a local atomic configuration with a broad range of structures (variable amounts of, planar threefold carbon bonding (sp^2), tetrahedral carbon bonding (sp^3) and negligible amount of trigonal, triple carbon bonding (sp) and compositions (variable hydrogen concentration) but crystallites size are small enough that electron diffraction patterns indicate an amorphous material. DLC truly an amorphous solid like glass, lacks any degree of crystallinity and has no long-range order but forms a random

stable network. As a result, DLC is generally considered to be amorphous. It has also been clearly demonstrated that the physical and chemical properties of the DLC films are closely related to both the chemical bonding that occurs and the microstructure of the film [190]. Though it is called "diamond-like", DLC is in fact not like crystalline diamond for it is black, not as hard, and is virtually amorphous. As opposed to diamond, which occurs naturally and can be synthesized at both high and low pressure; DLC is not a natural material and can only be produced at low pressure. DLC has two disadvantages: low deposition rate and high internal stress. Unlike diamond, it cannot be obtained as thick shapes, at least with the present technology.

Its microstructure allows the incorporation of other species, and DLC comprises a family of such materials, the properties of which can be tailored far more readily than those of diamond. Hydrogen is frequently present, occupying regions of low electron density in the matrix. Recently, there have been several attempts to improve the mechanical and tribological behavior of conventional hydrogenated and non-hydrogenated carbonaceous coatings by the addition of elements such as silicon, nitrogen, fluorine and various metals. DLC can be divided into two closely related categories known as amorphous DLC and hydrogenated DLC. A sizeable proportion of the sites in amorphous DLC (a-C) have the sp^3 coordination (indicating diamond nature) in the form of individual or polycrystalline diamond in small clusters, interspersed with amorphous regions. The sp^2 carbon (indicating graphitic nature) sites are generally lacking in this structure. The hydrogen content is less than one atomic percent and a small amount of argon may remain trapped in the lattice. Moreover, a fraction of the hydrogen may be unbound to carbon. The exact overall structure is still uncertain. The material is generally produced by sputtering from a solid carbon target and is usually referred to as "a-C".

Hydrogenated DLC (a-C: H or H-DLC) is also considered amorphous but, unlike a-C, it contains a variable and appreciable amount of hydrogen (up to fifty atomic percent). Its structure consists of an essentially amorphous network with isolated clusters dominated by the sp^2 configuration (graphite) with some sp^3 (diamond). Hydrogen is believed to play an essential role in determining the bonding configuration by helping to form the sp^3 bond. The exact location of the hydrogen atoms is still conjectural but hydrogen, being monovalent, can serve only as a terminating atom of the carbon network [191]. The ratio between the different carbon hybridizations (especially the sp^3: sp^2 ratio) is difficult to quantify and was found to be strongly dependent on the total hydrogen content in the film. There is also some evidence of triple carbon bonding (sp). The material is produced by

plasma action in a hydrocarbon atmosphere and is referred to as hydrogenated DLC (H-DLC or a-C: H).

Advantages and main limitations of using DLC in wear and tribological applications

Due to the tightening of environmental restrictions on the use of lubricants, and the increase in costs associated with disposal, there is increasing demand for solid lubricant coatings that allow contacting surfaces to rub against one another with reduced friction and wear. During the last few years hard, diamond like carbon (DLC) coatings have been used in different tribological application such as solid lubricant (particularly well suited for abrasion and wear applications). It was found that the coatings exhibit properties such as very low friction, high surface smoothness, high hardness, high resistance to wear and corrosion, all of which are desirable for engineering and biomedical implants materials [6-10]. They also provide a surface, which is biocompatible and non-toxic when implanted in the body for extended periods [192]. Another very important aspect is the property of DLC to graphitise the surface at high pressures (the transformation of DLC into graphite), so the coating develops self-lubricating properties[193]. Coatings that are very hard, have low friction and are fully biocompatible have obvious applications in hip implants, as wear is the most common mode of failure in all this applications.

DLC coatings have shown good potential in tribological applications, particularly in non-lubricated conditions and in vacuum environments. These applications include textile machinery, bearing surfaces, measuring instruments, air bearings, precision tooling, gears, fluid engineering systems, engine components, nozzles, and rotating equipment. Some typical examples of wear applications of DLC coatings include coating on video tapes and high-density magnetic-recording disks, where the coatings are applied by sputtering with facing targets. The disks are made of polyvinyl acetate. The coatings are extremely thin and smooth and allow the smallest-possible clearance between the recording head and the surface of the disk. Like MoS_2, the super low friction behaviour observed in DLC is associated with weak Van der Waals interactions between DLC hydrocarbon chains [194,195]. These coatings, when rubbed against themselves, have a remarkably low coefficient of friction. The coefficient value depends on the nature the DLC film and the tribotesting conditions, and is strongly governed by tribochemical effects [194]. Because of the superior hardness of DLC coating they are much more wear resistant than MoS_2 DLC coating protect against wears because of their graphitic nature (a solid lubricant); when this material is used in wear applications, a so-called transfer layer of hydrocarbons builds up from the rubbed film to the soft counterpart surface. The layer is oriented along the sliding

direction. Then DLC slides against its own transfer layer by easy-shear within the interfacial material, although it is the harder surface, only the DLC is worn at a very low wear rate, whereas the softer counter surface will not be worn [196]. However, the shearing ability strongly depends on the nature of the surrounding environment present in the contact [197]. Low wear friction coatings like Diamond like Carbon (DLC) are candidates for substituting lubricants or combinations of lubricants and hard coatings such as titanium carbide, titanium nitride, and other thin film materials.

The tribological behaviour of DLC films depends on the environmental conditions, the nature of the coating, and mechanical properties of the substrate. The current range of applications is limited. Most commercially available DLC coatings suffer from poor levels of adhesion, high intrinsic stresses and low load-bearing capability that means the coating is unable to support normal and tangential loads, particularly when deposited on soft and low alloy steels. It was reported that if DLC coatings can be applied to soft substrates, the application field of DLC films would be broaden [198], but this is limited in cases due to the very thin nature of the DLC coatings. The soft substrate carries the applied load, which can lead to catastrophic premature failure (distortion) of the thin film when subjected to high-applied load, through the collapse of the layer on the plastically deformed soft biomedical substrate such as 316L stainless steel, Ti alloy and so on having insufficient strength (that means, low load bearing capacity) [105,199,200]. In order to perform well as a use as tribological coating, the DLC film must also adhere well to the substrate material; the adhesive forces having to overcome the high internal stresses that otherwise would cause film delamination. Adhesion depends on the substrate material and can be affected by the deposition method. It was found that inadequate adhesion to the soft substrates due to the generation of the high residual stress (a large difference in the modulus of elasticity caused by a mis-match at the coating/substrate interface) in the film as it grows on the surface [201-203]. This leads to debonding and hence failure of the film.

2.5. TRIBOLOGICAL PROBLEM INVOLVING IN COMMON ENGINEERING MATERIALS

In this section, the present status of the common and promising engineering materials, such as 316L stainless steel, Ti-alloy and polymer materials is reported. A problem with all these material is that they usually show poor tribological performance due to their low hardness and stiffness in combination with a tendency to stick to the countersurface. In a tribological contact this means plastic deformation, abrasive and adhesive wear and high friction.

(a) Stainless Steel

Austenitic stainless steels have been widely using in diverse industrial sectors such as biomedical, food, offshore and chemical processing industries, nuclear reactor technology and so on, because of their superior corrosion resistance resulting from a native passive layer (Cr_2O_3) [204,205]. The addition of nickel causes the austenite structure to be maintained at room temperature. Thus, this steel is known as an austenitic stainless steel. Nevertheless, they have poor tribological (that means, high friction and wear rate) and mechanical (that means, low hardness, low load-bearing capacity) properties and also can suffer pitting or crevice corrosion in specific environmets, can limit the number of possible industrial applications [206]. Thermochemical diffusion processes, such as nitriding, can improve the tribological and mechanical properties of these steels by enriching the near surface region with nitrogen. The conventional nitriding processes (that means, gas nitriding and salt-bath nitriding) have several disadvantages such as higher distortion of the workpiece, longer processing time, poor surface finish and so on compared to plasma or glow discharge nitriding. On the other hand, Czerwiec et al. [32] identified some problems with conventional plasma nitriding. A higher sample temperature, which is set by the discharge parameters and cannot be controlled independently, and a comparatively higher operating pressure increases the possibility of surface contamination, which retards the diffusion of nitrogen. Higher current density, required to maintain an abnormal glow discharge, leads to overtempering of the workpiece. Plasma nitriding at high temperature (around 500 ^{0}C or higher) also reduces the corrosion resistance of the austenitic steel [204,207]. This fact is explained by the precipitation of chromium nitride, which results in the depletion of chromium in the austenitic solid solution [74]. This chromium depletion layer is very prone to corrosion.

Recently, more attention has been given to the use of low temperature (below 500 °C) plasma nitriding to control nitride layer formation compared to the conventional plasma nitriding processes, and thus to acquire enhanced surface properties (that means, tribological and mechanical) without losing corrosion resistance [32,35,77,106,206,208-210]. This effect can be correlated with the formation of a layer composed of a phase generally recognized as the S phase [211] or expanded austenite [212,213] with a face centred tetragonal (fct) crystal structure, which is a metastable and supersaturated solid solution of nitrogen in the face centred cubic (fcc) austenitic phase [209,214,215]. The resulting nitrided layer is precipitation-free and retains the corrosion resistance of a nitrided surface formed at low temperature. Furthermore, the S phase produces a significant hardening effect on the austenite stainless steel surface due to the solid solution strengthening. Again, plasma nitriding at low pressure where the plasma source is separate from the workpiece, such as RF discharge, microwave discharge, plasma source ion implantation, triode discharge and so on produces plasma containing a large number of active species. This increases the nitriding efficiency and allows more flexibility in controlling the process parameters [34,212]. The low-pressure nitriding processes can be used to form duplex coatings: deposition of hard coatings on the nitrided surface in the same processing chamber [77].

(b) Ti-based Alloy

Since the emergence of titanium as a 'wonder metal' [216-218], the titanium industry has developed a wide range of alloys with different compositions. Titanium is the fourth most frequently occurring structural metal on Earth. Its concentration within the Earth's crust is about 0.6 % [219]. Titanium is mainly extracted from ores such as rutile (almost pure TiO_2) and ilmenite ($FeO{\cdot}TiO_2$), with a content of 50 to 65 % TiO_2 [219]. Titanium belongs to the group of refractory metals and has an atomic number of 22 and its atomic weight is 47.90 [219]. With a density of 4.5 g/cm^3 [220], titanium belongs to the category of light metals. At ambient temperature the crystal structure of pure titanium is hexagonally close-packed (hcp, α-titanium). At 882 °C [219], an allotropic transition to a body-centered cubic structure (bcc, β-titanium) takes place. Titanium melts at 1668 °C, and has a Young's modulus of 106-108 GPa [219].

Ti and its alloy are very attractive materials for different engineering applications due to their several outstanding properties, such as high strength to weight ratio, good fatigue properties, excellent corrosion resistance, the formation of a native passive oxide layer TiO_2, and so on. They are particularly attractive materials for biomedical applications

due to their excellent biocompatibility [221]. One of the most common applications is the artificial hip joint, which consists of a bearing (femoral head and shell) and stem (details in appendix A3). For orthopedic load-bearing implants alloying elements are added to titanium to increase the strength of the material. Titanium alloys are categorized into α, α + β, and β-alloys based on their room temperature crystalline structure and alloy composition. Ti-6Al-4V (α + β-type), which was developed for the aircraft industry, was one of the first alloys used as implant material [222].

However, titanium and titanium alloys have poor tribological properties such as poor abrasive wear resistance, poor fretting behaviour, low surface hardness and high co-efficient of friction [223-227]. Therefore, the practical use of this material as a biomedical application (total hip, knee replacement, dental and so on) and in other engineering applications (such as aerospace, marine, sports equipment, chemical and automobile industries, pumps, turbine, combustion motor for racing car and so on), involving surfaces in mutual contact and under load or relative motion, is limited in many cases by the need for the hard surface to attain specific mechanical properties (wear, hardness, and so on) [223,224]. For example, there is a possibility of high wear of artificial implant material inside the human body, which can break down total hip and knee replacements. Wear debris produced by different wear mechanism can dissolved into human body by corrosion-fatigue and cause a harmful biological reaction with the tissue [223] (details in appendix A3). Research into the surface modification of the Ti base materials by different plasma and ion base techniques is on-going in order to overcome the current problems with conventional gas or liquid nitriding [228-230]. However, the conventional high pressure and low energy ion implantation or plasma/ion nitriding produces very thin nitrided layer (~0.1-0.2 μm) even after a long treatment time, which is not economical and thus not favourable for different application [231,229]. As Ti base materials are receiving much attention in many industrial applications, further research on different surface modification strategies that can be used for these materials or the development of the new Ti base alloys is necessary in order to improve their tribological properties (that means, hardness and wear).

(c) Polymer-based Alloy

Polymer materials have been used in many fields ranging from everyday life to low and high-technology engineering due to their unique advantages such as lightweight, processibility, inexpensive, corrosion resistance, impact load damping and low manufacturing cost [232]. Polymers can be natural or synthetic. They are long-chain

molecules that consist of many small repeating units. Polymers are widely used as implant materials as they have physical properties that are most similar to the natural tissues (details in appendix A3).

Figure 2.13: The acetabular components of a contemporary total hip replacement (adapted from [233])

Ultra-high molecular weight polyethylene (UHMWPE) consists of long chain of $-(CH_2)_n-$ and is commonly used polymer materials in load-bearing articulating surfaces, as in bearings, cams, gears, and followers, guides, seals and artificial joints because of its superior properties such as ductility and impact load [232,234] (details in appendix A3). However, compared to metallic and ceramic systems, these materials have low mechanical strength and poor tribological properties, such as low hardness and wear resistance, and are not suitable, in many cases, for long term consideration in human body. For example, wear and wear debris produced in the polymer articular surface has been recognized as one of the common cause's for the loosening and premature failure of the artificial hip joints [235]. The liner of the shell made of ultra-high molecular weight polyethylene (UHMWPE) is worn easily and fractures in a brittle manner when sliding against the metal femoral head (Figure 2.13).

Thus, various surface modification techniques have been evolved to enhance chemical, physical, mechanical and tribological functionality of these polymers. For example, surface cross-linking and chemical functional group are induced on the polymer surface by a suitable surface modification technique to enhance the mechanical properties of the polymers [234]. Surface crosslinking is a process in which polyethylene molecules are bonded together as shown in figure 2.14 [233,236].

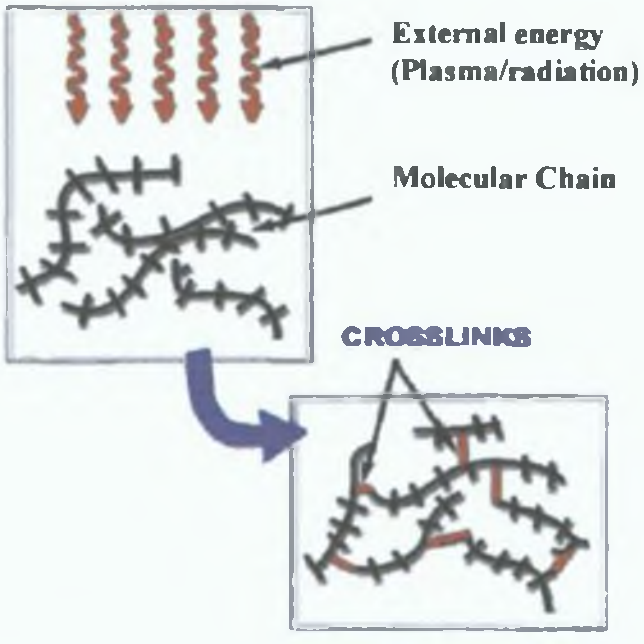

Figure 2.14: Typical crosslinking process of polymer materials (adapted from [233]).

The activity of the plasma or radiation creates a higher cross-linking density within the material to a depth of a few thousand angstroms [237]. The resulting structure has significantly increased hardness, good resistance to plastic deformation and increased stiffness (E), which ultimately leads to improved tribological properties [237,238] and can be used to enhance performance in many applications. On the other hand, plasma or irradiation induced chemical functionalisation or changes in surface topography can increase wettability of the polymer surface, which would improve lubrication conditions between contact surfaces, thus leading to high wear resistance [234].

Conventional ion beam implantation methods have been used to improve wear properties of polymer materials for few years [239,240]. But the conventional ion beam

processes have several disadvantages such as charge development on the surface, line-in-sight implantation, problems with surface coverage of the complex shaped substrates, and so on. The line-in-sight implantation problem has been overcome by the development of plasma immersion ion implantation technique (PIII) [232,241]. However, ion implantation of insulating materials (polymer, and so on) by using PIII technique are still facing several problems like surface charging, electrical arcing, plasma sheath distortion, and so on [242,243]. Again, surface wettability (hydrophilicity) is known to influence the interactions between the implant surface and the surroundings. High wettability ensures biocompatibility, and allows better cell adhesion. It have been also reported that wettability reduces friction and wear by establishing a low shear strength boundary film and low frictional coefficients (increasing the lubricity) [240]. However, bulk polymer surfaces have low surface tension and high chemical inertness and show low wettability in human body with interfacial plasmon liquid due to the presence of low polar part on its surface [244]. Many researchers reported [237,238] that the wettability properties of polymer materials can be improve by submitting the polymer materials to a surface treatment process such as for instance a plasma treatment. When a polymer is exposed to plasma, the surface changes to a high-energy state (increase in surface tension) as a result of the formation of polar groups. That is to produce a specific functional chemical group (polar groups surface such as-C-N,-C=N and so on) at the surface of the polymer to improve the surface wettability and biocompatibility of materials.

2.6. OBJECTIVE OF THIS WORK

Based on the review of relevant literature presented in this chapter, it is evident that there is still much work to be carried out in the area of surface engineering in order to overcome the current problems, particularly in tribological application. The following is a summary of the literature review presented in this chapter.

A problem with common and promising engineering materials, such as 316L stainless steel, Ti-alloy and polymer , that is widely used in biomedical (such as total hip, knee replacement, dental and so on) and in other engineering applications (such as aerospace, marine, sports equipment, chemical and automobile industries, pumps, turbine, combustion motor for racing car and so on), is that they usually show poor tribological performance due to their low hardness and stiffness in combination with a tendency to stick to the countersurface. It is hard to find a material that meets all the requirements of a given application. Changing the bulk material severely limits options in materials selections, and often is not economically or technologically viable. Surface engineering, either by surface treatment, or surface coating, has become a well-established technology or is an extremely versatile means of improving component performance in mechanical and tribological applications.

(i) Surface treatment of a material can improve its surface properties without changing its bulk properties. Several methodologies have been considered and developed for improve properties of materials; plasma surface modification (plasma nitriding / ion beam) is one of these methodologies. But the conventional plasma nitriding / ion beam processes have several disadvantages as presented earlier in literature review section. Nevertheless, nitrided layers produced by nitriding process may not be sufficient enough to combat severe wear. For example nitrided layer may be suitable for small movement and low contact pressure parts application but not in case of high contact pressure/stress application such as forming, die casting hot forging parts, and so on.

(ii) As nitrided layers produced by different nitriding process may not be suitable in severe wear and corrosion conditions, a significant number of hard coatings such as TiN, TiCN, and TiAlN and so on, have been used to improve the performance and extend the life of a component. But many of these coatings are very hard and they can form hard particles which act like grit when the coatings are worn and have a higher co-efficient of friction. Solid lubricant based hard Diamond-like-carbon (DLC) and MoS_2 coating has been used to

overcome this problem. This coatings exhibit very low friction, high surface smoothness and high hardness.

(iii) All these coating face a number of problems on soft substrate such as insufficient load bearing capacity, poor adhesion strength, higher stress development, poor tribological properties. The soft substrate carries the applied load, which can lead to catastrophic premature failure (distortion) of the thin film when subjected to high-applied load, through the collapse of the layer on the plastically deformed soft biomedical substrate such as 316L stainless steel, Ti alloy and so on having insufficient strength (that means, low load bearing capacity). In order to perform well as a use as tribological coating, the film must also adhere well to the substrate material. Inadequate adhesion to the soft substrates due to the generation of the high residual stress (a large difference in the modulus of elasticity caused by a mis-match at the coating/substrate interface) in the film as it grows on the surface. This leads to debonding and hence failure of the film.

(iv) The complex requirements for surface engineering cannot be realized in a single homogeneous coating or a single surface treatment. Duplex coatings systems (i.e., coatings deposition on plasma nitrided substrates) therefore seem to be the best compromise. As these systems can improve adhesion, prevent catastrophic premature failure and improve the further wear resistance of the components, their life spans can be extended. Also, plasma nitriding followed by in-situ coating deposition in the same process chamber (continuous process) is considered to be advantageous over the discontinuous processes which have been reported by other researchers. This area is still under investigation and no industrial applications of the duplex process have yet been established and so much research needs to be carried out in this area.

Therefore, further research needs to be undertaken to establish suitable methods of nitriding that can be used for (a) a wide range of materials efficiently and (b) duplex treatment to overcome current problems with the coating such as load bearing capacity of the soft substrate, improvement of composite hardness and adhesion. Attention will also need to be paid to select an appropriate coating design and material that can reduce friction and improve overall tribological properties of the bulk material. By considering the present shortcoming, an important objective of this work has been set up: to develop a plasma nitrided system that can treat a wide range of material and can use the duplex technique to further enhance the load bearing capacity and composite hardness of the solid lubricant based coating-substrate system. The focus is also on a thorough characterization of the microstructure and tribological properties of both plasma nitrided and coated sample to evaluate the ability and performance of the new process, material and design. Additionally,

in order to acquire a preliminary approximation of different process parameters finite volume and finite element methods will be employed. The objective of this project was achieved in three phases as follows.

Phase I: In the first phase of this work, in order to acquire a preliminary approximation of different process parameters, finite volume and finite element methods have been employed to determine the (i) gas mixture pattern inside the sputtering chamber and (ii) thermal stress inside the coating with and without considering the graded interlayer respectively. Gas flow and mixing pattern simulation has been undertaken using the computational fluid dynamics software FLUENT. The effect of the graded interlayer on thermal stress development has been analyzed using the finite element method ANSYS.

Phase II: In the second phase of this work, a new low pressure and low temperature plasma nitriding (below 500 °C) process has been developed for plasma nitriding a wide range of material (both conductive and non-conductive) using an existing carbon-based coating system. It is believed that this process will overcome the disadvantages of the conventional plasma nitriding and ion nitriding method as described in the literature section. Plasma nitriding was performed on 316L stainless steel, Ti-6Al-4V and UHMWP using Plasma enhanced chemical vapor deposition (PECVD) based Saddle field neutral fast atom beam source, and also an auxiliary heater to provide substrate heating. This objective can be schematically seen from figure 2.15.

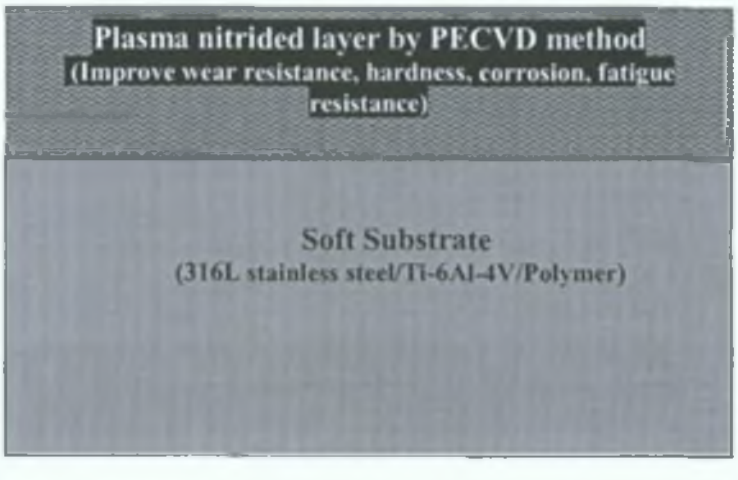

Figure 2.15: Plasma nitriding of soft sample

Phase III: In the third phase of this work, (a) continuous and (b) discontinuous duplex coating systems have been investigated in order to realize additional improvement in mechanical and tribological properties.

The main focus has been given to the improvement of the load bearing capacity and the adhesion of the coating-substrate system.

(a) Continuous duplex coating:

A continuous duplex process (two separate process completed by same techniques) was investigated consisting of the plasma nitriding followed by in situ deposition of the diamond like coating (DLC), which have been carried out in a single process chamber (PECVD based Saddle field neutral fast atom beam source) without any interlayer or post nitriding treatment. The configuration for the continuous duplex coating is shown in figure 2.16.

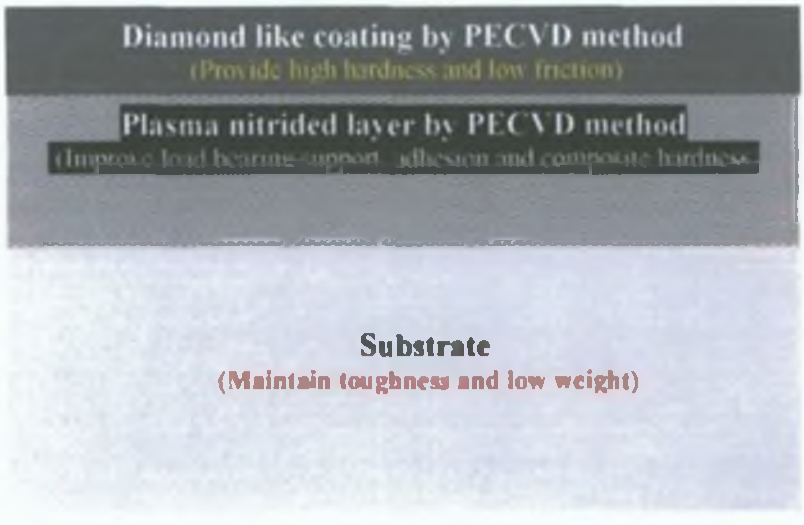

Figure 2.16: Continuously deposited duplex, solid lubricant based DLC coating on plasma nitrided sample

(b) Discontinuous duplex coating

A discontinues duplex treatment (two separate process completed by two different techniques) consisting of plasma nitriding and TiN+MoS_x coatings with and without a graded interlayer (Ti-TiN_x) on the stainless steel substrate was also investigated. The configuration for the discontinuous duplex coating is shown in figure 2.17.

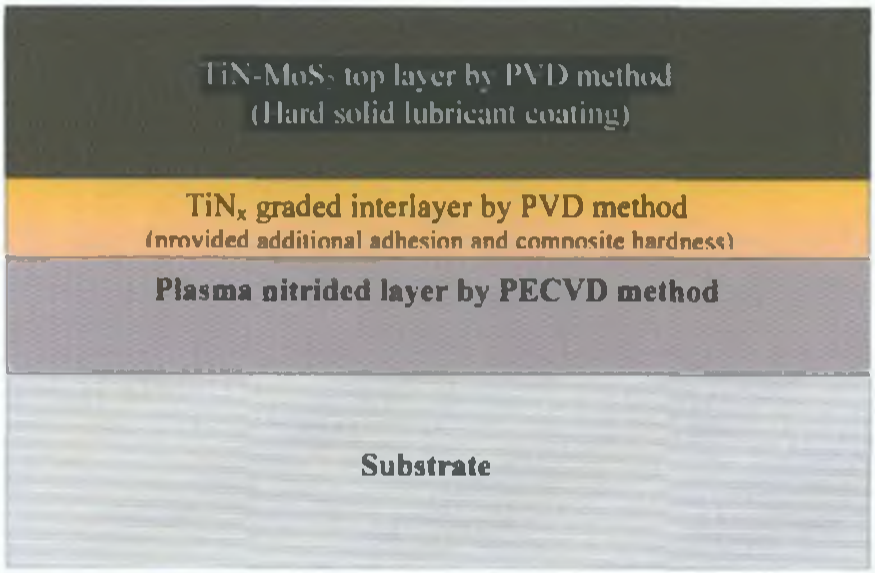

Figure 2.17: A solid lubricant based discontinuous duplex coating on plasma nitrided sample with graded interlayer.

Low-temperature plasma nitriding was performed with the newly developed process (Saddle field fast atom beam source) and coatings were deposited by Physical vapor deposition (PVD) based closed-field unbalanced magnetron sputtering.

CHAPTER 3: SIMULATION WORK DESIGN, EXPERIMENTAL WORK AND CHARACTERIZATION TECHNIQUES

3.1. INTRODUCTION

In order to acquire a preliminary approximation of different process parameters, finite volume and finite element methods have been employed. In the second section (3.2) of this chapter, a brief description, design and procedure of the simulation work is presented. In this work, plasma nitriding and coating deposition experiments have been carried out by PECVD based fast atom beam and PVD based closed field unbalanced magnetron sputtering methods. The plasma nitriding and coating deposition methods and procedures are described in the third section (3.3) of this chapter. As no previous work has been reported involving the use of the above methods for plasma nitriding and duplex coating deposition, a thorough characterization of plasma nitrided and coated sample is deemed to be a very important part of this work. Therefore, different methods for characterizing physical, structural, chemical, mechanical and tribological properties of the treated samples are discussed in the last section (3.4) of this chapter

3.2. SIMULATION WORK

3.2.1. GAS FLOW SIMULATION

Magnetron sputtering is the most versatile deposition procedure in the PVD techniques having the additional advantage of low deposition temperature. In this process, gas (preferably argon) is introduced into the chamber at low pressure (in the order of 10^{-3} mbar) to create a plasma after applying the electrical field. The positive ions of the plasma sputter the negative biased target and the consequent sputtered materials are deposited on a substrate placed in front of the target. During reactive sputtering, a reactive gas is usually introduced inside the chamber to allow the reaction with the sputtered material and formation of compound material (nitride, oxide and so on) on the substrate. Sputtering deposition is a complex phenomenon and it can be divided into four different stages: gas flow and mixing of gases (in case of reactive sputtering), plasma generation, physical sputtering of the target and transport of the sputtered neutral species to the substrate. As there is a different physical phenomenon involved in each stage, any single model will not be enough to describe all the situations. For each of the steps different kinds of mathematical and numerical modeling are required, as suggested by other researchers [245]. A Computational Fluid Dynamic (CFD) model is required to calculate the velocity

and pressure distribution of the working gases in the deposition chamber. This can be done using commercially available computational fluid dynamic software based on the finite element, finite volume or finite difference method.

A number of studies can be found in the literature about CFD modeling of deposition reactor designs and film growth effects in Chemical Vapor Deposition (CVD) applications. Kotecki et al. [246] developed a CFD model to enhance the performance of the CVD process. But there are very few studies [245] so far on the gas flow simulation of PVD deposition process. Knowledge of the gas flow and mixing characteristics in the PVD chamber is required to gain an understanding of the flow phenomenon. The determination of the flow and mixing pattern of the component gases inside a complex physical vapor deposition chamber is very difficult. Computational fluid dynamics seems to be an appropriate means to obtain some information regarding to the flow behaviour. The results of the fluid model, that means, gas pressure and velocity, might give some useful information during plasma modeling or sputtered particle transport modeling mentioned before. In this study the main focus will be on the first phase of the sputtering process: CFD modeling of the gas flow inside the magnetron-sputtering chamber. CFD modeling can provide a better visualization of the flow and gas mixing inside the entire deposition chamber, as it is quite difficult to understand that experimentally. This can also provide information for designing the chamber for smooth flow and mixing of gases. In this part of work, a FLUENT simulator was used to study the velocity, concentration of species and pressure inside different portions of the chamber. Several parametric studies were investigated, including the effect of operating parameters and the position of the substrate inside the chamber on the gas flow and mixing behaviour (which indirectly impact on deposition of thin film) under isothermal condition.

3.2.1.1. PROBLEM DESCRIPTION

This research used a commercial fluid dynamics code (FLUENT) with a 3-D model for momentum and mass transport throughout in a custom made PVD chamber [247]. Numerical simulation is an effective way to conduct parametric studies since they can be carried out at relatively low cost and short time period. The deposition chamber is considered as a cylinder with a height of 610 mm and the internal diameter of 603 mm; these dimensions are the same as the actual dimension of the chamber (Figure 3.1).

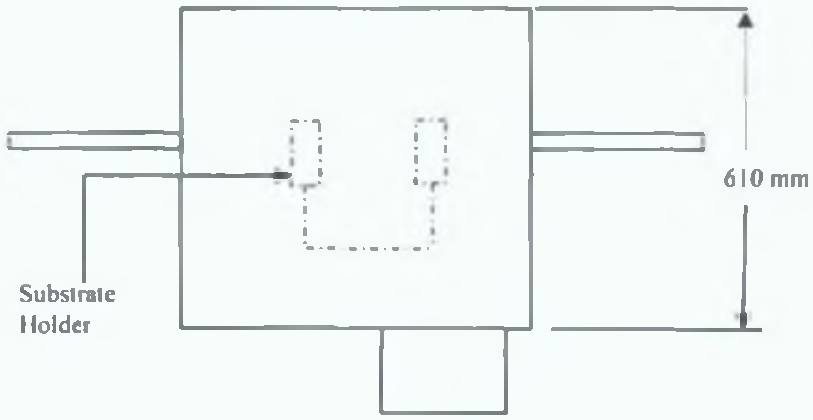

(a) Simplified front view

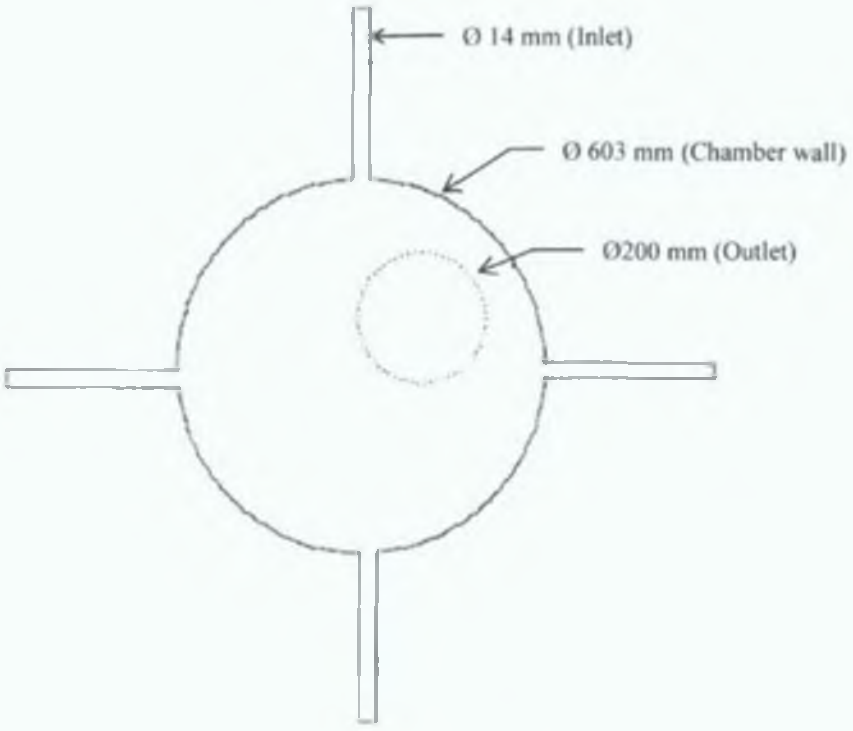

(b) Simplified top view

Figure 3.1: Cross sectional (2-D) view of the gas flow chamber (a) front view and (b) top view.

There is a total of three closely spaced inlet layers at the middle of the chamber wall along the periphery and each layer contains four inlets positioned at equal intervals (90°) around the chamber. For simplicity only one layer has been considered along the periphery of the chamber in this model. The diffusion pump is connected off axis with the bottom plate of the chamber. There is a rotary substrate table with substrate holders inside the chamber. The holder can be placed at different position on the table. A cross-sectional (2-D) view of the simplified chamber with dimensions is shown in figure 3.1. All dimensions used in the model were in SI units. A detailed description of the deposition system and process that was used in this work is discussed in Section 3.3.3 of this Chapter.

3.2.1.2. NUMERICAL MODELING

(a) Simulation tools

The gas flow and mixing behaviour was simulated in this study using the commercial computational fluid dynamics (CFD) software FLUENT [248]. This software used the finite volume method to numerically solve transport equations of mass, momentum and energy conservation. For all flows, FLUENT solves conservation equations for mass and momentum [248]. For flows involving heat transfer or compressibility, an additional equation for energy conservation is solved. For flows involving species mixing or reactions, a species conservation equation is solved or, if the non-premixed combustion model is used, conservation equations for the mixture fraction and its variance are solved (details in appendix A1). Additional transport equations are also solved when the flow is turbulent.

(b) Assumptions and conditions used taken in this study

The following assumptions have been made for simplicity in this analysis:

(1) At low pressures, the continuum hypothesis may become invalid. The important parameter here is the Knudsen number [249]. The Knudsen number is used in momentum and mass transfer in very low pressure gas flow calculations. The Knudsen number can be expressed by the following equation (3.1)

$$K_n = \lambda / L \quad \ldots\ldots\ldots\ldots\ldots\ldots\ldots\ldots\ldots\ldots\ldots (3.1)$$

Where λ is the mean free path and L is a geometrical length which describes the size of flow features. Different flow regimes are defined according to the Knudsen number as follows:

(i) N-S equations (Navier-Stokes equations) with "no-slip" wall boundary condition (BC) valid for $K_n < 0.001$, (ii)N-S-equation with "slip wall BC" valid for 0. 001 $< K_n < 0.1$, (iii) Transition Regime $0.1 < K_n < 10$ and (iv) Free molecule flow $K_n > 10$.

Therefore, the molecular regime deals with a Knudsen number greater than 10; the transition regime corresponds to a Knudsen number greater than 0.1 and smaller than 10; the viscous (continuum) regime deals with a Knudsen number smaller than 0.1. Note that no-slip wall Boundary condition breaks down first ($K_n \sim 0.001$) but N-S equations with continuum assumptions are still valid for another two decades of the Knudsen number. At low pressure used in the PVD chamber, the mean free path of the gas molecules is much smaller than the chamber dimensions and as such, a continuum analysis is adequate to study the transport and kinetics inside the chamber. The calculated value of the Knudsen number in this study showed that the value is sufficiently small to allow the flow to be considered as continuum (the Navier-Stokes equations are valid). The gases in the plasma reactor are assumed to be ideal, so the ideal gas law can be used. The viscous region can be divided into laminar and turbulent. The Reynolds number is small enough to allow the flow to be considered laminar.

(2) At Mach number much less than 1 (M<0.1 and so on), compressibility effects are negligible [248,250-252], that's mean, the effects of the pressure variations on the density of the gas mixture can be neglected. The Mach number for this study has been given below.

- Mach number, M= Velocity of gases/Velocity of sound,
- Speed of sound = 347 m/s [253] and Maximum velocity of the system = Maximum velocity of the Ar + maximum velocity of N_2 = (0.00379 +0.00162) = 0.00541 m/s

Therefore, Mach number, M = (0.00541 /347.3) = 0.0000155. The calculated value of the Mach number (0.0000155) in this study showed that the value is sufficiently small to allow the flow to be considered as incompressible and Newtonian. The viscous heating of the gas due to the dissipation is neglected since velocity gradients are not large. Due to low Reynolds numbers in the mixing chamber, the mixing of gases can be considered to be mainly by diffusion. Systems become steady state after a certain period of time. As a result, a steady state model has been considered. As both fluids are likely to be weightless, gravitational acceleration can be neglected. As Argon gas is inert, no reaction is considered between the gas species argon and nitrogen. The temperature of the surrounding surface of the chamber is equal to the ambient temperature that means, the system is isothermal and obviously no temperature dependant properties were included in the calculations.

3.2.1.3. SIMULATION EQUATION

The laminar, incompressible and steady state cases have been considered in this model. These flows have not taken into account any heat transfer, compressibility or reaction, that is, only transport of species (not kinetics of species) inside the deposition chamber has been considered. As a result these solutions have excluded any equation that deals with the energy and reaction of gasses. A details description of the simulation equation is given in appendix (A1).

3.2.1.4. THERMOPHYSICAL PROPERTIES

When an analysis is started in FLUENT, the control volume of the model (in this case chamber) is not empty. The control volume initially contains the fluid that was specified last in that system (species editing list in FLUENT software) as shown in figure 3.2.

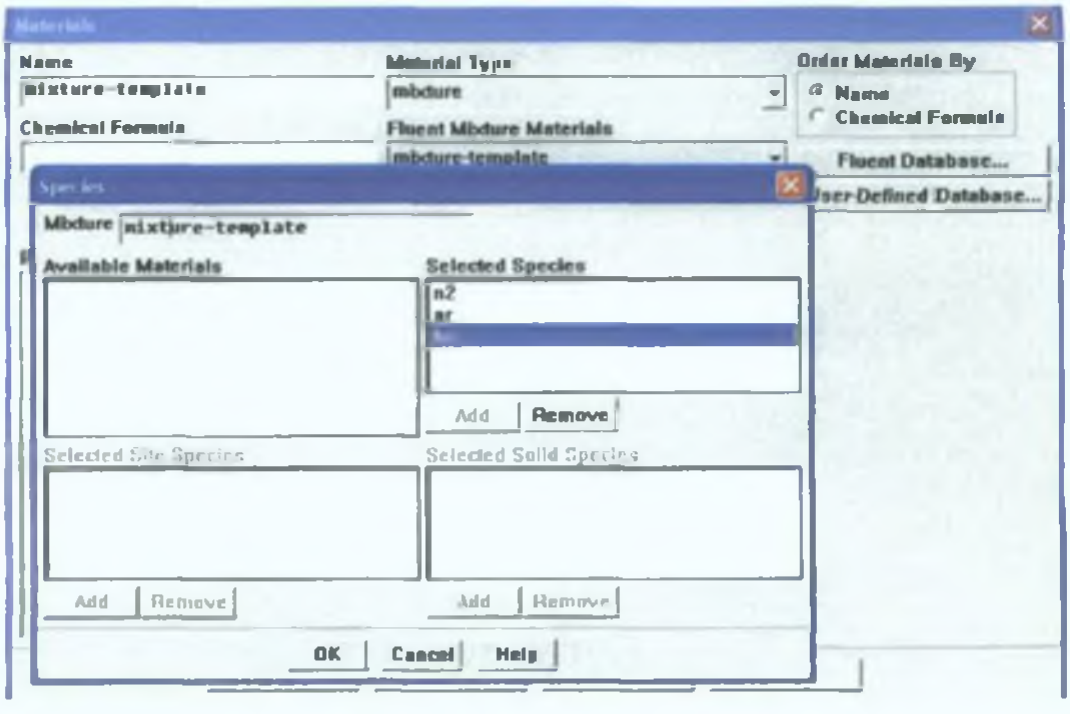

Figure 3.2: Species editing list in FLUENT software

If one fluid exists at the bottom of the list then this is the fluid that fills the system (chamber) before starting the iteration. It was observed after a long solution period that there was a very little change in the gas concentration in many positions of the chamber. For example, if N_2 was taken as a last gas in the list then the N_2 mass fraction was observed to be at a maximum (~1) in every part of the chamber, although flow of the nitrogen in inlet was considered very low. Therefore, this is not the exact nature of the gas pattern in chamber with a small mass flow. An easy way to overcome this problem is to come up with a third gas. This gas should preferably be inert and light, not a part of any reaction and not an inlet gas. It has to be added last to the element list. This gas will have been eliminated from the system by the time the solution is converged. If the code is solving for the n-1 species then n is the number of species in the system where the nth species should be the reference element.

Table 3.1: Thermophysical properties of Ar and N_2 and He (Helium) [254]

Gas	Density ρ (Kg/m^3) at 300K, 1 atm	Thermal conductivity (W/mK) at 300 K	Dynamic viscosity μ (Pa. s) at 300 K	Gas diffusivity at 300 K, 1 atm	Specific heat C_p (J/Kg K) at 300 K	Molecular Weight (Kg /kg-mole)
Ar	1.6228	. 0158	2.125×10^{-5}	1.31×10^{-5}	520.64	39.948
N_2	1.138	. 0242	1.663×10^{-5}	1.37×10^{-5}	1040.67	28. 0134
He	0.1625	0.152	1.99e-05	1.46×10^{-5}	5193	4. 0026

In this work, He gas (nth element and edited last in the list) is used as the reference gas in the system and it thus filled up the domain (volume) before starting the analysis and specifying Ar and N_2 as inlet gas in the system. The species are accepted as isotropic. The required thermodynamic and transport properties of Ar, N_2 and He gases for the simulation include viscosity, specific heat at constant pressure, thermal conductivity, mass and density. All the properties are taken at standard pressure ($1.1x10^5$ Pascal) and temperature (298 K). The values of the thermo-physical properties are chosen from the Fluent database (Table 3.1) [254].

3.2.1.5. MODEL GEOMETRY AND DISCRETISATION

Simulations performed in the numerical study are restricted to an axisymmetric configuration in order to reduce the computing time by solving a 2-D or partial 3-D problem instead of a fully 3-D one. But as the chamber has no axial symmetry, it would be very difficult to get the perfect symmetry of all the features by taking into consideration a single cross section either through the vertical or horizontal axis in a 2-D model.

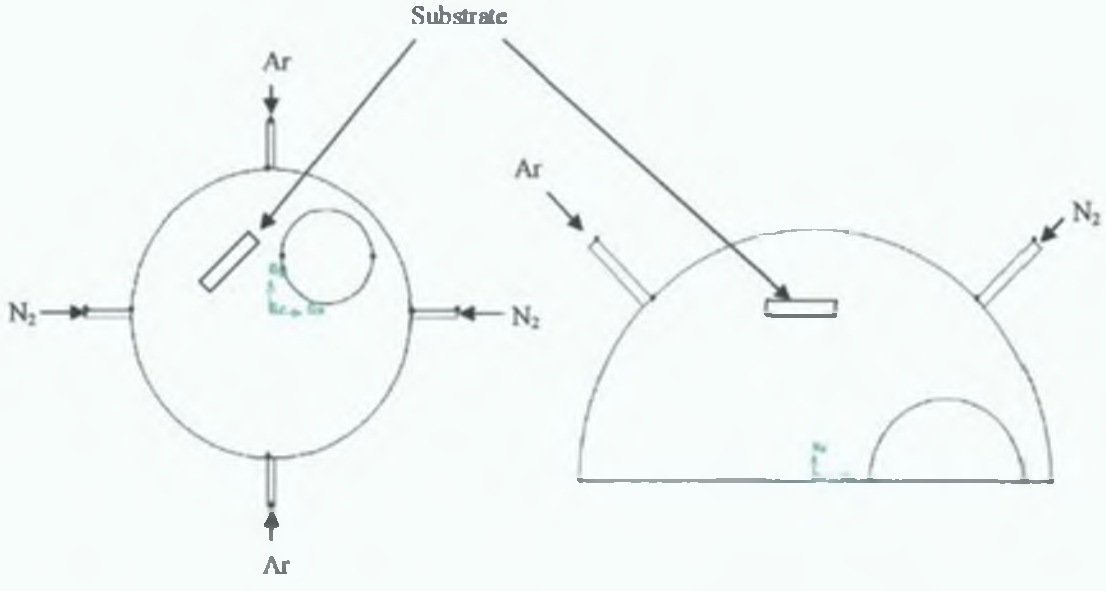

Figure 3.3: Top Cross-sectional view of (a) Full Model and (b) Half model

In this work, a 3D half model has been considered to get perfect symmetry of all the major parts of the real chamber. Top cross-sectional views of (a) the full Model and (b) the half model are shown in figure 3.3 and the schematic of full and half-symmetry of the 3D model are shown in figure 3.4. The grid size was halved by considering a 3D half model instead of considering a full 3D model. The half models consist of one nitrogen inlet, one argon inlet and one half outlet, cut mid-way by symmetry plan.

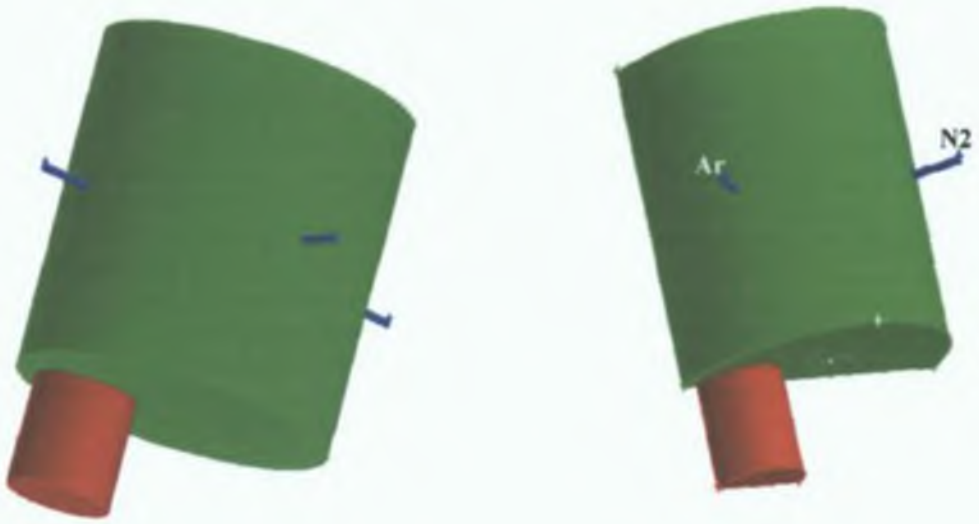

(a)

Figure 3.4: Schematic view of the (a) Full Model and (b) Half model

Grid selection is an important factor in ensuring solution accuracy in most numerical simulation methods. There are two methods of grid generation adopted in FLUENT. For a simple geometry without an edge or curve, the Cartesian coordinate grid system can be used. Otherwise, the body fitted coordinate (BFC) grid system is applied. In this study, the Cartesian coordinate grid system was chosen to generate the grid. The flow field model geometry were constructed and meshed by the software package GAMBIT Version 2.0.4 [255] and computed by FLUENT [248]. The acceptability of the grid generation is checked by GAMBIT and also by the FLUENT software. Geometry was formed by the step-by-step creation of a vertex, a line, a face and finally a volume. At first individual volumes (chamber, inlets, outlet and substrate) were created and after proper placement of all the components, they were combined together. First line meshing and then volume meshing with tetra/hybrid elements was adopted. This model was discretised into almost 146360 tetrahedral cells elements and 32114 nodes shown in figure 3.5.

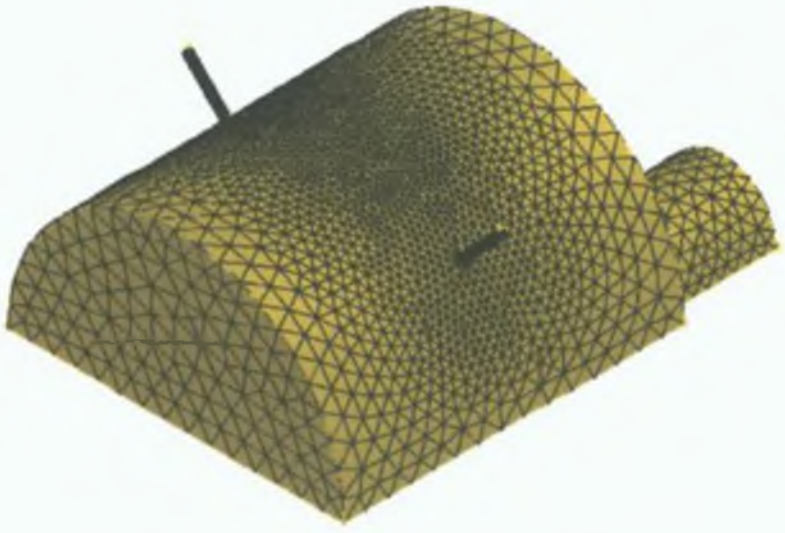

Figure 3.5: Meshing scheme of half model

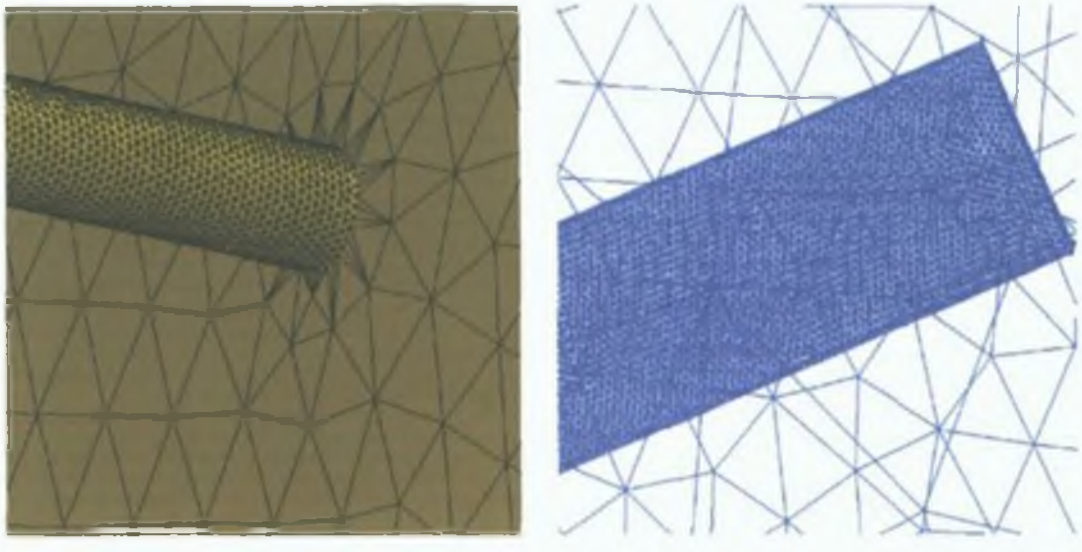

(a)

Figure 3.6: Meshing scheme of (a) substrate and (b) Inlet

In order to avoid an unphysical mathematical behavior related to local variations of flow values, the density of cells in the grid has been taken to be non-uniform. The mesh size is smaller near the substrate where the concentrations gradients of species are high. At critical flow point such as the inlet and outlet, the number of elements used also has been increased, as shown in figure 3.6.

3.2.1.6. BOUNDARY CONDITION

When solving partial differential equations, boundary conditions of different types are needed. For flow inside a chamber these are the wall boundary conditions, which are easy to define, and the inlet and outlet conditions. The inlet condition is of major importance for the flow simulation because the inlet profile determines the flow inside the chamber completely. There are several possibilities to define the inlet profile in a pipe. Complete problem definition requires specification of boundary conditions. The following boundary conditions are being applied as shown in figure 3.7.

<u>At the walls</u>

Velocity components at all the outer walls and substrate surface of the model were set to zero to comply with the non-slip condition at the wall ($V_x = V_y = V_z = 0$).

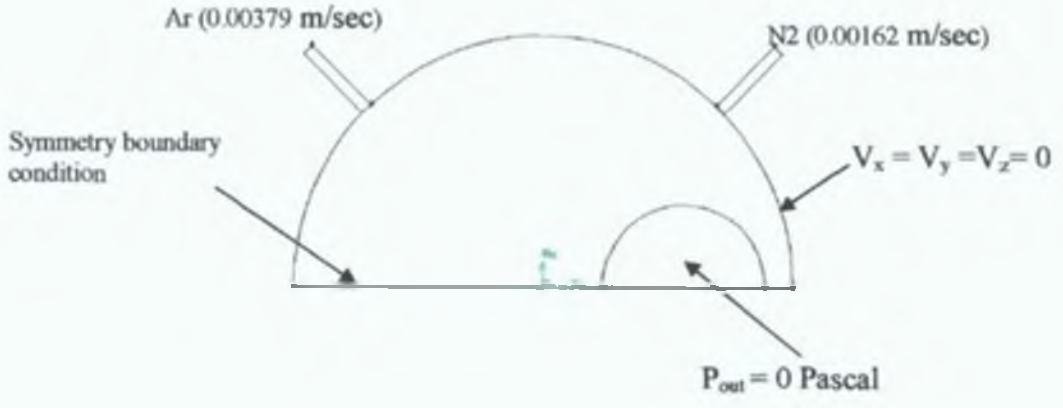

Figure 3.7: Boundary conditions applied in the model

<u>At Inlet</u>

The velocity inlet boundary condition was applied at inlet. The velocities of the gas species were calculated by dividing the flow rate by the inlet cross-sectional area by using equation (3.2).

$$v = \frac{Q}{A} \quad \text{----------(3.2)}$$

Where, Q, A and v represented respectively volumetric gas flow rate, cross-sectional area of inlet and velocity of the gases. An argon velocity of 0.00379 m/sec and nitrogen velocity of 0.00162 m/sec are applied perpendicular to the entrance of the inlet. Table 3.2 gives the recorded values of steady-state chamber pressure, flow rate of the gas species and their corresponding velocities at the inlet with constant nitrogen and constant argon flow rates as found from experimental work. Pure gas is passed though any particular inlet, in the case of argon inlet species mass fractions of argon and nitrogen are set 1 and 0 respectively.

Table 3.2. Chamber pressure and velocities of Ar and N_2 corresponding to their flow rate (* sccm= standard cubic centimetre per minute)

Pressure (Pa)	**Ar flow rate (*sccm)**	**N_2 flow rate (*sccm)**	**Ar velocity (m/s)**	**N_2 velocity (m/s)**
0.46	35	15	0.00379	0.00162

At Outlet

The pressure outlet boundary condition is applied at the outlet, that means, Gauge pressure at the exit: P_{out} = 0 Pascal. The operating pressure was set to 0.46 Pa corresponding to the flow rate. For all flows, FLUENT uses gauge pressure internally. Anytime an absolute or real pressure is needed, it is generated by adding the operating pressure to the gauge pressure. (Absolute pressure= Operating pressure + Gauge pressure). A constant temperature of 298 K was kept all over the domain.

At symmetry plan

A symmetry boundary condition was applied on symmetry plan of the half model.

3.2.1.7. SOLUTION PROCEDURE

Numerical simulation, in contrast to the algebraic models, is based on the resolution of Navier-Stokes equations at each point of the field. FLUENT uses a finite volume approach to solve the Navier-Stokes equations for fluid flow in addition to the basic conservation equations, in this case the fluid is considered incompressible. The governing equations in this model are solved sequentially (segregated from one another). Because the governing equations are non-linear several iterations of the solution loop must be performed before a converged solution is obtained. Each iteration consists of the steps illustrated in figure 3.8.

There is no explicit option for the segregated solver. Therefore, species transport models have been used using the segregated solver and implicit option. The solver specifications for the discretization of the domain involved the following procedures: a first-order discretization scheme for momentum, pressure and the volume fraction of nitrogen and argon gas, SIMPLEC for the velocity–pressure coupling. The under-relaxation factors, which determine how much control each of the equations has in the final solution, were set to 0.2 for the pressure, 0.3 for the momentum with the laminar model and the volume fraction equations were set at 0.6. The under-relaxation factors for density and body forces were set to 0.6. After setting all boundary conditions and initial conditions the solver iteration is started. At the beginning, the whole domain of the chamber filled with the last species gas, helium. This gas then replaced with nitrogen and argon gas over time. The iteration number was set depending on convergence of the problem.

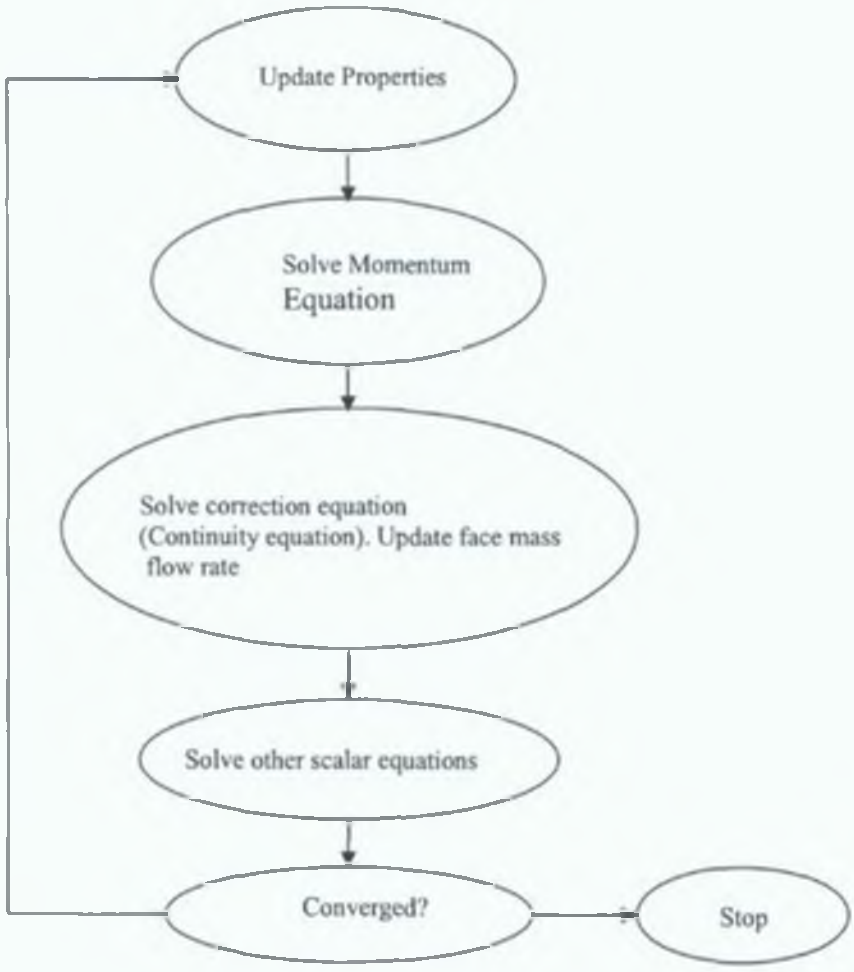

Figure 3.8: Overview of solution method (adapted from [248]).

There are a number of ways to define a problem as converged [256]. In this problem, as the first criteria, the residual of all parameter was set to a value roughly equal to the 10^{-4} level [257]. When it was observed that the residual value was no longer changing, it was primarily confirmed that the solution was converged. Figure 3.9 shows a typical residual curve. Secondly, it is recommended that a surface monitor be used at points where the flow is not dominated by one component of flow (for example a point right inside an inlet should not be selected).

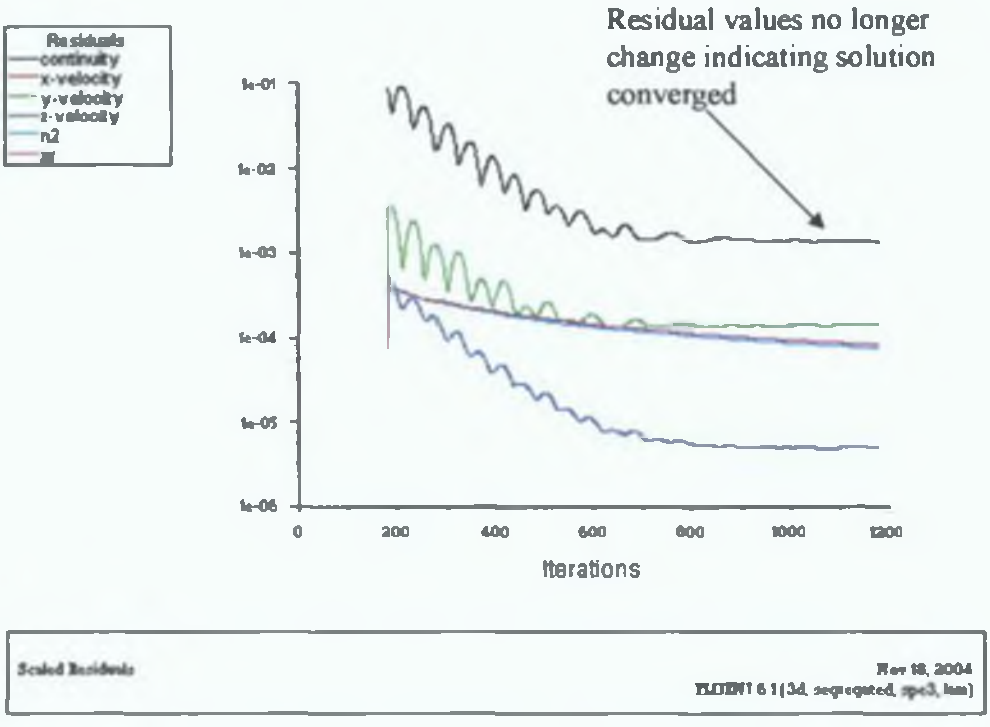

Figure 3.9: A typical residual curve.

The values should be monitored until they converge to a constant value. Convergence is difficult to define. To define a solution as converged, it would be better to get some initial idea about the flow pattern of a particular problem and if possible monitor the progress of certain variables towards known values, either obtained experimentally or from an educated guess. In this work, the facet average velocity at the symmetry plane was monitored for the convergent criteria.

3.2.2. THERMAL STRESS SIMULATION

Residual stress is a stress under no external loading and is the sum of growth stress and thermal stress. Residual stress is very common in coating deposition techniques such as plasma spraying, physical vapour deposition, chemical vapour deposition and so on. The stress state in the coating is very complicated and can vary through the thickness of the coating. A higher stress gradient between the coating and substrate is observed in the case of a thin coating system. Residual stress can strongly influence coating quality and the performance of a coated system since it is directly related to other coating properties such as hardness, adhesion, fatigue strength and so on [258]. Near the edges of a coating, a complex stress state will be present, but away from the edges, this appears to be a simple stress state where the stresses normal to the substrate and the shear stresses are zero [259-261]. Thermal mismatch stress results from the physical and thermal property mismatch between the coating and the substrate when cooled to the room temperature from the deposition temperature. The various physical parameters of both the coating and the substrate on which thermal stress depends can be listed as the coefficient of thermal expansion (CTE), Young's modulus, Poisson's ratio, coating thickness, thermal conductivity, temperature histories during deposition and cooling and stress relaxation mechanisms. Sometimes thermal stress can be high enough to cause to cracking or spallation of the coating. In general, thermal stresses develop at the interface between coating and substrate [262]. One of the major factors causing film failure during deposition processes or application of the coated parts is the stress discontinuity at the interface between the deposited coating and substrate. Graded coatings with a gradient microstructure and material properties is a new concept for designing hard coating and soft substrate systems to reduce the thermal stress [114] by reducing the abrupt discontinuity of material properties [263].

Generally, analytical solutions have been developed to describe the average biaxial thermal stress states in coating substrate system for linear-elastic or simple elastic-plastic materials [264]. Recently, for a more general 2-D or 3-D problem numerical methods such as finite element analysis (FEA) has been accepted as an attractive tool to simulate thermal stress in single layer or graded coating substrate systems [265-268]. Most of the analyses have been done for thick coatings deposited mainly by thermal spraying. Thermal stress simulation of thin coatings using FEA is often performed in wafer processing technology to

test the wafer reliability [269]. There are few studies of thermal stress modeling in thin hard coatings for mechanical applications [270-272]. The objective of this study is to study the distribution of thermal stress developed in a thin TiN coating on stainless steel substrate due to cooling from the deposition temperature to room temperature and to study the effect of TiN_x ($0 < x < 1$) graded interlayer on the coating substrate system by FEA.

3.2.2.1. FINITE ELEMENT CONSIDERATIONS

(a) Model formulation

For the modeling of residual thermal stresses generated in TiN coatings deposited by the sputtering method, a simple cylindrical shaped stainless steel sample (30 mm diameter and 0.05 mm thick) with coating on top of the sample (typical thickness 5 micron) was considered. These dimensions have been chosen to allow the coating substrate system to bend after the development of thermal stress [273].

Table 3.3: Graded coating design schemes.

Model	Schemes
M1	Substrate/ Top layer (5 μm)
M2	Substrate/3rd layer (2.5 μm) / Top layer (2.5 μm)
M3	Substrate/2nd layer (1.66 μm) /4th layer (1.66 μm) /Top layer (1.68 μm)
M4	Substrate/1st layer (.83 μm) /2nd layer (.83 μm) /3rd layer (.83 μm) /4th layer (.83 μm) /5th layer (.83 μm) /Top layer (.85 μm)

For 2-D analysis, an axisymmetric plane parallel to the global XY plane through the thickness of the coating and the substrate was considered, as shown in figure 3.10. In order to understand the effect of graded TiN_x sub-layer, four typical coating models (M1,M2, M3,M4) were adopted as shown in Table 3.3. The schemes of the graded coating were designed in such a way that number of layers increases and property gradient decreases from model M1 to M4.

Total thickness of coating in all models was kept constant to 5 μm. Several assumptions were made for simplicity of calculations [271,272]. It is assumed that the coating and substrate materials are isotropic and linear thermoelastic: that there was perfect bonding between each layer, that plain biaxial stress existed, and that uniform temperature were established in both the coating and the substrate at both at the processing temperature (500 ^{0}C) and at the temperature after cooling (25 ^{0}C).

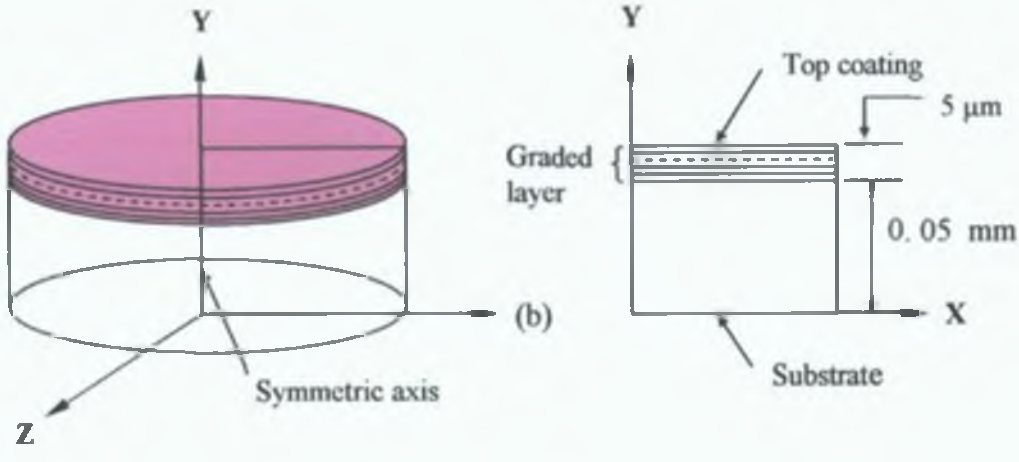

Figure 3.10: Schematic diagram of axisymmetric 2-D solid model of graded layer coating system.

(b) Material properties

The physical and thermal material properties of Ti coating, TiN coating and stainless steel (substrate) are shown in Table 3.4 [274,275]. The coating properties are not consistent in literature due to differences in deposition techniques, coating quality and thickness and of course the techniques used to evaluate the properties.

Table 3.4: Physical and thermal properties of the substrate, coating and graded layers (derived from known property of pure Ti and TiN coating).

Material properties	Stainless steel	Ti	Graded layers					Top Layer (TiN)
			1st	2nd	3rd	4th	5th	
Young's modulus (GPa)	200	140	217	294	371	448	525	600
Thermal expansion coeff. ($/^{o}C$) × 10^{-6}	13. 00	10.48	10.30	10.12	09.94	09.76	09.58	09.40
Poisson's ratio	0.30	0.41	0.38	0.35	0.33	0.30	0.27	0.25

The modeling of the graded coating is even more difficult due to lack of information regarding the material properties of the layers. As the properties of the graded TiN_x layers were unknown, the properties of these layers were allocated assuming that they vary linearly between known properties of pure Ti and stoichiometric TiN_x (x = 1) coating (Table 3.4). The assumption was reasonable due to the fact that the properties of TiN_x coating varies with the N_2 content in the coating [274,276,277].

(c) Analysis details

Numerical simulation of residual thermal stresses generated after the deposition of the coating was simulated using ANSYS finite element analysis code [278]. All coatings were modelled using the four-node structural and quadratic element PLANE 42, using the axisymmetric option. Mapped meshing with quadrilateral-shaped elements was used to mesh the model. Element size is minimized in a graded fashion near the interface across the plane between each layer, as this area is very prone to high stress concentration [262,273]. A fine mesh was also introduced near the edge across the thickness of the coating and substrate as shown in figure 3.11. The mesh was refined until the results showed only a small change [273,279].

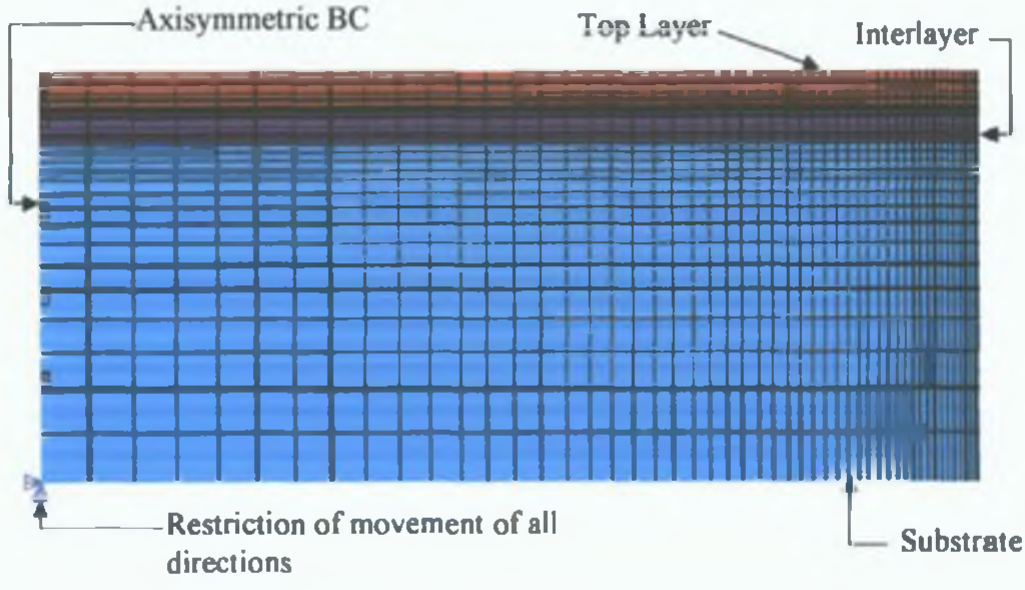

Figure 3.11: Schematic diagram of the meshing scheme and structural boundary condition

The left side of the model is used as the axis of the axisymmetric mode as shown in figure 3.11. The bottom left corner of the axisymmetric model is pinned to restrict any movement. All other edges are free so that bending is permitted to take place during cooling. Thermal loading was applied by setting the reference temperature as the deposition temperature (500°C) and the uniform temperature as the room temperature (25°C). The coating failure mechanisms are mainly controlled by the magnitude and the distribution of radial stress (σ_x), tangential stress (σ_z), axial stress (σ_y) and shear stress (σ_{xy}) at or near the radial free edge of the specimen or near the specimen's axis of symmetry (y-axis). These stresses are obtained and analysed in the following sections.

3.3. EXPERIMENTAL METHODS AND PROCEDURES

3.3.1. SAMPLE SELECTION AND PREPARATION

3.3.1.1. SAMPLE SELECTION

The samples used for this research work were designated as Ti based alloy (Ti-6Al-4V), Stainless steel 316L and ultra high molecular weight polyethylene (UHMWPE). These are common materials which are frequently used in different engineering applications, especially in biomedical applications due to their good biocompability properties. Chemical composition of these materials is given in Table 3.5.

Table 3.5: Chemical composition of the samples material used in this project

Materials	Chemical Composition (wt-%) / Structure
Stainless steel 316L	C (0.03 max), Mn (2), Ni (10), Cr (18), Mo (3) and Fe (balanced)
Ti-6Al-4V	Al (6), V (4), and Ti (balance)
UHMWPE	long chain of $-(CH_2)_n-$ (Medical grade polymer supplied by Impact Ireland)

Thick samples of 10 mm × 25 mm (thickness × diameter) cut from long a rod were prepared for hardness testing and microscopy (optical and SEM) studies. Thin samples of 0.2 mm × 25 mm (thickness × diameter) were also used to allow X-ray diffraction (XRD), testing to be carried out after being treated under the same operating conditions. Sample preparation for both the thick and thin substrates is a time consuming process as the surface is extensively modified to produce a mirror finish. Cleaning of the substrate and equipment is required between each step in the process to prevent large particles of materials which were removed from the previous step from interfering with the following step. The samples were prepared to a smooth, clean and flat surface in order to allow uniformity in the nitriding layer depth and coating thickness across the surface and hence a homogeneous

process. The clean and smooth surface of the sample enhances plasma interaction (resulting in a more active reaction on surface) and coating adhesion. Furthermore, this also allows the samples to be tested using different sophisticated characterization technique such as such as XRD, EDX, SEM, XPS, AFM, Optical microscopy, wear and hardness tests. It also allows accurate results to be obtained with very little variation along the surface. During each stage of preparation it is important not to touch the surface as this can leave organic materials on the surface which evaporate slowly and can be burned by the electron beam resulting in contamination within the chamber. This contamination results in difficulties when pumping down to required levels and also interferes with the resulting properties of the material.

3.3.1.2. PREPARATION OF SAMPLE FOR NITRIDING, COATING DEPOSITION AND CHARACTERIZATION

(a) Thick Sample Preparation

The samples were supplied with a turned surface and had to be polished to a mirror finish. There are many steps to this process as outlined in this Chapter. For the thick sample all of the following steps are untaken.

- (1) Mounting: This step mounts each sample separately in a phenolic resin in order to make them of uniform size to allow them to fit into the clamp of the polishing machine. The surface of the sample is left exposed so that it may be polished. Mounting is done using a Simplimet 2000 Automatic Mounting Press. This is a hot-compression mounting machine which heats the substrate and powder to 150 ^{0}C for Ti-6Al-4V and 316L sample (for polymer samples a temperature below 100 ^{0}C was used to retain its original structure) at a pressure of 290 bar for six minutes and then allows water to pass around the chamber for three minutes for cooling.

- (2) Grinding: This step was carried out using a Motopol 2000 Grinder/Polisher which wet polishes up to 6 samples at one time using different grades of SiC emery papers (240, 600, 800, and 1200). This plane grinding step was to establish a flat surface on the samples so that they were all that the same level. Progressively finer papers were used to obtain a smooth surface, each one

removing material of smaller sizes from the surface of the substrates at each stage so that a flat surface is obtained. This is semi-automated process reduces any variation in result as the applied force and rpm used during the process remain constant.

- (3) Polishing: Once flat the samples are then further ground with progressively finer grit papers. They are finally polished on Micro cloth for Ti-alloy and 316L samples and textmet paper for polymer materials by using 1.0 μm alpha alumina paste and 0.3 μm alpha alumina powders to produce a reflective finish. The mirror finished samples are then rinsed in acetone to remove residues from the unpurified water supply used during this wet-polishing process.

- (4) Mounting Remove: Due to the strong bond of the resin to the substrate the mounting does not peel off easily. To remove the mounting the samples are place in a vice, gripped along the circumference of the resin. A hacksaw is then used to cut through the resin and 5-10 mm is needed to be made depending on the substrate diameter before the resin can be tapped off using a hammer. Great care was taken to ensure that this process did not damage the prepared face of the sample.

- (5) Storage/Hand Polishing: All prepared samples are kept in a desiccant. However, an oxide layer may build up on the surface of the material between preparation and use. Therefore, they were hand polished before use in order to remove this. They were individually polished on a velvet pad with 0.3 micron alpha alumina abrasive applied to its surface for five minutes.

- (6) Ultrasonic Cleaning: The ultrasonic cleaning was carried out in acetone for thirty-five minutes at a temperature of 35 ^{0}C. Ultrasonic cleaning removes grease, oil and any organic elements that may be on the surface of the sample due to fingerprints or air contaminants.

- (7) Drying: They are then rinsed in water and dried using compressed air to prevent water stains on the material.

- (8) Etching: The samples are etched in situ once placed in the chamber by an argon rich plasma beam. As the argon ions collide with the surface of the substrate their kinetic energy forces any contaminant away from the surface and so results in a clean face. This is the final preparation step and removes any remaining contaminant.

(b) Thin Sample Preparation

Thin samples were provided with a flat surface and so only the final three steps are required hand polishing, ultrasonic cleaning and etching. Hand polishing is carried out in progressive steps from a 3 micron to a 0.3 micron alpha alumina abrasive, and the other two steps are carried out as described for the thick samples.

(c) Preparation of post-treated samples for facilitating different characterization techniques

The nitrided and coated samples were sectioned with a Beuhler Abrasimet 2 cut off saw machine. Sectioning was initiated from the edge of the coated or nitrided surface to get a smooth interface between the coating or nitrided layer and the substrate material. The sectioned part of interest was mounted and polished (both machine and hand polish) as described above, in order to reveal the cross-sectional properties. Sectioning of the nitrided sample allowed different types of measurement, such as, the depth hardness, cross-sectional microstructure of the nitrided layer and thickness of nitrided layer. Sectioning of coated samples allowed measurement of coated layer thickness, coating-substrate interfacial morphology and compositional depth profiling by EDX. A glyceregia (15 ml HCl, 10 ml acetic acid, 10 ml HNO_3 and 2-5 droplets of glycerol) etchant was used to chemically etch the non-nitrided and nitrided 316L samples, both coated and uncoated. Kroll's etchant (6 ml HNO_3, 3ml HF and 100ml H_2O) was used to display the surface microstructure of the non-nitrided and nitrided Ti-6Al-4V alloy sample.

3.3.2. PLASMA NITRIDING AND CONTINUOUSLY DEPOSITED DUPLEX DLC COATING SYSTEM

PECVD based Microvac 1200 DB system have been used in this project for both plasma nitriding and continuously deposited duplex Diamond like Carbon (DLC) coating.

(a) **(b)**

Figure 3.12: (a) vacuum Chamber and (b) control panel

The basic mode of operation of this equipment involves the creation of a vacuum in the chamber and the introduction the gas into the chamber. This gas becomes ionized and forms the plasma which is directed towards the substrate. This is controlled by a push-button control panel. The vacuum chamber and control panels are shown in figure 3.12.

3.3.2.1. MAIN COMPONENTS OF THE SYSTEM

The machine is broken down into five main sections: the chamber pump down equipment which creates the vacuum, the gas flow system, the substrate holder, the heating system of substrate and the plasma generation unit. In addition, there are a number of auxiliary components associated with the microvac 1200 DB. These components aid both

the pumpdown of the chamber and operation process and include valves, the chamber, the cooling water supply, the gas inlet supply and the control panel.

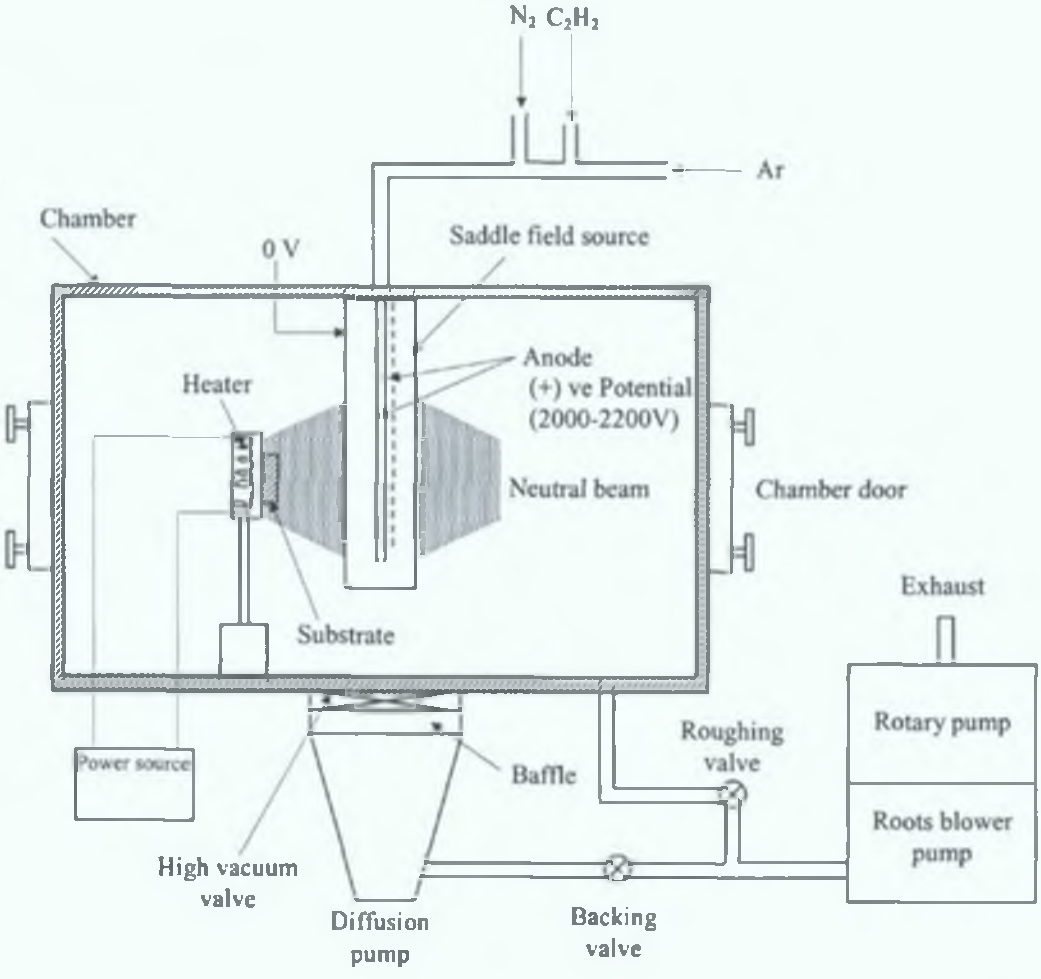

Figure 3.13: PECVD based FAB experimental rig

The pumpdown system in the chamber consists of three pumps and a series of valves and gauges which monitor and maintain the required levels. The three pumps used to create the vacuum within the chamber are the rotary pump, the diffusion pump and the roots blower as shown in figure 3.13. The rotary pump reduces the pressure in the chamber to a magnitude of 10^{-3} mbar and then the diffusion pump reduces the pressure further down to magnitudes of 10^{-7} mbar. The roots blower was added to the original design in order to increase the ability of the rotary pump and hence speed up the process. Due to the fact that the vacuum created within the chamber by the operation of the pumps has a great affect on

the treatment process three pressure gauges are used to monitor the vacuum levels. Two Pirani gauges are used which can display lower vacuum levels up to 10^{-3} accurately. One of these is used to display the pressure within the chamber before activation of the high powered diffusion pump and the second is used to monitor the pressure of the oil which is used within the diffusion pump. This ensures the chamber can be monitored as well as the pump as the pump can be damaged if operated at pressures other than in the region of 10^{-3} mbar. A Penning gauge is used to monitor the higher vacuum generated within the chamber with a magnitude of 10^{-7} mbar.

The gas inlet network for the system caters for four inlets; two for each source (B95 and FAB 104 source). Currently only the B95 source is operating. This source has two inlets one of which was used for passing the argon gas (Ar) to etch the substrates in to the chamber and another was used for passing the acetylene (C_2H_2) to deposit carbon base coating in to the chamber. A new inlet has since been attached with this B95 source for passing nitrogen gas (N_2) into the chamber separately to facilitate the system as a duplex process.

Figure 3.14: Gas flow controller of the deposition chamber

The system has been updated with a separate mass flow controller for the Ar, N_2 and C_2H_2. With the current system setup the argon, the carbon carrier gas and the nitrogen gas can be introduced inside the chamber independently by controlling respective inlets from the flow controller, shown in figure 3.14.

Nitriding of a material requires that the surface of the substrate be heated to a temperature of between 350-900 ^{0}C to allow the nitrogen molecules to penetrate into the substrate to interact with the other elements within the material and so change the properties of the material. This system contained a substrate holder facilitating with a heater, shown in figure 3.15, which provided heat to the substrate. This unit consists of a grooved monel plate with hollow ceramic tubes inserted into the grooves. Tungsten is

woven through the tubes which allow the current to pass through the entire plate and heat it. The ceramic tubes are covered with a flat mantel plate and the substrate is attached to this plate. The current is applied to the tungsten wire via a feed through into the machine from an external source, the value of this can be varied which allows the temperature of the unit and substrate to be altered. The substrate holder and heating unit are connected by the ceramic rods which insert into both. The electric wires are then connected through the ceramic connectors to the tungsten wire of the heating unit. Thermocouple wire is used for measuring the temperature of substrate.

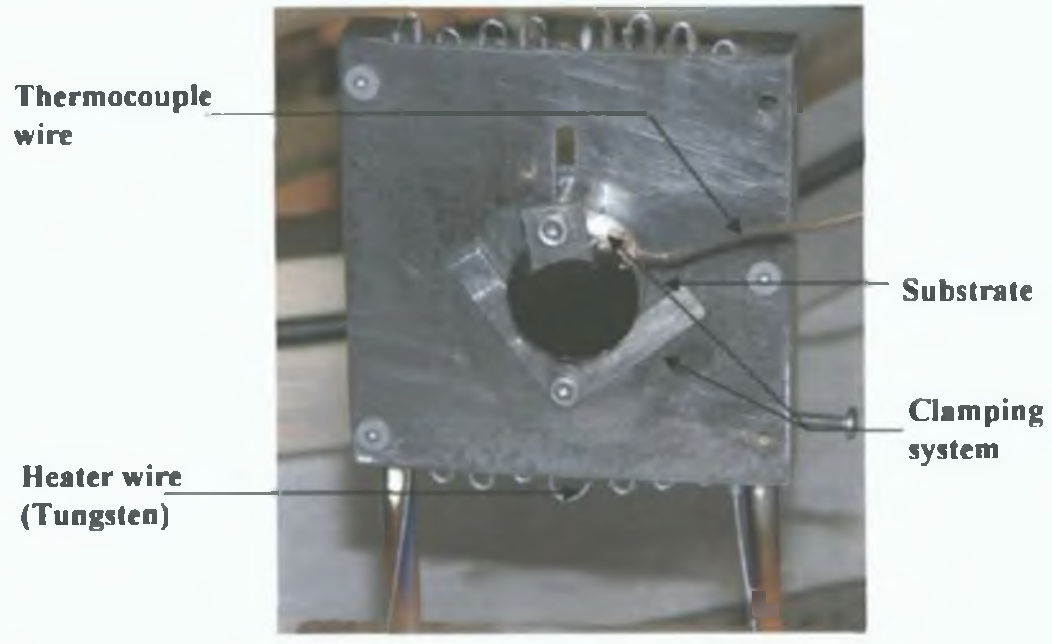

Figure 3.15: Substrate holder with heater on backside

There are many ways which can be used to create plasma, however, the process used in this project is Microvac 1200 DB system. It is based on two Saddle field sources both of which produce a neutral fast atom beam (FAB). These sources are the Saddle field B95 and the Saddle field FAB 104. As discussed in this work only the B95 source has been used, as shown in figure 3.16. The source has its own power supply and cooling water supply. This process works within a vacuum chamber which is created by a diffusion pump, rotary pump and roots blower which are connected to it.

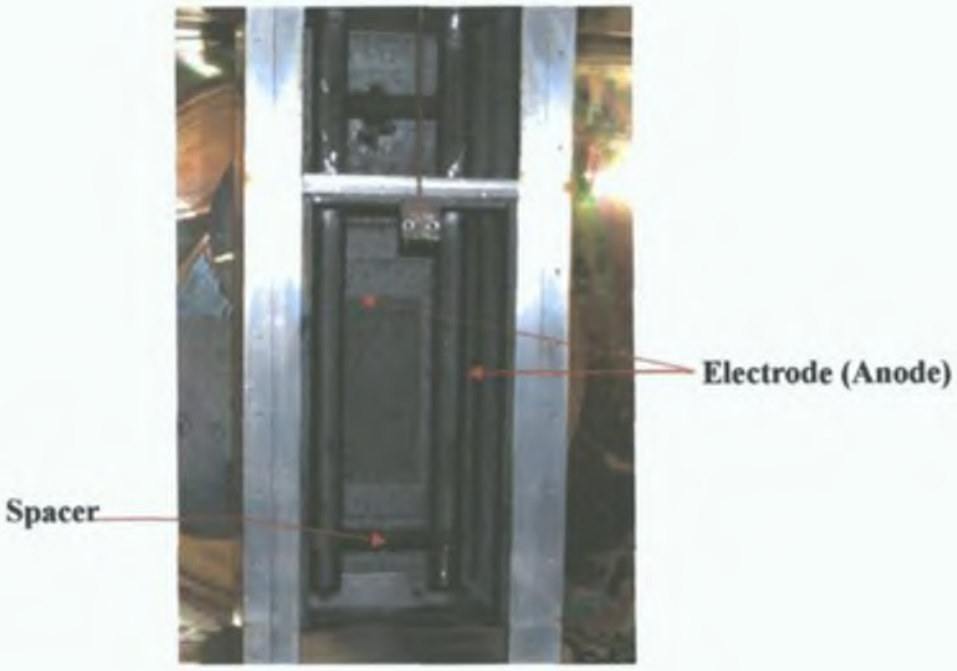

Figure 3.16: Saddle field source type B95

3.3.2.2. THE SADDLE FIELD FAST ATOM BEAM (FAB) SOURCE AND ITS ADVANTAGE

A Saddle Field Fast Atom Beam (FAB) is defined to consist of energetic neutral particles ranging in energy from a few electron volts to several thousand electron volts [280]. In the FAB plasma source there are two positive parallel anode rods symmetrically arranged around the main axis of a rectangular cathode cylinder based on McIlraith's principle of an electron electro-static oscillator [281]. By the application of high voltage to the rod anodes, electrons oscillate at high frequency backward and forward through a saddle point of the electrostatic field between the anodes. With this arrangement the electrons can follow a long oscillatory path and a large number of ions are produced when these electrons collide with gas a molecule that means, a high intensity cold cathode discharge is produced at low pressures. The cathode attracts the ions and the majority of those ions are then converted into fast atoms either by neutralization in charge-transfer collisions with neutral gas molecules or by recombination with the emitted secondary electrons produced by collisions of the ions with the cathode. The atoms produced from the

source escape through the aperture, in the cathode wall, in the form of a highly energetic atom beam [280,282]. A cross section of this plasma generator is shown in figure 3.17.

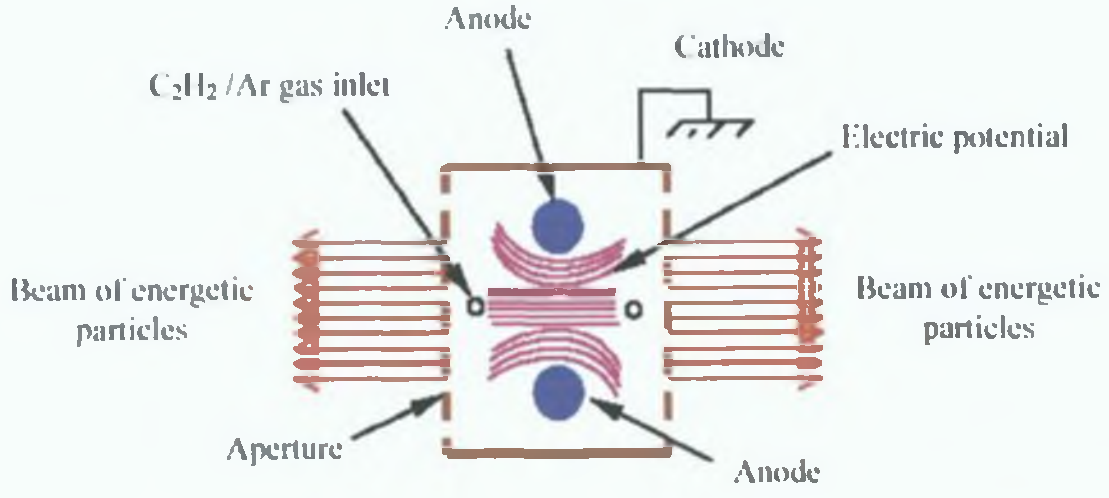

Figure 3.17: Schematic of plan view of the saddle field fast atom beam source (type B95)

Figure 3.18: Inside PECVD chamber

Glow discharged (Plasma) decomposition by either dc or RF excitation of the gases have certain draw backs. The potential profile [283] of the saddle field FAB discharge is almost same as RF diode. Therefore this system achieves some of the advantages of the RF source but only requires a dc supply. A very low processing temperature (near room temperature in the range of 20-100 ^{0}C) can be maintained when operating the saddle field source equipment. This FAB technique is advantageous for processing insulator and composite materials, because the sample surface does not become charged. In summary, once the chamber has reached the desired pressure, the process gas is introduced into the source above the aperture. The gas becomes ionized, plasma is produced and molecules of the gas are dissociated. The aperture is a carbon grid which allows the plasma pass though. The beam is directed towards the substrates on the substrate holder. The positions of the beam aperture and substrate holder are shown in figure 3.18.

3.3.2.3. EXPERIMENTAL PROCEDURE (PECVD BASED FAST ATOM BEAM SOURCE)

(a) Plasma nitriding

Plasma nitriding was performed with a PECVD based saddle field neutral fast atom beam source (as described above) and an auxiliary heater was used for controlling the sample temperature. The experimental set-up for plasma nitriding is shown in figure 3.13. After loading the sample the nitriding chamber was evacuated to a low pressure (~ 10^{-4} Pa) by the diffusion pump backed by rotary pump and roots blower pump and the sample was etched by the argon plasma beam with an overall pressure of 2×10^{-1} Pa for 15 min (constant for all experiment). As the argon particles collide with the surface of the sample the kinetic energy of the particles forces any contaminants away from the surface resulting in a clean surface. The sample (Ti-6Al-4V and 316L) was then heated to the required level (depending on the substrate materials used) by the auxiliary heater and nitrogen along with argon gas was introduced into the beam source to produce a neutral beam by the application of high voltage (1000-2200 V) to the anodes of the source. The resulting beam then bombards the sample with the high-energy molecules and produces nitriding surface. No external heating was applied for polymer (UHMWPE) samples and the beam current was set sufficiently low to avoid heating (temperature maintained below 100 °C) and thus any degradation of the samples. For this aim the beam current is low compared to that commonly employed for metal samples. Nitriding was performed at a range of beam currents and at a stable pressure of around 1×10^{-1} Pa (constant for all experiment) for a

range of treatment times. Experimental parameters and specification for different materials are given in Table 3.6.

Table 3.6: Plasma nitriding experiments for different substrate materials

Material	Parameter	Specification
316L stainless steel	Variable • *Beam current:* 0.4 A to 0.7A • *Nitriding time:* 1 to 12 h. Fixed parameter • *Temperature*: 420 ^{0}C • *Gas mixture:* 80% argon and 20% nitrogen	Low temperature and low pressure plasma nitriding to retain corrosion resistance of 316L stainless steel
Ti-6Al-4V	Variable • *Nitriding time:* 4 and 8 h • Temperature: 500-900 ^{0}C Fixed parameter • *Beam current:* 0.5 A • *Gas mixture:* 25% argon and 75% nitrogen	Low pressure plasma nitriding to enhance the activity of plasma at the sample surface
UHMWPE	Variable • *Beam current:* 0.2 A Constant parameter • *Gas mixture:* 25% argon and 75% nitrogen • *Nitriding time:* 3 h • *Temperature:* kept below 100 ^{0}C (In this case no external heating was applied. Heat is generate due to plasma)	Plasma nitriding of the insulator material at low pressure

A mixture of argon and nitrogen was used for each experiment in this present investigation. The distance between the cathode and substrate was 320 mm in all cases. A K-type thermocouple placed in contact with the sample front surface was used to measure the surface temperature. The samples were allowed to cool down to room temperature from nitriding temperature under vacuum before taking them out.

(b) Continuously deposited duplex coating: Low temperature plasma nitriding of 316L followed by in-situ deposition of DLC coating

Plasma nitriding of substrate (316L) was performed with Saddle field fast atom beam source as described above. The following parameters were used for the plasma nitriding experiments using the duplex treatment methods: Temperature: 420 ^{0}C, Pressure: 1×10^{-1} Pa, Gas mixture: 80% Ar + 20% N_2, time: 6 h, Voltage: 2000-2200 V, Beam current: 0.6 A.

Table 3.7: Design of continuous duplex coating

Coating type	Description
UT+DLC	DLC coating on untreated (UT) 316L sample Parameters used for DLC coating Deposition pressure: 1.5×10^{-1} Pa, Time: 80 min, Beam current: 0.9A, process gas: Acetylene gas (C_2H_2)
PN+DLC	Continuously in-situ deposited DLC coating on Plasma nitrided (PN) 316L samples. Parameters used for plasma nitriding experiment Temperature: 420 ^{0}C, Pressure: 1×10^{-1} Pa, Gas mixture: 80% Ar + 20% N_2, time: 6 h, Voltage: 2000-2200 V, Beam current: 0.6 A. Parameter used for DLC coating Same as above

The deposition of the DLC coatings on the non-nitrided and plasma nitrided substrate (duplex treatment) was performed in a same system used for plasma nitriding experiment. Non-nitrided substrates were ultrasonically cleaned and subsequently etched by argon plasma beam with an overall pressure and anode current of 1.5×10^{-1} Pa and 0.8 A (1900 V) respectively for 15 min. The plasma nitriding sample was allowed to cool down to room temperature from the nitriding temperature, under vacuum. Plasma nitrided sample

was etched by argon plasma beam in a same condition as non-nitrided sample before continuous in situ film deposition. After achieving a base pressure of 10^{-4} Pa the deposition pressure was fixed to 1.5 $\times 10^{-1}$ Pa by controlling acetylene gas (C_2H_2) flow inside the deposition chamber. In all cases anode currents of the source were kept constant to 0.9A and the voltage of the source was in the range of 1200-1400 V. The time for coating deposition was 80 min. The distance between the cathode and substrate was 320 mm and deposition temperature was in the range of 80-90 ^{0}C. A summery of the process parameters and design of the continuously deposited duplex coating is given in Table 3.7. The deposited sample was allowed to cool down to room temperature from the nitriding temperature, under vacuum before being taken out of the chamber.

3.3.3. DEPOSITION OF GRADED AND DISCONTINUOUS DUPLEX COATING

The PVD based magnetron sputtering system, which was constructed for the experimental work, comprised of different part. Whilst the vacuum equipment was generic, one of the most important features of this system is the custom-built chamber. The basic requirement of the chamber was versatility and adaptability in a research environment. The system is shown in figure 3.19.

Figure 3.19: Magnetron sputtering system

In first two years of this research work, the magnetron sputtering rig was developed to produce the Closed Field Unbalanced Magnetron Sputtering (CFUBMS) arrangement. This development work evolved re-establishing different systems such as the magnetron, vacuum, electrical, water-cooling, reactive sputtering controller and so on. The design and installation of the one-axis and two-axis rotary substrate table has enabled the deposition of a new generation of coatings, such as graded, multilayer, composite and so on. A brief description of the whole process is described in the later part of this section. TiN+MoS_2

coatings with and without having graded interlayer have been deposited on nitride and non-nitride samples in a physical vapour deposition (PVD) chamber equipped with a closed field unbalanced magnetron sputtering (CFUMS) system. Coatings are deposited using the d. c magnetron sputtering source, from Ti and MoS_2 targets. N_2 is used as a reactive gas for depositing TiN.

3.3.3.1. BASIC COATING DEPOSITION STEPS IN THIS SPUTTERING PROCESS

- The target, in the form of a plate, is made of the material to be deposited and is connected to a DC power supply capable of supplying several kilovolts.
- The deposition chamber is first evacuated roughly by the rotary pump from atmospheric pressure to 5×10^{-2} mbar (5 Pa). And finally the chamber is evacuated to low pressure with a value of 5×10^{-6} mbar (5×10^{-4} Pa) by the diffusion pump. At this position the working gases (Argon as a sputtering gas and N_2 as a reactive gas) are continuously feed into the chamber and vacuum pumps continuously drive the gases out of the chamber. As the inlet gas flow rate is higher than the pumping speed (measured by outlet flow rate) a residual pressure will build up in the chamber. By controlling the inlet gas flow rates the chamber pressure is raised to the required working pressure value $1\text{-}5\times10^{-3}$ mbar ($1\text{-}5\times10^{-2}$ Pa). Pressure difference between inlet and outlet drives the gas flow through the channel. Eventually steady flow states are established inside the channel.
- After pumping down to base pressure (10^{-6} mbar) and backfilling the chamber with the sputtering gas (usually Ar) as discussed in the previous step, a negative voltage is applied to the target to initiate the plasma.
- The positive ions in the plasma bombard the negative target surface and eject mostly neutral atoms of the target, which are then condensed onto the substrate to form a film.
- Substrates are sometimes negatively biased with a relatively lower voltage to bombard the growing film for dense and well-adhered coating.
- For depositing compound material, a reactive gas is introduced into the chamber. The reactive gas will then react with the sputtered target material and form a compound on the substrate.
- Typical operating conditions for metal deposition in a planar DC sputtering system are as follows: cathode current density of 1 mA/cm^2, discharge voltage of 1000-5000V, operating pressure of 10^{-1} mbar and deposition rate of 40 nm/min.

- The basic process is shown in the figure 3.20. This technique has the problems of low deposition rate and high power supply. For eliminating this problems magnetron sputtering and more specifically unbalanced magnetron sputtering is introduced.

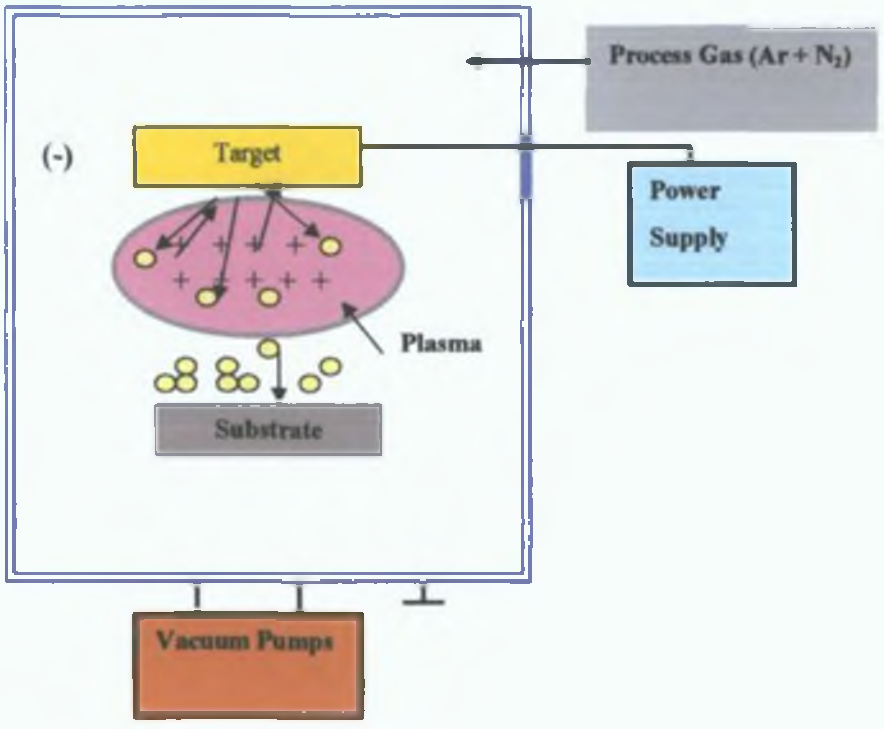

Figure 3.20: Basic DC sputtering process.

3.3.3.2. MAIN PARTS OF THE DEPOSITION SYSTEM

The magnetron sputtering system, which was constructed for the experimental work, comprised of a vacuum chamber, standard high-vacuum equipment, rotary substrate table and magnetrons with power supplies. The vacuum chamber was designed to maximise versatility. Thus, by using the four side magnetrons, large samples can be coated by rotating the sample in the chamber. By utilising only one or two magnetrons, smaller samples can be coated without rotation.

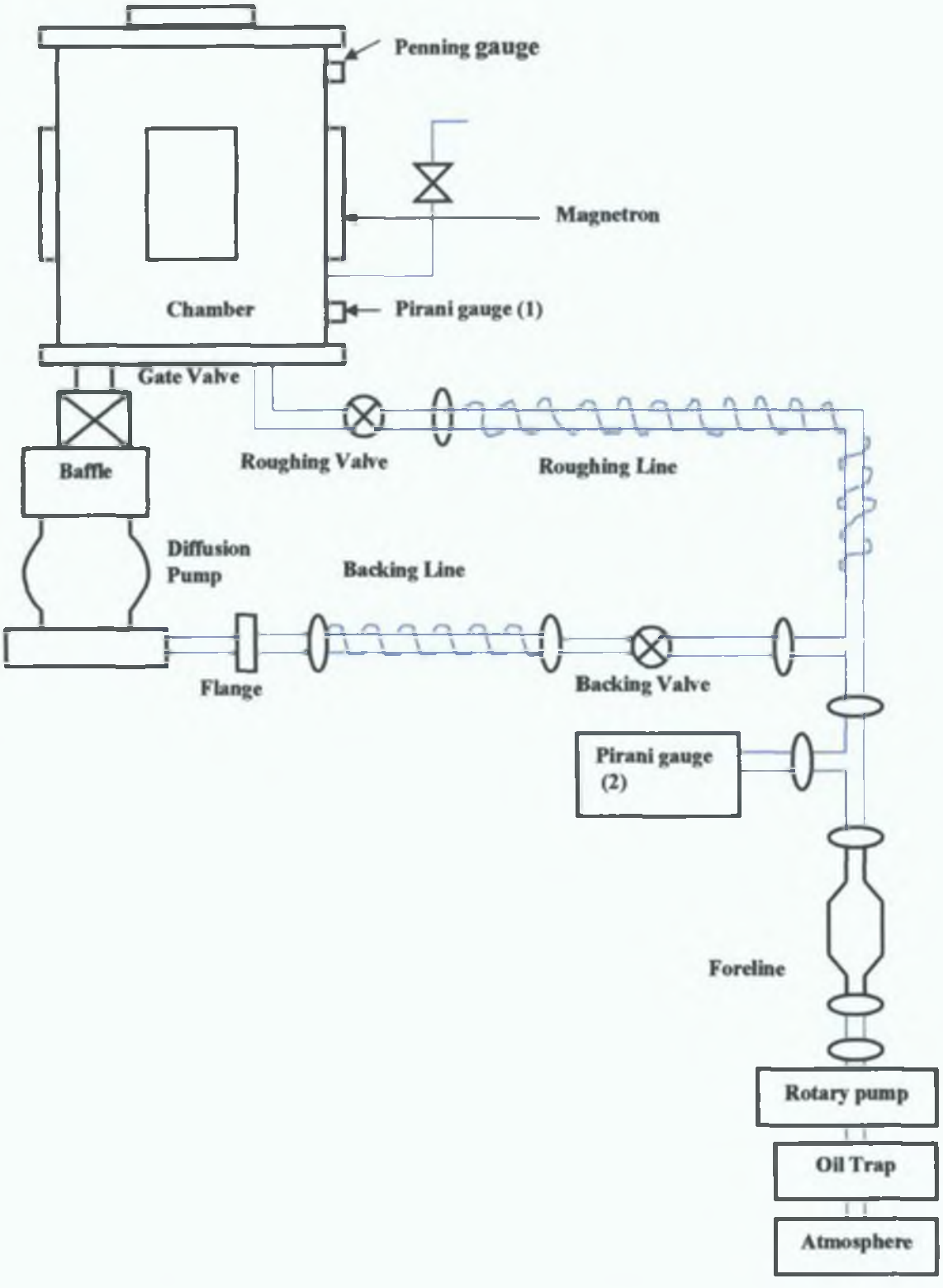

Figure 3.21: Schematic diagram of the pump down system

The chamber was fabricated using non-magnetic AISI 304 stainless steel. The chamber, of approximately 200 litres (0.2 m^3) is evacuated using a combination of the rotary backing pump, which could rough pump the vacuum chamber from atmosphere to 0.03 bar in 5 minutes. A high vacuum is pumped using the diffusion pump to 5 x 10^{-6} bar in a further 5-6 hour. No cryogenic trap was employed. Leak detection was aided by the mass spectrometer and a helium sniffer. The ultimate pressure achieved was approximately 10^{-6} mbar level. The schematic diagram of the pump down system is shown in figure 3.21. The chamber is evacuated using a diffusion pump (2400 l/s) and backed by a rotary backing pump (765/min). A Gate valve controls the diffusion pumping. The roughing and backing lines are controlled by Block valves. These valves are electropneumatically controlled and are actuated by an air compressor (~ 5 bar). The backing line is filtered by using a foreline trap in between the rotary and diffusion pumps. The rechargeable Zeolite molecular was used in the forline trap.

Normally with a stationary substrate table, it is almost impossible to deposit a coating on a three-dimensional object. For three-dimensional coating, the rig has been provided with a single axis and two-axis rotary substrate table.

Figure 3.22: Substrate holding table

Substrates can also be placed in the middle of the table for single-axis rotation instead of two-axis rotation. Ferrofluidic feedthrough is incorporated for dynamic sealing of the table shaft with the chamber. The rotary motion is provided by a belt-driven external motor. The rotary shaft is cooled by Deublin rotary union. The rotary table is shown in figure 3.22.

The flow rates of both working and reactive gas were controlled by a Tyln mass flow controller and a Tyln mass flow meter respectively. The gas flow were controlled and

monitored by a Tyln flow control unit. The total pressure of the chamber was monitored by the use of Edwards Penning gauges which were controlled by an Edward pirani-Penning controller. Another Pirani gauge monitored the pressure on the backing line. All valves were electro pneumatic. Three different types of gases are supplied during different kinds of film formation. Ar is mainly supplied for generating the plasma to deposit any metallic coating like Ti. Either Ar, N_2 or Butane is supplied for reactive deposition of bicomponent coatings like TiN or TiC respectively. N_2 and Butane can be supplied with Ar for depositing tricomponent coating like TiCN

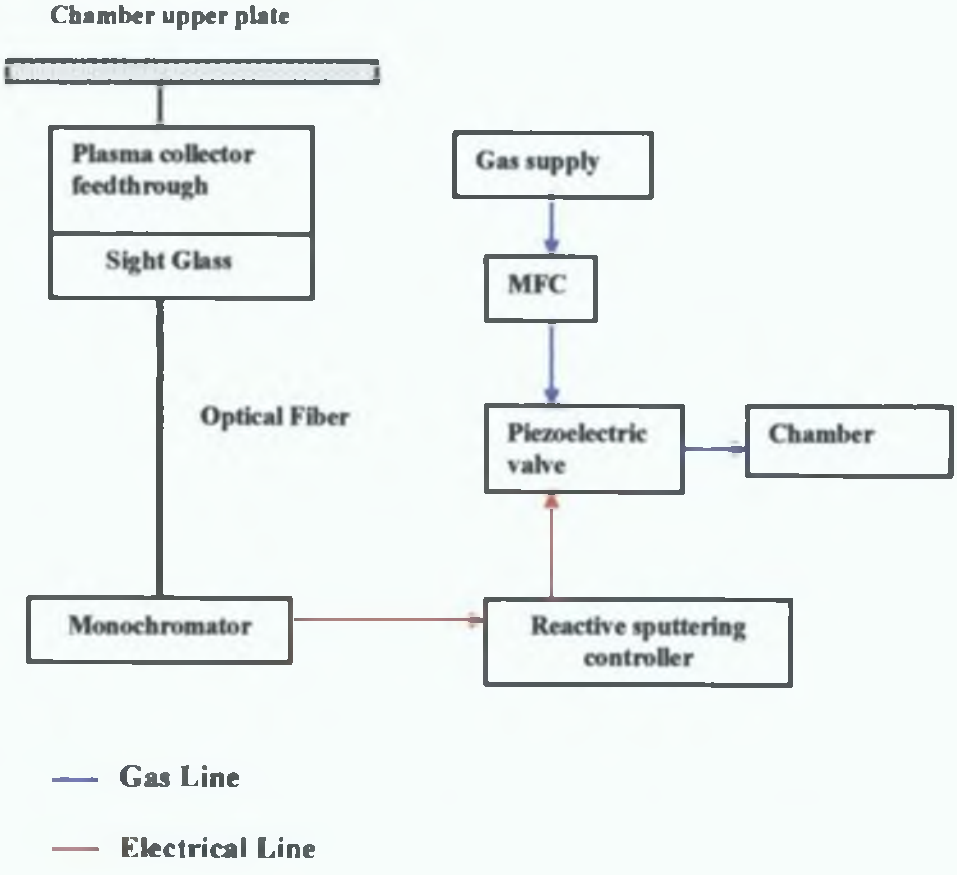

Figure 3.23: Schematic diagram of reactive sputtering control system.

A valve and a regulator are attached to each cylinder. The regulator controls the flow of gas to the plastic gas pipeline. After the regulator there is a Mass Flow Controller (MFC). This MFC controls the flow rate of the gas into the chamber. There is a valve between the regulator and MFC. This valve controls the gas flow to the MFC. A mass flow meter and a piezoelectric valve are attached to the gas supply system for close-loop control of the reactive gas during reactive sputter deposition. The closed loop control of reactive gas is discussed in the Reactive Sputtering Controller section. Each MFC is electrically connected to a flow control unit. During reactive sputtering, the target is poisoned with the coating material. The poisoned target produces films rich in reactive gas and deposition rate is low. Target poisoning reduces the reactive gas consumption leading to an increase in the reactive gas pressure.

The sputtered material passes through the plasma where it is excited and emits light at characteristic wavelengths. The emission intensity is proportional to the density of the excited species, and this is also proportional to the product of the excitation probability and the density of the unexcited species. The Reactaflo™ unit monitors this plasma emission and uses it as a control signal for the reactive gas supply. If the monochromatic is tuned to a metal emission line then this line will fall as the reactive gas is admitted (reverse control sense). If it is tuned to a reactive gas emission line then this will rise as the reactive gas is admitted (normal control sense). In either case the emission signal is a unique function of the reactive gas pressure. The Reactaflo™ unit dynamically controls the reactive gas flow to keep the chosen emission line constant. This eliminates the pressure instability and allows operation across the whole range of target conditions. The schematic diagram of the reactive sputtering control system is shown in the figure 3.23. For example, in the case of TiN film deposition, in order to maintain the correct stoichiometry, the optical emission intensity of titanium was observed and monitored. The emission intensity of a species in a plasma is a good indication of the density of that species in the plasma. By setting the level of target poisoning such that the deposition rate is optimised, the deviations from this set point are monitored as TiN is reactively sputtered and the fluctuations provide the feedback signal to the piezoelectric valve which admits the nitrogen gas into the chamber. For deposition of graded layer TiN coating, the optical emission intensity of titanium was observed and monitored and the set point of Ti was decreased gradually from 100 % to ~50% (stoichiometric) after a certain interval (depending on the thickness of each layer required). As a result a graded coating of Ti-TiN_x----$TiN_{stoichmetric}$ can be deposited. The main advantage of using an optical emission spectrometer is that it allows for the rapid

compensation in fluctuations of the plasma composition. The partial pressures of nitrogen and argon are monitored using the Reactaflo reactive sputtering controller. The dynamic control of the reactive gas flow eliminates pressure instabilities during target poisoning.

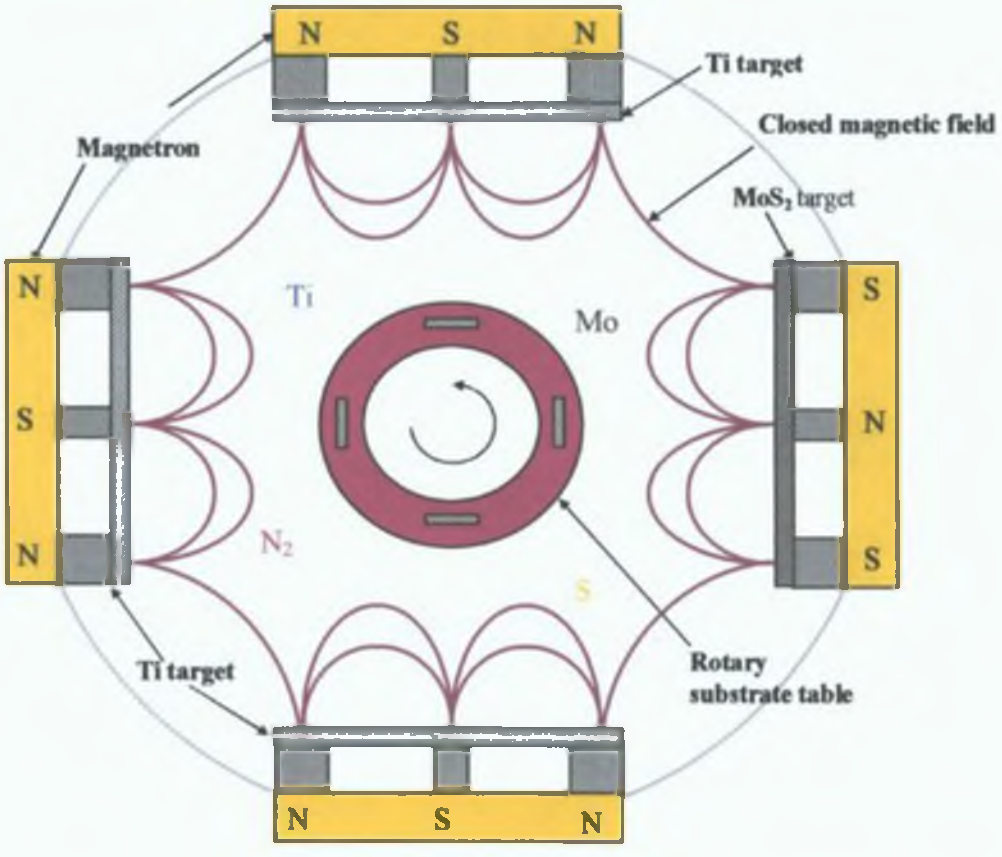

Figure 3.24: Cross-section of the closed-field magnetron sputtering chamber.

The magnetron employed in this project was supplied by Teer coating services, UK and comprised four magnetrons. The magnetron ordered were not only unbalanced, but they in themselves were of reversed polarities such that, for instance in the four magnetron case, a closed field arrangement ensued, where the magnetic field lines from the edges of the one magnetron closed with the edge of the adjacent magnetron as shown in figure 3.24. This effectively confines the plasma to the middle of the chamber where the substrate is placed [284,285]. A closed field system results in increased plasma densification and hence increased ionisation and ion bombardment of the growing film. Two facing magnetrons with Ti and MoS_2 targets were activated during deposition. The other two facing magnetrons with Ti targets acted as dummies, as shown in figure 3.24.

3.3.3.3. EXPERIMENTAL PROCEDURE (SPUTTERING)

(a) Deposition and design of the coating to see the effect of the graded interlayer

In this part of the coating design, the effect of different types of interlayer (soft, hard and graded interlayer) on the properties of the TiN+MoS_2 were study. The coatings were deposited on stainless steel substrates in a custom made sputtering chamber (inner diameter 603.00 mm and height 610.00 mm) with Teer unbalanced magnetron in a closed-field arrangement, (Figure 3.24) as reported earlier in detail. The substrate was ultrasonically cleaned and subsequently sputter cleaned in argon plasma with an overall pressure and voltage of 10^{-2} mbar and 1000 V respectively for 15-20 min. After achieving a base pressure of 10^{-5} mbar the deposition pressure was fixed to 3×10^{-3} mbar. Two facing magnetrons with Ti and MoS_2 targets (13.3×33 cm^2) were activated during deposition. The other two facing magnetrons with Ti targets acted as dummies to complete the closed magnetic field. The substrate was fixed to a rotatable substrate holder (1-fold rotation) and rotated at a speed of 3 rpm with a target to substrate distance of approximately 80 mm.

Table 3.8: Design of the TiN+MoS_x coating with different interlayers

Sample	Interlayer	Top layer	Interlayer description
G1	Ti	(TiN+MoS_x)	Soft interlayer
G2	Ti–$TiN_{0.33}$–TiN		Graded interlayer
G3	Ti–$TiN_{0.2}$–$TiN_{0.47}$–TiN		Graded interlayer
G4	TiN		Hard interlayer
G5	-		No interlayer

A range of coating systems with different interlayers was investigated, as shown in Table 3.8, to see the effect of graded interlayer. First the Ti target was powered and nitrogen was gradually (depending on the interlayer composition) introduced in to the chamber to form the graded interlayer (sample G2 and G3). Nitrogen flow rate was controlled by a Reactaflo reactive sputtering controller monitoring the Ti emission peak. For sample G1, no nitrogen was introduced to form a pure Ti interlayer. For sample G4, nitrogen was controlled to form a stoichiometric TiN interlayer. For sample G5 no interlayer was used. After interlayer deposition (for G5 no interlayer), the MoS_2 target was

powered with a small ramp time (1 min) and the top layer of all coatings was deposited by passing the substrate in front of the Ti and MoS_2 targets in the argon and nitrogen gas environment. In the top layer, nitrogen was again controlled to form stoichiometric TiN. In all cases the Ti and MoS_2 target currents were kept constant at 6.5 A (target voltage, 410V) and 0.4 A (target voltage, 460V) respectively. The deposition time of the top layer was kept constant at 50 min and the interlayer deposition time was varied between 15-30 min depending on the interlayer composition. An advanced Energy MDX 5 kW DC power source was used for supplying power to Ti and MoS_2 targets. During the entire process the substrate was negatively biased to -60 V with an Advanced Energy MDX 5 kW power source.

(b) Discontinuously deposited duplex coating

Discontinuously deposited duplex coating is a process where plasma nitriding and coating are performed in a separate process step. In this research, deposition of the TiN-MoS_2 coating with or without having graded layers was performed by the sputtering method whereas plasma nitriding was carried out using the PECVD based fast atom beam method as mentioned early. Plasma nitriding of the substrate (316L) was performed with Saddle field fast atom beam source as described in Section 3.3.2.3. The following parameter has been used for the plasma nitriding experiment for the duplex treatment: Temperature: 420 ^{0}C, Pressure: 2×10^{-1} Pa, Gas mixture: 80% Ar + 20% N_2, time: 5 h Beam current: 0.7 A. The deposition of TiN+MoS_x and TiN+MoS_x coatings with graded interlayers (Ti-$TiN_{0.2}$ - $TiN_{0.47}$ -TiN) on the non-nitrided and plasma nitrided substrate (duplex treatment) was performed by magnetron sputtering. Design of the coating-substrate system is shown in Table 3.9. Before coating deposition the nitrided substrates were manually polished by 0.3 μm alpha alumina powder to remove the superficial layer. Non-nitrided or nitrided substrates were then ultrasonically cleaned and subsequently sputter cleaned in the argon plasma with an overall pressure and voltage of 1 Pa and -1000 V respectively for 15-20 min. The procedure of deposition of TiN+MoS_x and TiN+MoS_x coatings with and without graded interlayer has been reported in the previous section.

Table 3.9: Design of the discontinuous duplex coating

Coating description (mark)	**Substrate condition**	**Interlayer**	**Top layer**
TiN+MoS_x coating on non-nitrided substrate (Coating)	Non-nitrided	-	(TiN+MoS_x)
TiN+MoS_x coating with graded interlayer on non-nitrided substrate (GI+Coating)	Non-nitrided	Graded interlayer	
TiN+MoS_x coating on plasma nitrided substrate (PN+Coating)	Nitrided	-	
TiN+MoS_x coating with graded Interlayer on plasma nitrided substrate (PN+GI+Coating)	Nitrided	Graded interlayer	

3.4. CHARACTERIZATION TECHNIQUES

3.4.1. STRUCTURAL PROPERTIES

3.4.1.1. X-RAY DIFFRACTION

In the X-ray diffraction process, the incident X-ray is scattered from electrons of the atom by two kinds of scattering: unmodified scattering (same wavelength) and modified scattering (longer wavelength). Because there is a change in wavelength, the modified scattering from the different electrons of the atom is completely incoherent. It develops a background and is therefore of no further use. Therefore, in X-ray diffraction only monochromatic and unmodified scattering is used for analysis of the sample. It is necessary to consider the different electrons of an atom to obtain the scatter interaction of an X-ray with an atom. The sum of the amplitudes per electron gives the amplitude of the unmodified scattering per atom. To determine the interaction of X-rays with a crystal, it is necessary to know the scattering factor of an individual atom. The amplitude of scattering from an atom is the sum of the amplitudes per electron and the scattering by a crystal is the sum of the amplitudes per atom. Unlike the electrons, the only difference is that for a crystalline material the positions of the atoms are more or less fixed. This necessitates the addition of a structure factor to the summation, to consider the spatial distribution of the atoms within a unit cell. However, a crystal is composed of multiple unit cells, which have a periodic distribution in space, resulting in, just as for the unit cell, an additional summation over all the unit cells in the crystal. The basic principle of the X-ray diffraction is derived from Bragg law. This law states that when the difference in the path lengths experienced by radiation scattered from two adjacent lattice planes are equal to the wavelength of the radiation or a multiple of this, constructive interference will occur. This can be represented by the following equation (3.3) [286].

$$n\lambda = 2d\sin\theta \quad \text{.....} \quad (3.3)$$

Where n, λ, d and θ are the order of reflection, the wave length, the spacing between plane and the incident diffraction angle of the X-ray beam (also called Bragg angle) respectively.

It is important to note that, the size of the crystals has a pronounced influence on the width of the diffraction peak and the intensity is linearly proportional to the number of unit cells that have the same orientation. Therefore, X-ray diffraction cannot only be used to determine the structure factor of a material or the lattice spacing, but it may also provide valuable information concerning the size and crystallographic orientation of crystallites.

(a) Lattice spacing

Lattice spacing of a cubic structure (d_0 *or* a_0) can be determined using Bragg's law, where (hkl), is the reflection plane [286].

$$n\lambda = 2d_{hkl}\sin\theta_{hkl} \quad \text{..... (3.4)}$$

$$d_{hkl} = \frac{d_0}{\sqrt{h^2+k^2+l^2}} \quad \text{..... (3.5)}$$

Therefore by using equation 3.4 and 3.5, it is possible to determine a_0 from each reflection. The accuracy in lattice parameter, d_0 is basically the accuracy with which θ and λ can be determined. Differentiating Bragg's law with respect to θ shows that the error in d_0 is proportional to cotθ. Therefore, the error in d_0 is smaller when a reflection at a higher 2θ angle is used. Although there are different sources of systematic errors in d_0 the predominant source of error is displacement of the specimen from the diffractometer axis. This results in an error in the lattice spacing defined by [286]:

$$\frac{\Delta d_0}{d_0} = -\frac{D}{R}\cos\theta\cot\theta \quad \text{..... (3.6)}$$

Where D is the horizontal displacement of the specimen from the diffractometer axis and R is the distance from the specimen to the detector. The procedure is as follows: first determine d_0 for different {hkl} planes using equation (3.6) and then plot this data as a function of the cosθ.cotθ (which is called a Nelson-Riley plot). Linear extrapolation to cosθ.cotθ=0 gives a lattice spacing which takes the systematic errors in consideration. Deviations from the linear relationship are due to accuracy limitations or are a result of the nature of the specimen.

(b) Grain size and deformation strain

The size of a grain and imperfections within a grain have an effect on its X-ray diffraction pattern [286,287]. By comparing modified X-Ray diffraction pattern with the perfect crystal pattern, it is possible to determine the grain refinement and, stress effect in the crystals after material processing. As mentioned above, the condition for Bragg's law (equation 3.3) is only fully satisfying for a perfect cubic crystal. The difference between plane y and plane y+n is n times the path difference, d_{hkl}. When this is equal to half a wavelength destructive interference will occur for these two rays. Therefore, when the size of a crystal is infinite this will occur for all non-ideal rays and the diffraction peaks are very sharp. Decreasing the crystal size will result in diffraction broadening because when there are only n-1 planes this difference of half a wavelength will not be reached. This broadening depends on the distance between the planes and is thus different for different {hkl} reflections. This can be is described by the following equation (3.7).

$$\beta = \frac{K\lambda}{L\cos\theta} \quad \ldots\ldots\ldots\ldots\ldots\ldots\ldots\ldots\ldots\ldots (3.7)$$

Where β is the width of the diffraction peak in radians, L is the size of the grain and K is a factor which depends on the shape assumed for the intensity distribution of diffraction. Its value is close to unity. The broadening of the diffraction line is not only due to size and micro-stress effects but also due to non-monochromatic radiation, slit sizes and an imperfect focus. The later broadening is called the instrumental broadening. When $\beta\cos\theta/\lambda$ is plotted as a function of $4\sin\theta/\lambda$ [288] by using equation 3.8, it is possible to determine the grain size and the deformation strain: the reciprocal of the intercept gives the grain size and the slope of the line relates to strain broadening.

$$\frac{\beta_i \cos\theta}{\lambda} = \frac{K}{L} + 4e_{hkl}^{max}\frac{\sin\theta}{\lambda} \quad \ldots\ldots\ldots\ldots\ldots\ldots\ldots\ldots\ldots\ldots . (3.8)$$

Therefore by using this equation separation of the finite grain size and strain broadening is possible.

(c) Thin film and XRD

In normal, Bragg-Brentano powder diffraction, two axes move in sequence with each other. The sample and the detector move together with a gear ratio of 1:2. In other words, the detector moves twice as fast as the sample or the sample position is half that of the detector. This type of geometry is known as theta-2-theta geometry. When the machine is operating in normal powder diffraction mode, there are also two axes moving in sequence with each other, but in this case the X-ray tube and the detector move together at the same speed and at the same angle. This is known as theta-theta goniometer geometry. When one looks at a thin film in normal powder diffraction in either of these mentioned geometries, there is generally a very large peak contributed by the sample substrate. The intensity of this peak is often so high that it swamps out the peaks of the film or it may directly overlap the film peaks of interest. This conventional X-ray diffraction geometry is not useful for the study of ultra thin, graded composition and multilayered thin films, partly because of poor sensitivity and partly because of the presence of the interfering effect of the substrate. A useful geometry must be based on a low X-ray incidence angle, so as to be able to probe the material up to a specific depth. By means of X-rays under the special condition of grazing incidence relatively to a sample surface it is possible to investigate thin films or buried interfaces in the layer system. Grazing angle diffraction is a technique employed whenever there is a need to see only the surface of a sample

In the case of grazing angle geometry, the only peaks visible are those corresponding to the thin film or coatings. The peaks depend on the magnitude of the angle. In this case the theta-theta geometry is used, which is based on slight modification of conventional Bragg-Brentano geometry. Instead of moving both the X-ray tube and the detector, the X-ray tube is fixed at a low angle while the detector scans across the 2-theta area of interest. Because the source is positioned at a very low angle relative to the surface of the sample, (~ 1-10 degrees), the X-ray "graze" the surface rather than penetrate into the sample. Thus, only the film diffracts, and not the substrate underneath. In this work, both a normal scan (locked couple) and Glancing Angle X-ray Diffraction (GAXRD) at an incident angle of 30^0, called a detector scan, have been performed using a Bruker D8 diffractometer with CuK_α radiation. The following parameter have been used at the time of scanning of sample: X-ray beam current and voltage were respectively 40 mA and 40 KV, scanning speed was 1.0 sec/step, increment per step was 0.05 degree, absorption mode was set up to auto and scan type was select as detector scan. For X-ray diffraction, very thin substrate samples have been used (0.5 mm). Penetration depth of the X-ray beam inside the

sample depends on the absorption co-efficient of this coating-substrate system as well as the magnitude of the grazing incident angle.

3.4.1.2. SCANNING ELECTRON MICROSCOPY (SEM) WITH ENERGY DISPERSIVE X-RAY (EDX)

In this work, SEM has been used for investigation of surface topography of the samples. The Princeton Gamma-tech EDX was employed to obtain the chemical composition of the nitrided and coated samples and the elemental line profile analysis of the graded interlayer.

(a) Principle of SEM

In a SEM instrument, the electron gun accelerates the electrons down the column towards the sample with energies typically ranging from hundreds to tens of thousands of eV. The electrons emerge from the gun as a divergent beam. The condenser lenses, objective lens and several apertures in the column converge and focus the beam on the sample surface. A set of scanning coils deflect the beam in a scanning pattern over the sample surface. The beam exits from the column into the specimen chamber, which incorporates a stage for manipulating the sample and one or more detectors. The signals, emitted from various positions of the specimen surface as the specimen is scanned by the electron probe, are detected by a detector (located near the specimen) and the signal induced in the detector is sent to the video amplifier. The interaction volume between the incoming primary electrons and the sample can be divided into regions associated with a specific signal type, such as secondary electron, backscattered electron, X-ray and so on. Not all of these effects will be large enough to be detectable. However, virtually all materials will exhibit usefully large secondary electron currents and X-ray emissions. Secondary electrons (SE) are caused by inelastic collisions with the atoms in the target area and generally have a low energy. Because of their low energy, they can escape only from a shallow region at the sample surface. As a result, they offer the best imaging resolution (in the order of 5-20nm). The contrast arises primarily from sample topography. This makes the interpretation of secondary electron images very intuitive. The characteristic X-rays are excited by the electron beam with a distinct line spectrum used in for EDX instrument for chemical analysis of the sample as described below.

(b) Specimen preparation for SEM

Good imaging necessitates contamination-free surfaces, resistance of the specimen to high vacuum and to the electron beam, absence of electrical charging and a sufficiently high electron yield. Charging effects can be avoided by operating at a low accelerating voltage or applying conductive coatings, which is a widely used technique. The coating layer must be thick enough to provide a conductive path, but should be as thin as possible to avoid obscuring fine details. The minimum thickness depends on the surface roughness. The coating can be applied by cathode sputtering under vacuum. The investigated samples in this work have been coated with a sputtered gold layer by the Scan Coat Six Sputter Coater. This is a compact bench-top unit designed to thinly coat non-conductive samples with gold or carbon for use in Scanning Electron Microscopes

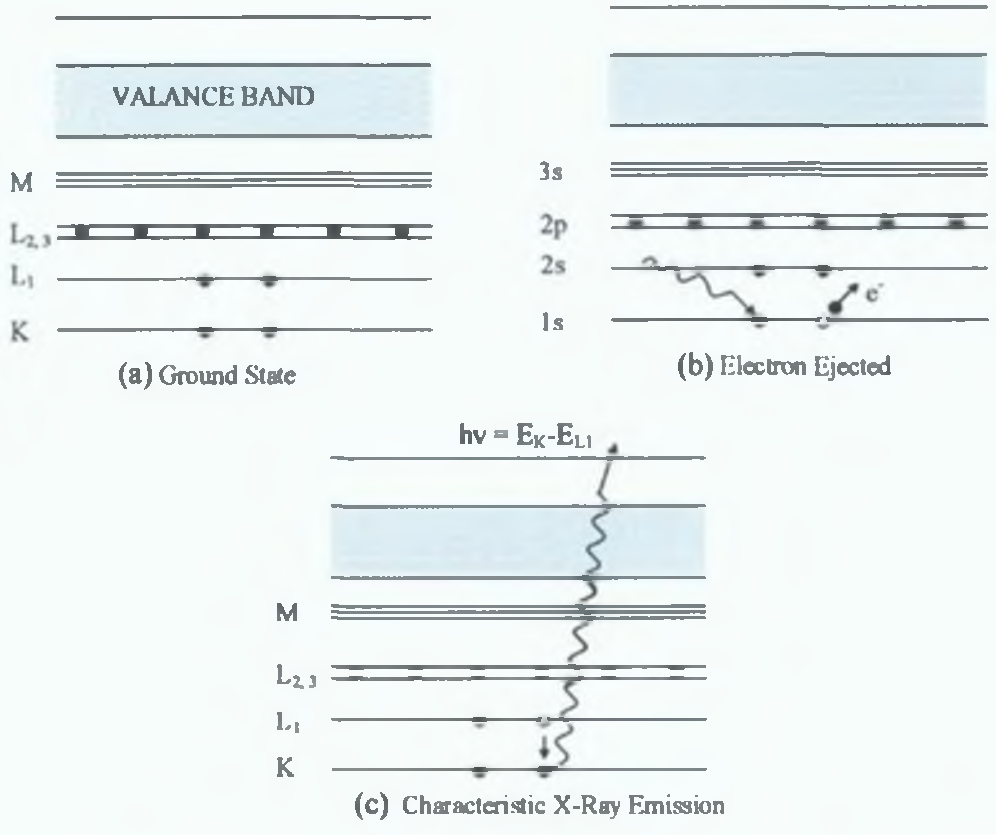

Figure 3.25: Schematic diagram of electron energy transition: (a) Ground state; (b) incident photon (or electron) ejects K shell (1s) electron (c) X-ray emission when 2s electron fills vacancy of 1s (adapted from [289]).

(c) Chemical characterization by EDX

EDX analysis stands for Energy Dispersive X-ray analysis. If an electron is exited by photon energy (in SEM electrons are used as photon energy as described above) from ground or initial state (Figure 3.25 (a)) to leave an atom or to go into a higher unoccupied level an electron hole is formed (Figure 3.25 (b)). This electron hole is filled by one of the outer shell electrons, conserving energy by emitting an X-ray photon (Figure 3.25 (c)). X-rays excited by the electron beam form two types of spectra, the Bremsstrahlung (electromagnetic radiation emitted by electrons when they pass through matter) with a continuous spectrum, and the characteristic X-ray radiation with a distinct line spectrum. This X-ray spectrum is unique to each element and therefore an analysis of the X-ray emission of any specimen can give an analysis of the constituent elements in the specimen. The X-ray line spectrum can be analysed by EDX and an EDX spectrum plot identifies the element corresponding to each of its peaks. It is a technique used for identifying the elemental composition of the specimen, or an area of interest thereof. The higher a peak in a spectrum, the more concentrated the element is in the specimen. The information depth of X-ray emission depends on the energy of the primary electrons and the elements in the specimen, but is generally of the order of micrometers (for solids). This technique has one disadvantage, namely it is not very suitable for lighter elements. The EDX analysis system works as an integrated feature of a scanning electron microscope, and can not be operated on its own without the latter.

3.4.1.3. OPTICAL MICROSCOPY

The optical microscope is useful for quantitative metallographical analysis, using an automatic image analyser connected to the microscope. This instrument provides a powerful tool for examining, evaluating and quantifying microstructure of various, materials. When the microscope operates in its reflective mode, the instrument is well cable of revealing polished and etched material specimens. But the information derived depends critically upon the metallographic preparation procedure. In this research work, the Reichert "MeF2" Universal Camera Optical Microscope has been used to examine plasma nitriding and coated sample.

3.4.1.4. X-RAY PHOTOELECTRON SPECTROSCOPY (XPS)

Basic Principle: In the XPS technique electrons (photoelectrons) are emitted from the core level of an atom by the absorption of photon energy, as illustrated in figure 3.26. Photoelectron emission occurs when a photon transfers its energy to an electron, and a photoelectron can be emitted only when the photon energy is larger than the binding energy of the electron. In this technique, in general X-rays of known and fixed photon energy (hv), usually Mg K_α (1253.6 eV) or Al K_α (1486.6 eV), are used to excite and eject the core level electron. The emitted electrons (photon) have kinetic energies, given by the following equation (3.9):

$E_b = h\nu$ (known quantities)-)- E_k (measured by the analyzer of XPS instrument) ... (3.9)

Where, hv is the energy of the absorbed photon (X-ray), E_b is the binding energy of the atomic orbital from which the electron originates and E_k is the kinetic energy of the ejected photoelectron. The kinetic energy of the ejected photoelectron (E_k) is analyzed by retarding or accelerating the detected electron in the spectrometer. It is forced by an electron lens system and then dispersed in terms of kinetic energy by a hemispherical electrostatic analyzer.

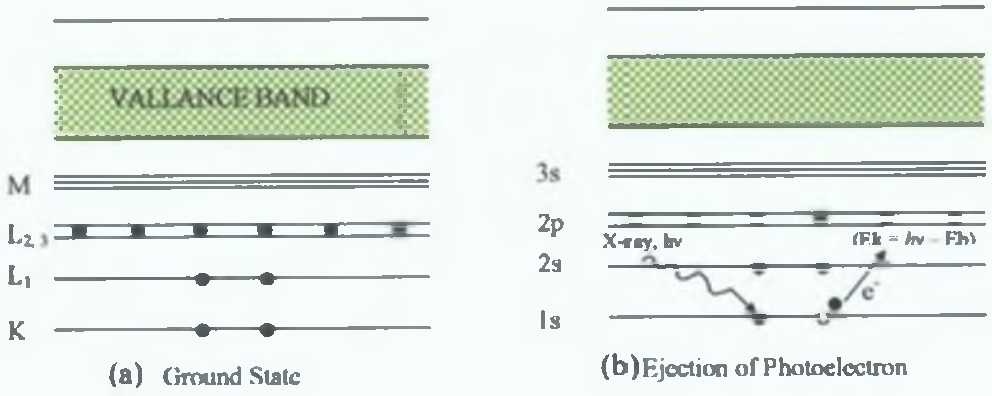

Figure 3.26: Schematic diagram of electron energy transition: (a) ground state and (b) incident photon (X-ray) ejects K shell electron (photoelectron).

The photoelectrons are subsequently detected via a multichannel system consisting of multichannel plates, a phosphor screen and a CCD camera. Therefore, the binding energy of the core level electron, E_b, is measured by the difference between the known energy of the X-ray photon (hν) and the kinetic energy (E_k) of the electrons (measured by the analyzer of XPS instrument). Binding energy (E_b) measurement provides an atomic identification and chemical state information as E_b is constant and a fixed value (fingerprint) of a particular atom. The XPS technique provides and means for the identification of elements and gives information about their chemical states present in the outermost ~5 nm of the sample's surface due to the relatively short inelastic mean free path of the photoelectrons. The transportation of emitted electrons, generated in the solid, to the surface can thus only occur from a certain depth. The XPS technique can detect all elements except for H and He due to its excellent element selectivity and quantitative character. An XPS spectrum shows a background due to inelastic scattering in the substrate (before reaching the spectroscopy some of the electron loss there energy further). Nevertheless, the main advantage of using the XPS-technique lies in the fact that the binding energy of a photoelectron is sensitive to the chemical surrounding of the atom, that means, there is a chemical shift in the binding energy. These shifts are very important since they provide a tool to identify the individual chemical states, or bonding states, of an element.

In this work, the X-ray photoelectron spectroscopy (XPS) analysis of the samples was carried out in VG Microtech electron spectrometer at base pressures in the preparation and analysis chambers of $2x10^{-8}$ and $1x10^{-8}$ Pa, respectively. The photoelectrons were exited with X-ray source using MgKα (hν =1253.6 eV) and the pass energy of the analyser was 20 eV yielding a resolution of 1.2 eV. The C1s, O1s, N1s, Ti2p, Al2p and V2p3/2 peaks were recorded along with 20-1000 eV survey scans. The intensities of the peaks were determined as the integrated peak areas, assuming the background to be linear. The elemental concentrations were calculated by an approach in which the transmission function of the analyser is taken into account. The values of respective cross sections were taken from literature [290]. Depth profiling of samples was carried out by in-situ sputtering using an argon ion gun which was operated at an energy of 3 keV and a sample current of 90 mA.

3.4.1.5. ATOMIC FORCE MICROSCOPY (AFM)

AFM is one of the many techniques, which fall into the Scanned Probe Microscopy (SPM) family of instruments. In all of these SPM techniques a small probe (10-100 nm radius of curvature) is raster scanned by a piezoelectric device over a sample to produce an image of the sample surface, or the near the surface region. A simple schematic of an AFM instrument is given in figure 3.27.

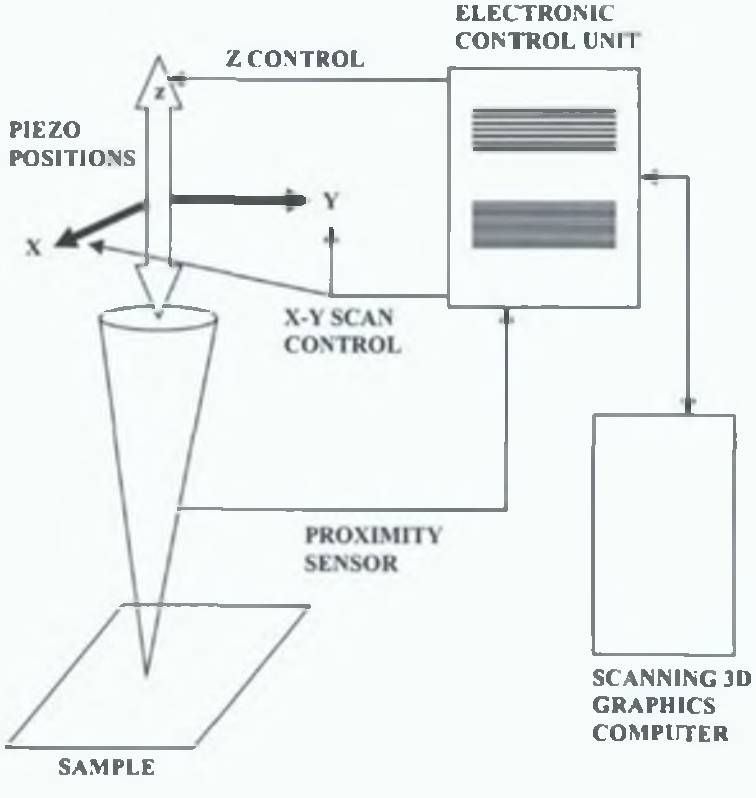

Figure 3.27: Scanning probe microscopy system.

In this instrument the probe tip is mounted on the end of a triangular cantilever arm, similar to a diamond stylus mounted on the end of a record player arm. A piezoelectric device raster scans the sample beneath the probe tip. As the probe is brought close to the sample, it is first attracted to the sample surface due to attractive Van der Waals force and the cantilever will bend. When it is first attracted to the sample surface, the electric orbitals

of the atoms on the surface of the probe and sample start to repel each other. As the gap decreases, the repulsive force neutralizes the attractive forces and then becomes dominant. Hooke's law calculates the force of the interaction between probe and sample. This bending of the cantilever can be monitored by bouncing a laser beam off the cantilever on to a 2-element photodiode as shown in figure 3.28.

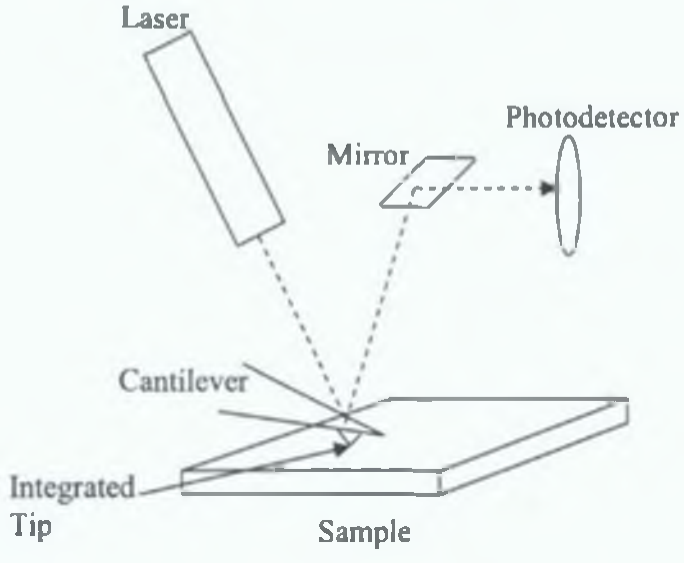

Figure 3.28: AFM force sensor drawing

In normal operation the tip-sample force is held constant by a computer controlled feedback loop that examines the force (bending of the cantilever) and tells the piezoelectric device whether to move the sample closer to further away in order to maintain the set force value. The AFM image produced by taking the feedback signal at each pixel of the raster scan is a measured of the topography of the sample. Tip-sample force depends on the nature of the samples, the distance between the probe and sample, the probe geometry and in any contamination on the sample surface. The AFM can be divided into two primary scanning modes: contact and noncontact, which simply refers to whether or not the scanning probe actually comes into physically contact with the sample surface. The contact mode takes advantage of Van der Waal's attractive forces as surfaces approach each other and provides the highest resolution. In the non-contacting mode, a vibrating probe scans the surface at a constant distance and the amplitude of the vibration is changed by the surface morphology.

As there is no current flow, the AFM can be used on electrically conductive or non-conductive surfaces and in air, vacuum, or a fluid environment. AFM is capable of visualizing and imaging surface features as small as a carbon atom (.25nm) and as large as the cross section of a human hair (80 μm) depending the resolution of the particular instrument. Tradition microscopes have only one measure of resolution, the resolution in the plane of an image. An atomic force microscope has two measures of resolution, the plane of the measurement and in the direction perpendicular to the surface. The in-plane resolution depends on the geometry of the probe that is used for scanning. In general, the sharper the probe the higher the resolution of the AFM image. Getting the maximum vertical resolution requires minimizing the vibrations of the instrument during measurement. By AFM, the surface roughness can be quantifying in many ways such as: Area R_a (Average Roughness), Area RMS (Root-mean-square roughness), Average Height (sum of all height divided by the number of data points), Maximum Range (Maximum peak-to valley range in the area). RMS roughness values have been measured in this study. Feature size and thickness of the film can be also be determined by the line analysis in AFM. In this work, the Pacific Nan Technology Nano-RTM AFM scanner was employed with a scan rate of 1 Hz, a scan area 3.25 μm x 3.25 μm and a resolution of 256 to perform the top surface morphology analysis and surface roughness of the coating on a silicon substrate using the contact mode. The NanoRule^{+TM} AFM image analysis software was used to analyze the image.

3.4.1.6. VIBRATIONAL SPECTROSCOPY

The mechanical molecular and crystal vibrations are at very high frequencies, which places them in the infrared (IR) region of the electromagnetic spectrum. Coupling between incident infrared radiation and the electronic structure of the chemical bond produces the infrared absorption spectrum as a direct means of observing molecular and crystal vibrations (FTIR). The Raman spectrum arises from an indirect coupling of high-frequency radiation (usually visible light, but also ultraviolet and near infrared) with the electron clouds that make up the chemical bonds. Although both IR absorption and Raman spectroscopy measure the vibrational spectra of materials the physics of the IR process is quite different from that of Raman spectroscopy (absorption instead of scattering), the information content is very similar. Both are characterization probes that are sensitive to the details of atomic arrangement and chemical bonding.

(a) Micro Raman Spectroscopy

Raman spectroscopy is primarily a structural characterization tool. It is a commonly used technique for analyzing molecular vibrational frequencies in carbon based materials which can be related to the strength of the inter atomic bonds. Thus, the different bond type in a material can be determined. The Raman spectrum is more sensitive to the lengths, strengths, and arrangement of bonds in a material than it is to the chemical composition. The Raman spectrum of crystals likewise responds more to details of defects and disorder than to trace impurities and related chemical imperfections. In Raman spectroscopy, a sample is irradiated with a strong monochromatic light source (usually a laser). Some of this light may be transmitted or absorbed by the sample (infrared studies). But most of the energy of the incident light (radiation) distorts the electron clouds that make up the chemical bonds in the sample, storing some energy. When the field reverses as the wave passes, the distorted electron clouds relax and the stored energy is released. Most of the released radiation energy will scatter at the same wavelength as that of the incoming laser radiation, a process known as Rayleigh scattering. However, a small amount, approximately one photon out of a million will scatter from that sample at a wavelength shifted from the original laser wavelength. This shift of wavelength is caused because of the light scattered due to vibrations in the molecules. Scattering in which the scattered photons have either higher or lower photon energy, is called Raman scattering. A schematic diagram of Raman spectroscope is shown in figure 3.29. The Raman spectrum for a sample is an expression of its vibrations. Individual peaks of this spectrum may be ascribed to particular phase of molecular groups within that sample. Since the peaks are a function of the energy of the scattered photons they correspond to the energies of the vibrational transitions or the frequencies of its vibrational modes.

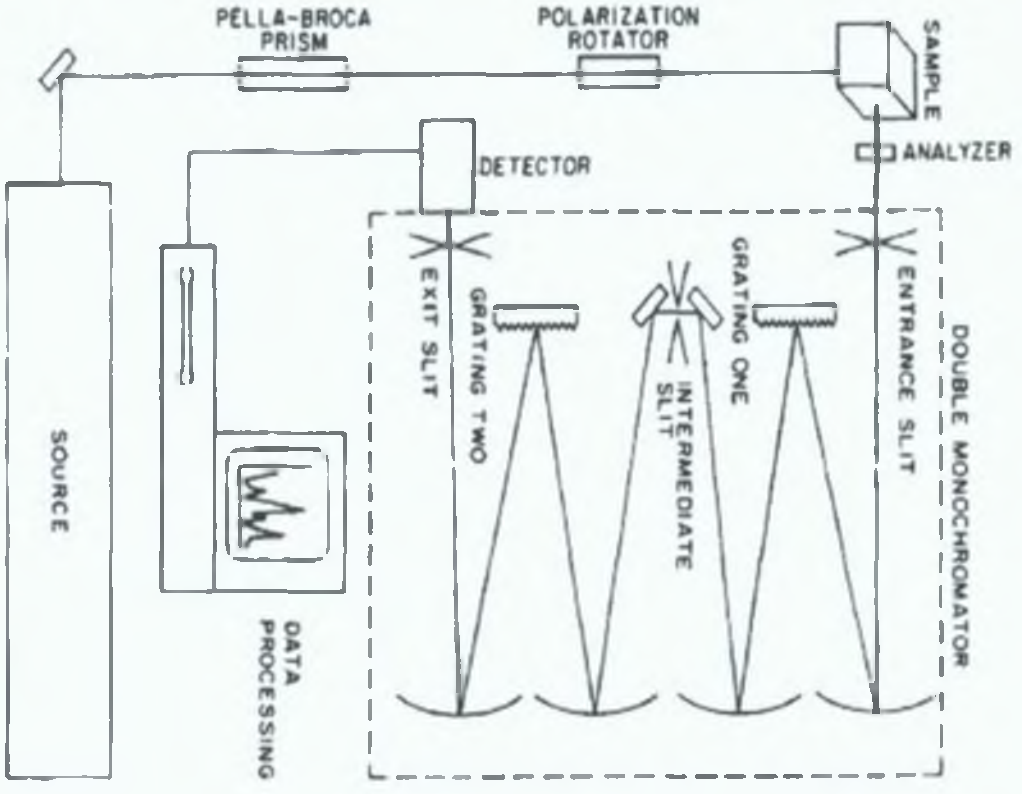

Figure 3.29: Schematic diagram of Raman spectroscope [291]

The spectra that can be produced are dependent upon the interatomic forces operating in that molecule. A sensitive measure of the structure and bonding is provided by analysis of the positions, symmetries and relatives intensities of individual peaks. Importantly, a samples vibrational spectrum is the characteristic of those species/molecules/samples. Thus Raman experiments are principally studies of the vibrational behavior of molecular systems. The Raman spectrum has axes of intensity and wave number, whose units are cm^{-1}. This unit is most commonly employed and describes the frequency, or Raman shift from the frequency of the incident monochromatic laser light. When the laser encounters a molecule, vibrational energy of the different bonds in molecules will be different and different bonds will vibrate at different frequencies. The vibrational frequencies of crystal and molecules lie between 0-5000 cm^{-1}. Routine analysis of materials usually concerns those vibrations with frequencies between 100-2000 cm^{-1}. In Raman, probe depth varies from μm to mm depending on materials and laser power used.

In this work, Micro-Raman measurements were performed in backscattering geometry using 488 nm Ar^{+} laser excitation at room temperature on a Jobin Yvon Libran HR800 μRS system equipped with a liquid nitrogen cooled CCD detector (wavenumber resolution = 0.4 cm^{-1}) to find out chemical bonding information of the film. With an Olympus MPlan 100_x microscope objective, the laser was focused on the sample surface to a diameter of approximately 1μm. All the Raman Spectra were registered with the same accumulation time of 10 s and averaged for 15 accumulations to increase the signal to noise ratio. Deconvolution of the Raman spectrum performed using Microcal (TM) origin software with a Gaussian/lorentzian peak fit.

(b) Fourier Transmitted Infrared Spectroscopy (FTIR)

The potential utility of infrared spectrophotometry (IR) is a function of the chemical bond of interest, rather than being applicable as a generic probe. The ratio of the intensity before and after the light interacts with the sample is determined. The plot of this ratio versus frequency is the infrared spectrum. The aim of the basic infrared experiment is to determine the intensity ratio I/ I_0 as a function of the frequency of the light (λ), where I_0 is the intensity of the light incident upon the sample and I is the intensity of the beam after it has interacted with the sample. A plot of this ratio versus the frequency is the infrared spectrum. The infrared spectrum is commonly plotted in one of three formats: as transmittance, reflectance, or absorbance. In this study, Raman result was verified with Fourier transform infrared spectroscopy (FTIR) measurement using a Perkin-Elmer 2000 system and measurement have been made in transmission mode. The scanning resolution was 1 cm^{-1}. All the scans were performed at room temperature and normal atmorpheric conditions.

3.4.2. PHYSICAL AND MECHANICAL PROPERTIES

3.4.2.1. THICKNESS

The thickness of a thin film and nitride layer on a substrate can be measured by large variety of different methods. In this work, the stylus profilometer and the ball cratering method have been used for measuring the thickness of the coatings and nitride layers.

(a) Stylus Profilometer

One of the most accurate methods of thickness measurement is to use a step-height measurement facility on a Stylus Profilometer-which of course necessitates leaving or producing an uncoated region, over which the step can be measured. A contact-type surftest Profilometer was used to evaluate film thickness easily by measuring the step increase between the uncoated substrate and the coated substrate. The procedure is the same as that in the measurement of surface roughness, which is measured along a single line profile, and is characterised as the arithmetic average of the heights of the peaks and troughs of the surface. The surface profiler measures the average height of the irregularities from the mean line along a specified sample length. The mean line is defined such that the areas between the surface profile above and below the mean line are equal. The stylus instrument amplifies and records the vertical motion of a stylus while moving at a constant velocity relative to the specimen surface. By positioning the stylus over the uncoated portion of the sample, and allowing it to traverse along a path such that it crossed the uncoated/coated boundary onto the coated sample side, a measure of the coating was given. However, it was found that the 'step' was not as sharp or well defined as anticipated. By this method surface roughness of the coated and uncoated sample also can be measured.

(b) Ball Crater

Ball cratering is a very simple method originally used for assessing the thickness of thin films. This is achieved by grinding a small crater in a coating with a ball of known geometry to provide a tapered cross-section of the film when viewed under an optical microscope. This method can be used for characterizing different type of properties for single layer, multilayer or graded layer coating [292,293]. Measurements of the resultant

crater can then be made to allow the calculation of the film thickness. Wear rate of coating can also be made using additional techniques. Examination of the crater can also give qualitative information on coating adhesion and interface condition.

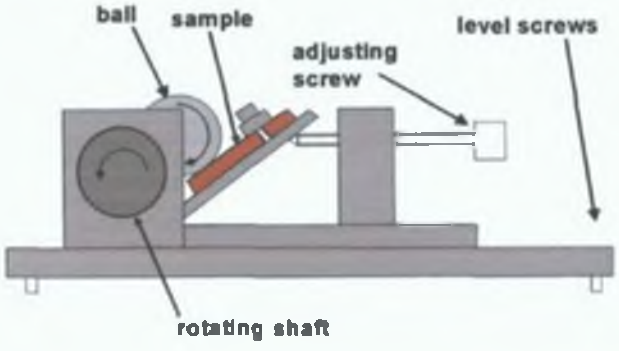

Figure 3.30: A schematic diagram of the side view of the Ball Crater device

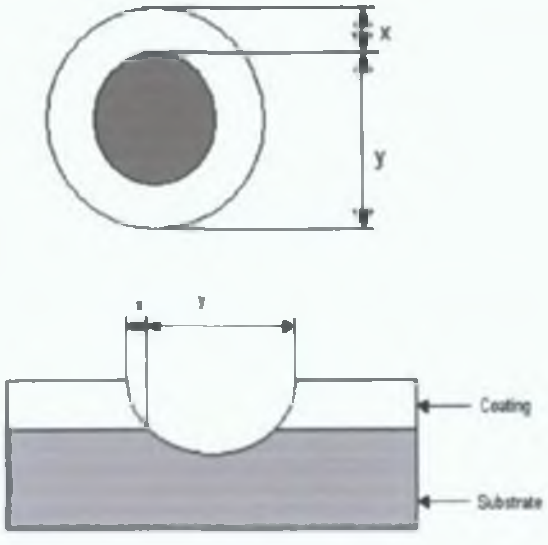

Figure 3.31: Schematic views of the ball crater apparatus and the crater profile.

Application to complex graded and multi-layered coatings allows the analysis of adhesion layers, layer colours, thicknesses and interfaces. Structural or compositional analysis of thin films can also be made using additional techniques such as Auger Electron Spectroscopy or Transmission Electron Microscopy. Schematic diagrams are shown in figure 3.30 of the side view of the device. In this work, a Teer bc-2 ball cratering device was used in

conjunction with the Reichert "MeFe2" Universal Camera Optical Microscope to measure the thickness of the coating and to reveal the graded layer structure.

(i) Coating Thickness Determination

Optical inspection of the depression reveals the projected surfaces of the abraded coating and substrate sections. By measuring the parameters x and y as shown in figure 3.31, the thickness of the coating t can be calculated by a simple geometrical equation (3.10)

$$\text{Thickness, } t = \frac{x.y}{\text{Ball diameter}} \quad \ldots\ldots\ldots\ldots\ldots\ldots \quad (3.10)$$

Where ball diameter = diameter of the ball used to make the crater (in microns).

(ii) Individual layer thickness determination

Layer thickness is determined in the same way as total coating thickness by measuring the distances x1, x2 and y1, y2, as shown in figure 3.32 in microns. The layer thickness is then given by the following equations (3.11 and 3.12). In this way individual layer thicknesses of graded, multilayer coating can be measured.

$$\text{Outer layer thickness, } t_{out} = \frac{x1.y1}{\text{Ball diameter}} \quad \ldots\ldots\ldots\ldots\ldots\ldots\ldots\ldots\ldots\ldots\ldots\ldots\ldots\ldots\ldots\ldots\ldots\ldots \quad (3.11)$$

$$\text{Middle layer thickness, } t_{mid} = \frac{x2.y2}{\text{Ball diameter}} \quad \ldots\ldots\ldots\ldots\ldots\ldots\ldots\ldots\ldots\ldots\ldots\ldots\ldots\ldots\ldots\ldots\ldots\ldots\ldots\ldots \quad (3.12)$$

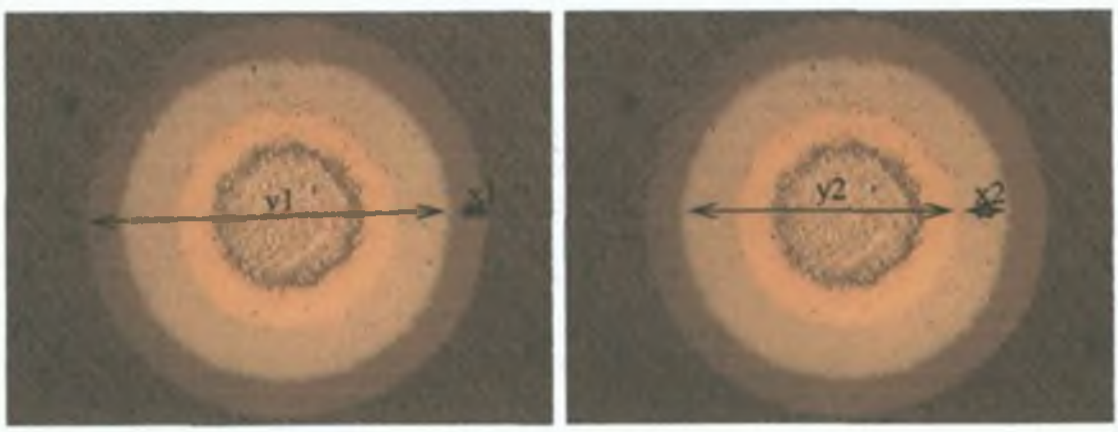

Figure 3.32: Measurements made to calculate individual layer thicknesses [292]

3.4.2.2 ROUGHNESS MEASUREMENT

(a) Optical Profilometer

Optical profilometer was also used for the measuring surface roughness of materials, as well as Stylus Profilometer. By this technique 3D/2D surface structure image can be extracted and by analyzing this image different topographical properties of the material can be measured. In this research, 3D/2D image and roughness of surface were measured using a WYKO NT1100 optical profilometer.

3.4.2.3. CONTACT ANGLE MEASUREMENT

Contact angle is a simple, rapid and sensitive method to measure the wettability and hydrophilicity (water attraction) of a solid surface.

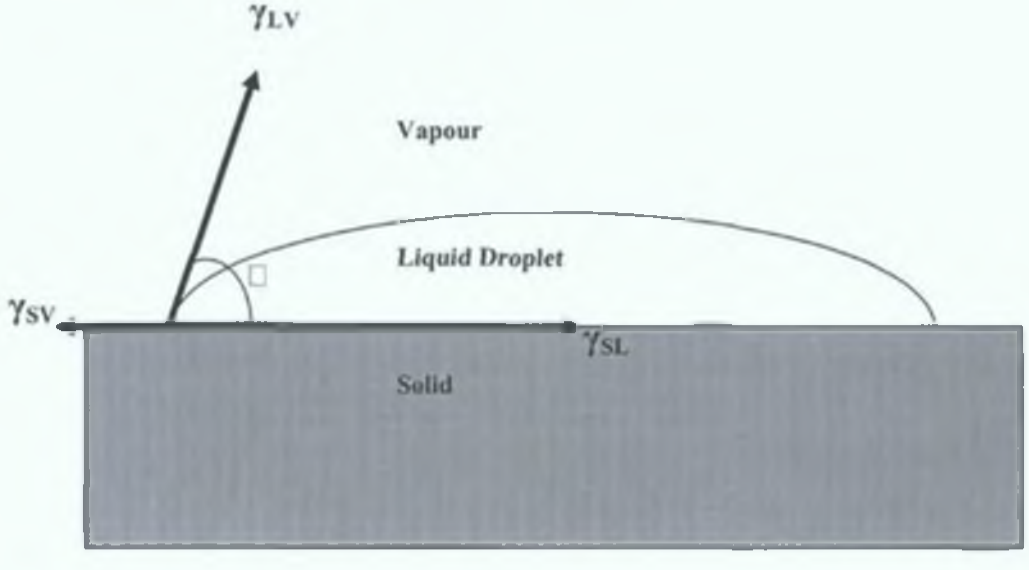

Figure 3.33: Schematic presentation of contact angle measurement. The resultant interfacial tension γ_{ij} are related to the contact angle, Θ, though young's equations (3.13). Where, L=Liquid, S=Solid; V=Vapour

Wettability, indicating the spreading of a fluid drop over a surface, is a measure of adhesion performance. This can be indicated by the water contact angle (Θ), which is taken as the angle between the sample surface, inside the drop and the tangent of the drop at the sample surface, as shown in figure 3.33. The drop of a liquid put on a solid surface will modify its shape due to the different surface/interfacial tensions, until equilibrium is reached and equilibrium can be represent by the Young equation (3.13) [294]. A smaller angle indicates better wettability and adhesion.

$$\gamma_{SV} - \gamma_{SL} = \gamma_{LV} \cos \theta \quad \text{..... (3.13)}$$

In this work, the wettability measurement was made using an OCA 20 Video-Based Contact Angle Meter from Dataphysics. The measurement of was carried out through the sessile drop method. For this measurement 1 microl. droplets of de-ionised water was left to sit on the solid substrate surface for 10 seconds before the contact angle was measured. A Sequence of images was obtained with a high-speed video camera mounted on a microscope starting from the moment of the drop deposition. The images were analysed by the software which automatically determines the contact angle between liquid and solid. These angles were measured at 18.4 °C. For each sample 3 contact angle measurements were taken and an average was then calculated.

3.4.2.4. HARDNESS MEASUREMENT

The hardness of a material is generally defined as its resistance to permanent indentation or a measure of a material's resistance to localized plastic deformation. The depth or size of the resulting indentation is measured, which in turn is related to a hardness number: the softer the material, the larger and deeper the indentation and the lower the hardness index number. Various techniques (Macro, Micro, and Nano and so on) have been developed to measure the hardness of the thin films and nitride layers and the choice of methods depends on the thickness and material of this layer. First microhardness tester was developed by Smith and Sandland in 1925 [295]. They designed a square-based diamond pyramid indenter with a face angle of 136°, whose geometry gave hardness numbers values identical to the Brinell numbers using a hardened steel ball. This fact made the Vickers hardness test widely accepted and very easy to implement. Microhardness is carried out at

extremely low loads of 5 grams to 100 grams depending on the thickness and hardness of the layer to be measured. The Vickers hardness number, H_v, is obtained as the ratio of the applied load to the area of the resulting indentation. With the given pyramid geometry the hardness is expressed as

$$H_v = 2\sin(\theta/2) * (P/d^2) \quad \ldots\ldots\ldots\ldots\ldots\ldots\ldots\ldots \quad (3.14)$$

Where θ is the angle between opposite faces of the diamond, P is the applied load in kg_f, and d is the indentation diagonal in mm. As the measured hardness value is largely dependent on the load range, it is therefore important to indicate in for every hardness measurement which load was applied. In order to account for the hardness-load dependence, several models [296-298] have been proposed for both bulk materials and coated samples. There are limitations when measuring the microhardness of nitride layers and especially thin films. It has also been stated [299] that if the substrate was indented more than one tenth of the overall thickness then the hardness values were thought to be substrate dependent. Care should be to taken when selecting the load for measuring the hardness of a thin layer. It is better to select a load as low as possible in the case of thin films and nitride layers. In this work, Vickers microhardness was measured for an average of 6-10 indentation per sample using a Leitz MiniLoad microhardness tester with a range of load 10-50 g (depending on the thickness and hardness of the tested materials). A 500 g load was used for toughness investigation of the coating.

3.4.2.5. FILM ADHESION

Adhesion of coating to the substrate is of primary importance in surface engineering applications. There are number of qualitative and quantitative method that can used to measure adhesion between the coating and substrate. Among them Rockwell C is a very simple method for quick qualitative measurement of adhesion.

(a) Rockwell C adhesion Tests

Rockwell indenters (Indentec 8150BK) in conjunction with the Reichert "MeFe2" Universal Camera Optical Microscope were used to measure the adhesion properties of thin films on steels. A number of papers have been reported to measure adhesion of the coating-substrate system using this method [300,301]. This test method is very easy to perform. The Rockwell-C adhesion test was developed in Germany and is standardized in the VDI guidelines [302]. A 120^0 sphero-conical diamond indenter (Brale) is used for Rockwell-C

adhesion test. The hardness tester (maximum applied load is 100 kg) causes layer damage adjacent to the boundary of the indentation. When the indenter penetrates the coating, cracks propagate from the indentation point. The comparative adhesion properties of the coatings can be determined by analysing the crack network from the indentation spot. After indentation an optical microscope with a magnification of 80X was used to evaluate the test. Three indentations were produced on each sample.

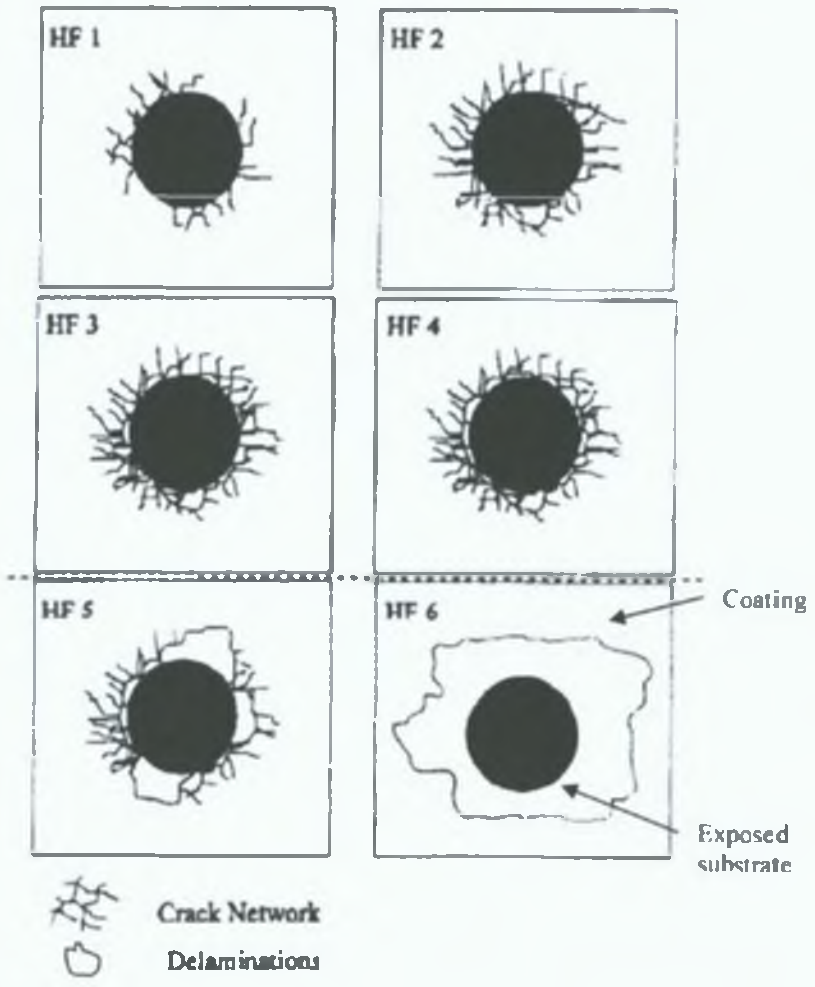

Figure 3.34: Adhesion strength quality HF 1 to HF 6. Where HF1 represents good adhesion with very few crack networks around the periphery of the indention and HF6 represents the worse adhesion with complete delamination of the coating near the edge of the indentation. [301].

The damage to the coating was compared with a defined adhesion strength quality shown in figure 3.34. A scale was considered from HF1 to HF6 showing the adhesion properties in a sequential way. HF1-HF4 defines a sufficient adhesion whereas HF5 and HF6 represent

insufficient adhesion (HF is the German short form of adhesion strength). HF1 shows excellent adhesion properties with a few crack networks while HF6 shows the poorest adhesion properties showing complete delamination of the film.

3.4.2.6. WEAR PROPERTIES MEASUREMENTS

Tribological properties of materials, such as friction co-efficient, wear rate/depth, wear track topography and so on, can be measured by a tribometer (Pin-on-disk) following the ASTM G-99-90a standard in conjunction with a profilometer, optical microscope, ball crater, and so on.

(a) Pin-on-disk

The Pin-On-Disc wear tester uses a high torque drive motor to rotate a flat sample under a loaded wear pin. The wear pin is a 3 mm diameter ball made either from Cr steel, WC, and so on. The wear pin creates a circular wear track of the required diameter by offsetting the pin relative to the sample's centre of rotation. The sliding motion of the sample under the wear pin provides a frictional force which is a property of the film and is proportional to the load applied. Different wear track diameters allow a number of tests to be performed on one sample. The same linear speed can be used for all tests by adjusting the rotational speed for each diameter. The frictional force is detected by a load cell and the analog friction output signal is transmitted to the computer where it is detected. Examination of the resulting plot of friction versus time gives an indication of the friction characteristics and endurance of a particular coating. Information on the pin/disk material can be entered into the computer for Hertzian pressure calculation between the pin and disk. The load can be varied by adjusting the amount of dead weight hung at the loading beam. The test can be carried out under dry or lubricated conditions. The control of the test parameters such as speed, frequency, contact pressure and time, and environmental parameters such as temperature, humidity and lubrication allow a close reproduction to the real life conditions of practical wear situations.

Test method

The coated sample is positioned on the sample table. A schematic view of pin-on-disk testing machine is shown in figure 3.35.

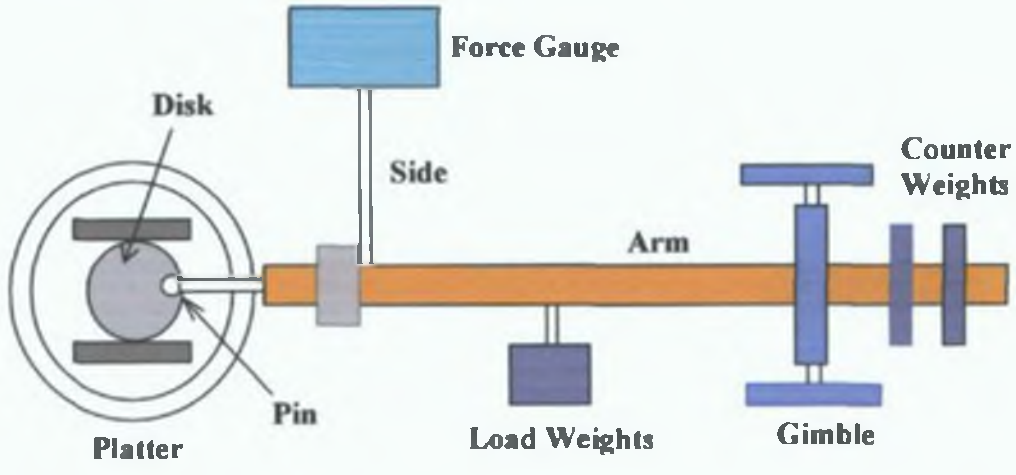

Figure 3.35: Schematic view of main components of Pin-on-desk tester

The following parameters are selected before staring testing; the maximum number of revolutions (which determines the test duration), load applied, track diameter and the rotation per minute, R. P. M, (which controls the sample speed of rotation). Before a test is started, it is essential that the ball surface is clean and free from debris is essential. This is ensured by moving the wear pin (ball) in its holder until a clean surface can be seen under a microscope. The ball holder is then tightened to ensure no movement of the ball during testing. Once the diameter and the load of the test are selected the loading beam is lowered until the ball is in contact with the coated sample. The test is then started through the computer and data acquisition begins. After the pin on disc test is completed the computer displays a graph of the friction against time. The graph is automatically saved to the hard disc during the test. The recorded data can be further processed after the end of the test. In this research, the pins on disk wear tests were carried out using an Implant Sciences ISC-200PC tribometer. It is a device for measuring the wear on a material's surface and it is consists of a tribometer and a computer for data acquisition. The pin-on-disk test involves rotating either the disk or the pin. The pin and disk are in contact with each other (above), so the rotation creates a wear groove on the surface of the disk. The system can be used to measure the coefficient of friction, the wear behaviour between materials, and the integrity

of thin films or coatings. The ISC tribometer was originally developed by Lewis Research Center as an in-house wear test apparatus.

Figure 3.36: Implant Science Corporation ISC-200PC Tribometer (Pin-on-disk) for friction measurement

Before wear tests, the ball and the disk specimens were cleaned with ethanol to remove any remaining contaminants. Samples were tested for 2500-20,000 revolutions at a speed of 85-60 rpm, a range of loads (50-200g) on a 3 mm diameter tungsten carbide ball (pin) and a cylindrical track diameter of 7-10 mm in laboratory air (40-50 % RH) and room temperature (25 ^{0}C) depending on the material of the tested sample. A picture of the standard pin-on-disk machine used in this research is shown in figure 3.36. The test was carried out under dry or unlubricated conditions. The friction coefficients were continuously recorded in the hard disk. The morphology of the wear track was observed by the Reichert "MeFe2" Universal Camera Optical Microscope (2D) as well as by WYKO NT1100 optical profilometer (2D and 3D). Optical profilometry was carried out across the wear track on each sample at ten different locations in order to measure the wear depth and width. The wear rate can be determined by measuring the wear volume or wear depth. EDX analyses were performed on the wear track to find out the composition of the worn surfaces. The wear lifetime of the sample coating was defined by observing the point at which friction coefficient value to raise abruptly that of the substrate.

CHAPTER 4: RESULTS AND DISCUSSION

4.1. INTRODUCTION

In this chapter, the results of the simulation work, plasma nitriding and duplex coating experimental work are presented and discussed. Gas flow simulation results are presented in the sub-section 4.2.1 of this chapter. In sub-section 4.2.2, the generation of thermal stresses in graded and single layer coatings are discussed to see the advantage of using a graded layer design. Then detailed results regarding the plasma nitrided of different materials are presented and discussed in section 4.3. A result relating to the possibility of applying the plasma nitrided system as a duplex coating process is discussed in section 4.4. In the last section of this chapter, a summary of the results and discussion of the simulation work, plasma nitriding and duplex coating experimental work are presented.

4.2. SIMULATION WORK

4.2.1. GAS FLOW SIMULATION

4.2.1.1. VELOCITY PROFILE

The velocity contours of Ar and N_2 gases are shown in figure 4.1(a). Gases were introduced into the deposition chamber through the Ar and N_2 inlets and transferred inside the chamber as a result of the pressure difference. It was observed that the velocity of the gases was higher near to the inlet and it became smaller away from inlet region. This was due to a sudden expansion of gases from a small inlet into a large chamber volume. Velocity was also found to be higher at the outlet area due to the suction effect of the low pressure. The pressure at the outlet is lower than at any other point of the chamber as a result the flow is driven through the outlet, as shown in figure 4.1 (b). Near the outlet, the flow approached fully developed (Parabolic) and the velocity was found to be higher in the centre line of the outlet. The same type of flow was also found near the inlet.

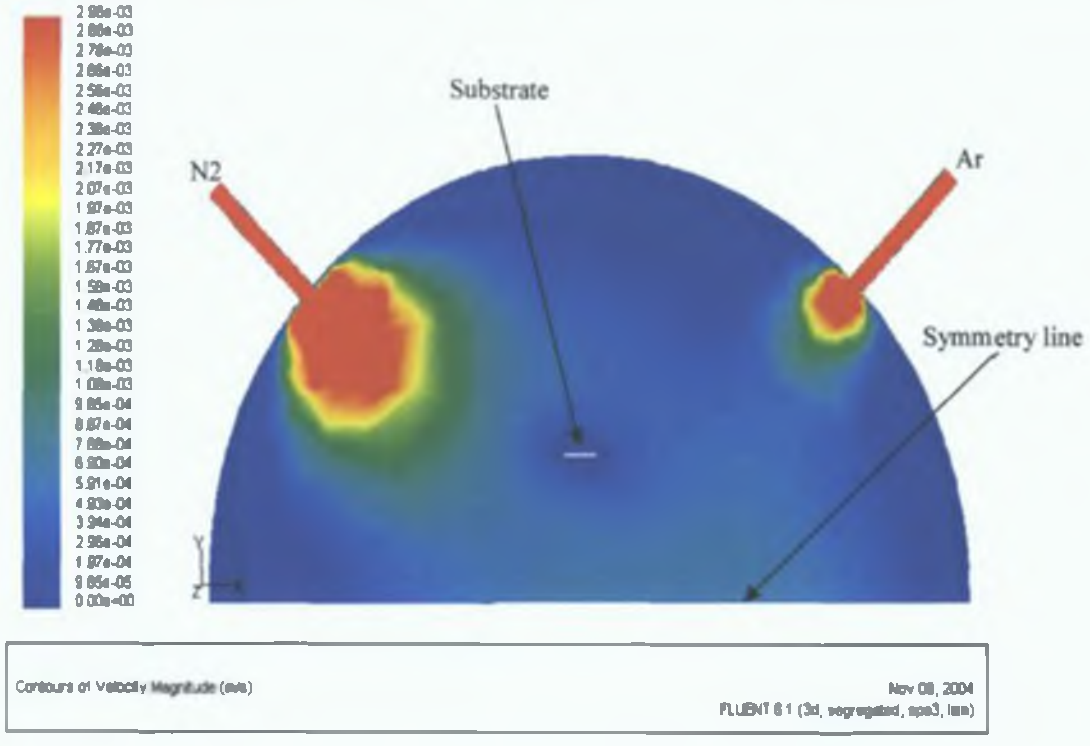

(a)

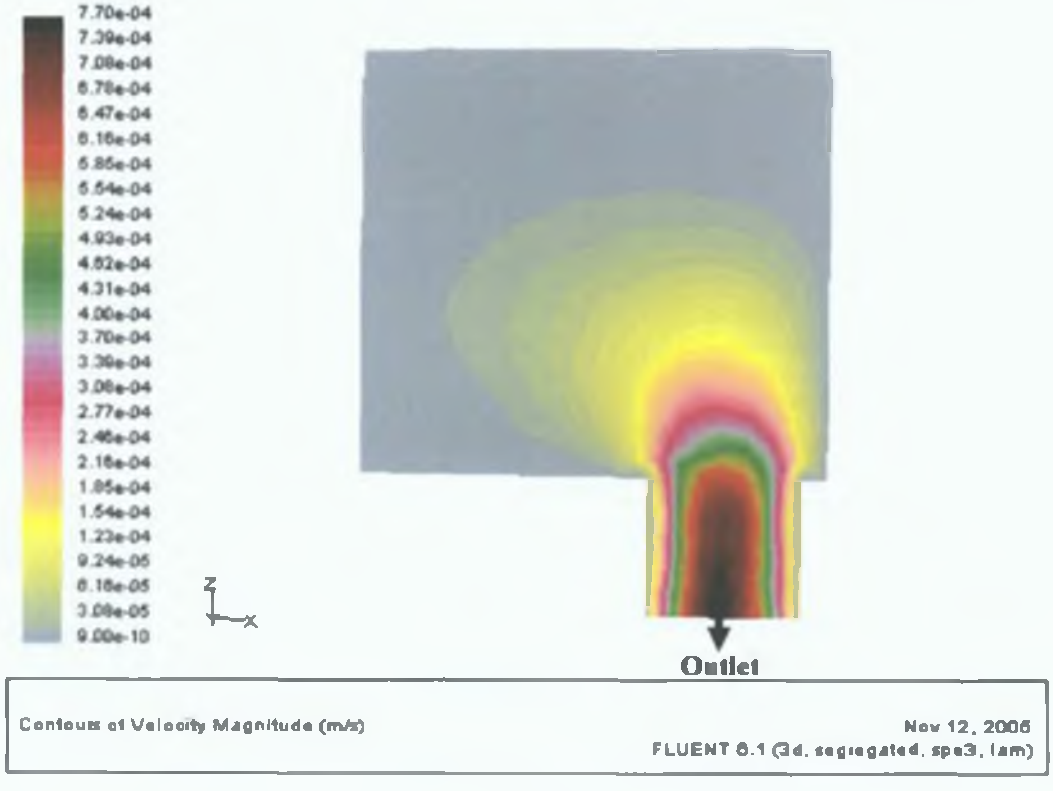

(b)

Figure 4.1: Velocity magnitude contour of the Ar and N_2 gas mixture at (a) plan though inlets and (b) symmetry plan

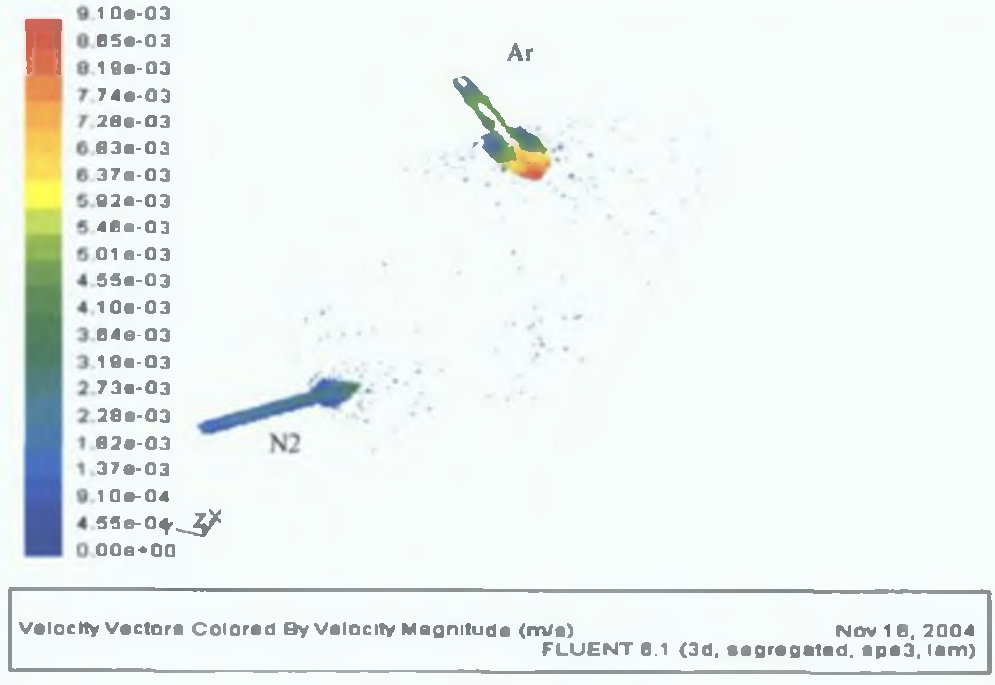

(a)

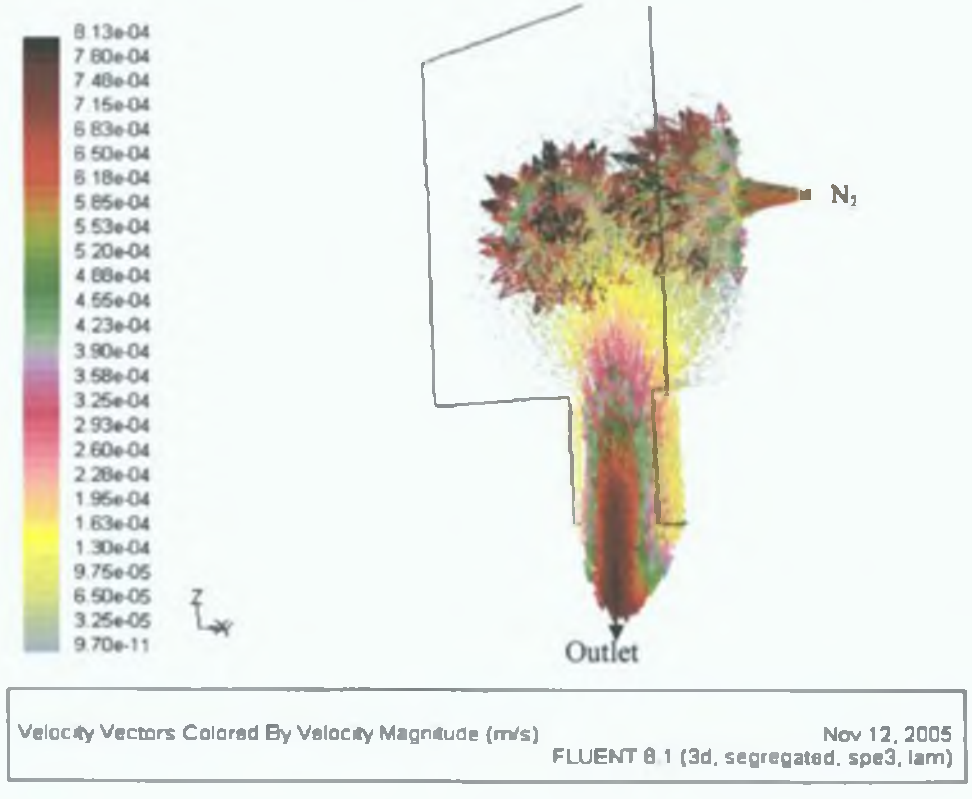

(b)

Figure 4.2: The velocity vector contour of the gas mixture on (a) plan though inlet and (b) symmetry plan.

It was observed that a gas circulation zone was created around the substrate surface, as shown in figure 4.1 (a), and the flow of gases was directed parallel to the substrate surface (towards the outlet). The gas the velocity was recorded to be very low near to the substrate surface.

The velocity vector contours of the Ar and N_2 gases are shown in figure 4.2. The velocities are illustrated by arrows whose length is proportional to the speed of the gas and whose orientation indicates the directions of flow. No backflow was observed at either the inlet or outlet. The velocity was found to be low near to the chamber wall and substrate surface. As the boundary layer grows, the flow near the wall is retarded by viscous friction. Sloping arrows were observed in the near wall region close to the outlet. This sloping indicates that the flow in the near-wall region slowed down as a result of an injection of fluid into the region away from the wall. Thus in order to satisfy mass conservation, the velocity outside the boundary layer increases.

Figure 4.3: Pressure contour of the chamber

4.2.1.2. PRESSURE PLOT

Higher pressure was observed at the inlets (a higher positive velocity region) as pressure is proportional to the velocity at any point. As the velocity of the argon inlet was higher compared with the nitrogen inlet, higher pressure was found at argon inlet, as shown in figure 4.3.

4.2.1.3. MASS FRACTION

Figure 4.4 (a) and (b) shows the mass fraction pattern of nitrogen and argon gas respectively at a plane through the inlet where the substrate was placed in front of the nitrogen inlet. The nitrogen concentration is seen to be higher nearer to the inlet.

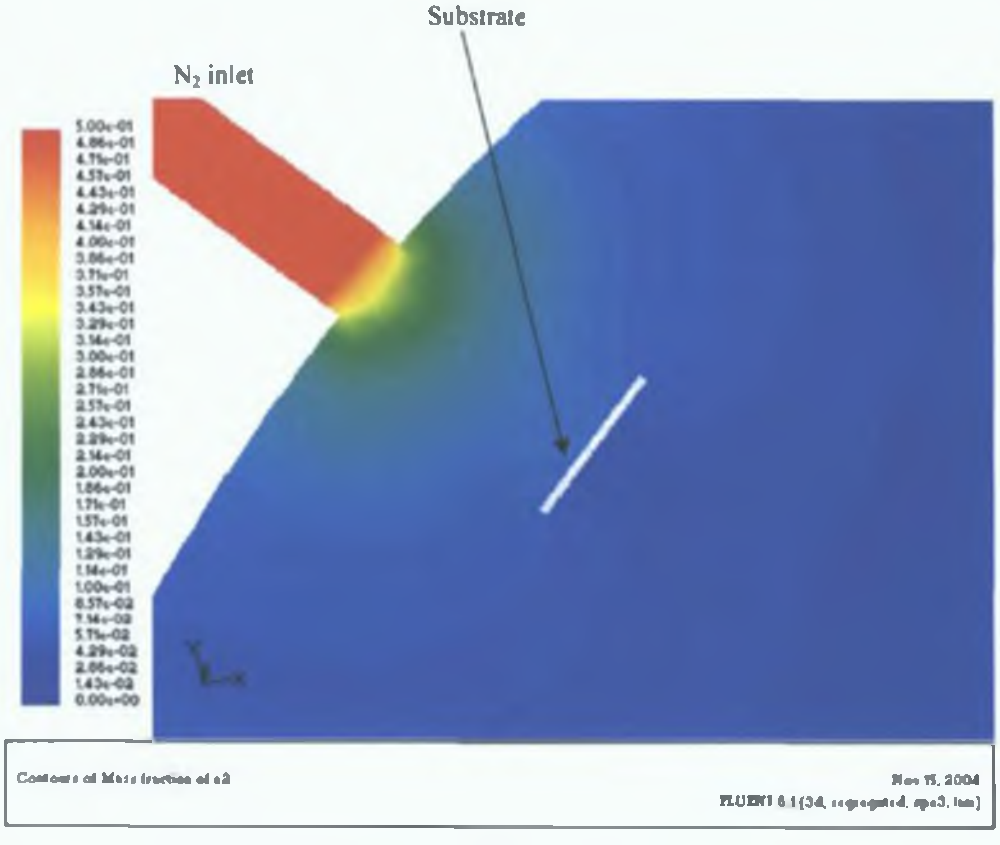

(a)

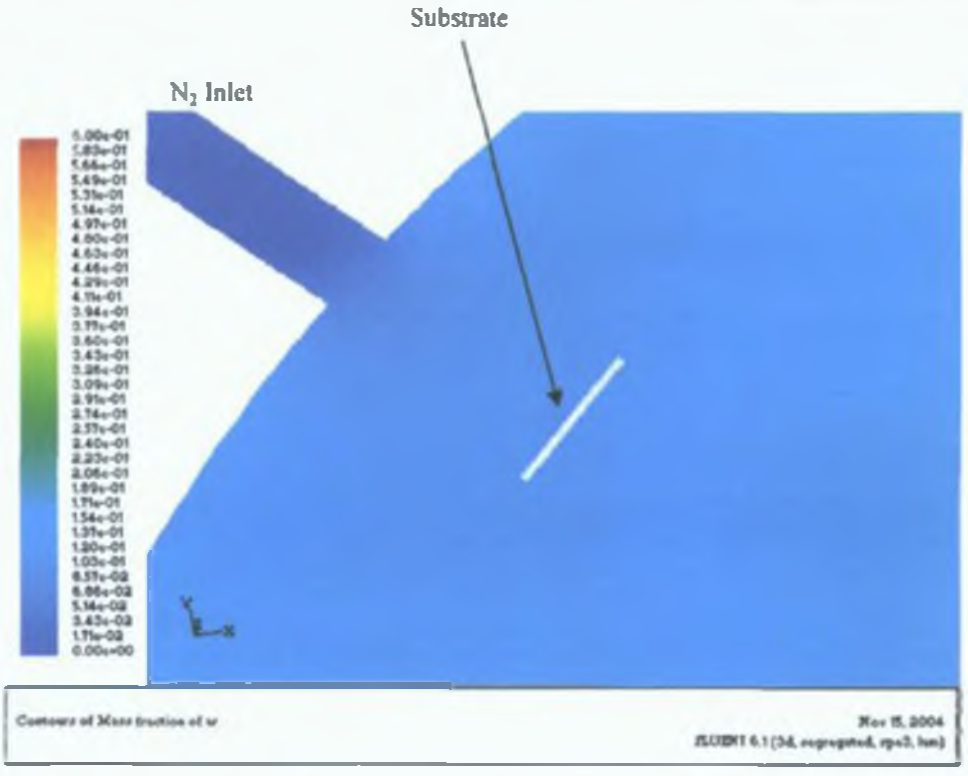

(b)

Figure 4.4: Mass fraction contour of the (a) nitrogen and (b) argon gas at plan though N2 inlets. Substrate was placed 40 mm distance away from chamber wall and faced infront of the nitrogen inlet.

Nitrogen concentration was found to decrease with increasing distance from the inlet in expanding wave pattern until it reached the substrate surface. Higher nitrogen concentration could be observed at the middle of the substrate surface than at the edges. On the contrary, argon concentration was found to be lower near to the nitrogen inlet and started to increase away from the inlet.

4.2.1.4. EFFECT OF SUBSTRATE POSITION AND TEMPERATURE

In most cases, two important properties need to be considered for successful deposition of TiN, TiCN coatings, these are stoichiometry and uniformity. The ultimate performance of the coating more or less depends on these properties. To deposit a stoichiometric and uniform coating, a minimum amount of reactive gas/species needs to be supplied homogeneously on the substrate surface. To achieve this goal, different substrate

positions were considered to see its effect on the N_2 mass fraction distribution and concentration on the substrate surface.

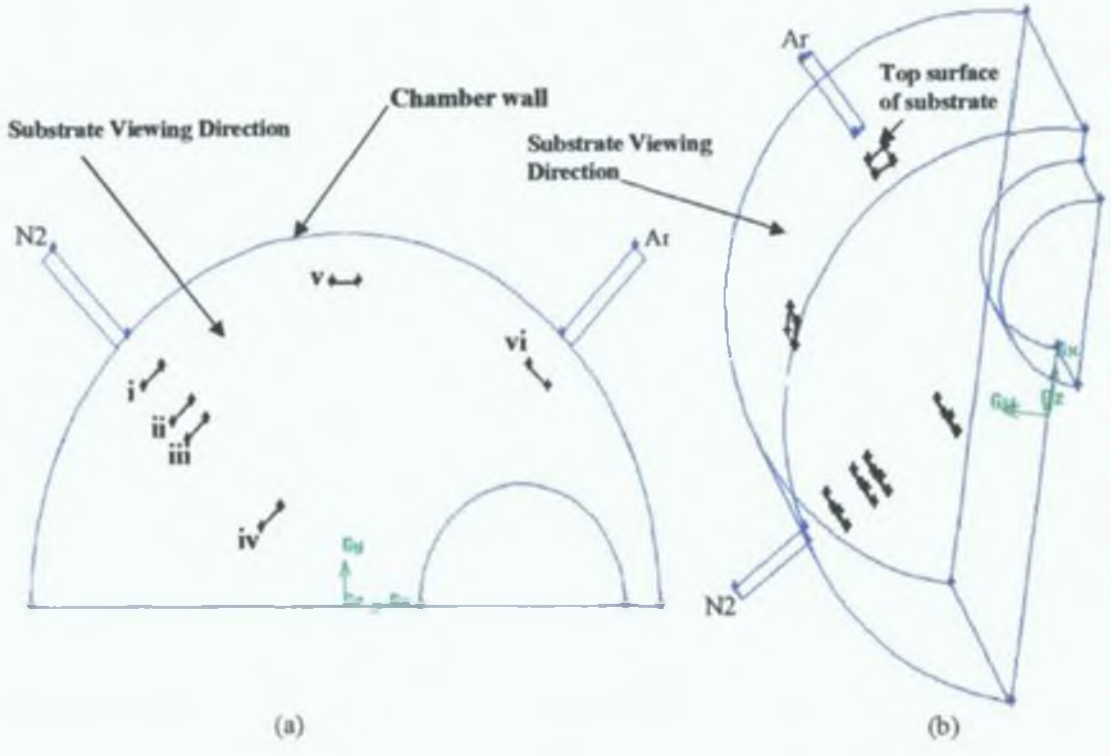

Figure 4.5: Different substrate position inside deposition chamber (during analysis one substrate have been taken at a time) to see there effect on the mass fraction distribution, (a) top view and (b) 3D view.

The substrate positions were investigated as shown in figure 4.5. Where points i, v and vi are the positions of the substrate (located 40 mm away from the chamber wall), faced in front of, the nitrogen inlet, the chamber wall at the middle of two inlets and the argon inlet respectively. Whereas points i, ii, iii and iv are the positions of the substrate located 40 mm, 80 mm, 120 and 200 mm away from the chamber wall respectively and faced in front of the nitrogen inlet. A summary of the maximum, minimum and differences in the mass concentration of the nitrogen gas on the substrate surface at different substrate positions of the substrate and temperatures is given in table 4.1. These results give an indirect indication of the nitrogen concentration and uniformity in coating over the substrate surface.

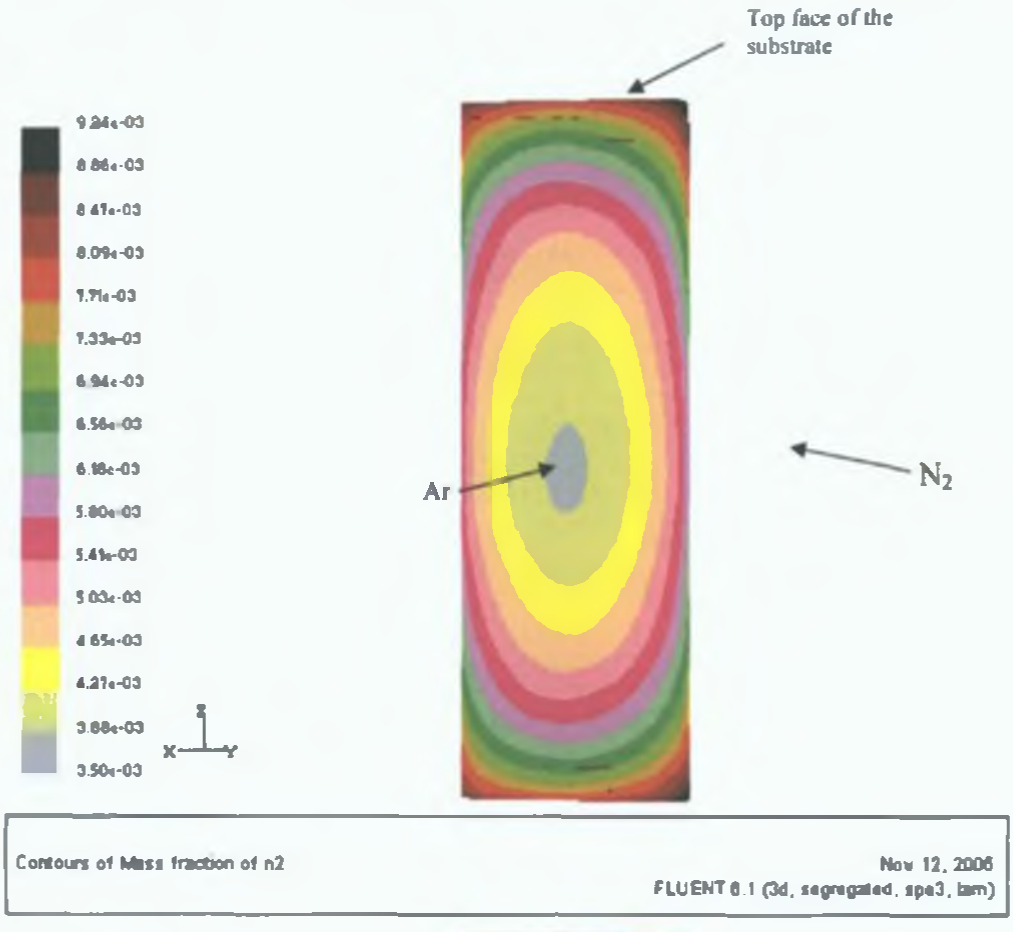
Top face of the substrate
Ar
N_2
Contours of Mass fraction of n2
Nov 12, 2006
FLUENT 6.1 (3d, segregated, spe3, lam)

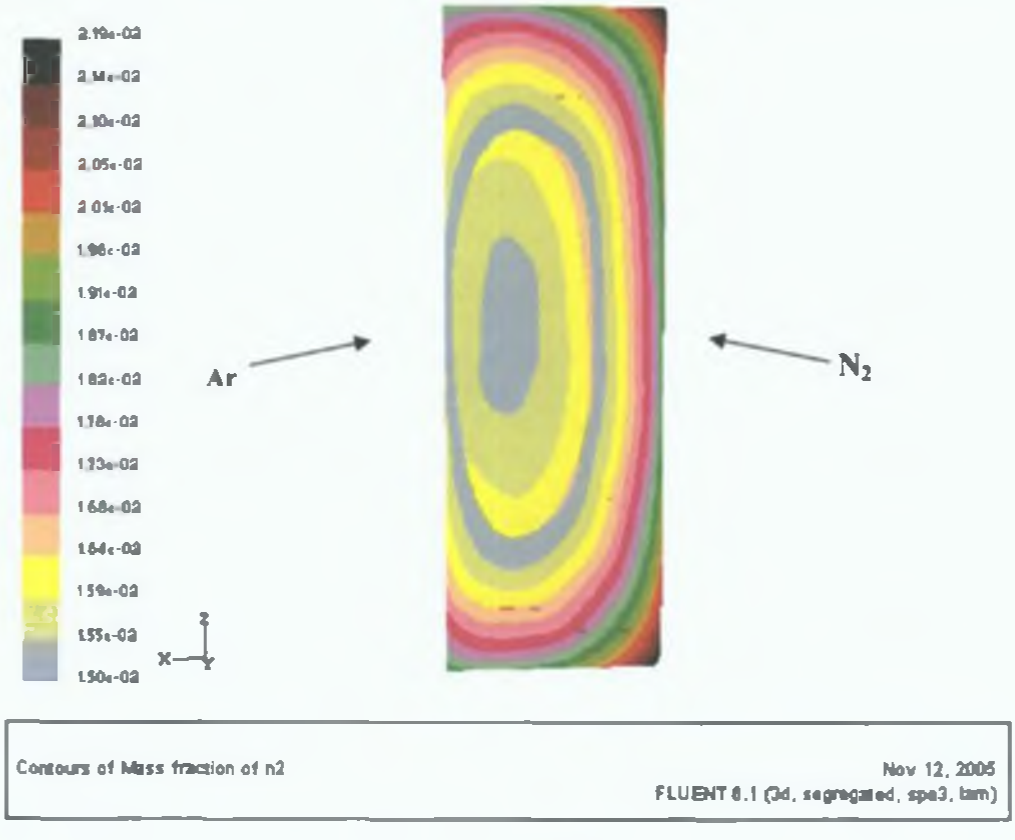
Ar
N_2
Contours of Mass fraction of n2
Nov 12, 2006
FLUENT 6.1 (3d, segregated, spe3, lam)

(b)

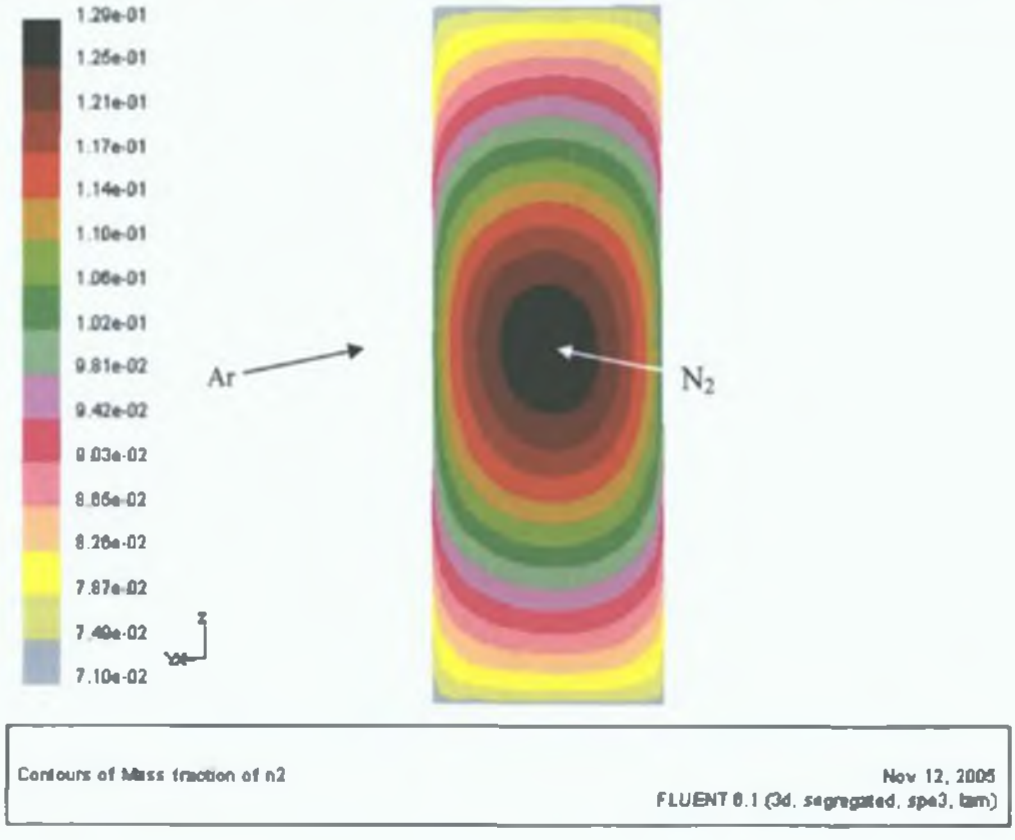

(c)

Figure 4.6: Mass fraction contour of nitrogen gas at the substrate surface placed 40 mm distance away from chamber wall and faced infront of (a) the argon inlet, i (b) the chamber wall at the middle of two inlets, v and (c) the nitrogen inlet, vi. Where, i, v and vi are the postion of the substrate as shown in figure 4.5. Substrate viewing direction is also shown in figure 4.5. Arrows indicates relative flow direction of the Ar and N2 gas with respect to substrate.

(a) Substrate placed at different positions inside the chamber but at a fixed distance from the chamber wall

When the substrate was placed in front of the argon inlet (postion vi), the concentration of the reactive nitrogen gas was found to be low at the middle of substrate compared to the edges, as shown in figure 4.6 (a). This can be attributed to the strong flow of the argon at the middle of the substrate hindering penetration of the nitrogen in the middle of the substrate. This would be not a perfect position for deposition of stoichiometric coating, as the maximum concentration that could be attained, was very low (0.00924).

Again, when the substrate was in front of the nitrogen inlet (position i) as shown in figure 4.6 (c), the nitrogen concentration on the centre of the substrate surface was found to be approximately 0.129, which was very high compared with the concentration of the edge (0.0710). It may be due to the weakening of the flow of nitrogen, at the edge by the dominating Ar flow. This difference caused a very significant variation in concentration (0.058) over the substrate surface compared with all other substrate locations. Therefore, this location was not suitable for uniform coating deposition. On the contrary, nitrogen gas concentration was found to be more uniform over the substrate surface compared with position (i), when the substrate was placed in the middle between the argon and nitrogen inlets (position v), as shown in figure and table 4.1. It was also observed that in this position, (v), nitrogen concentration was much higher than in position, (vi). This result indicated that the location of the substrate in middle between the inlets is the optimum position (v) for getting a uniform and stoichiometric coating.

Table 4.1: Maximum, minimum and differences in mass concentration of nitrogen on the substrate surface for different substrate positions and temperatures. Where, i-vi represented the position of the substrate as shown in figure 4.5.

Position of substrate	Substrate distance from the chamber wall (mm)	Testing temperature (K)	Maximum mass concentration	Minimum mass concentration	Difference in concentration (maximum-minimum)
In middle between Ar and N_2 inlet (v)	40	300	0.0219	0.0150	0.0069
In middle between Ar and N_2 inlet (v)	40	773	0.0307	0.0189	0.0118
In front of Ar (vi)	40	300	0.00924	0.00350	0.00574
In front of N_2 (i)	40	300	0.129	0.0710	0.058
In front of N_2 (ii)	80	300	0.0565	0.0487	0.0078
In front of N_2 (iii)	120	300	0.0389	0.0353	0.0036
In front of N_2 (iv)	200	300	0.0272	0.0215	0.0057

(b) Substrate placed at different distances from the chamber wall but fixed infront of the nitrogen inlet

From this analysis it was observed that the concentration of nitrogen on the substrate decreased if the substrate to chamber wall distance was increased (maximum mass concentration at 40 mm = 0.129 and at 200 mm = 0.0272), as shown in figure 4.7 and table 4.1.

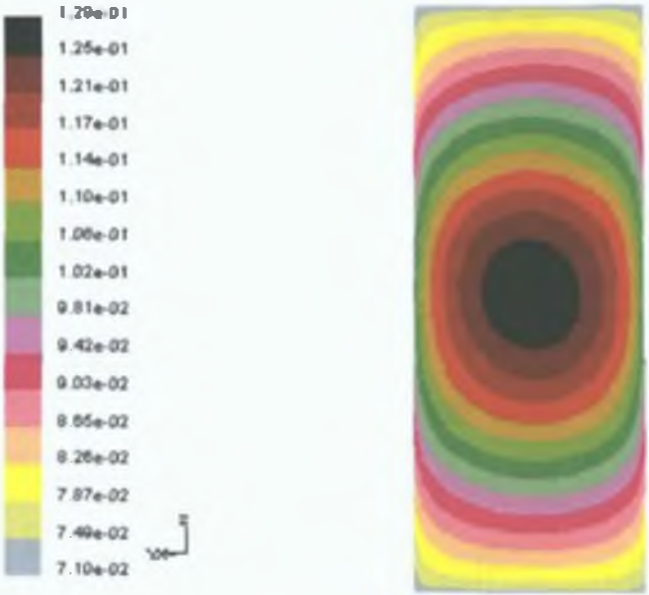
1.29e-01
1.25e-01
1.21e-01
1.17e-01
1.14e-01
1.10e-01
1.06e-01
1.02e-01
9.81e-02
9.42e-02
9.03e-02
8.65e-02
8.26e-02
7.87e-02
7.49e-02
7.10e-02
Contours of Mass fraction of n2
Nov 12, 2006
FLUENT 6.1 (3d, segregated, spe3, lam)

(a)


5.65e-02
5.60e-02
5.55e-02
5.49e-02

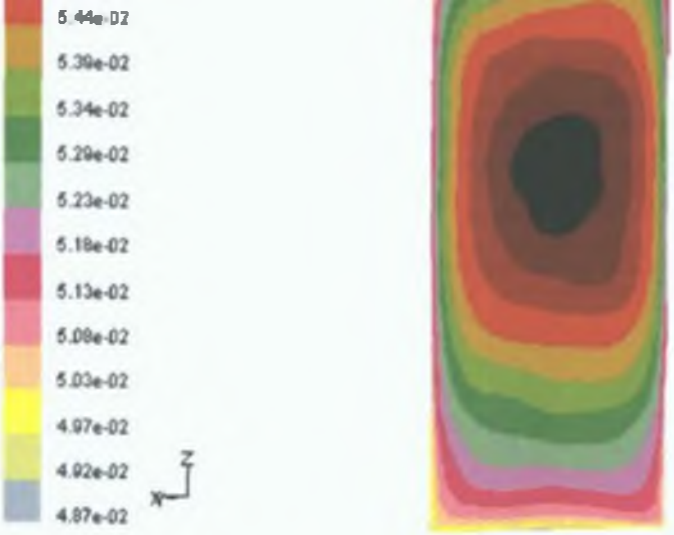

Contours of Mass fraction of n2

Nov 12, 2006
FLUENT 6.1 (3d, segregated, spe3, lam)

(b)

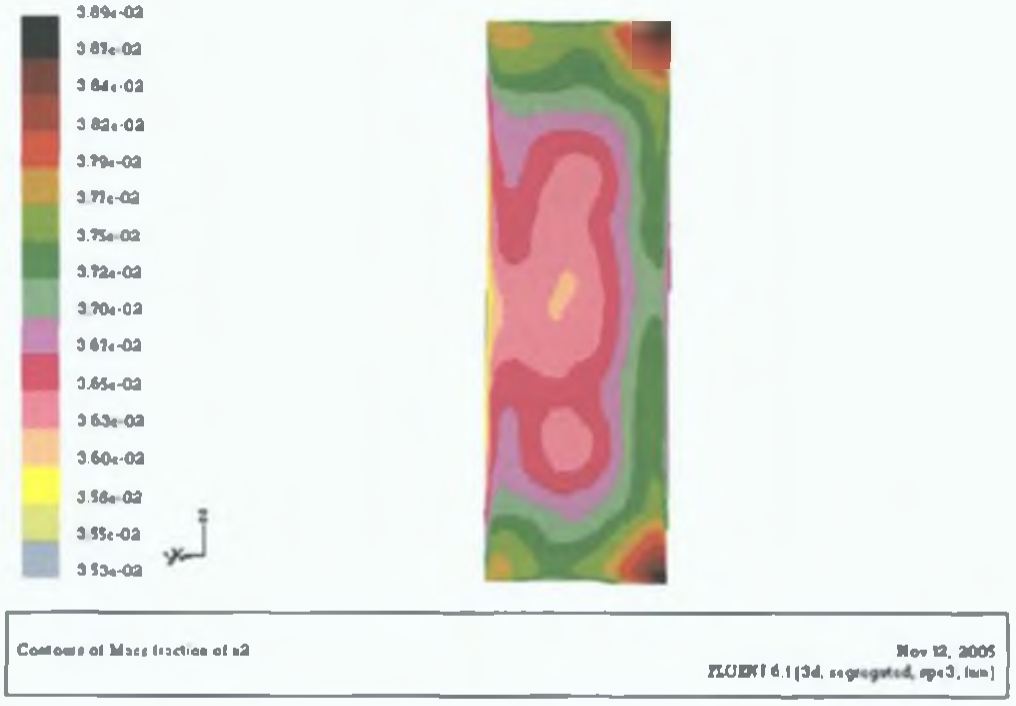

(c)

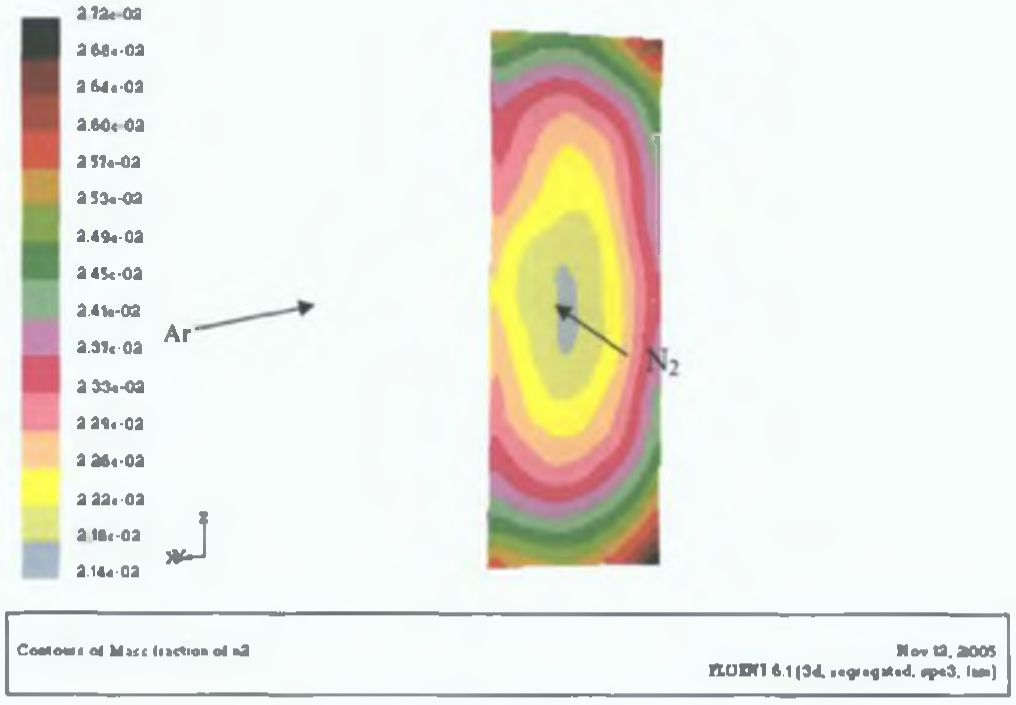

(d)

Figure 4.7: Mass fraction contour of the nitrogen gas at the substrate surface when placed, (a) 40 mm, i (b) 80 mm, ii (c) 120, iii (d) 200 mm, iv distance away from chamber wall and faced infront of the nitrogen inlet. Where, i, ii, iii and iv are the postion of the substrate as shown in figure 4.5. The substrate viewing direction is shown in figure 4.5.

This can be explained by the weakening of the nitrogen flow at a greater distance from the chamber wall causing enhanced mixing of gases in to with other. However, nitrogen concentration became uniform when the substrate was moved away from the chamber wall (mass concentration difference at 40 mm = 0.058 and at 200 mm = 0.0057) at the expense of mass concentration. This may be due to the increased in mixing capability of Ar and N_2 gases at a distance far from the chamber wall as a result of the decrease in the dominating flow nature of nitrogen gas near the N_2 inlet. When the substrate was placed near to the chamber wall a higher nitrogen concentrate was found at then centre of the substrate and a lower concentration on the top and bottom of the substrate surface as shown in figure 4.7. However, interestingly this trend changed when the substrate to the chamber wall distance was increased. The nitrogen concentration was observed to decrease at the centre of the substrate surface and increase at the edges. This analysis confirmed that the distance of the substrate from the chamber wall has considerable influence on the mass concentration and uniformity of the coating as well.

(c) Effect of substrate temperature on the N_2 mass fraction distribution on the substrate

To study the effect of the substrate temperature on the mass concentration and distribution, two different temperatures have been considered, room temperature (300K) and deposition temperature (773 K).

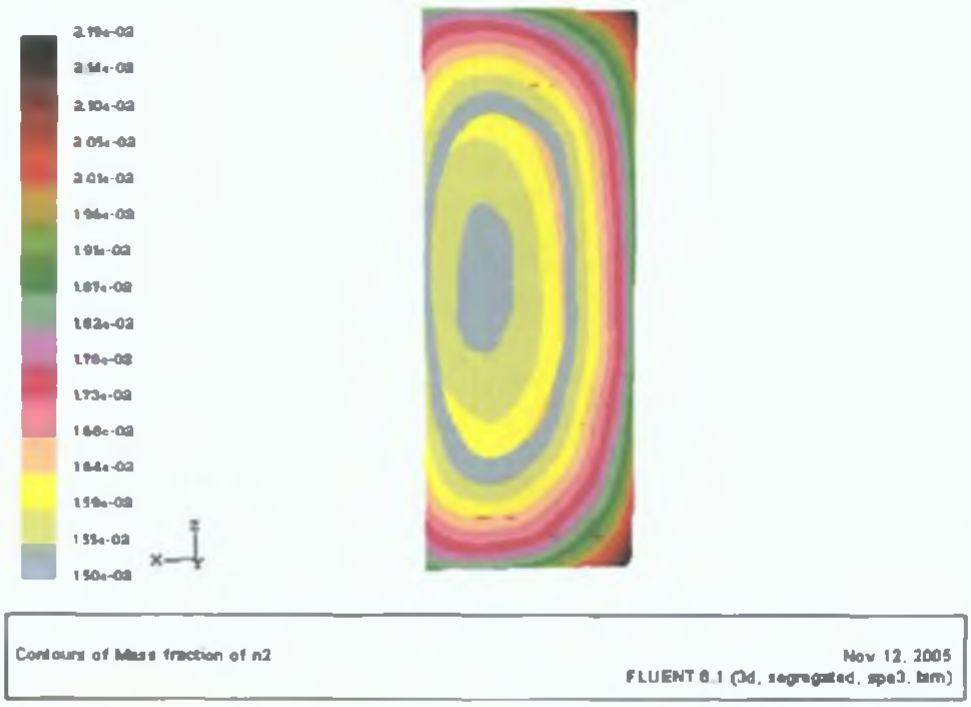

(a)

(b)

Figure 4.8: Mass fraction contour of nitrogen gas at the substrate surface placed 40 mm distance away from chamber wall and faced infront of the chamber wall at the middle of two inlets, v, with the substrate at (a) room temperature (300K) and (b) deposition temperature (773 K). Where, v is the postion of the substrate as shown in figure 4.5. The substrate viewing direction is shown in figure 4.5.

This study confirmed that the temperature has an effect on the mass concentration at the substrate surface. A higher mass concentration was attainable at a higher substrate temperature with almost the same gas distribution as shown in figure 4.8. An increase in the mass concentration at substrate surface at high temperatures may be attributed by the higher mass diffusivity of the gases at higher temperatures. The maximum mass concentrations found for the 300K and 773K temperature samples were 0.0219 and 0.0307 respectively.

4.2.1.5. VERIFICATION OF THE MODEL

As there are no experimental facilities in DCU and data relating to gas mixture inside the vacuum chamber, mass imbalance and velocity profiles were used to verify the model. It was observed that the total mass flow rate at the inlets was almost the same as that at the outlet. Velocities along the thickness of inlet and outlet were given a parabolic profile. It was also found that the velocity was fully developed at a certain distance from

the inlet or outlet positions. This result was also compared with ANSYS software (CFD Flotran) which afforded almost the same result. All of these results confirmed the validity of the model.

4.2.2. THERMAL STRESS SIMULATION

4.2.2.1. PARAMETRIC STUDIES

In order to examine the effects of the parameters on thermal stress generation within the coatings (maximum Von Mises stress in the coating), several sets of analyses were performed on the single layer coatings by varying one parameter and holding the other parameters constant and comparing them with the general equation of thermal stress (equation A.9 in appendix chapter).

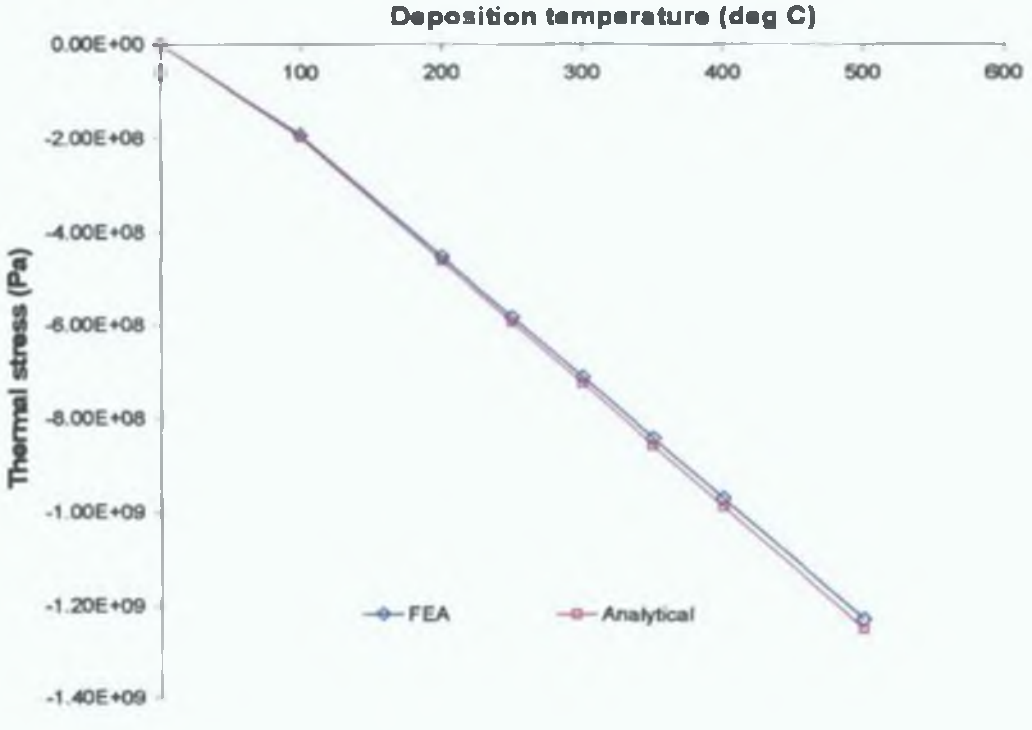

(a)

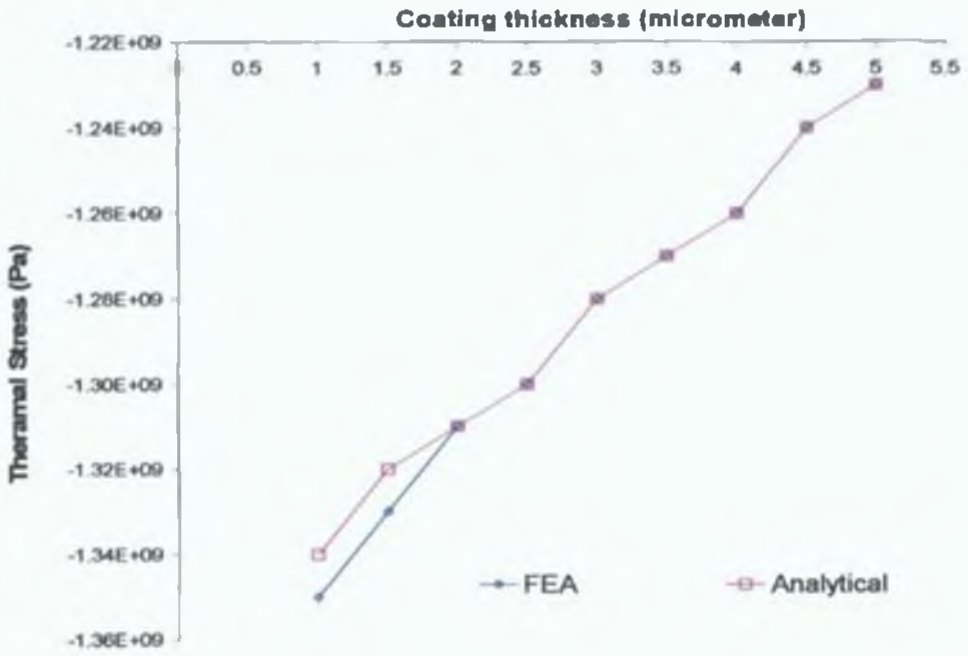

(b)

Figure 4.9: Variation of the analytical (average) and FEA thermal stress (Max Von mises stress) with (a) deposition temperature and (b) coating thickness.

Typically in the sputtering method, the deposition temperature varies between 100-500 ^{0}C depending on operating parameters. From figure 4.9 (a), it is seen that the thermal stress varies linearly with the deposition temperature. This proportionality has been reflected in the graph, both for analytical (average stress) and finite element analysis. The tensile thermal stress increase with increasing in the coating thickness, as seen in figure 4.9 (b) according to equation A.9, given in appendix A2.

4.2.2.2. SHEAR STRESS DISTRIBUTION

Figure 4.10 (a) shows the distribution of shear stress (σ_{xy}) through the thickness of the coating and substrate at different distances away from the edge of the M4 model. The shear stress values are far less than the other stress components except near the edge. At the

edge tensile stress exists throughout the coating and near the top surface of the substrate. Away from the edge the shear stress values decrease.

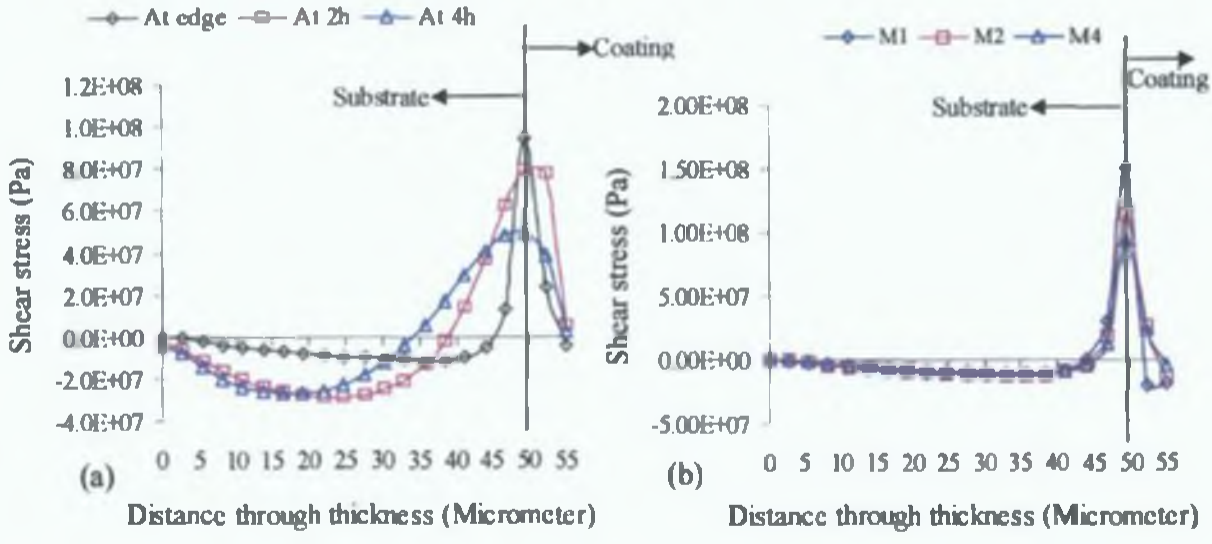

Figure 4.10: Shear stress (σ_{xy}) through the thickness of coating and substrate (a) at different distances away from the edge of the M4 model and (b) at the edge of the different models (Note: 2 h is a distance of two times the coating thickness away from the edge).

The shear stress is equivalent to the adhesion strength of the coating [260]. As the maximum shear stress is at the interface between the coating and substrate, the spallation of the coating is expected to occur from this position if the shear stress is greater than the bonding strength between the coating and substrate [303]. As expected there is small shear stress along the axisymmetric line and top surface of the coating. From figure 4.10 (b) it can be seen that increasing the number of graded interlayers can reduce the shear stress significantly. A shear stress reduction of approximately 36 % reduction was observed with the graded coating system containing five interlayers (M4) when compared to a single layer coating (M1). This reduction in shear stress will decrease the probability of cracking or spallation of the coating from the substrate. The reason behind the decrease of thermal stress in the graded coating is the smooth transition of material properties between the substrate and top layer of the coating.

4.2.2.3. TANGENTIAL STRESS DISTRIBUTION

Figure 4.11 (a) shows the distribution of tangential stress (σ_z) through the thickness of the coating and substrate at different distances away from the edge of the M4 model. From the bottom to the top surface of the substrate, a stress gradient and stress reversals (compressive to tensile) are observed. They reach a maximum value near the interface between the coating and substrate. Compressive tangential stress exists through the thickness of the coating from the bottom to the top surface with a slight stress gradient but no stress reversal is observed.

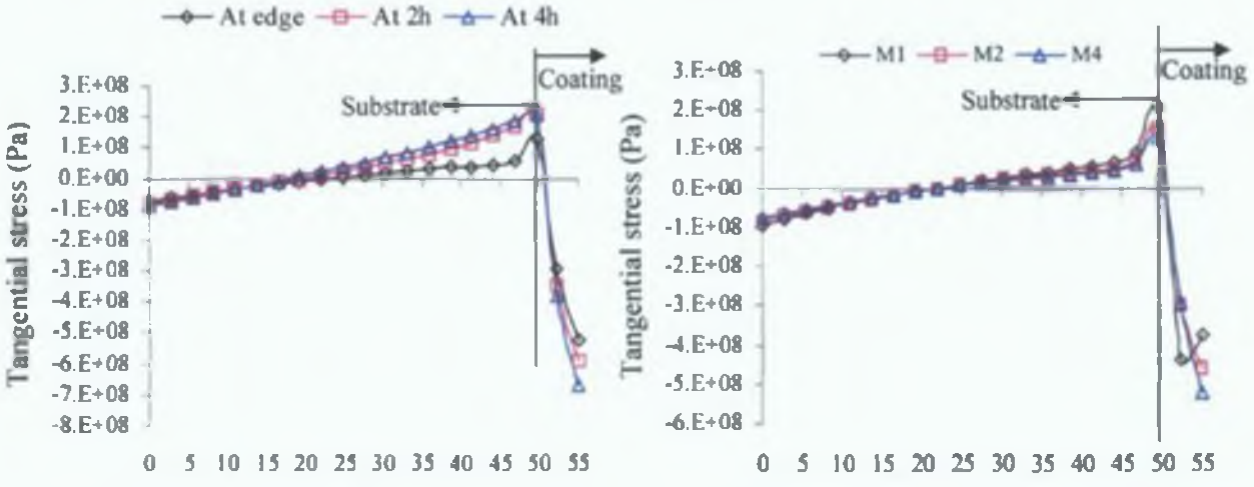

Figure 4.11: Tangential stress (σ_z) through the thickness of coating and substrate (a) at different distances away from the edge of the M4 model and (b) at the edge of the different models (Note: 2 h is a distance of two times the coating thickness away from the edge).

The minimum tangential stress value in the coating appears at the edge and it increase with increase distance from the edge. At around a distance of 4 h, (where h is coating thickness) stresses reach the maximum value and remain constant throughout the rest of the coating. Since the substrate-to-coating thickness ratio is large, the compressive tangential stress in the coating is much larger than the tensile stress in the substrate [273]. Like the shear stress, the tangential stress at the interface decreases with the increase in number of graded interlayers, as observed in figure 4.11 (b) due to the smooth transition of material properties. A similar stress distribution was found for the radial stress (σ_x)

component, which confirms the biaxial stress state in the coating. Small axial stress (σ_y) values were found all along the coating and the substrate. At the edge, the compressive stress in the substrate is higher than the tensile stress in the coating due to the thinness of the coating. The graded coating system also reduced the axial stress substantially.

4.2.2.4. MODEL VERIFICATION

As there are no appropriate experimental facilities available in DCU to evaluate thermal residual stress in PVD deposited coating, following indirect verification has been done at the time of simulation work. They are given below:

- Numerical verification of the model for the single layer coatings was done by putting the different coating and substrate properties values into the thermal stress equation A.9, in appendix A2.
- No stress was found when the room temperature was set equal to the deposition temperature
- Radial stress distribution (σx) ≅ tangential stress (σz) distribution: this confirms the biaxial stress state in the coating.

4.3. PLASMA NITRIDING

4.3.1. LOW TEMPERATURE PLASMA NITRIDING OF 316L STAINLESS STEEL

4.3.1.1. SURFACE MORPHOLOGY AND SURFACE ROUGHNESS

The surface morphology of non-nitrided samples (with and without chemical etching) is shown in figure 4.12. It was observed that in the chemically etched non-nitrided sample austenitic grain boundaries and twins, which are the common characteristics of austenitic steel, were clearly visible (Figure 4.12a).

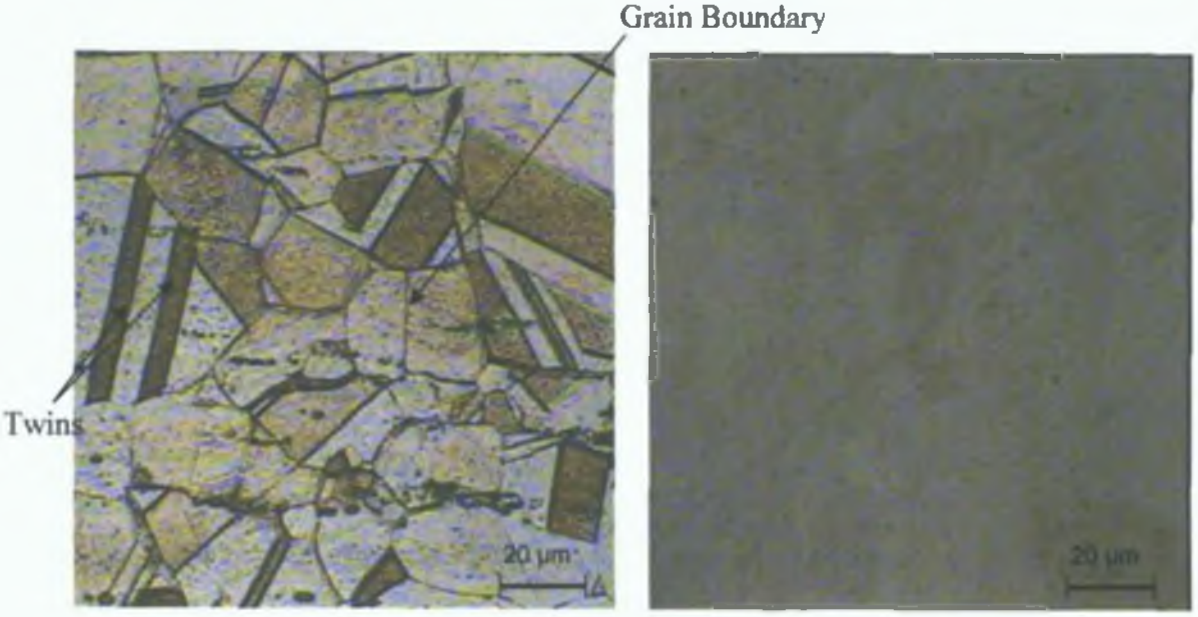

(a) (b)

Figure 4.12: Optical surface morphology of the non-nitrided samples (a) chemically etched and (b) without chemical etching.

On the other hand, no twins were observed in the un-etched, non-nitrided sample (Figure 4.12b). Similar microstructures to the etched non-nitrided sample were also observed in the surface of the nitrided samples without chemical etching shown in figure 4.13 (a-c). However, twins were more visible when nitriding time was increased. This irregular surface is possibly due to the formation of the nitrided layer [213,304].

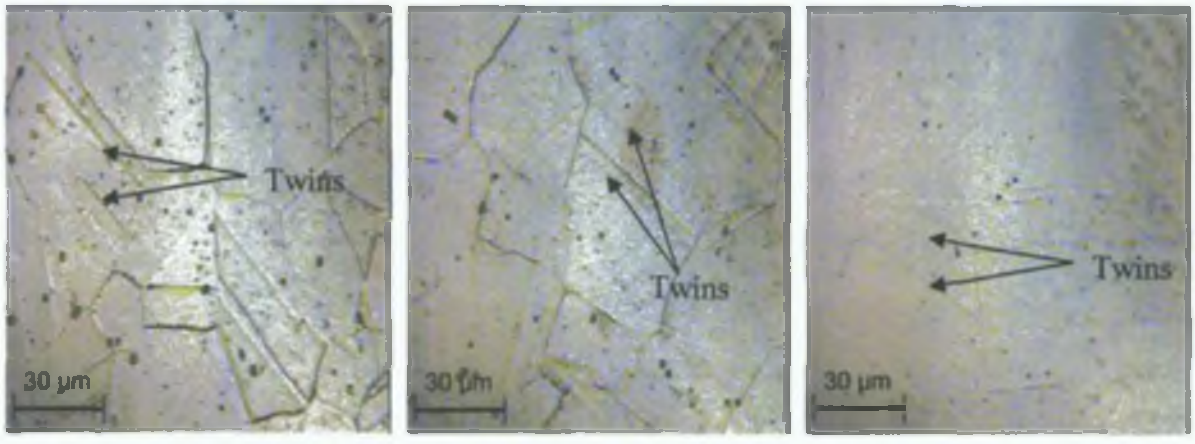

(a) (b) (c)

Figure 4.13: Surface morphology of the nitrided surface (without chemical etching), nitriding at 420 ^{0}C by using 0.4 A current for (a) 9 h, (b) 6 h and (c) 3 h.

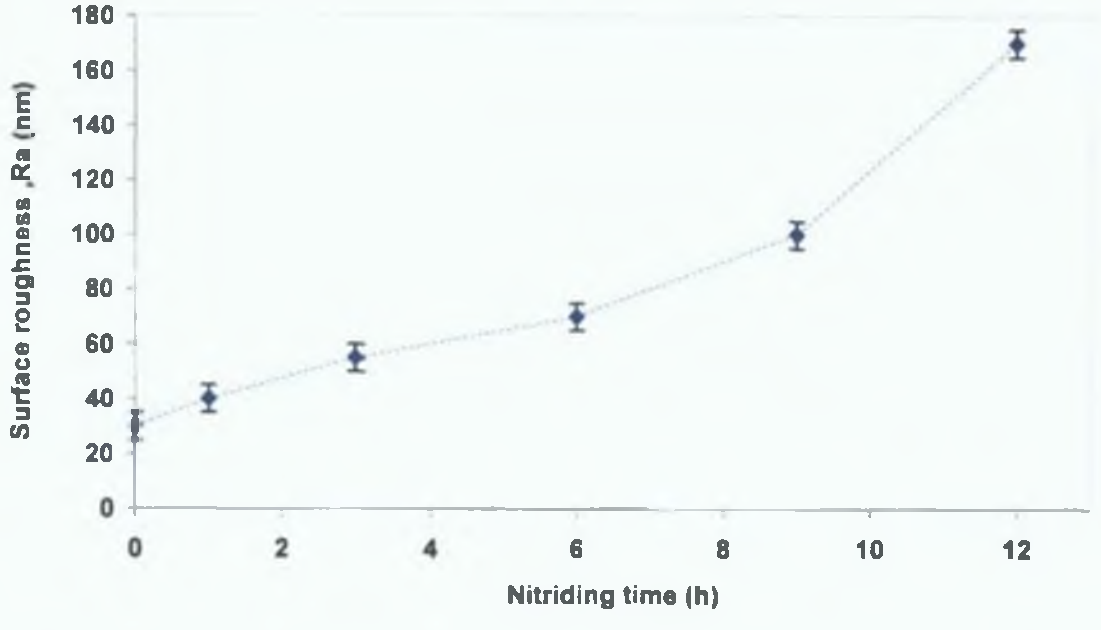

Figure 4.14: Average surface roughness (R_a) of the 316L stainless steel samples, nitrided at 420 ^{0}C by using 0.4 A current for different times (Two samples have been used for each experiment and three measurement have been carried out for each samples. Error has been originated from the non-uniformity of the samples surface).

The average roughness value (R_a) increased as the nitriding time increased, as shown in figure 4.14. The average surface roughness of the nitrided samples increased from 30 nm for the non-nitrided sample to a value of approximately 170 nm after 12 h. A slight increase in surface roughness (30 nm for non-treated sample and 50 nm for etched sample) was found when only argon etching was carried out. Therefore, the increase of surface roughness cannot be entirely attributed to the argon etching effect [305]. The reason for the increase in surface roughness is not fully clear. However, it could be possibly due to the formation of a distinct surface microstructure during nitriding. This distinct surface was more clearly visible with increased plasma processing time as mentioned before.

4.3.1.2. CROSS-SECTIONAL MORPHOLOGY AND NITRIDED LAYER THICKNESS

The cross section of the treated 316L samples using the same experimental parameter (0.4 A current, and so on) for different processing times is shown in figure 4.15.

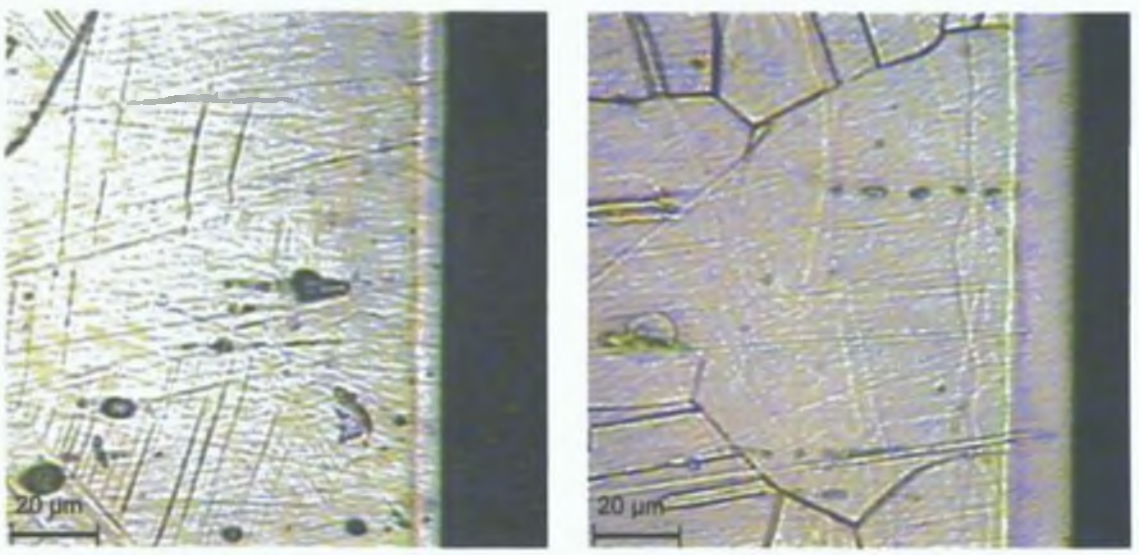

(a) (b)

Figure 4.15: Cross-sectional morphology of the chemically etched 316 stainless steel samples nitrided for (a) 1 h and (b) 12 h.

The nitrided samples etched with the glycergia agent clearly revealed a well-defined nitrided layer separated from the core material by a visibly etched line. A similar characteristic was also found by Li and Borgioli et al. [209,304] in the plasma nitrided AISI 316 samples. A very thin nitrided layer was observed in the case of the 1 h nitriding sample (Figure 4.15a) whereas a comparatively thick layer was observed in the case of the 12 h nitriding sample (Figure 4.15b). The thickness of the nitrided layer increased as nitriding time increased as shown in figure 4.16.

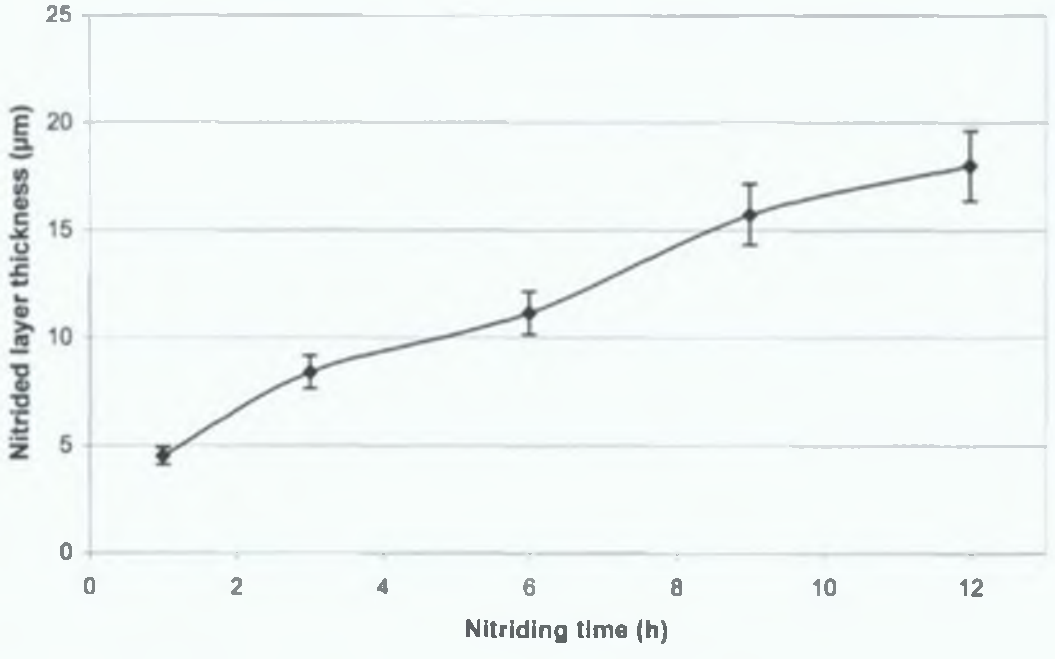

Figure 4.16: Nitrided layer thickness of the 316L stainless steel samples nitrided at 420 ^{0}C by using 0.4 A current for different times.

However, the average growth rate of nitrided layer = (Nitriding layer thickness / Nitring time), was found decreasing with increasing nitriding time (for example, average growth rate for the 3 hr and 9 hr nitriding sample were 4.5 µm/hr and 1.7 µm /hr respectively). From these observations, it can be confirmed that the growth of the nitrided layer was apparently influenced by nitriding time. The literature relating to low temperature nitriding reports that the nitrided layer (S phase layer) thickness is usually less than 3-10 µm depending on the treatment time, which can range from 5 to 10 h and the nitriding processes used [209,304,306]. The featureless nitrided layer had a thickness, which was measured to be around 25 µm (with beam current 0.7 A and time 12 h) and 18 µm (with beam current 0.4 A and time 12 h) in this study. The formation of the nitrided layer within a

short processing time, compared to other nitriding processes, can be attributed to the bombardment of the energetic neutral particles, which possibly favour the surface conditions and enhance diffusion kinetics. In the literature [214] it was reported that the microstructure of the samples nitrided at higher temperatures shows a dark layer when viewed using an optical microscope after etching. This dark phase indicates the precipitation of chromium nitrides, which leads to a decrease in the corrosion resistance of the steel. On the other hand, low temperature nitriding exhibits a bright nitrided layer after etching, which indicates no precipitation of chromium nitride. As the low temperature nitrided layer is free from precipitation, the etchant cannot attack the layer and the microstructure appears bright [214]. In this investigation the nitrided layer was found to be bright and homogeneous with no evidence of pores (figure 4.15). This finding also agrees with other nitriding studies performed at low temperatures [307].

4.3.1.3. ELEMENTAL ANALYSIS BY EDX AND PHASE ANALYSIS BY X-RAY DIFFRACTION

Figures 4.17a and 4.17b show the EDX spectra of non-nitrided and nitrided samples respectively. In the spectra of the elements in the nitrided samples, a nitrogen peak was clearly visible indicating the presence of nitrogen. In the spectra of the non-nitriding sample, the position of the nitrogen peak was shown but no noticeable nitrogen peak was observed. A more intense nitrogen peak was observed when the sample was nitrided for longer time. Typical X-Ray Diffraction patterns of low temperature plasma nitrided layers and untreated 316L stainless steel are shown in figure 4.18. γ_{111} and γ_{200} peaks of austenite phases were observed in the case of the untreated 316 stainless steel sample. However, in the plasma nitrided sample a set of peaks, which do not match with any existing ASTM X-Ray Diffraction index, were observed. These peaks have been associated with a metastable phase called "expanded austenite" or "S phase" and designated by S1 or γ'_{111} and S2 or γ'_{200}. Both the S1 and S2 peaks were similar to the γ_{111} and γ_{200} austenite peaks in the untreated sample.

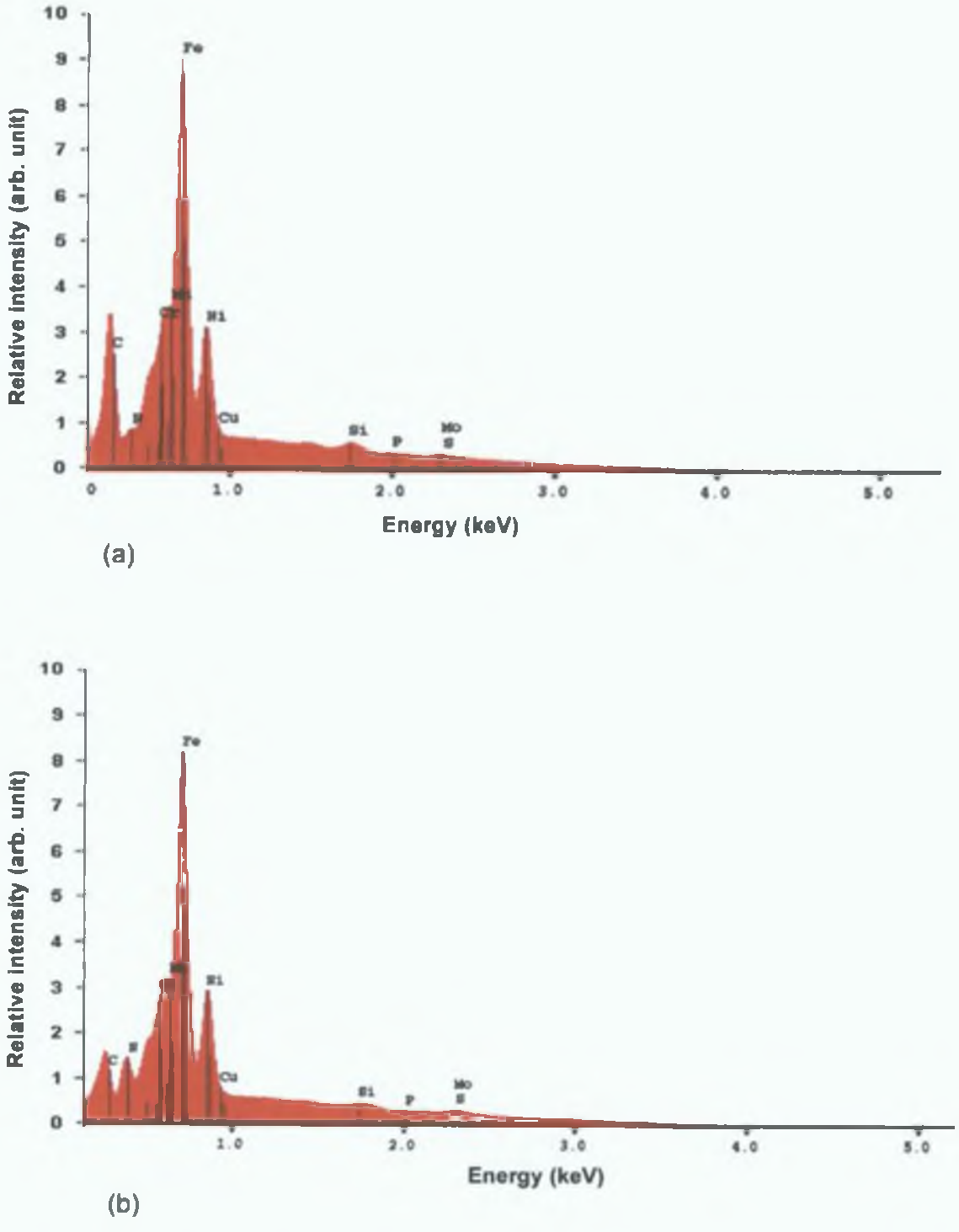

Figure 4.17: EDX spectra of (a) non-nitrided and (b) nitrided 316 stainless steel samples.

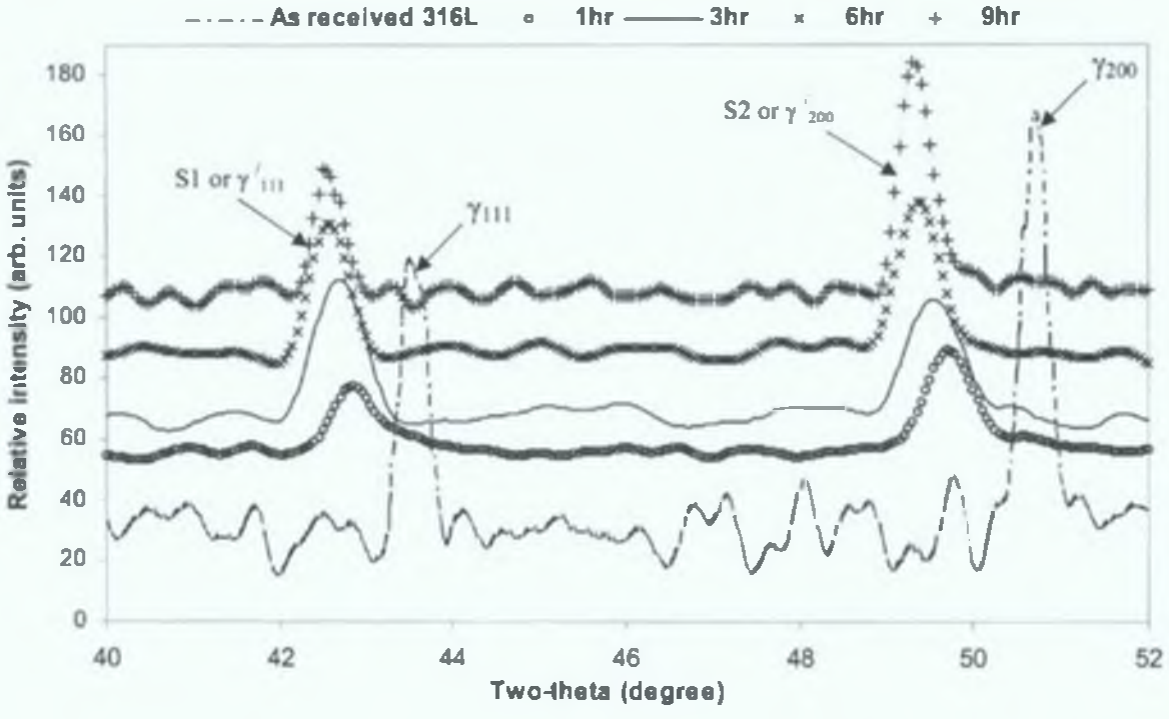

Figure 4.18: XRD patterns of the 316L stainless steel samples nitrided at 420 ^{0}C by using 0.4 A current for different times

The S1 and S2 peaks appeared at lower angles, compared to the austenitic phases in the untreated sample, indicating an expansion of the lattice, as shown in figure 4.19, due to the incorporation of nitrogen in the interstitial position of the fcc austenite structure [209,214]. Broadening of the S peaks was also observed compared to the non-nitrided sample. This may be due to the residual stress, defects inside the nitrided layer or may be due to refinement of austenite grain size [308].

From figure 4.18, it was observed that S peaks were gradually moved to lower diffraction angles as the nitriding time increased. This fact can be explained by an increase in nitrogen concentration inside the nitrided surface as nitriding time increased. However, the maximum peak shifting was found for the 6 h nitride samples. No further significant peak shifting was observed after this time. It was also observed that shifting of the γ_{111} peak was higher than that of the γ_{200} peak. Lattice parameters were calculated from planes (111) and (200) for all samples. It was found that there was a difference of lattice parameter value between (111) and (200) crystallographic planes for the 6 h nitriding time sample, as shown in figure 4.19, whereas little difference of lattice parameter was observed in the case of the 1 h nitriding samples. This fact can be explained by the step by step changing of the cubic

symmetry of the nitrided layer as the lattice parameter value gradually becomes unequal with increasing nitriding time. This finding also agrees with other nitriding studies performed at low temperatures [308].

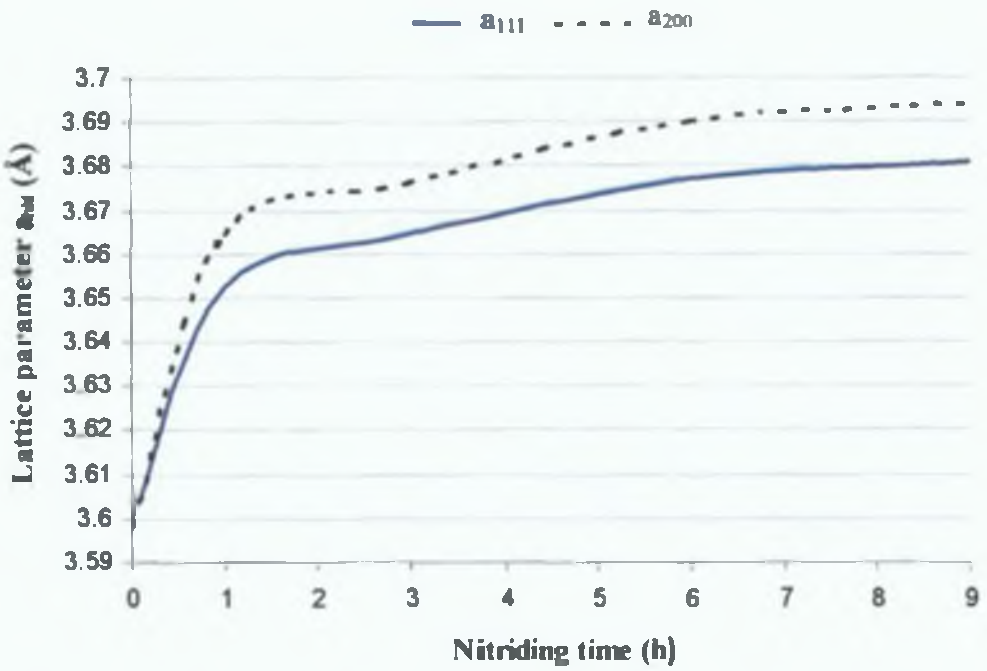

Figure 4.19: Variation of the lattice parameter a_{111} and a_{200} (calculated from diffraction angle of (111) and (200) planes respectively) of the nitrided stainless steel samples as a function of the nitriding time under given conditions.

The X-Ray Diffraction analysis did not reveal any peak for CrN, which is usually encountered in association with the formation of a black layer. This result was also in agreement with the optical investigation of the nitrided cross-section where no such black layer was observed.

4.3.1.4. HARDNESS OF NITRIDED SAMPLES

The hardness depth profile of the sectioned nitrided samples (with 0.7 A beam current and 9 h) carried out by Vickers microhardness testing is shown in figure 4.20. Near the surface of the nitrided the layer hardness values remained almost constant upto a value of slightly above 1200 HV. The higher hardness value in the nitrided layer sharply decreased to a lower hardness value corresponding to the non-nitrided sample [306]. This suggested that a thin hard layer was formed without any significant diffusion of nitrogen underneath this hard nitrided layer. The hardness depth profile was also in agreement with the microstructural observation of the thin nitrided layer followed by the core material (Figure 4.15).

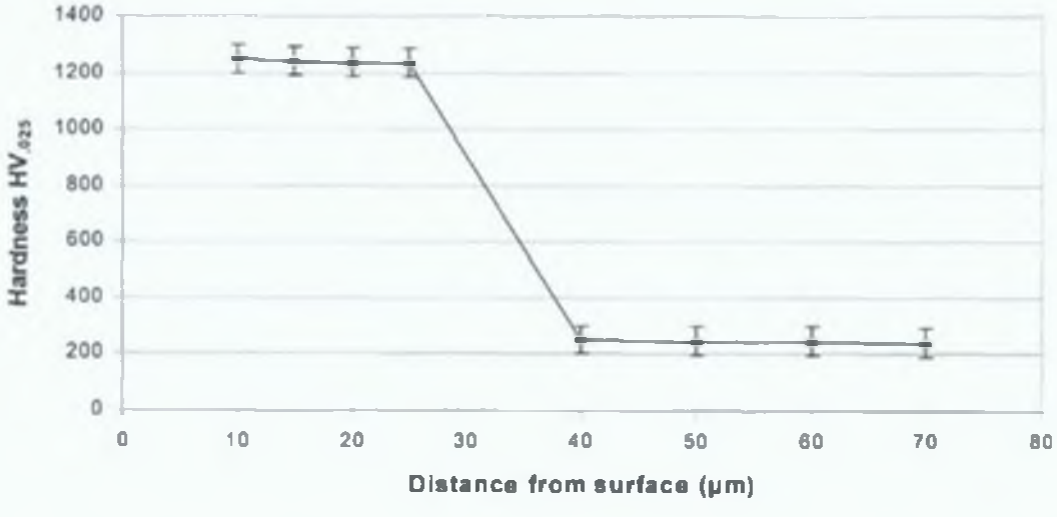

Figure 4.20: Hardness depth profile of the nitrided 316 stainless steel sample (Two samples have been used for each experiment and three measurements have been carried out for each samples.).

The Vicker microhardness as a function of nitriding time is shown in figure 4.21. The hardness values increased as the nitriding time increased. This fact can be explained by the formation of a relatively thick nitriding layer with increased nitriding time, which is in agreement with the cross-sectional morphology of the nitrided substrate. This thick layer increases the composite hardness of the samples. The increase in hardness with increasing nitriding time may also be due to a greater concentration of nitrogen in the austenite phase

at long nitriding time samples compared to that of short nitriding time samples, which is in agreement with the XRD findings.

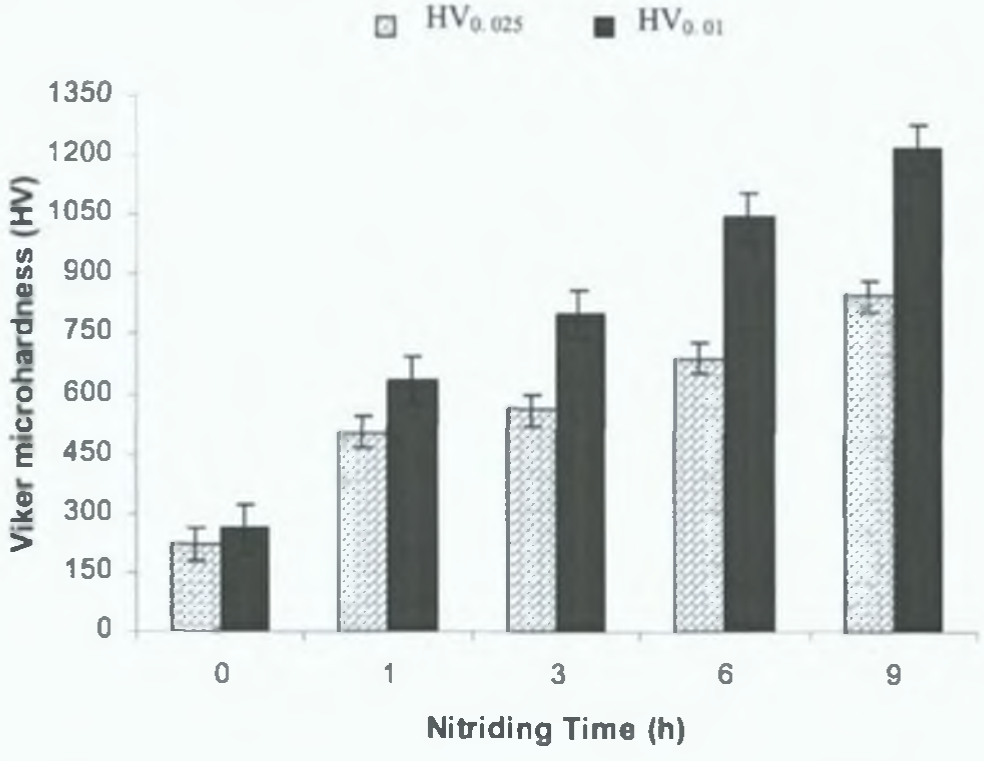

Figure 4.21: Surface hardness of the stainless steel samples nitrided at 420 ^{0}C by using 0.4 A current for different times (Two samples have been used for each experiment and three measurements have been carried out for each samples).

This higher concentrated of nitrogen induces a further solid solution strengthening effect in the nitrided layer for long nitriding time samples compared to short nitriding time samples, which in turn increase hardness [206,214]. Plasma nitriding by this method showed that the surface hardness of the nitrided sample (12 h) was approximately 1250 $HV_{0.01}$, which was roughly four times higher than the hardness of the non-nitrided samples.

4.3.1.5. WEAR PROPERTIES

Before pin-on-disk wear test as-nitrided samples were polished to a surface roughness range from 30 nm to 50 nm in order to gains a better understanding of the tribological properties. The friction co-friction curves for the nitrided and the non-nitrided samples are shown in figure 4.22, where all pin-on-disk wear tests were performed with same conditions.

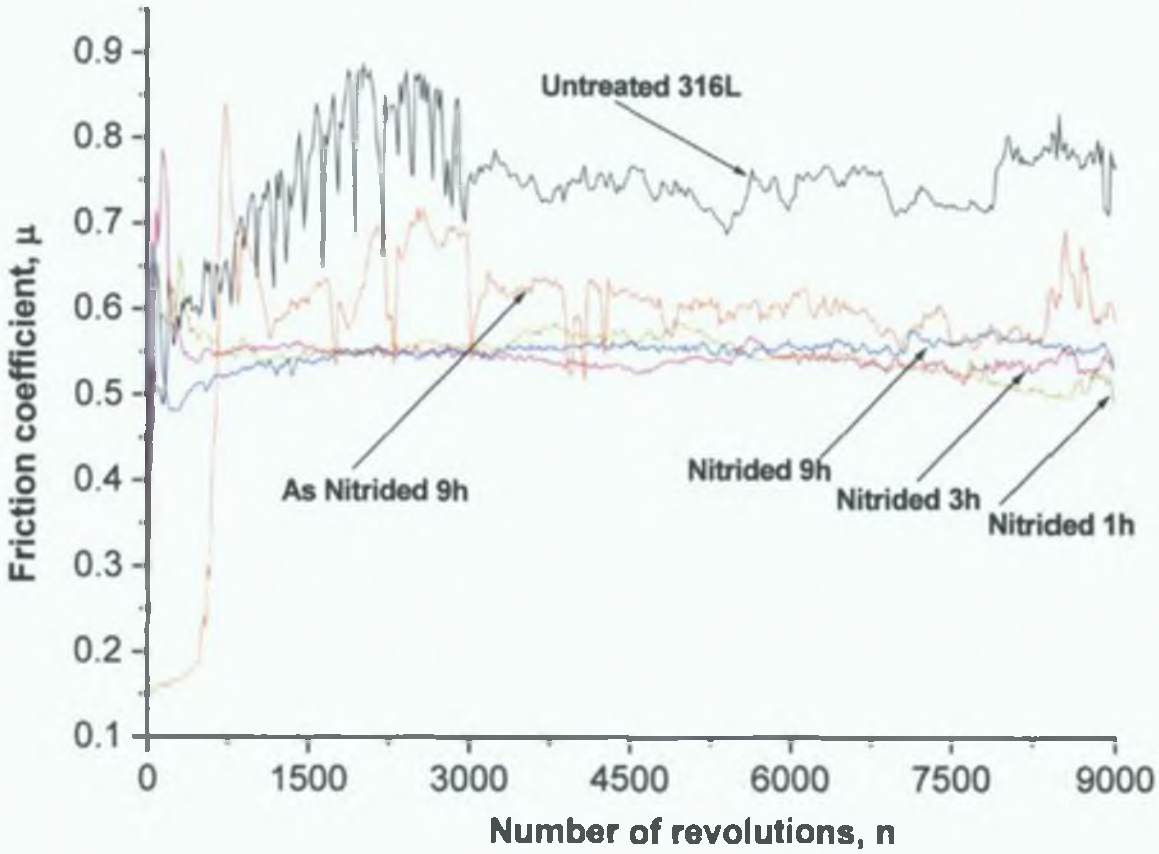

Figure 4.22: The friction coefficients for pin-on-disk tests of the untreated sample, the polished nitrided samples treated for different times, and the as-nitrided sample.

The non-nitrided and as-nitrided (9 h) samples showed a steady state friction value of approximately 0.76 and 0.64 respectively. However, the steady state friction co-efficient values for all polished nitrided samples were approximately between 0.49 and 0.55. This is

lower than the as-received nitrided sample. The reason for this may be due to the high surface roughness of as-treated nitrided samples. The plasma nitrided samples showed lower, stable and smoother co-efficient of frictions compared to non-nitrided substrate. This was because the hard nitrided surface lead to a lower contact area when tested on the pin-on-disc machine [210]. This prevents the asperity welding of hard nitrided samples with the counterface materials [309]. The friction value was found to be increased as nitriding time increased and the 1 h nitriding sample (polished) showed the lowest friction value compared to all other samples.

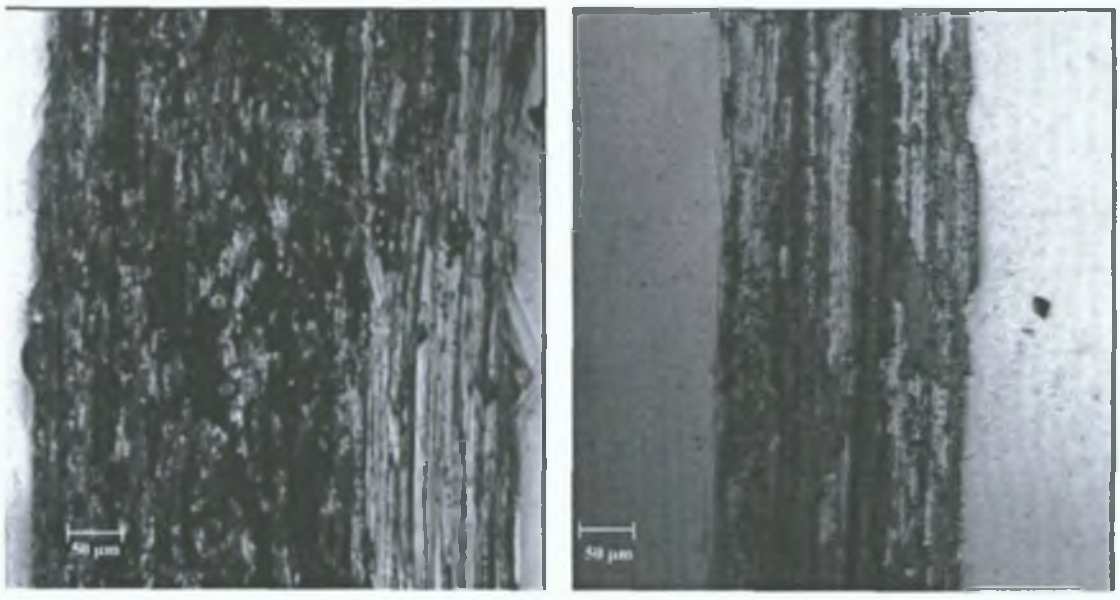

(a) (b)

Figure 4.23: Low magnified optical wear track morphology image of (a) the non-nitrided and (b) the nitrided sample

The wear track morphology of the treated and the untreated samples are shown in figure 4.23a and 4.23b respectively. Macroscopically a very wide, rougher and deeper wear track was clearly observed for the untreated sample (Figure 4.23a). The wear track of the untreated sample showed large plastic deformation and deeper ploughing line on wear track and severe material pile up at the edge of the wear track shown, in figure 4.24a and 4.24b respectively.

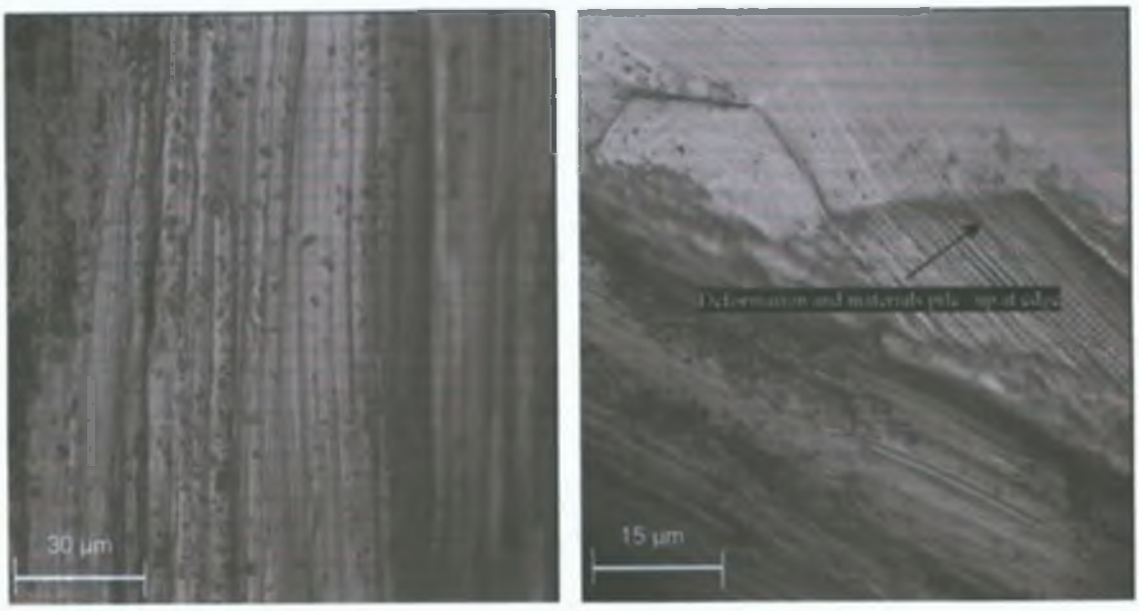

(a) (b)

Figure 4.24: The optical wear track morphology image of the non-nitrided sample at (a) middle of wear track and (b) edge of the wear track

Two types of wear are believed to have occurred in the untreated sample: (i) at the first stage a two-body (adhesive) wear mechanism by adhesion between counterpart and soft 316L and (ii) a three-body mechanism (abrasive) at the next stage of the wear test by producing a materials transfer layer and wear debris [310]. A large amount of wear debris was distinctly found on the untreated sample wear track and this wear debris produced a parallel deep ploughing line along the wear track (Figure 4.24a). So there was a severe adhesive, abrasive and deformation wear mechanism for the untreated samples. On the other hand, different wear behaviour was characterized for the nitrided sample compared to untreated sample, due to its high hardness. From figure 4.23b, a narrow, less rough and shallow wear track was observed in treated samples. Nitrided samples showed no deformation and no material pile up at the edge of the wear track due to a very hard load, supporting layer of nitride, shown in figure 4.25. A magnified picture (Figure 4.25b) showed the formation of a transferred layer on plasma nitrided layer.

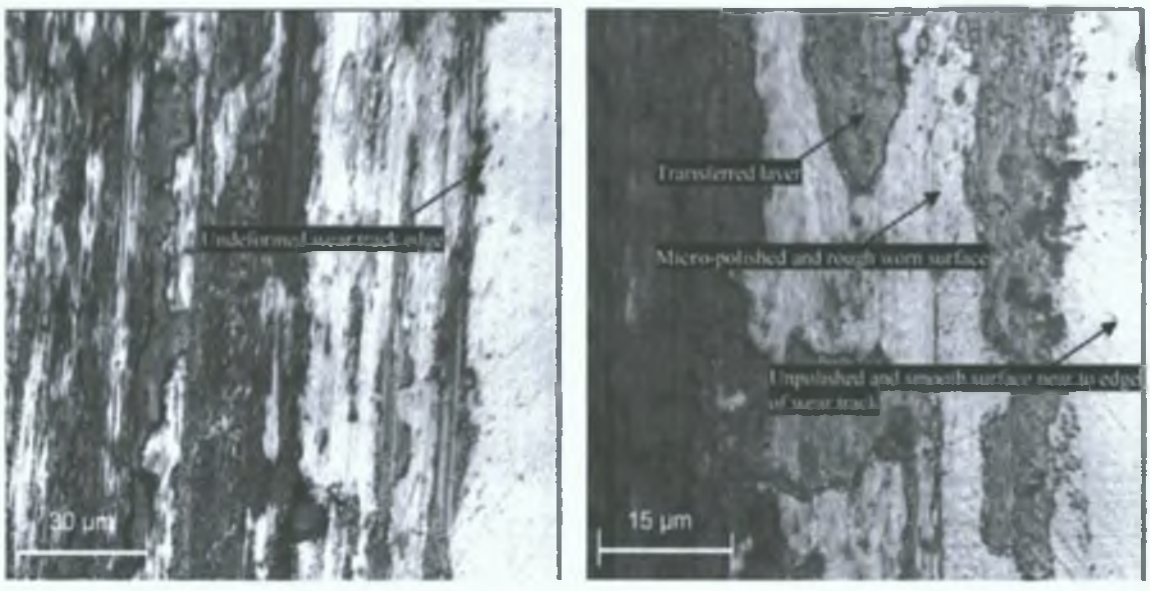

(a) (b)

Figure 4.25: The optical wear track morphology image of the nitrided sample showed (a) an undeformed wear track edge and (b) a polished, transferred layer and an unpolished region

C. X. Li et al. [310] reported that this transferred layer came from repeated oxidation of very fine particles generated from micro-abrasion of the hard nitrided sample asperities and this was based on the well established theory of oxidation wear [311]. So a micro-abrasive and oxidation wear mechanism was characterized for the treated samples. The absence of adhesive wear mechanism on nitrided surface may be due to the prevention of hard nitrided surface asperity welding. The low temperature plasma nitriding sample, that were treated for a long time, showed relatively large micro-abrasive particles and a large transferred layer, compared to samples nitrided for short time. Figure 4.26 shows the wear depth value of both nitrided and non-nitrided samples. It was found that low temperature plasma nitriding significantly improved the wear resistance of the 316 stainless steel. The wear depth value of the 1 h nitrided sample (polished) was recorded to be as low as 0.5 μm, which was approximately thirteen times lower than untreated samples. This was due to hard nitrided surface leading to a decreased contact area with the counter-part surface at the time of wear test, as well as the difference in wear mechanism described above. This was also in agreement with the wear track width of the nitrided and the non-nitrided samples.

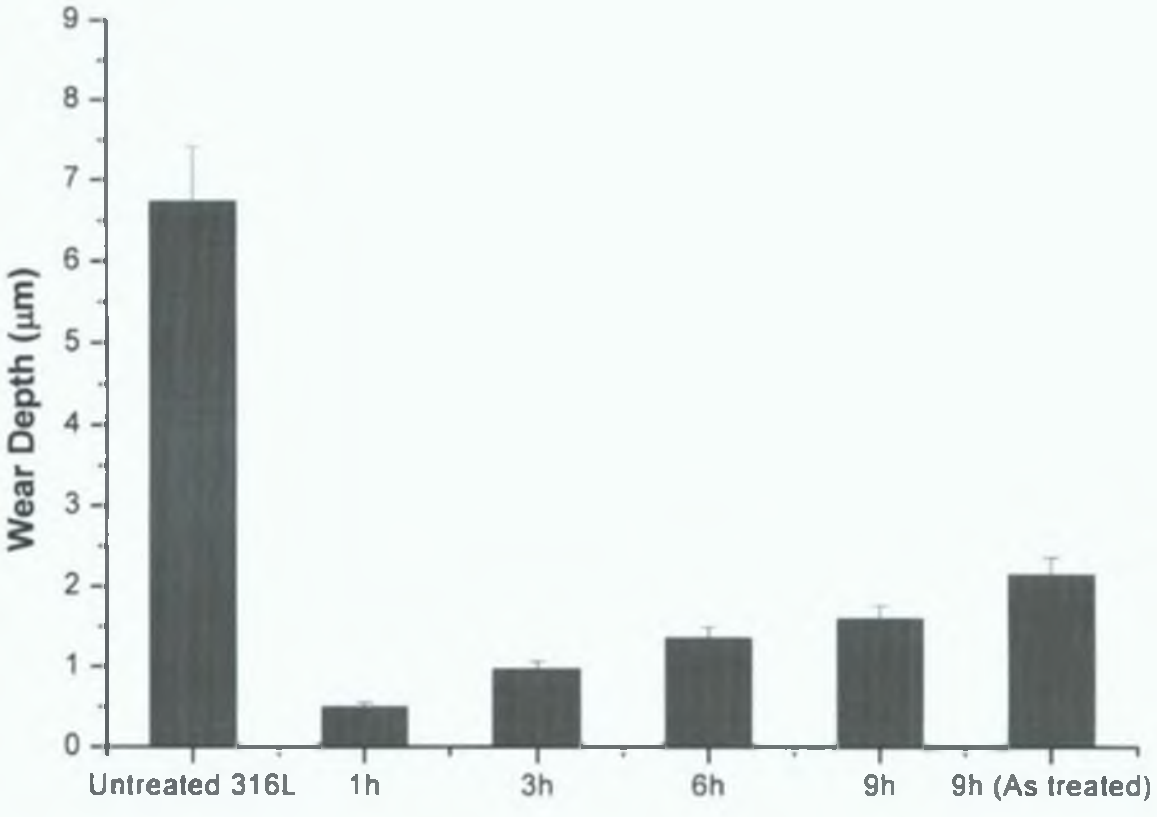

Figure 4.26: Wear depth value of the untreated, the polished nitrided samples treated for different times, and the as-nitrided sample

The wear track width of nitrided sample treated for 1 h (240 μm) was found to be almost half that of untreated samples (503 μm) as can be seen from figure 4.23. However, an interesting relationship was established between the wear depth values of the samples nitrided for different length of time. It was observed that the wear depth value increased as the nitriding time increased. This fact can be explained by the build up of more residual stress in the top most layer of sample nitrided for the longest time and the formation of more harder and larger abrasive wear particles than found for a sample nitrided for a shorter length of time. This result also agreed with XRD result, which showed that the lattice parameter of the 316L stainless steel sample increased as the nitriding time increased, which was an indirect indication of increased stress in nitrided layer. But the wear depth of all of the nitrided samples was significantly lower than those of the untreated samples. The polished nitrided samples showed a lower wear depth value than the as-treated nitrided

samples due to greater contact between the counter-part surfaces and the rougher surface which lead to more damage of the surface. This result also could be correlated with the friction co-efficient and wear track morphology results of the treated and the untreated samples.

4.3.2. LOW PRESSURE PLASMA NITRIDING OF TI-6AL-4V

4.3.2.1 MORPHOLOGY OF NITRIDED SAMPLES

The surface morphology of the non-nitrided and the nitrided samples without chemical etching, observed using optical microscopy and the SEM, are shown in figure 4.27 and 4.28 respectively.

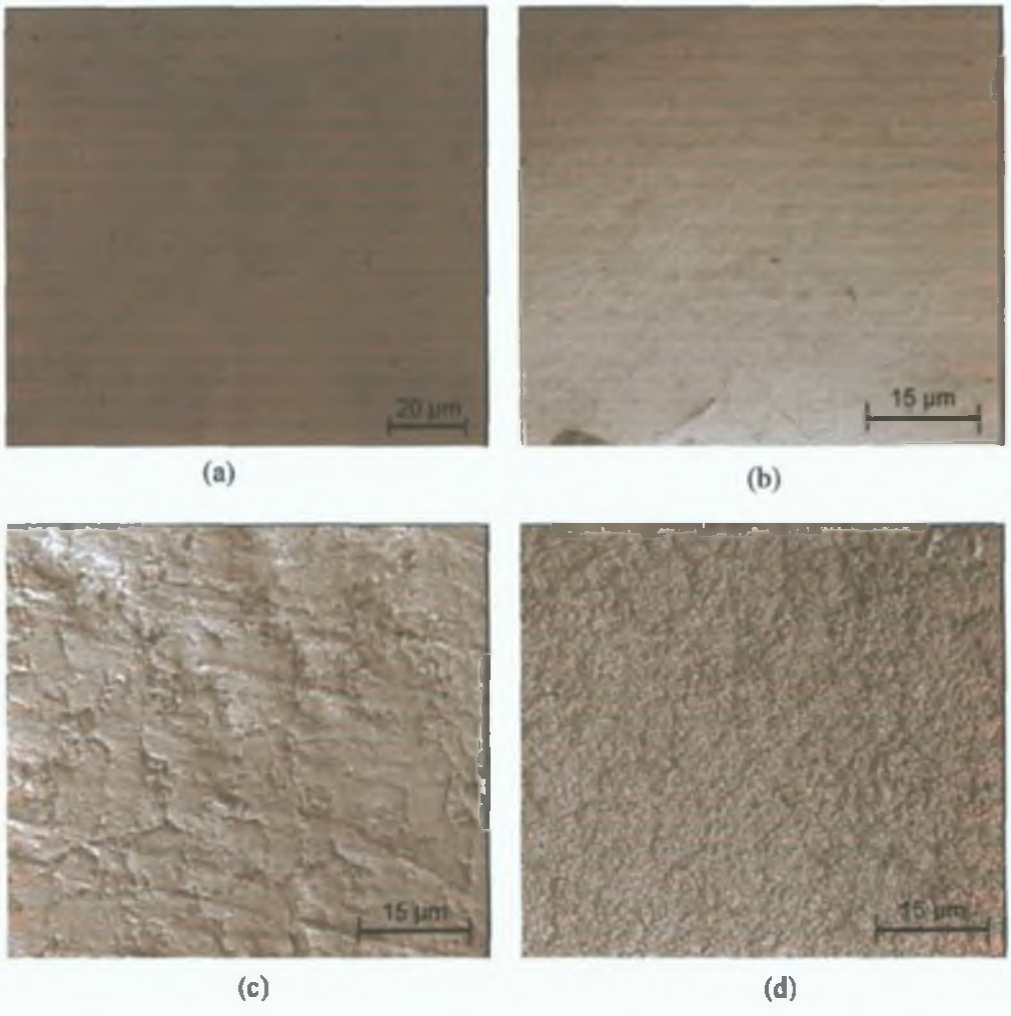

Figure 4.27: The surface morphology of (a) the non-nitrided Ti-6Al-4V samples and the nitrided Ti-6Al-4V samples, with nitriding carried at (b) 500 ^{0}C (c) 600 ^{0}C and (d) 900 ^{0}C, as observed using optical microscopy

The grey colour of the untreated samples contrasted with the intense gold as the nitriding temperature increased from 500 ^{0}C to 900 ^{0}C, which was an indirect indication of the formation of TiN phase on the surface of the nitrided sample. A very smooth and featureless surface was noticed in the non-nitrided samples (Figure 4.27a and 4.28a). However, a very irregular and rough surface (like grain refinement) consisting of many peaks and valleys was visible from the picture of the sample nitrided at 900 ^{0}C (Figure 4.27b and 4.28b) and this feature was less visible for the sample nitrided at low temperature (below 700 ^{0}C). The average surface roughness of the nitrided samples was found to increase as the nitrided temperature increased. The surface roughness was recorded to be 100 nm and 170 nm for the sample nitrided at 700 ^{0}C and 900 ^{0}C respectively. As 900 ^{0}C is close to the transition temperature of the α-Ti to β –Ti, the significant increase in surface roughness at 900 ^{0}C may be due to the interaction of the plasma with active the sample surface contain β–phase [228,312].

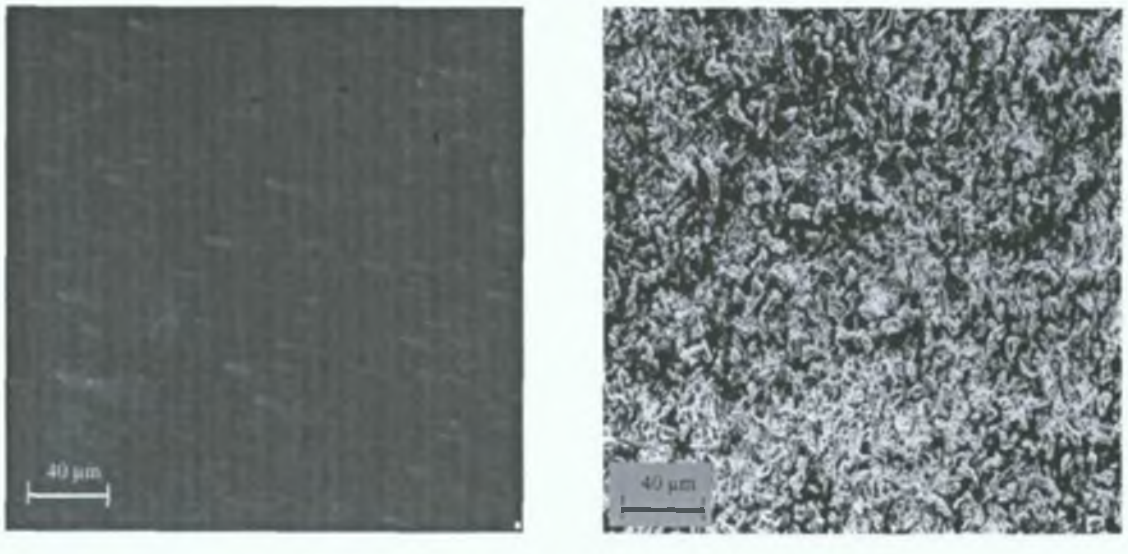

(a) (b)

Figure 4.28: SEM surface morphology of (a) non-nitrided and (b) nitrided Ti-6Al-4V samples.

A minor contribution of the increase in surface roughness for the sample nitrided at high temperature (at or above 700 ^{0}C), may be due to the bombardment of the energetic neutral particles on the sample surface [231]. Bombardment of the surface with the energetic neutral particles was believed to be main factor for increasing the surface roughness of the sample nitrided at low temperature.

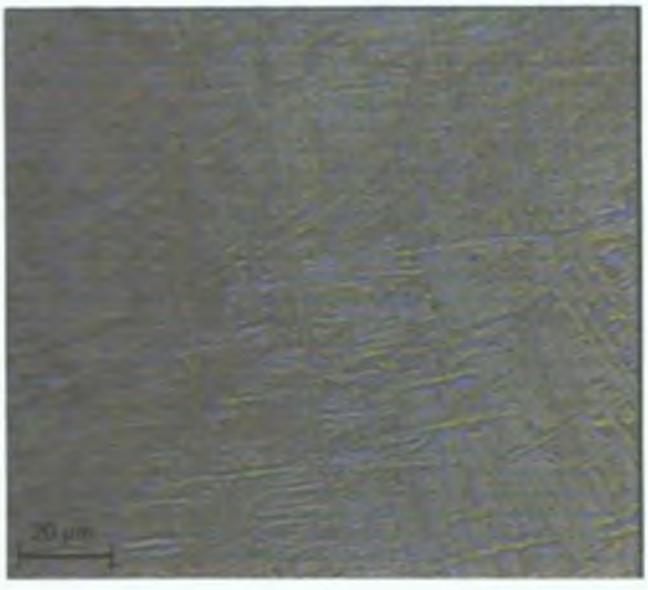

Figure 4.29: Optical micrograph of the etched nitrided Ti-6Al-4V samples.

The microstructure of the as-received Ti-6Al-4V alloy consisted of transformed β-Ti containing acicular α-Ti (where the α-phase was found at prior β-phase grain boundaries) with colonies features called Widmanstten structures [313,314] as shown in figure 4.29. The colonies are characterized by a cluster of acicular α-Ti phase arranged with the same orientation and so the structure of a large number of acicular α-Ti phases has a basket weave feature. The grey colour of the untreated samples contrasts with the intense gold after nitriding, which is an indication of the formation of TiN on the nitrided sample surface. The cross-sectional surface microstructure of the nitrided samples was seen to clearly include a well-defined continuous compound nitrided layer after chemically etching with Kroll's reagent, when nitriding was performed at or above a temperature of 700 ^{0}C (Figure 4.30b and 4.30c) and growth of this layer was found to increase as the nitriding temperature increased. The TiN containing compound layer [225,226,315] has not been attacked by the etching reagent and can be seen as a white layer.

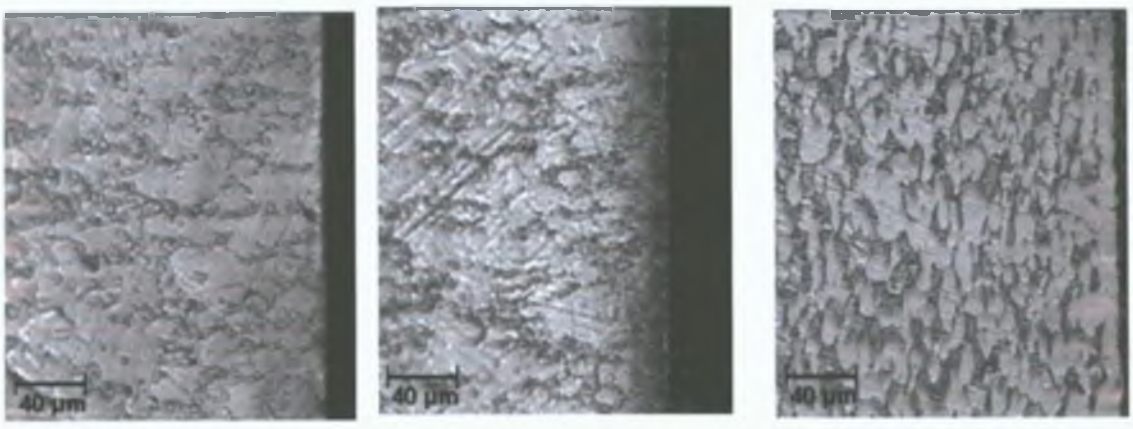

(a) (b) (c)

Figure 4.30: Cross-sectional optical micrographs of the nitrided Ti-6Al-4V samples, nitrided at (a) 600 ^{0}C (b) 700 ^{0}C and (c) 900 ^{0}C

The thickness of the compound layer was measured to be approximately 3 µm and 9 µm for the sample nitrided for 4 h at temperatures of 700 ^{0}C and 900 ^{0}C respectively. The optical micrographic result did not reveal any compound layer when samples were nitrided at temperature below 700 ^{0}C. However, underneath the compound layer or top surface (in the case of samples nitrided below 700 ^{0}C) a well recognized nitrogen diffusion layer can be seen for all the nitrided samples. This has been reported by several researchers [226] and is supported by the hardness depth profile of the sectioned nitrided samples [316].

4.3.2.2. PHASE ANALYSIS BY XRD AND XPS

Typical X-ray diffraction patterns of the low pressure plasma nitrided and untreated Ti-6Al-4V samples are shown in figure 4.31. A number of peaks (diffraction lines) of both the hexagonal close packed (hcp) α-Ti phase and the body-centred-tetragonal (bct) β-Ti phase were observed for the as-received Ti-6Al-4V samples.

As there are no databases for the spectra of the Ti-6Al-4V in the powder diffraction file, the α-Ti and the β-Ti peaks were indexed in accordance with the reference powder diffraction file (PDF), number 44-1294 and 44-1288 respectively, as shown in figure 4.31.

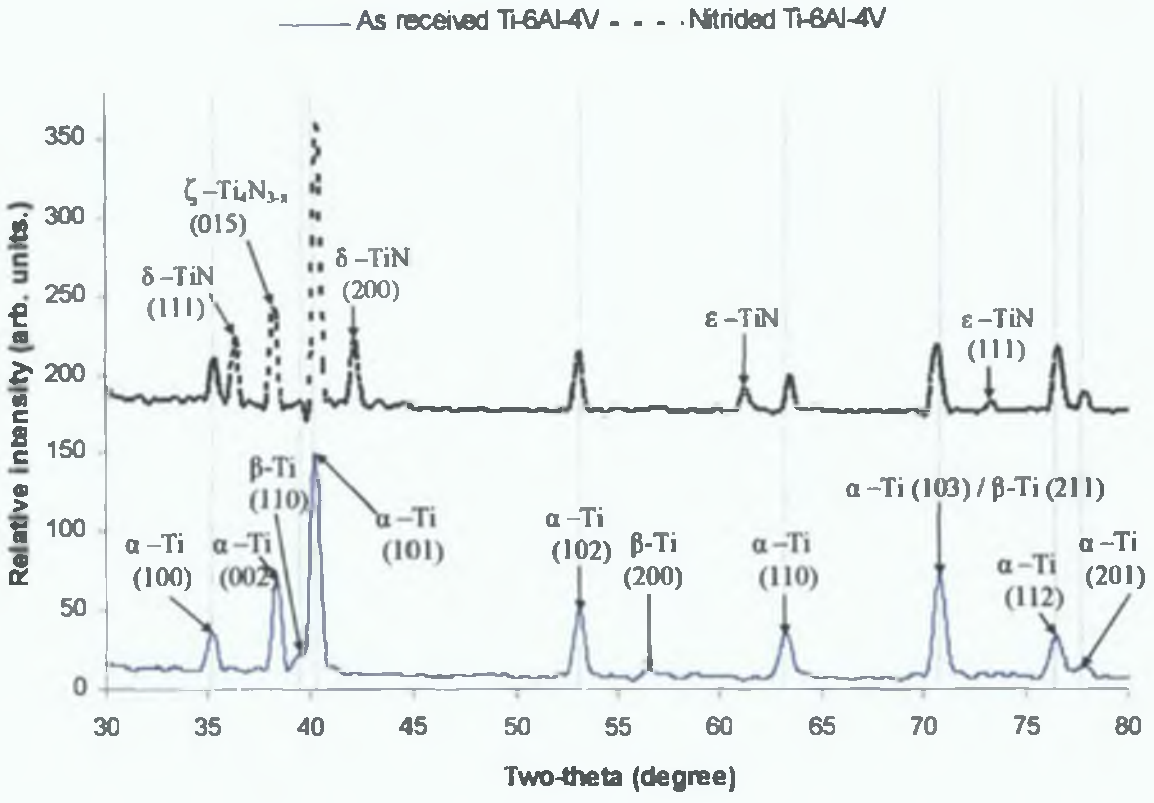

Figure 4.31: XRD patterns of the Ti-6Al-4V sample, nitrided at 900 ^{0}C for 4 h and the as-received Ti-6Al-4V (untreated) sample.

A set of new peaks along with peaks from the α-Ti and the β-Ti were observed when samples were nitrided at 900 ^{0}C. After analysis of the nitrided sample peaks, it was confirmed that the nitrided layers consisted of the face-centred cubic (fcc) δ-TiN phase, the tetragonal ε-TiN phase and the rhombohedral ζ-Ti_4N_{3-x} phase, as indexed in accordance with the reference powder diffraction file (PDF) numbers 65-965, 08-418 and 39-1015 respectively. The peaks of the nitrogen rich cubic δ-TiN phase were observed at $2\theta \approx 36.35$ and 42.25 which corresponds to the (111) and (200) diffraction planes respectively. At $2\theta \approx$ 61.25 and 73.35 clear peaks of a tetragonal ε-TiN phase were also observed.

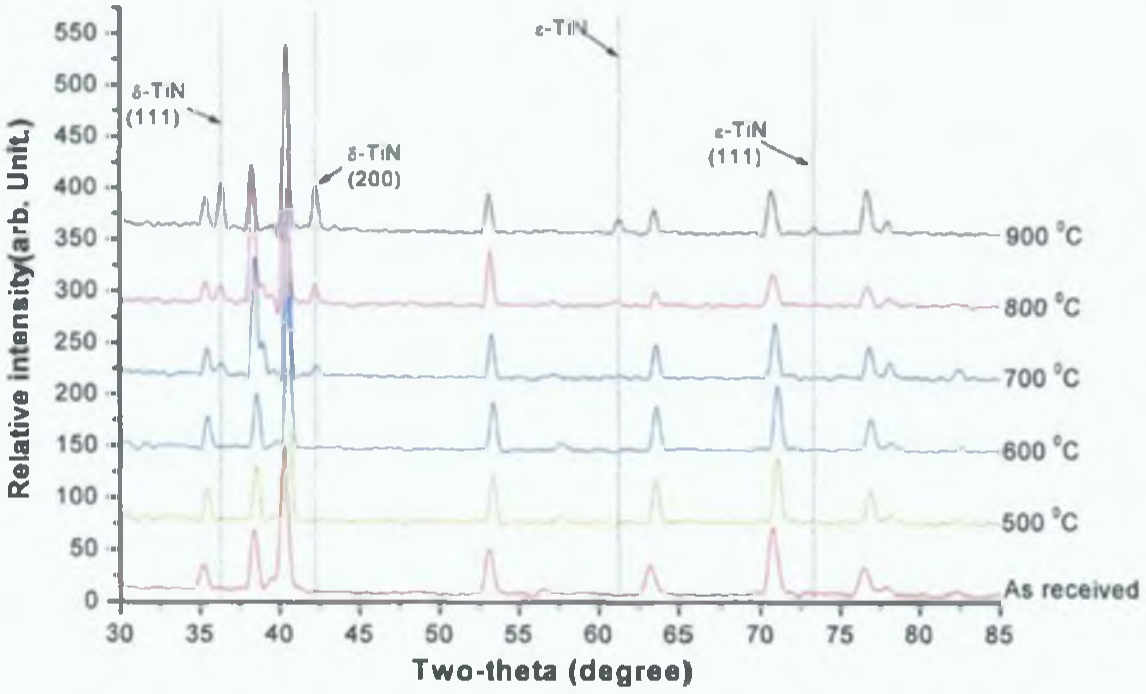

Figure 4.32: The XRD patterns of the nitrided Ti-6Al-4V sample, with nitriding carried for 4 h at different temperatures (500, 600, 700, 800 and 900 ^{0}C) and the as-received Ti-6Al-4V (untreated) sample showing the position of the TiN peaks.

In the XRD spectrum of the nitrided sample, it was found that lines corresponding to the (102) and (103) diffraction planes in the α-Ti phase were shifted to slightly lower angles compared to the untreated samples. This can be explained by the solid solution effect of nitrogen in the α-Ti phase (that means, the enlargement of the lattice parameters of the Ti). On the other hand, peaks for the (110) and (201) crystal planes of the α-Ti phase and the (110) crystal plane of the β –Ti phase, were shifted to slightly higher angles when compared with the untreated samples. This could indicate a tendency for both of the Ti phases to transform into the tetragonal ε-TiN phase. The existence of a nitrogen rich α-Ti phase and the tendency to form an ε-TiN phase from the α-Ti phase were also observed by other authors when the technique of plasma nitriding of α+β Ti alloys is used [229,317]. The diffraction line of the ζ-Ti_4N_{3-x} phase was observed at $2\theta \approx 38.25$ called nitrogen deficient nitride, which corresponds to the (015) diffraction plane. Other authors have reported similar findings [229,318]. All of these different peaks are believed to arise because of the complex structure of the nitrided layer.

The intensity of TiN peaks was found to increase as nitriding temperature increases. However, no X-ray spectrum lines of TiN phases were observed when nitriding was

performed at temperatures below 700 ^{0}C. This result confirmed that the formation of the TiN phase was limited by the nitriding temperature, as shown in figure 4.32. When the nitriding has been performed with high-energy atom beam and at a high temperature (900 ^{0}C), the conditions are suitable for the formation of TiN phases. This result is also supported by other authors [318]. All of these different peaks are believed to arise because of the complex structure of the nitrided layer. S. Yilbas et al. [319] believe that the complex diffraction patterns are composed of three different contributions. There is the contribution of the fcc δ-TiN phase on the top layer, the contribution of a phase of fcc δ-TiN and tetragonal ε-TiN in the intermediate layer and a solid solution of nitrogen in the Ti phases in the diffusion layer.

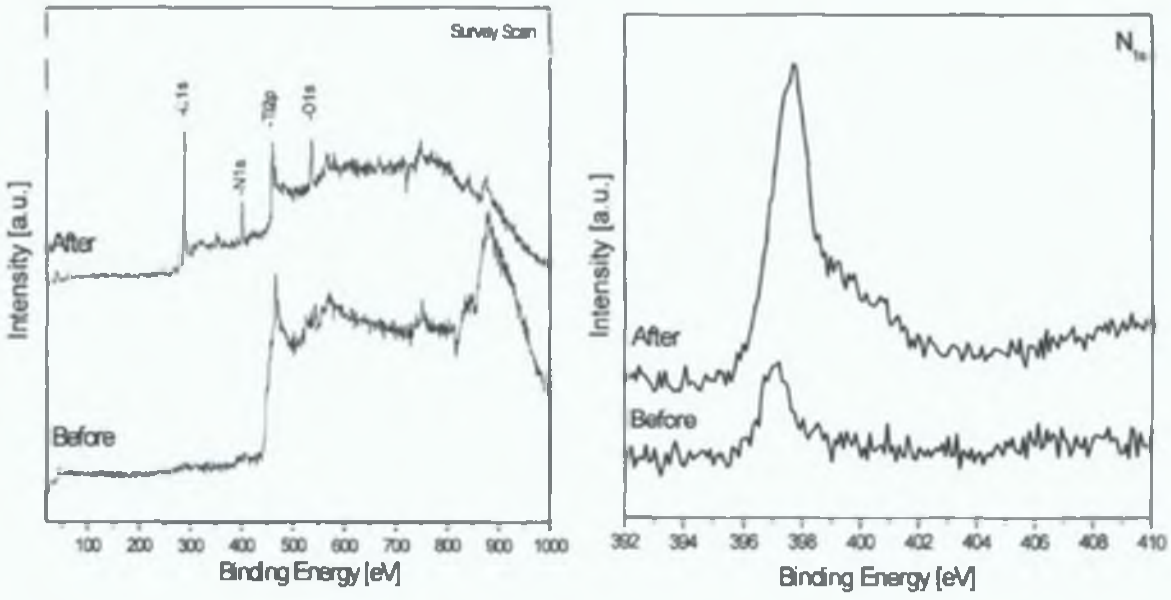

Figure 4.33: The XPS spectra of the (a) non-nitrided and nitride Ti-6Al-4V sample survey scan and (b) the non-nitrided and nitride Ti-6Al-4V sample N_{1s} peak.

XPS survey scan spectra of the treated (900 ^{0}C) and untreated samples showed the presence of Ti and O in the untreated sample and C, N, Ti and O in treated sample (Figure 4.33a). C in the sample is thought to mainly come from the chamber (as plasma source wall is made with carbon clad) and also from atmosphere. Similar result was also found by other researchers [227]. From figure 4.33b, a nitrogen peak was clearly visible in nitrided sample indicating incorporation of the nitrogen in treated sample.

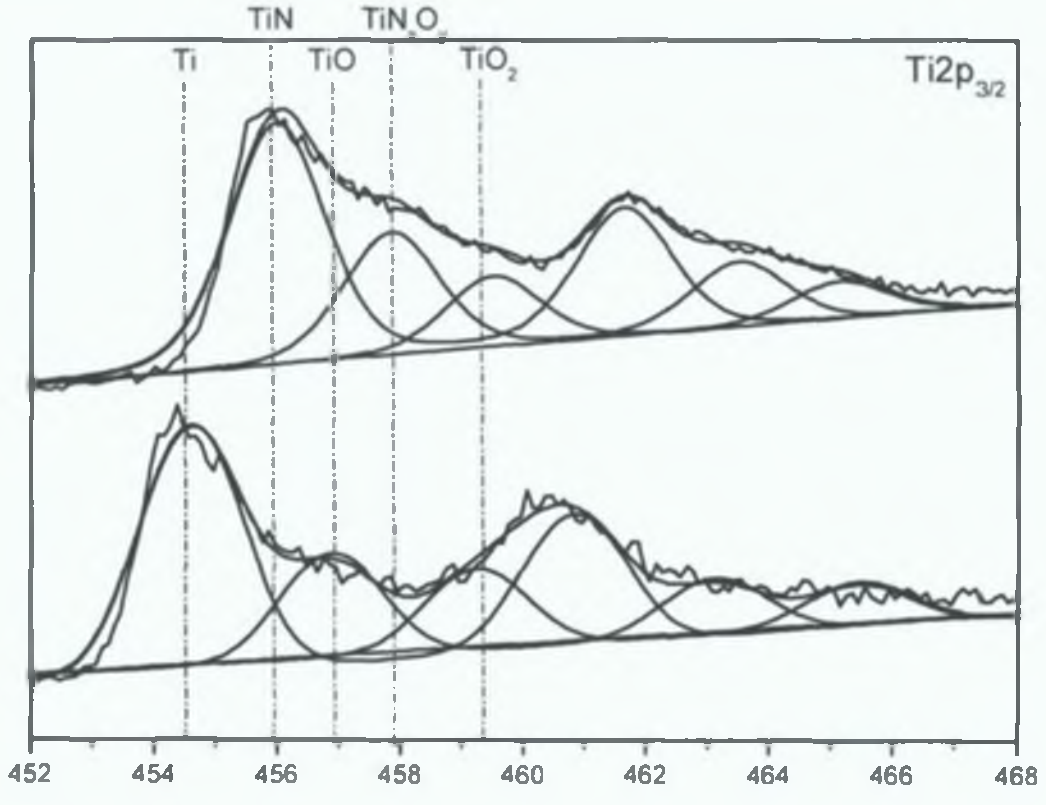

Figure 4.34: The XPS narrow scan spectra with peak deconvulation of the non-nitrided and the nitrided Ti-6Al-4V sample $Ti_{2p\ peak}$

In the spectra of the non-nitriding sample, no noticeable nitrogen peak was observed. The XPS Ti_{2p} peak fitting curve of the plasma nitrided sample confirmed that the nitrogen was retained in the nitrided layer predominantly as TiN phase (Figure 4.34), which was in agreement with the XRD results. However, a small peak of TiN_xO_y phase was also found in nitride layer (when samples were nitrided at 900 ^{0}C). On the contrary, the dominating phase of the metallic Ti and small amount of TiO and TiO_2 were detected in untreated sample.

4.3.2.3. HARDNESS OF NITRIDED SAMPLES

The hardness of a surface is very important due to its influence on the wear properties of the materials. The hardness depth profile of the sectioned nitrided samples was carried out by a Vickers microhardness tester with 15 gm and 25 gm loads and is shown in figure 4.35. Near the surface of the nitrided layer, the maximum hardness was found to have a value 1578 $HV_{0.015}$ which is roughly three times higher than the hardness of the non-nitrided samples (568 $HV_{0.015}$).

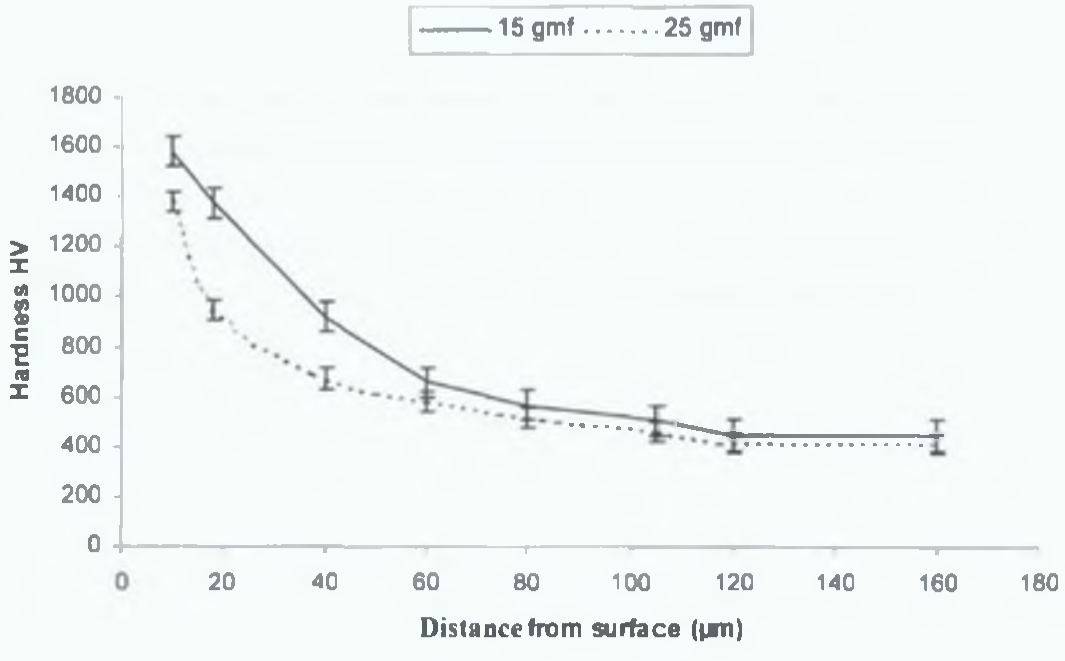

Figure 4.35: Hardness depth profile of the nitrided Ti-6Al-4V sample.

This high hardness value was only observed for a short distance (16 μm) from the top nitrided surface. The significant high hardness value for the top layer of the nitrided sample may be due to the presence of the very hard TiN in this layer. The presence of this phase was confirmed by XRD and the cross-sectional optical investigation of the nitrided samples. Due to the presence of the diffusion layer below the compound layer, the hardness value decreased gradually from the top compound layer. The hardness values near the interface between the diffusion layer and the core materials were nearly the same as the values for the untreated samples (568 $HV_{0.015}$). Values for the untreated region of the samples were constant whether the measurement was taken on the surface of the samples or a long way beneath the surface. This finding agrees with the results of other researchers

[319]. The presence of nitrogen in a solid solution enriching α-Ti phase in the diffusion layer, resulted in an increase in the hardness value for this layer [228].

The Vicker microhardness of the non-nitrided and nitrided samples at different temperatures is shown in figure 4.36. The samples nitrided at high temperatures (at or above 700 ^{0}C) showed higher hardness compared to samples nitrided at low temperatures due to the formation of a compound nitriding layer (composed of hard TiN and other phases) at higher temperatures. This was in agreement with the cross-sectional morphology of the nitrided substrate.

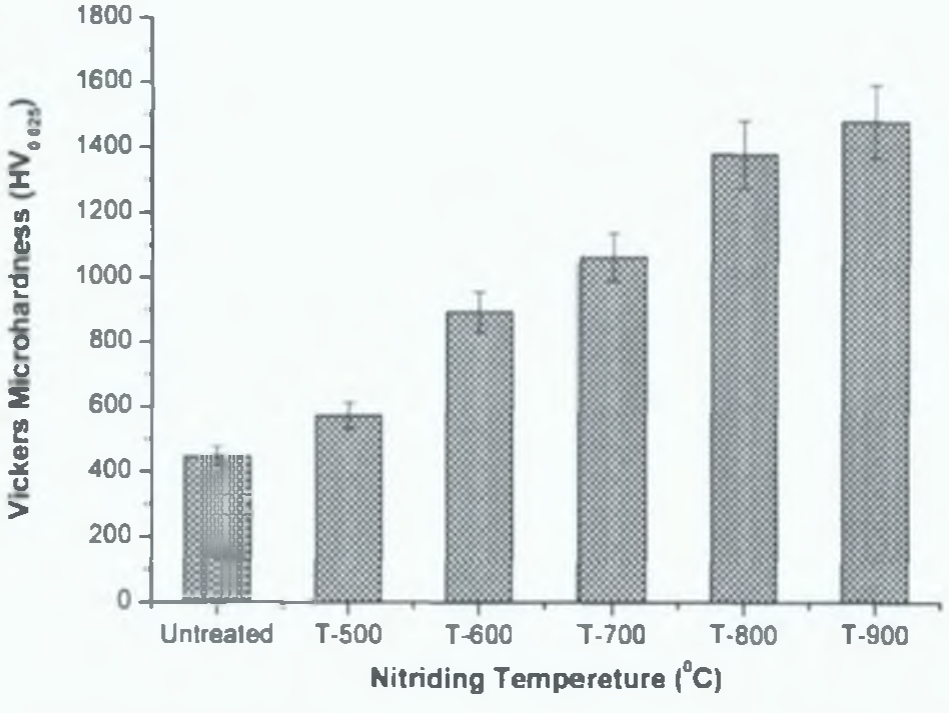

Figure 4.36: The surface micro hardness of the nitrided Ti-6Al-4V sample, with nitriding carried for at different temperatures (500, 600, 700, 800 and 900 ^{0}C) and the as-received Ti-6Al-4V (untreated) sample

In case of samples nitrided at high temperatures (at or above 700 ^{0}C), the increase in hardness with temperature can be explained by, (i) the formation of a relatively thick compound layer and (ii) the presence of a more concentrated hard TiN phase which was confirmed by XRD result. On the other hand, a slight increase in hardness of the samples nitrided at low temperature (below 700 ^{0}C) can be attributed to the combined effect of the diffusion layer and presence of oxide phases, as confirmed by XRD result.

4.3.2.4. TRIBOLOGICAL PROPERTIES

The friction co-efficient curves for the nitrided and the un-nitrided samples are shown in figure 4.37, where all pin-on-disk wear tests were performed with the same conditions mentioned earlier. Un-nitrided samples showed average friction values of 0.57 and a small change of the friction value was found for the sample nitrided at low temperatures (average friction values of 0.51).

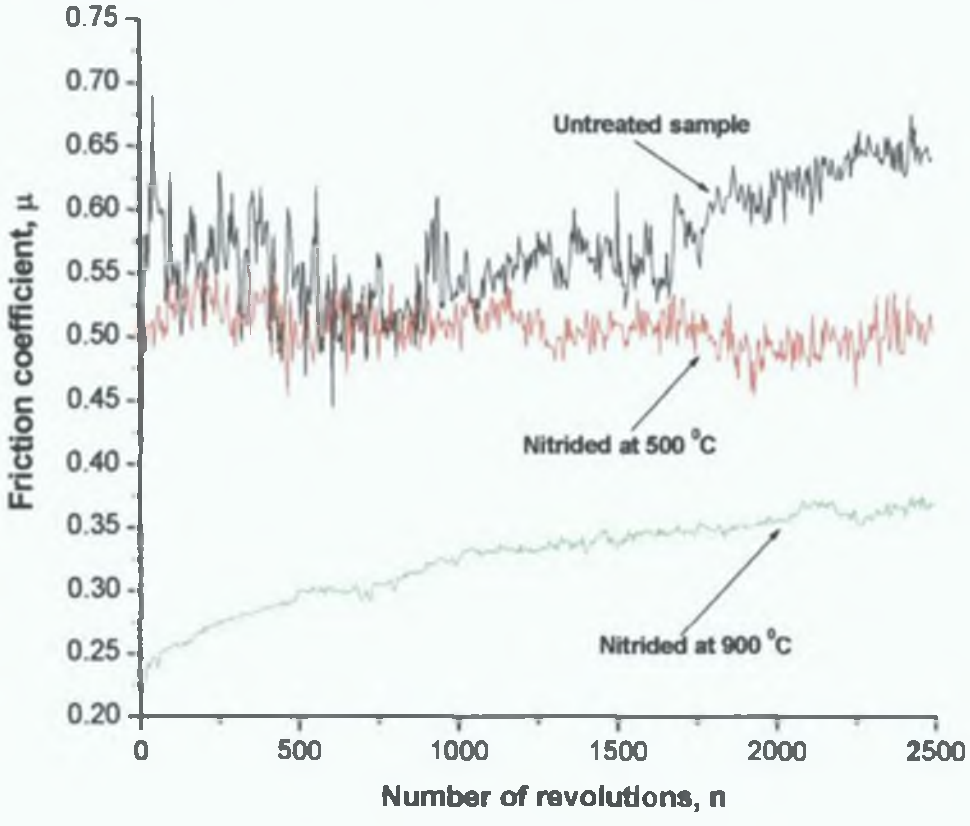

Figure 4.37: The friction coefficients for pin-on-disk tests of the non-nitrided and the plasma nitrided Ti-6Al-4V sample.

However, the sample that was plasma nitrided at high temperatures showed a lower (average friction values of 0.324), more stable and smoother co-efficient of friction compared to the non-nitrided and the low temperature nitrided samples. This can be explained by the presence of the hard nitrided surface, which leads to a lower wear contact area [210] due to the prevention of the asperity welding of the hard nitrided samples with the counterface materials when tested on the pin-on-disc machine [309]. The TiN_xO_y compounds which were confirmed by XPS result to have formed on the surface of the samples, exhibited low friction [229].

The wear track morphology of the nitrided (polished and as-treated) and the non-nitrided samples are shown in figure 4.38. A wide and rougher wear track with large plastic deformation and deep ploughing on the wear track were clearly observed in the un-treated sample (Figure 4.38a) due to the very low hardness of the soft untreated sample. A severe adhesive, abrasive and deformation wear mechanism was found for untreated samples. On the other hand, different wear behaviour was observed for the hard nitrided sample. The samples nitrided at high temperatures (900 ^{0}C) showed a narrow, less rough and shallow wear track compared to the non-nitrided and nitrided samples at low temperature (Figure 4.38). Nitrided samples demonstrated no severe deformation and ploughing line on the wear track due to the hard load supporting layer of the nitride (Figure 4.38c). Figure 4.38c and 4.38d clearly shows the formation of a transferred layer on the plasma nitrided layer and this layer was considered to come from asperities shearing and the burnishing of the nitrided surface with counterpart materials. A micro-abrasive and burnish type wear mechanism was characterised for the treated samples. The absence of an adhesive wear mechanism on the nitrided surfaces may be due to the asperity welding prevention of the hard nitrided surface [309]. The polished nitrided samples (900 ^{0}C) showed increased smoothness of the wear surface compared to the unpolished nitrided surface which may be due to less asperities shearing and the burnishing of the smooth nitrided surface (Figure 4.38d). The samples nitrided at low temperatures showed no significant improvement in the wear properties due to the low hardness of the nitride layer and an absence of TiN phase in the nitrided layer. This was confirmed from hardness and XRD test results respectively.

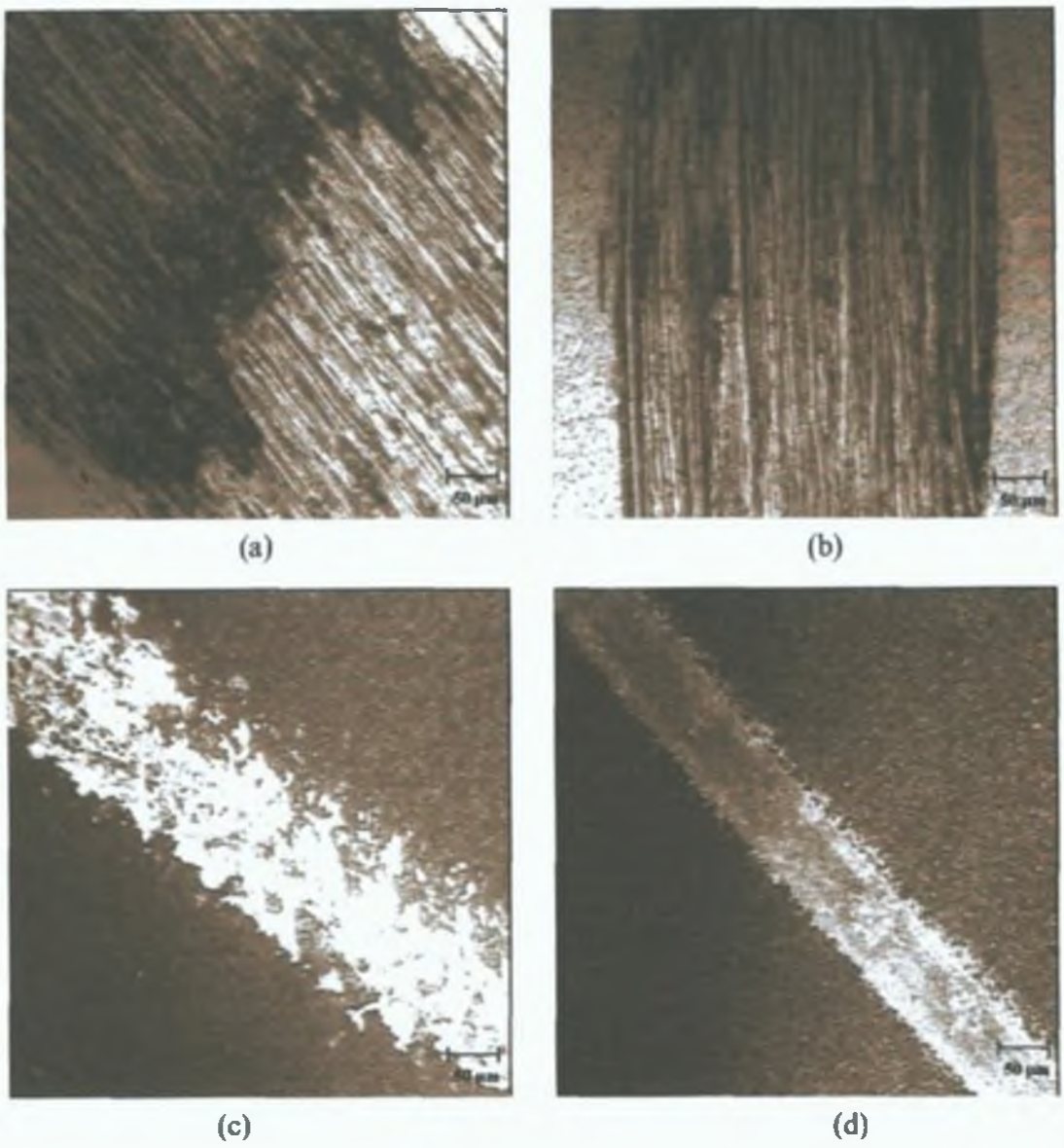

Figure 4.38: The optical wear track morphology of (a) the non-nitrided Ti-6Al-4V samples and the nitrided Ti-6Al-4V samples, samples after nitriding at (b) 500 ^{0}C (as nitrided) (c) 900 ^{0}C (as nitrided) and (d) 900 ^{0}C (nitrided and polished)

Wear depth results also confirmed that plasma nitriding of the Ti-alloy sample at high temperatures significantly improves the wear resistance when compared to the untreated samples. Wear depth values were recorded as low as 0.42 μm for the as nitrided samples (900 ^{0}C) and 0.2 μm for the polished nitrided samples (900 ^{0}C) which was respectively approximately eleven and twenty times lower than the untreated samples (wear depth 4.8 μm). This fact can be explained by the increases of the surface hardness caused by the presence of the hard TiN phase (which has a low adhesion against counter part and highest

strength) after nitriding which causes a decreased wear contact area with the counter surface during the wear test [210,320]. This was also in agreement with the wear track width of the nitrided and the non-nitrided samples. The wear track width was found to be as low 140 μm for the as-nitrided samples (900 ^{0}C) and 88 μm for the polished nitrided samples (900 ^{0}C). These values were significantly lower than those of the untreated samples (560 μm). The wear depths of the polish nitrided samples was also found to be lower than those of the as- treated nitrided samples. A greater amount of damage was caused to the surfaces of the as-treated nitrided samples, which in turn increased the wear rate. Higher wear depth and wear track width values were recorded for the samples nitrided at low temperatures compared to the sample nitrided at high temperatures, which is an also in agreement aforementioned finding.

4.3.3. PLASMA NITRIDING OF NON-CONDUCTIVE UHMWPE

4.3.3.1. TOP SURFACE MORPHOLOGY BY OPTICAL MICROSCOPE

It was observed by the naked eye that the surface coluor of the nitrided polymer samples changed from off-white to light yellowish. The changing of the surface color can be attributed by thermal effect of bombardment of the surface with energetic particle and dehydrogenation (which enhanced the formation of conjugated double bond) [241].

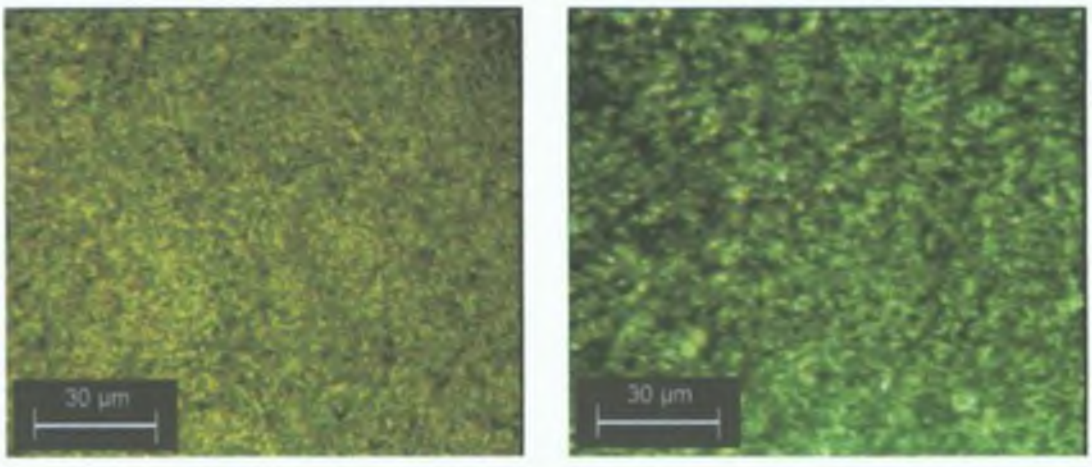

(a) (b)

Figure 4.39: Optical top surface morphology of the (a) untreated and (b) treated sample

From figure 4.39, a featureless and more irregular surface morphology (peak and valley) of the nitrided sample was observed comparing to the non-nitrided sample surface, may be due to etching effect at the time of nitriding process and due to the change in functional groups of the treated surface. A small increased in surface roughness was observed for the nitrided sample compared with the untreated sample. The average surface roughness of the untreated sample was recorded to be 357 nm compared with treated sample which had a value of 401 nm.

4.3.3.2. EVALUATION OF PHASE BY RAMAN AND XPS

The extended Raman spectra of as-received and nitrided UHMWPE, produced using a wavelength of 488 nm, are shown in figure 4.40. For the untreated polymer samples, several sharp peaks similar to polyethylene can be clearly observed at ~1070 and 1134, 1289, 1445 and 2186 cm^{-1} as shown in figure 4.40. The peaks with weak intensities at 1070 and 1134 cm^{-1} were corresponded to C-C skeletal stretching vibration of the carbons atoms. Bands at 1289 cm^{-1} originated from $-CH_2$ in phase twisting. Whereas, peaks at 1375 and 1450 cm^{-1} were generated respectively from $-CH_2$ symmetric and asymmetric deformation stretching modes. A significant changed in the shape and intensity of the peak was observed for nitrided samples [239].

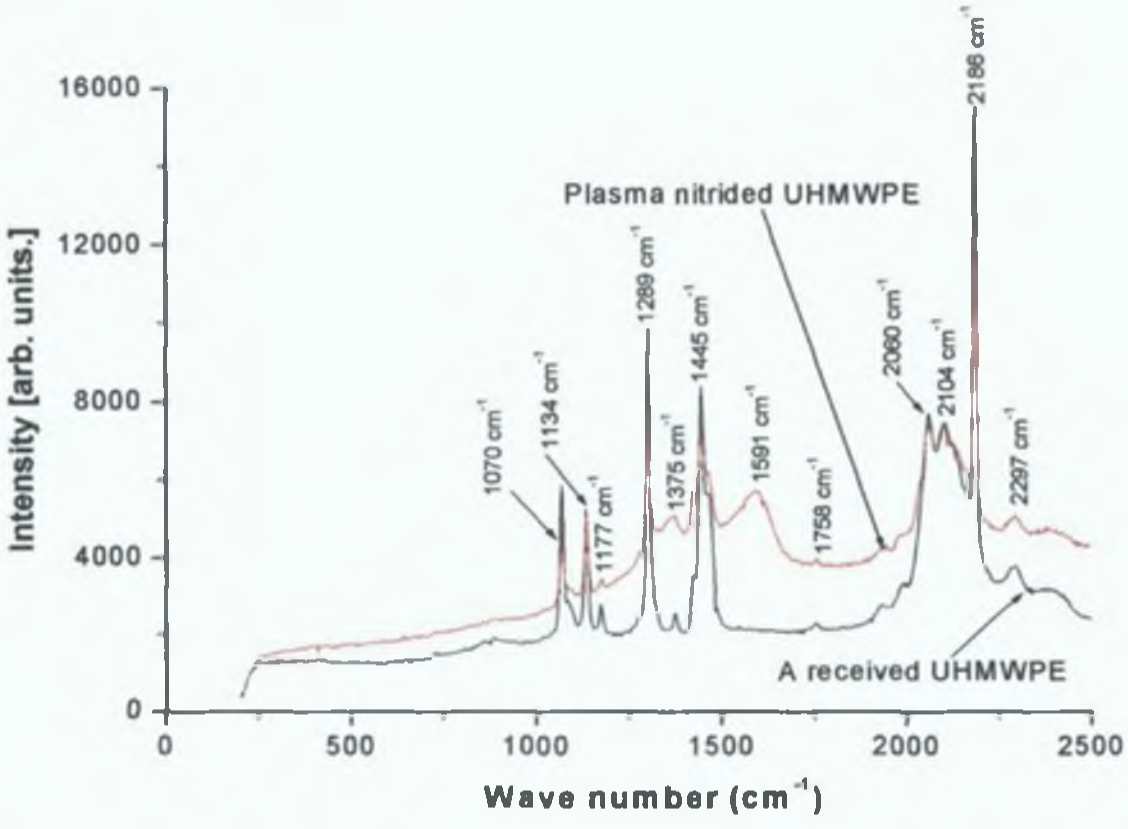

Figure 4.40: Survey Raman spectra of the Nitrided and Non-Nitrided UHMWPE sample

The photoluminescence effect (background) of the nitrogen implanted samples was found to increase. This may be due to an increase in the number of defects in the treated samples caused by the bombardment of the surface with high energy particles. The relative intensity of the peaks related to C-C and $-CH_2$-vibrations was found to decrease, indicating that the chemical structures of the surface change after plasma nitriding. In particularly, the intensity of the peak at 1289 cm^{-1} is related to the n value of the chain $[-CH_2-]n$ bond in untreated UHMWPE. The high intensity of this peak indicated a higher value of n which in turn represented a long polymer chain. That means, the intensity of 1289 cm^{-1} peak is inversely proportional to chain lengths. Therefore, a decrease in the 1289 cm^{-1} peak intensity suggests breaking and shortening of the long polymer chain (decrease n value) in the untreated sample. This indirectly represents the creation of the crosslinking effect in treated samples. Others research supports this result [239,321].

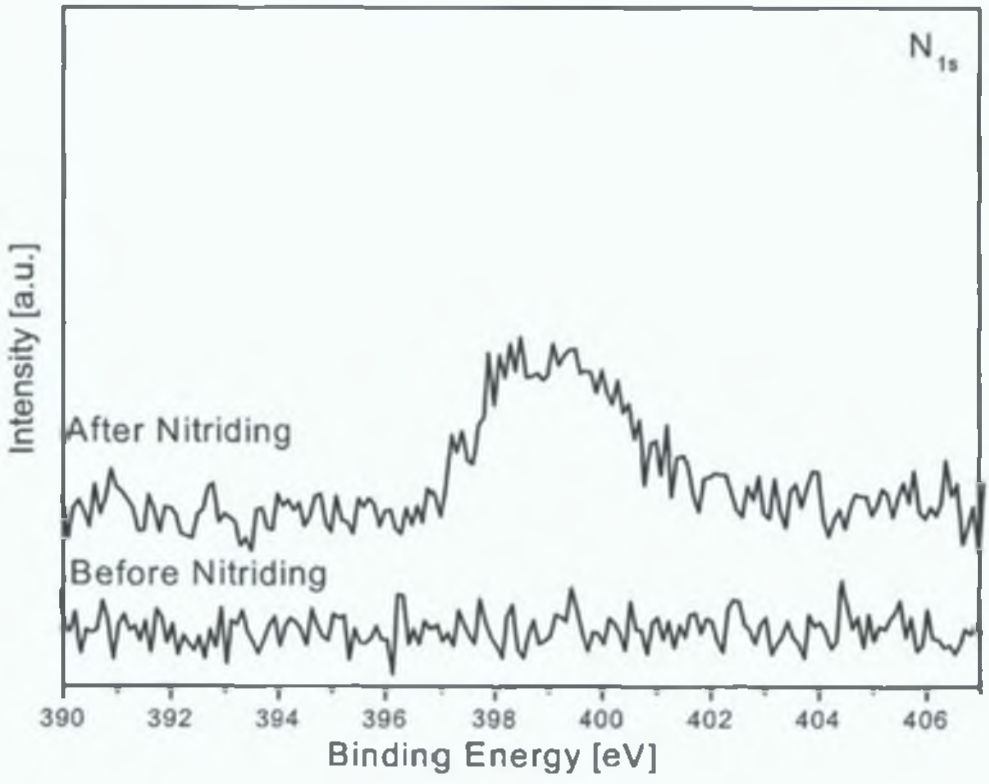

Figure 4.41: XPS, N1s peak of the nitrided and non-nitrided samples

The nitrogen (N 1s) peak positions of the as-received and nitrided samples are shown in figure 4.41. No nitrogen peak was observed in non-nitrided samples. However, a clear peak of nitrogen was found in the nitrided samples which confirmed the injection of the nitrogen in to the plasma nitrided sample.

In general, the unbounded or non-bonding nitrogen peak position is situated at a binding energy of between 402.0 - 403.0 eV [322]. However, a broad (full width at half maximum ~ 3.25 eV) and small intensity peak of N1s for plasma nitrided sample was found at a new position of ~399.2 eV, as shown in figure 4.42.

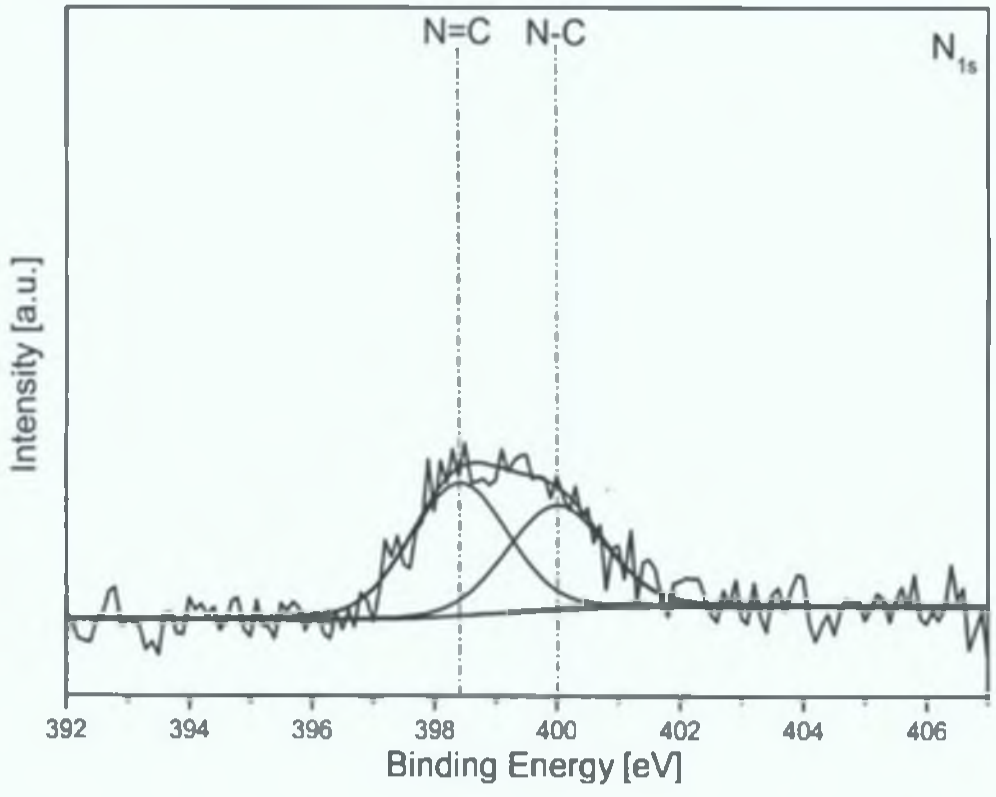

Figure 4.42: XPS narrow scan and peak fitting curve of the N1s peaks showed possible bonding in the nitrided sample

A peak at 399.4 eV was reported which corresponded to the nitrial (–C≡N) bond of CN_x phase [322,323]. Again, by decomposition of this broad peak using peak fitting software, it was confirmed that nitrogen peak of the plasma nitrided sample was composed of two major components. The nitrogen atom can be subtitutionaly bound by sp^2 or sp^3 hybridized carbon atom clusters. The peaks situated at the binding energies ~ 398.4 and ~

400.02 eV, correspond to a double bond, C=N (N-sp^3 C) and a single bond, C-N (N-sp^2 C), respectively. This is supported by other researchers [324,325]. The bonding explanation of nitrogen in the polymer samples is quite complicated and not fully clear as different researchers have used different processes/techniques and have reported different types of possible bonding. However, as in present investigation no peaks were found corresponding to the position of the unbound or precipitation of nitrogen (~ 402. 0-403. 0 eV), in any case it can be confirmed that the crosslinking effect was taking place in nitrided sample through the formation of chemical bonds between the of injected nitrogen atoms and with polymer carbon chain (-C≡N or-N-sp^3 C and N-sp^2).

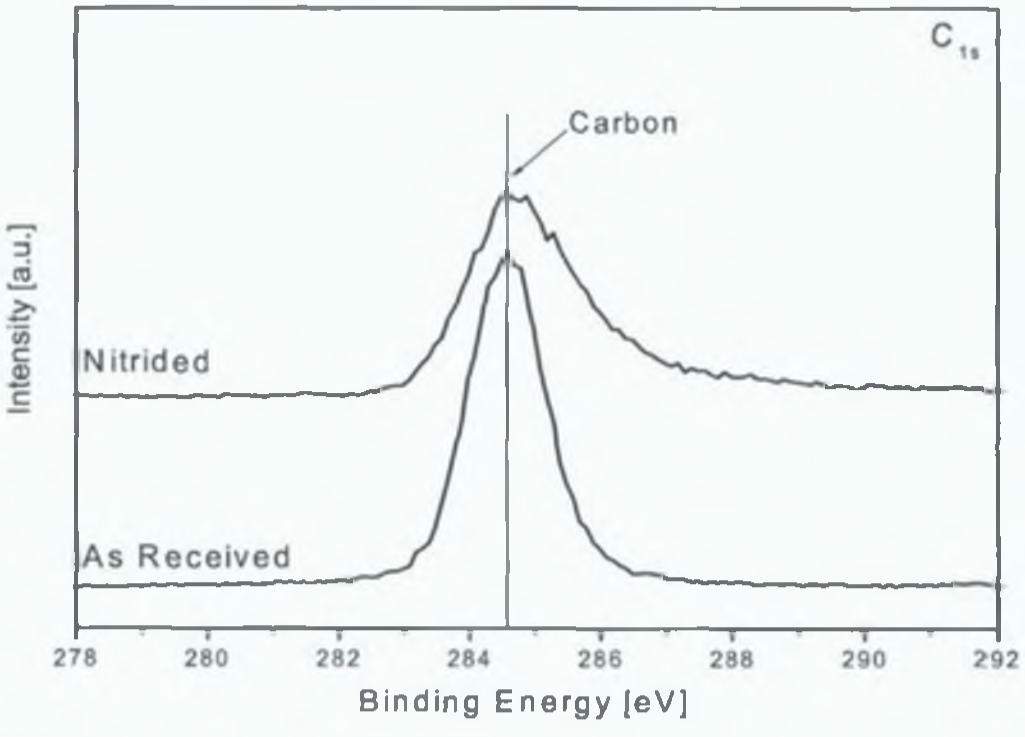

Figure 4.43: XPS narrow scan curve of the C1s peaks of the nitrided and non-nitrided samples

The carbon peak position of the nitrided and non-nitrided sample is shown in figure 4.43. The peaks were featureless in nature, as both peaks were found at same position (~ 284.66 eV) and had same shape.

4.3.3.3. WETTABILTY MEASUREMENT BY CONTACT ANGLE

The hydrophilicity or wettability of the materials was assessed through the measurement of the water contact angles. The contact angle measurement confirmed a small change in contact angle value for the treated sample compared to the untreated sample, as shown in figure 4.44. The untreated sample had contact angle of 126 ^{0} whereas the contact angle of the plasma nitrided sample was found to be around 117 ^{0}. The increased of the wettability property (decreased of the contact angle value) of the plasma nitrided samples compared with the untreated samples may be due to an increase in the polar component of the nitrided sample surface compared to the non-nitrided sample. The increased wettability or decreased contact angle after ion implantation on organic materials was confirmed by other researchers [326]

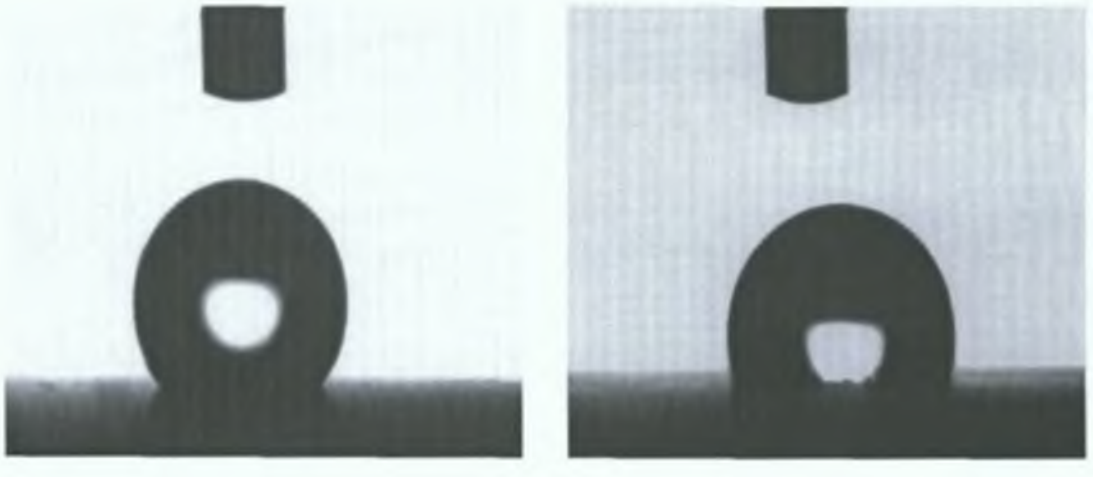

(a) (b)

Figure 4.44: Water droplet on the (a) non-nitrided and (b) Nitrided sample surface for measuring contact angle (wettability)

4.3.3.4. MECHANICAL AND WEAR PROPERTIES

Vickers microhardness testing results confirmed the increase of the plasma nitrided sample hardness compared with non-nitrided sample. This may be due to formation of a hard nitrided phase and also due to the cross-linking effect confirmed by XPS and the Raman results.

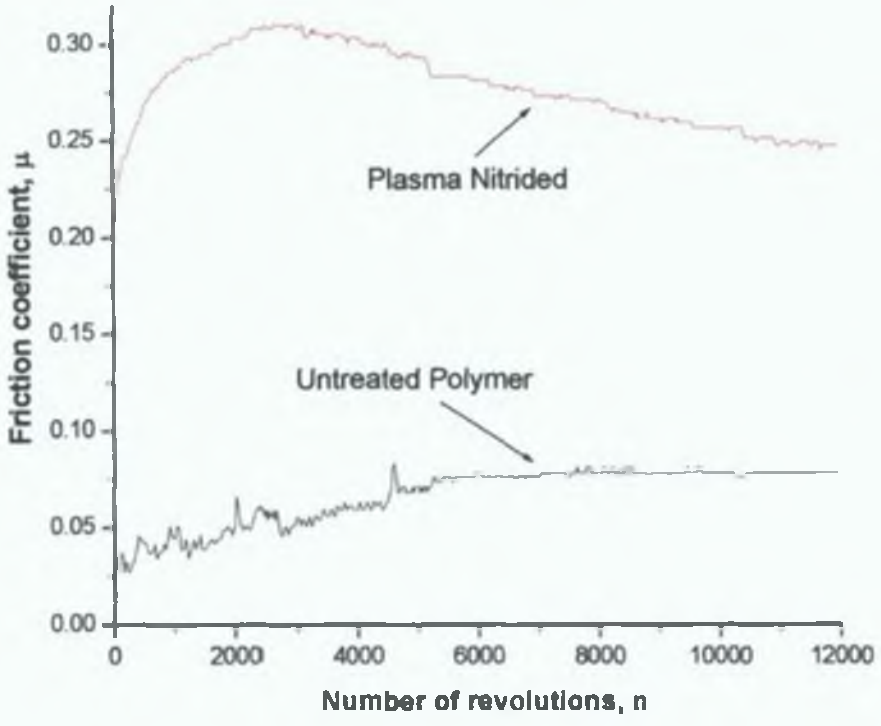

Figure 4.45: Co-efficient of friction curves for the untreated and treated samples

The dry sliding (un-lubricant) wear results (tested at room temperature in air on the pin-on-disk machine) confirmed the increase in friction value of the nitrided sample compared with the non-nitrided sample, as shown in figure 4.45, when all test were carried out in the same conditions (load = 100g, number of rotation = 12, 000, speed = 60 RPM, radius of wear track = 7 mm, and counterface material = tungsten carbide ball). The reason of the increase in friction value was not fully clear but it may be due to changes of the surface structure and the increase in surface roughness. Other researchers have supported this result [326]. However, this result was in contrary to those found in work carried by Allen et al. [240]. They carried out wear test in both dry and wet conditions, using Ti-6Al-4V as a counterface material, and found that the treated samples showed a lower co-efficient of friction compared with the untreated samples. A significant reduction in co-efficient value also was recorded by them when the wear tests were performed in wet conditions.

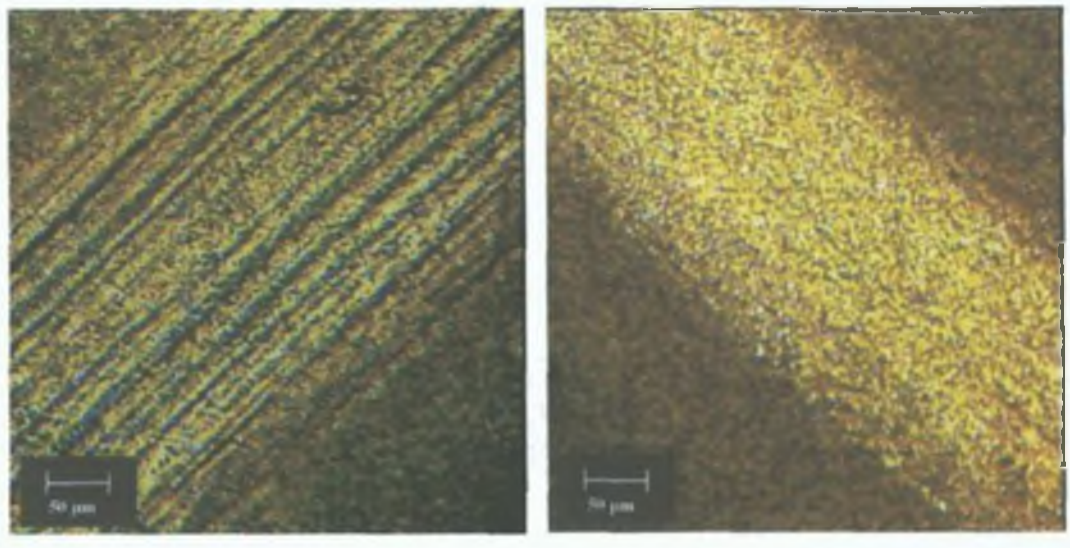

(a) (b)

Figure 4.46: Wear track morphology of (a) untreated and (b) treated sample

A deep, wide and ripple-like wear track with deformation and many abrasive grooves was clearly observed for the untreated soft UHMWPE samples, as shown in figure 4.46. Contrary to this, a relatively smooth wear track with a fine abrasive nature was observed in the wear track of the treated nitrided sample indicating an improvement in the wear resistance of the nitrided surface. The wear track image result supported the measured wear width and depth values as shown in Table 4.2.

Table 4.2: Summary of the wear test results for the polymer samples

Sample	Co-efficient of friction (steady state)	Wear depth (μm)	Wear width (μm)
Untreated polymer	0.055	1.44	312
Treated polymer	0.24	1.06	236

The improvement of wear-resistance of the plasma nitrided UHMWPE sample could be attributed to the surface strengthening induced via the formation of crosslinking and the

hard nitrided phase in the nitrided UHMWPE sample. The hard surface formed as a consequence of the effects of structural modification and crosslinking, as confirmed by the XPS and Raman results, increase the load bearing capacity of the soft polymer samples. Hence, the contact area with the counterpart surface was significantly reduced during the wear test. Crosslinking also reduced the sliding between molecules of treated surface. This result also was supported by other authors [235,241] using surface treatment methods other than fast atom beam. It was reported that a further significant improvement in wear properties could be recorded, when wear testing of the polymers samples with high wettability was carried out in wet conditions [240].

4.4. DUPLEX COATING

4.4.1. CONTINUOUSLY DEPOSITED DUPLEX BIOMEDICAL COATINGS

4.4.1.1. TOP SURFACE MORPHOLOGY BY ATOMIC FORCE MICROSCOPY (AFM) AND OPTICAL MICROSCOPY

A featureless smooth surface microstructure of the DLC coating on a silicon substrate was observed from the AFM micrographs, shown in figure 4.47. The scan was carried out over an area of 3.25 µm x 3.25 µm giving an RMS surface roughness around 2-3 nm.

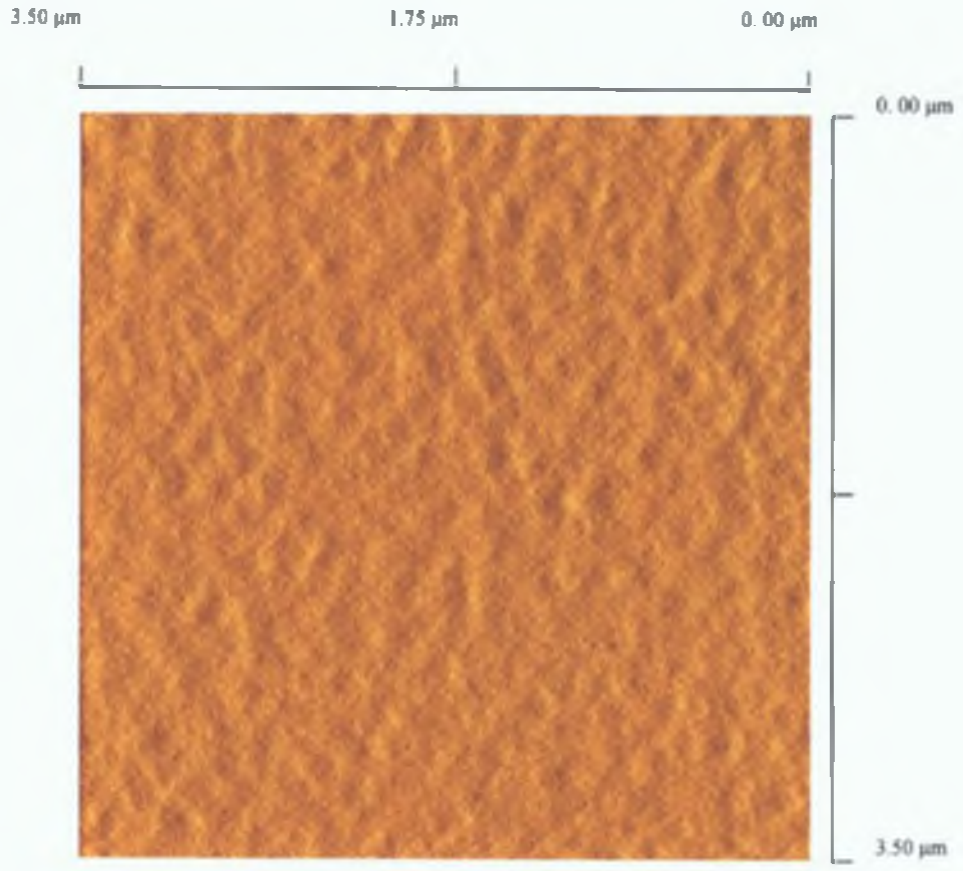

Figure 4.47: AFM top surface morphology of the DLC coating on silicon substrate.

Figure 4.48 shows the optical top surface morphology of the non-duplex treated and the duplex treated samples on 316L stainless steel. A featureless smooth surface with few pinholes was observed on the top surface of the non-duplex treated samples. However, as the coating was thin, a peculiar surface morphology of the plasma nitrided sample (austenitic grain boundaries and twins as described earlier) was observed on surface of the duplex treated sample. No pinholes were observed on the surface of the duplex treated sample. The surface roughness increased from 30 nm for the non-nitrided substrate to 100 nm for the nitrided substrates. The roughness value of the nitrided sample was found to decrease slightly after the deposition of the DLC coating.

(a) (b)

Figure 4.48: The optical top surface morphology of (a) the non-duplex treated and (b) the duplex treated samples on 316L stainless steel.

Figure 4.49 shows, the chemically etched (by glyceregia agent) SEM cross-sectional morphology of the duplex coating substrate system. The micrograph reveals a clearly visible nitrided layer, separated from the core material. This confirms the precipitation-free nitriding of the stainless steel at low temperature. These results agreed with those of other researchers [209]. A uniform and dense layer of the DLC coating on the homogenous thick plasma nitrided layer was found in the duplex treated samples.

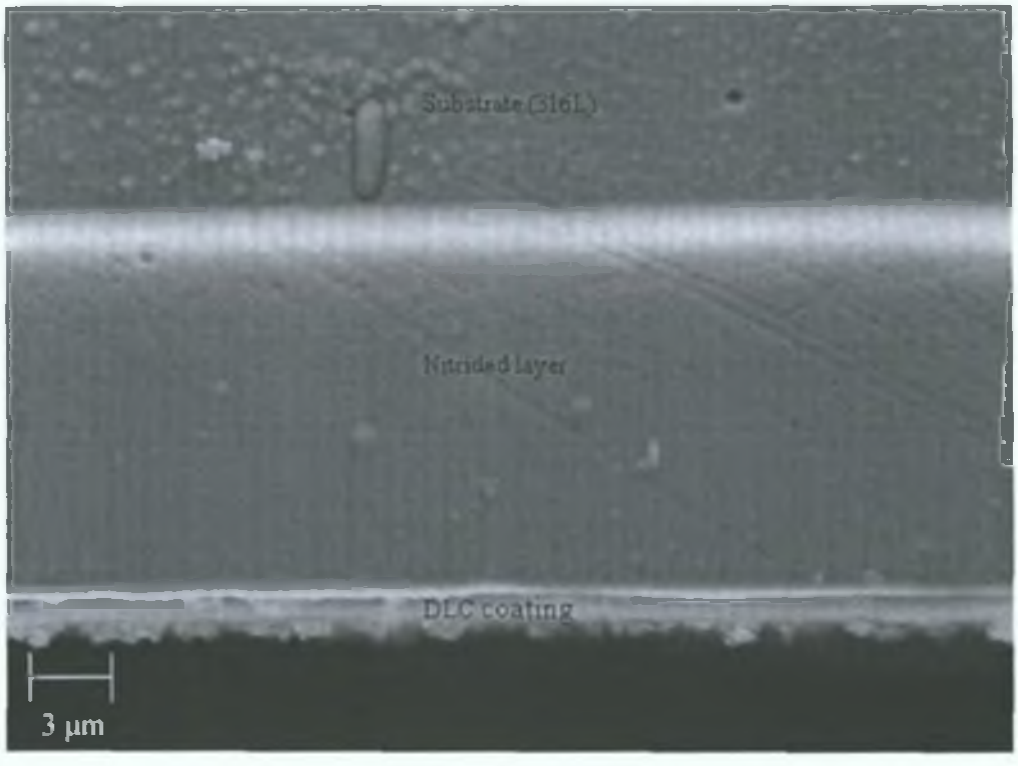

Figure 4.49: The chemically etched (by glyceregia agent) SEM cross-sectional morphology of the duplex coating substrate system.

A very good bonding with no delamination was confirmed at the interface between the coating and the nitrided layer. The thickness of the nitrided layer was measured to be approximately 13 µm and the thickness of the coating was between approximately 0.9 and 1. 00 µm.

4.4.1.2. PHASE ANALYSIS BY XRD, RAMAN AND FTIR

The XRD results confirmed the formation of the amorphous DLC coating on the silicon substrate as only the silicon substrate peak (402) was observed at ~2Θ = 69.7 from the diffraction line [327]. The C-C bonding structure of the coating was identified by Raman spectroscopy shown in figure 4.50. A broad peak around 1550, composed of a G (corresponding to the graphite phase) and a D (corresponding to the disorder phase) band was confirmed after Gaussian peak fitting.

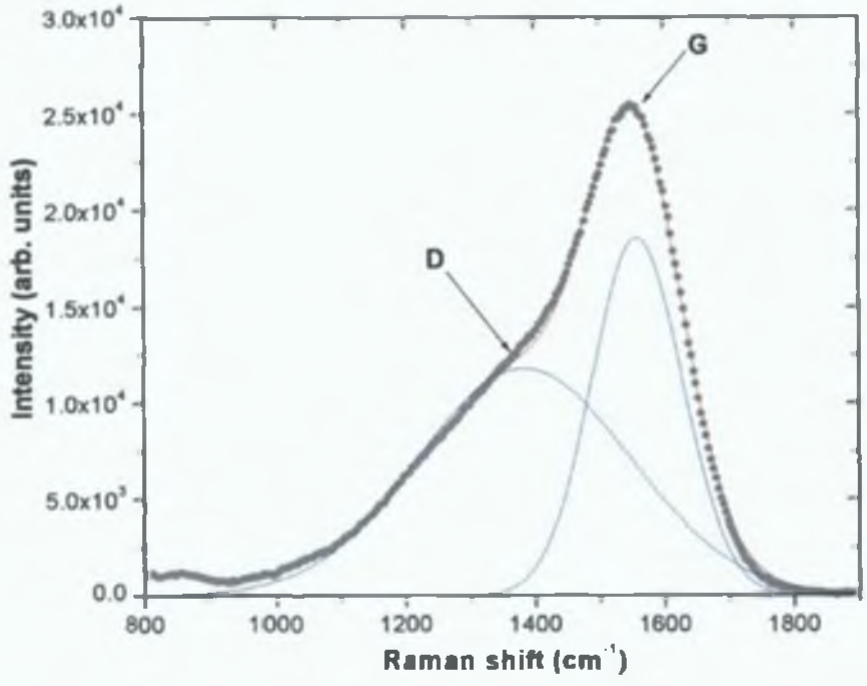

Figure 4.50: The Raman curve fitting spectra of the DLC coating on silicon

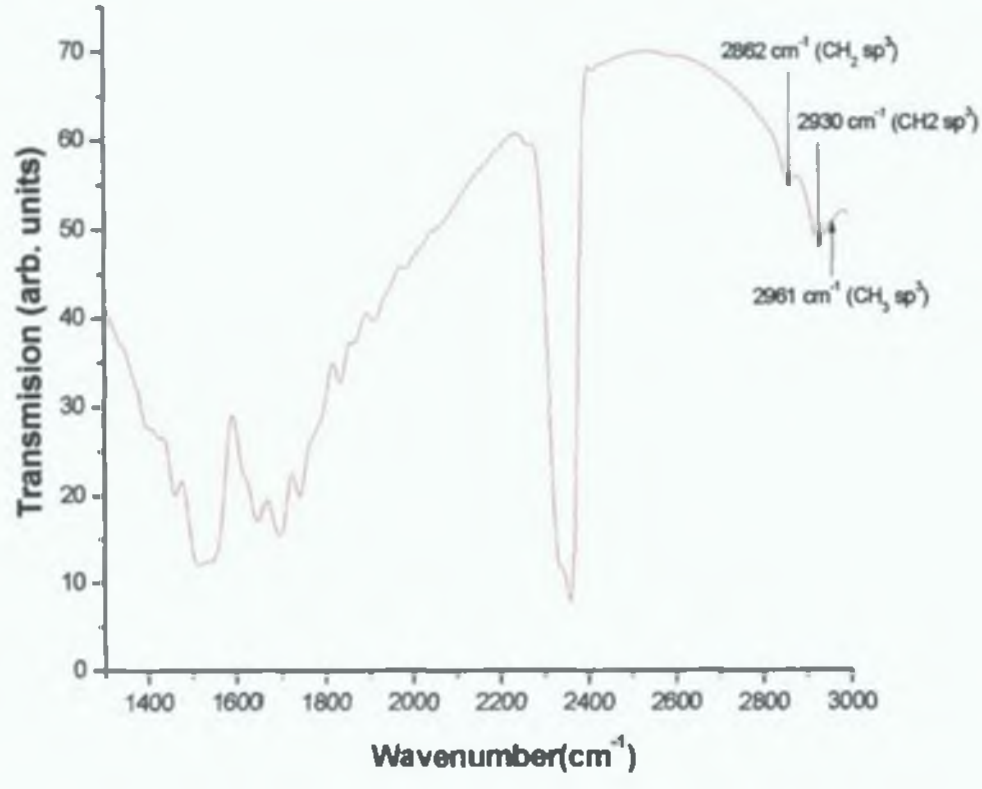

Figure 4.51: The FTIR survey spectra (transmitted) of the DLC coating on silicon

The position of the G peak was recorded approximately at 1558 cm^{-1} and the intensity ratio of D and G band (I_D/I_G) was found in this study to be 0.63, which confirmed the amorphous DLC nature of the coating [299,328]. The structure of the film was also confirmed by the FTIR study, where peaks at 2961 cm^{-1}, 2930 cm^{-1} and 2862 cm^{-1}, as shown in figure 4.51, were believed to be come from sp^3-CH_3 anti-symmetric, sp^3-CH_2 asymmetric and sp^3-CH_2 symmetric vibrations respectively [329,330]. This result indicated the presence of sp^3 bonds in the film and was supported by the Raman results.

4.4.1.3. ADHESION MEASURENT BY ROCKWELL-C

From the Rockwell C indentation spot of the duplex and the non-duplex coating system, it was found that plasma nitriding significantly reduced crack network formation and plastic deformation beside the edge of the indenter. It can be clearly observed from figure 4.52a that the coating on the untreated soft sample showed a large number of the crack networks around the indentation spot. This feature represents adhesion in HF3-HF4 scale (bad adhesion). Coating on soft substrate could not support the load and caused plastic deformation of the substrate, which ultimately partially detached (swelling) the coating from the substrate at the edge of the indentation.

However, no crack network and no swelling type detachment or deformation were observed around the edge of the duplex treated sample's indentation spot indicating relatively good adhesion, as shown in figure 4.52b. This feature represents adhesion in HF1 scale (good adhesion). The plasma nitriding effect in the duplex coating systems therefore produces an improvement in the adhesion. This is possibly due to the presence of the very hard thick nitrided sub-layer which may have reduced the hardness and residual stress gradient between substrate and coating [331] without the deposition of any interlayer.

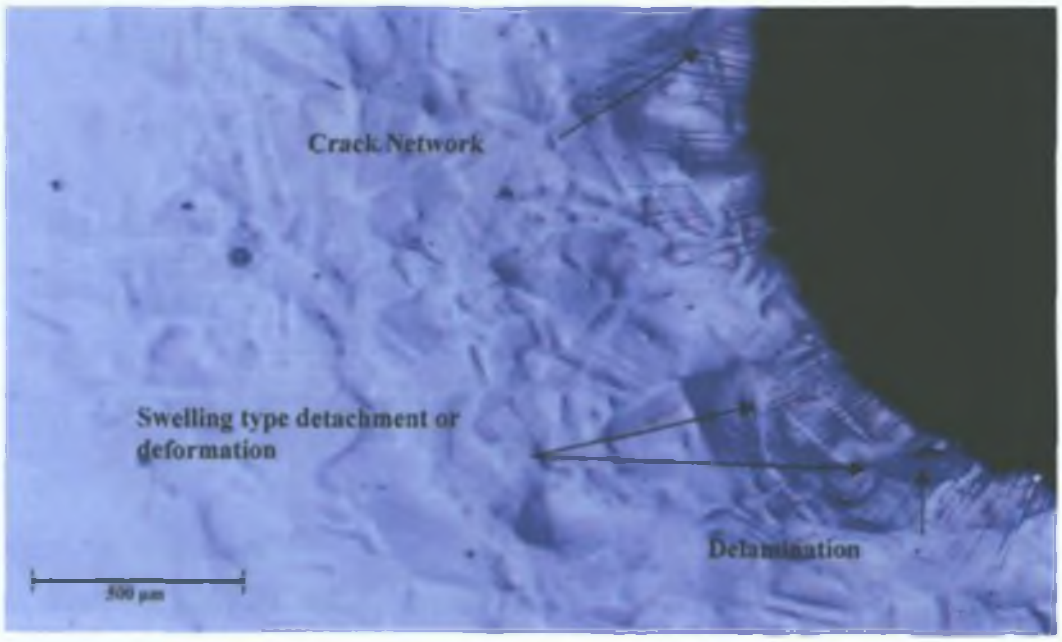

(a) Non-Duplex

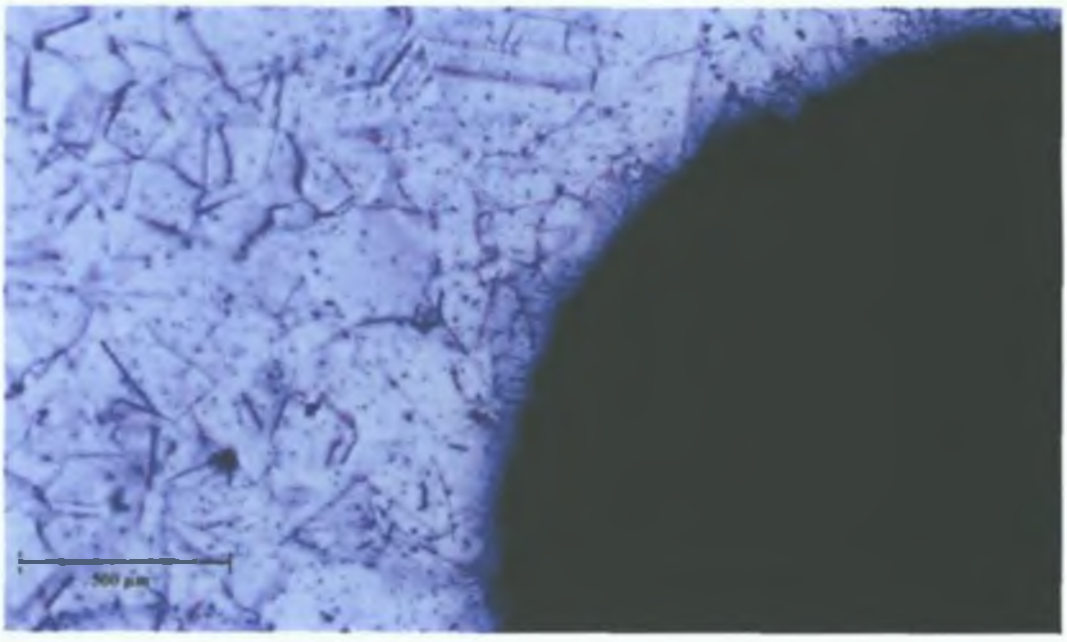

(b) Duplex

Figure 4.52: The Rockwell-C indentation spot of (a) the non-duplex and (b) the duplex coating system used for the adhesion evaluation

4.4.1.4. TRIBOLOGICAL PROPERTIES

Figure 4.53 shows the micro hardness of the different coating systems and substrates without coating (plasma nitrided and non-nitrided). The plasma nitrided substrate showed higher hardness than the non-nitrided substrate by at least a factor of four. The significant increase of the substrate hardness is believed to be increased by the load bearing capacity of the coating. The coatings on plasma nitrided substrates (that means, duplex coating systems) showed higher hardness values (3209 $HV_{0.015}$) than the coatings on non-nitrided substrates (1287 $HV_{0.015}$). A two and half fold increase in the duplex treated sample composite hardness compared to the non-duplex treated samples can be explained by the composite effect of the thick hard nitrided surface underneath the coating [138] as shown in figure 4.49 (Cross-sectional SEM image).

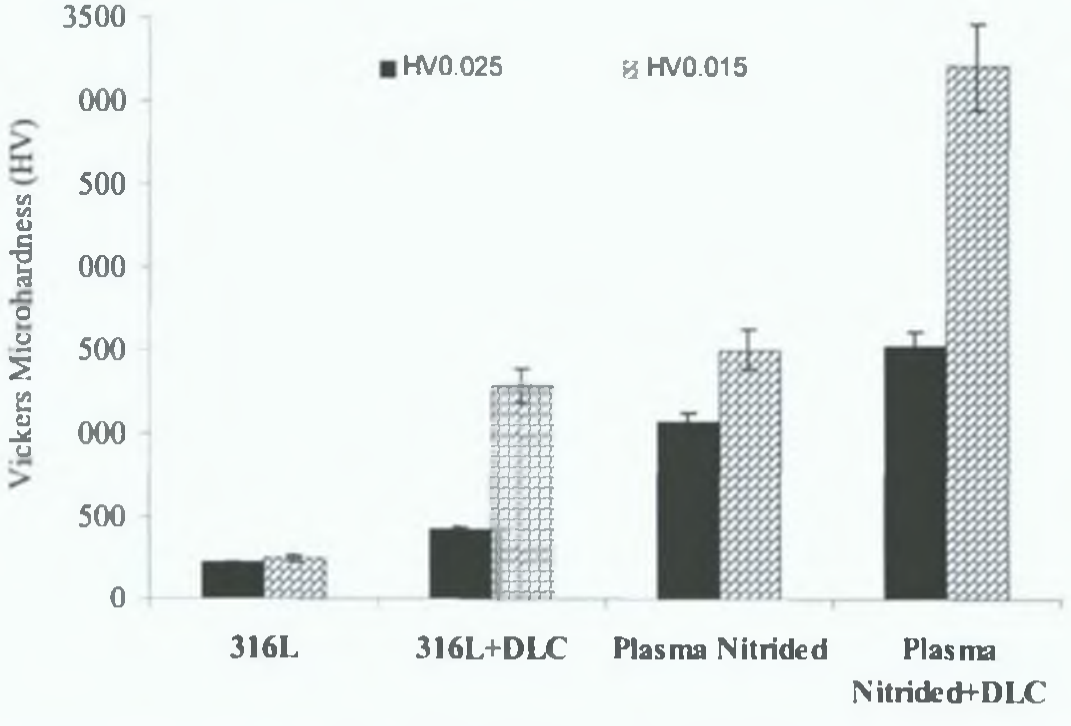

Figure 4.53: The micro hardness of the different coating systems and substrates without coating (plasma nitrided and non-nitrided).

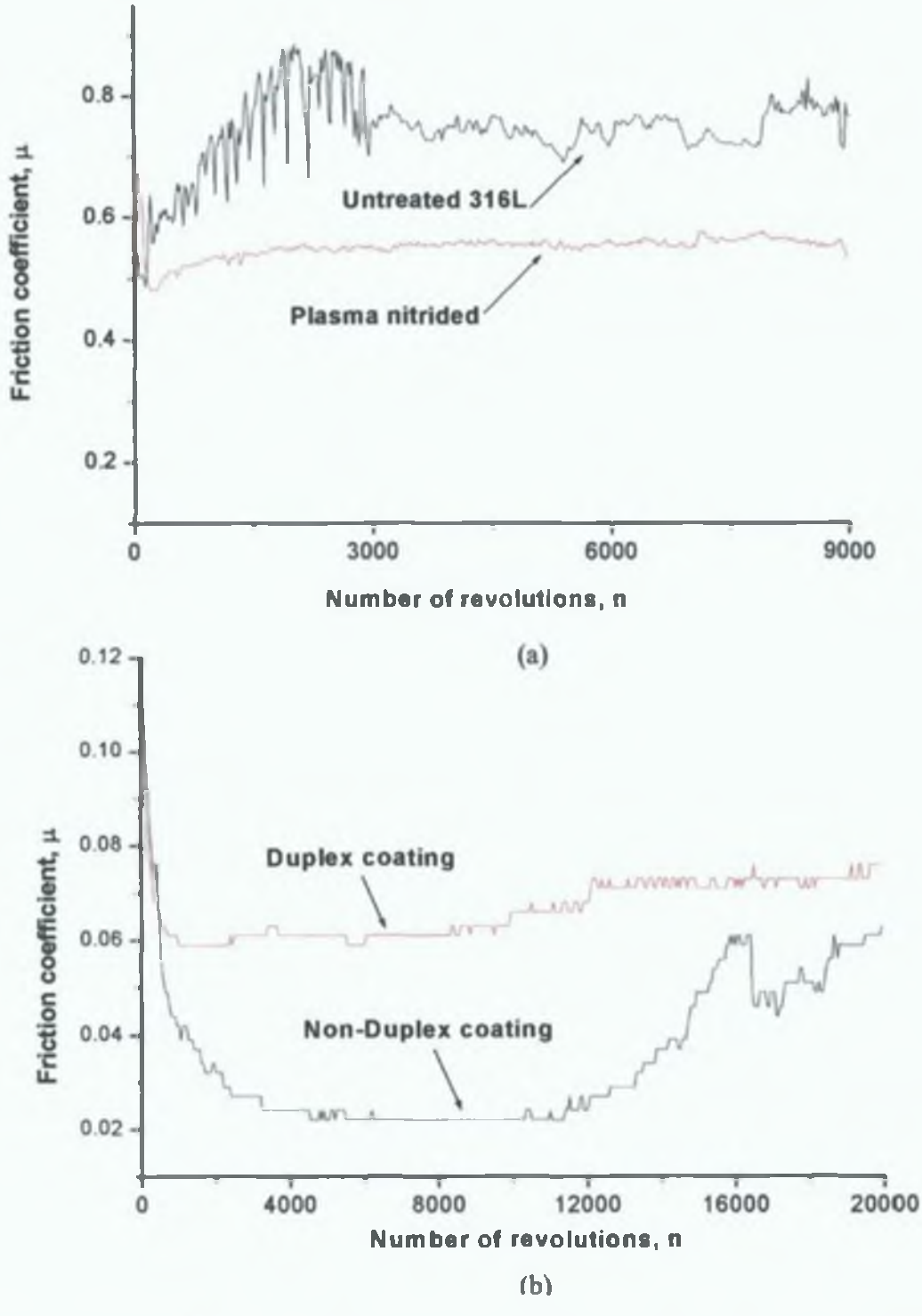

Figure 4.54: The friction coefficients for pin-on-disk tests of the (a) non-nitrided substrate and plasma nitrided sample and (b) non-duplex and duplex coated sample.

The plasma nitrided samples showed a lower co-efficient of friction compared to the non-nitrided substrate, as shown in figure 4.54a, as the hard nitrided surface lead to a

lower contact area during the pin-on-disc tests [210]. The non-duplex coating showed a slightly lower friction value than the duplex coating, which may be due to the higher surface roughness of the duplex samples, as shown in figure 4.54b. Both coating systems showed an average coefficient of friction value of between 0.06 and 0.1 in the steady-state period. These values were significantly lower than those found for the nitrided and the non-nitrided substrates. This fact can be explained by the solid lubrication effect of the DLC coating during the sliding operation [332]. However, the friction value of the coatings on the nitrided sample was smoother and more stable than those non-duplex systems due to the better load bearing effect of hard nitrided surface.

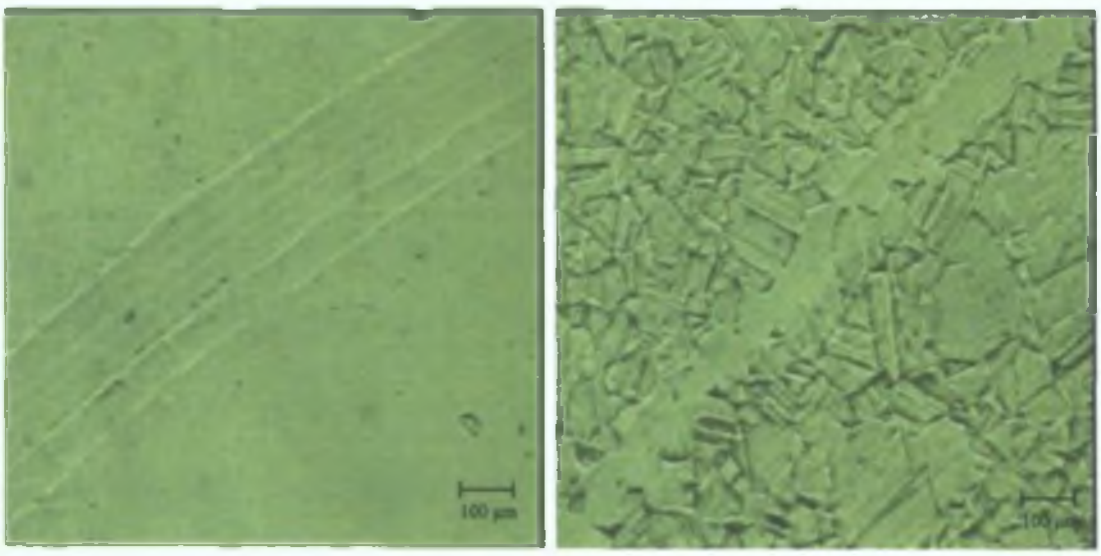

(a) (b)

Figure 4.55: The optical wear track morphology of (a) the non-duplex treated and (b) the duplex treated samples.

The wear track width and morphology have been taken as a measurement index of the coating substrate system wear behaviour. This method has also been reported by other researchers [333-335]. The coating on plasma nitrided substrate showed a very narrow and shallow wear track, as shown in figure 4.55a, when tested for up to 9, 000 revolutions at a speed of 60 rpm in laboratory air (40-50% RH) on the pin-on-disc. The width of the wear track was measured to be approximately 90 μm and there was a very small amount of wear visible on the duplex treated samples. This is may be due to the significant reduction in the wear contact area, as duplex treated coating samples consisted of a very hard and thick load

supporting nitrided layer below the coating layer [210] and also have relatively higher surface roughness compared to the non-duplex treated coating [336]. However, a wide and deep wear tack was observed on the non-duplex treated sample, as shown in figure 4.55b, when tested using the same condition as the duplex system on the pin-on-disk machine. The width of the wear track was measured to be approximately 230 μm, which was approximately two and half times greater than the duplex treated sample wear track width. A material deformation line at the edge as well as many grooves line was clearly observed on the wear track of the non-duplex treated sample. Since the non-duplex coating does not have any hard supporting layer, an increase in wear contact area was produced during the test, because the soft substrate material was deformed and pushed towards the edge of the wear track. Therefore, although the co-efficient of friction of both coatings were nearly the same, the wear track width and morphology suggest a significant improvement in the wear properties of the duplex treated samples compared to those of the non-duplex treated samples.

4.4.2. DISCONTINUOUS DUPLEX COATING WITH AND WITHOUT A GRADED INTERLAYER

4.4.2.1. EFFECT OF GRADED INTERLAYER

The thickness of all interlayers was between approximately 0.5 and 0.6 μm, whereas the thickness of all top layers was between 1.3 and 1.4 μm in different coating systems.

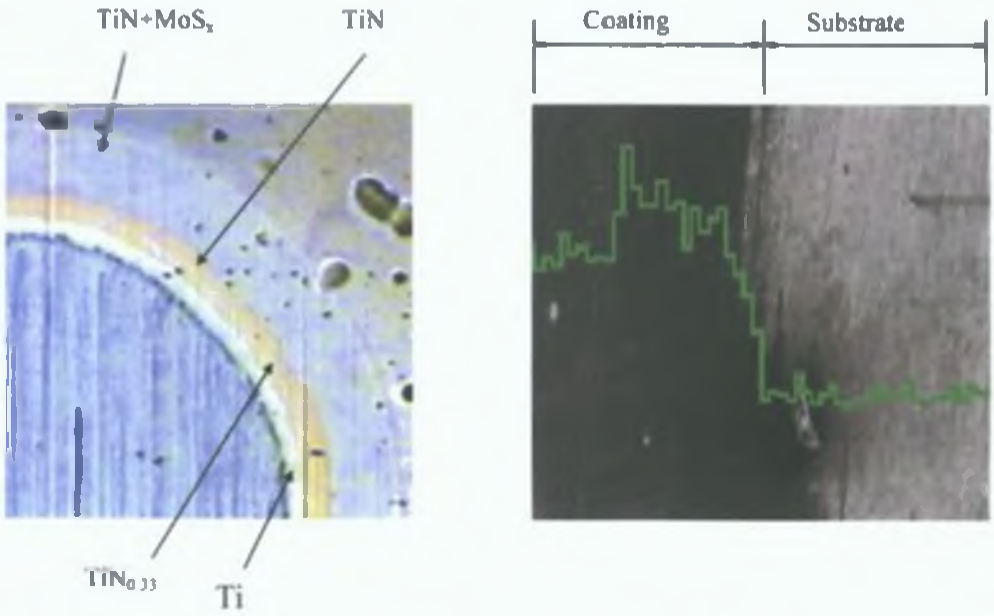

Figure 4.56: (a) Optical micrograph of the crater formed by ball cratering machine to reveal different layers (b) EDX line profile of nitrogen concentration from the substrate to the top of the coating.

Figure 4.56 (a) shows the optical micrograph of crater formed by the ball cratering device revealing the graded interlayer for sample G2. An EDX line profile analysis was performed on the crater, which starts at the substrate and ends at the top layer. As a characteristic element concentration of nitrogen was plotted. It showed that nitrogen concentration gradually increased from the substrate to the final TiN interlayer and so-called "step by step" composition of the graded interlayer was formed (Figure 4.56b).

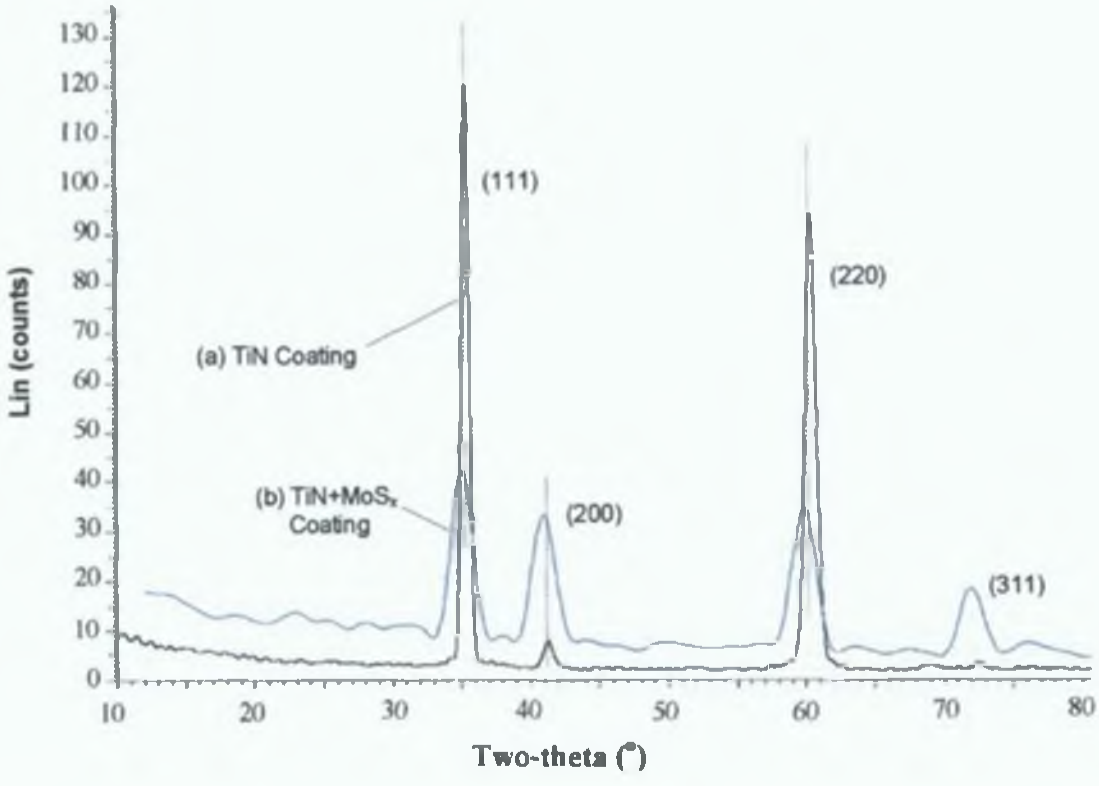

Figure 4.57: XRD spectra of TiN and TiN+MoS_x coatings , Where (xyz) is the crystal plan.

Curve (a) and (b) are the representative XRD line spectrum for the pure TiN and TiN+MoS_x coatings respectively as shown in figure 4.57. Peaks for the (111), (200), (220) and (311) crystal planes of the TiN phase and therefore both coating types exhibit the f. c. c. TiN structure. In the TiN+MoS_x coating, peaks were shifted to lower angles and slightly widen compared to the pure TiN coating, which indicated an increase in the lattice parameter and a reduction in grain size respectively. No MoS_x phase was found in the TiN+MoS_x coatings, which suggested that the Mo and S atoms were either incorporated into the cubic TiN lattice or segregated at the grain boundaries [185,337]. All the samples tested had Rockwell indentation values in the range HF3 to HF5, indicating moderate to poor coating adhesion. The coatings with graded interlayer (G2 and G3) had better adhesion due to the smooth compositional variation across the interlayer. The relatively low hardness of the steel substrate may have a significant influence on this measurement [338].

The microhardness result of the different TiN+MoS_x coatings confirmed that sample G1 showed the lower hardness value (490 $HV_{0.01}$) compared to all other coatings, due to the soft Ti interlayer. The hardness of the coatings with the graded interlayer was found to be higher than the coating with soft interlayer (G1) and the coating without any

interlayer (G5). Sample G4 (760-800 $HV_{0.01}$) in particular exhibited higher hardness due to the increased concentration of stoichiometric TiN in the interlayer.

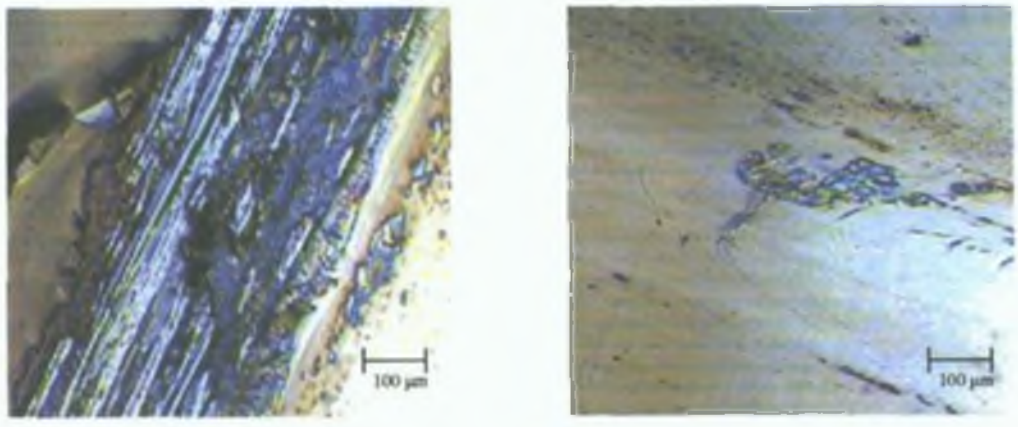

(a) (b)

Figure 4.58: Optical micrographs of the wear track created by the pin-on-disk test for (a) sample G1 (b) sample G3.

The top layer of all the coatings had the same TiN+MoS_x composition. When tested up to 9, 000 revolutions on the pin-on-disc machine they all exhibited coefficients of friction of between 0.4 to 0.5. These values are lower than those of 0.7 to 0.8 which were obtained for 'pure' TiN, but higher than the values of < 0.1 observed for MoS_x. This fact can be explained by the lubrication effects from the MoS_x formed by combining Mo and S during the sliding operation [185]. The coefficient of friction with the graded interlayers was smoother and more stable than the sample G1, G4 and G5. The wear depth value confirmed that coatings with the graded interlayer showed a lower wear depth value than the other coating systems due to the presence of the tough graded interlayer. This means that these coatings had better load bearing capacity.

Sample G1 containing a soft and thick Ti (~ 0.6 µm) interlayer, showed poor wear resistance due to low hardness and adhesion of the interlayer compared to other interlayers [339]. Again sample G4, containing a hard and brittle TiN interlayer (poor load bearing capacity and poor adhesion) also showed poor wear resistance compared to the coatings with the graded interlayer. Similar wear behaviour can also be observed from the morphology of the wear track of sample G1, which showed had severe grooving on the coating, (Figure 4.58 (a)), whereas in the coating with the graded interlayer (Figure 4.58 (b)) no such signs of grooving were observed. The coating, without any interlayer (G5) also showed a high wear depth compared with the graded interlayer coating.

4.4.2.2. THE EFFECT OF PLASMA NITRIDING

Figure 4.59 shows the microhardness of the different coating systems and the substrates without coating (plasma nitrided and non-nitrided).

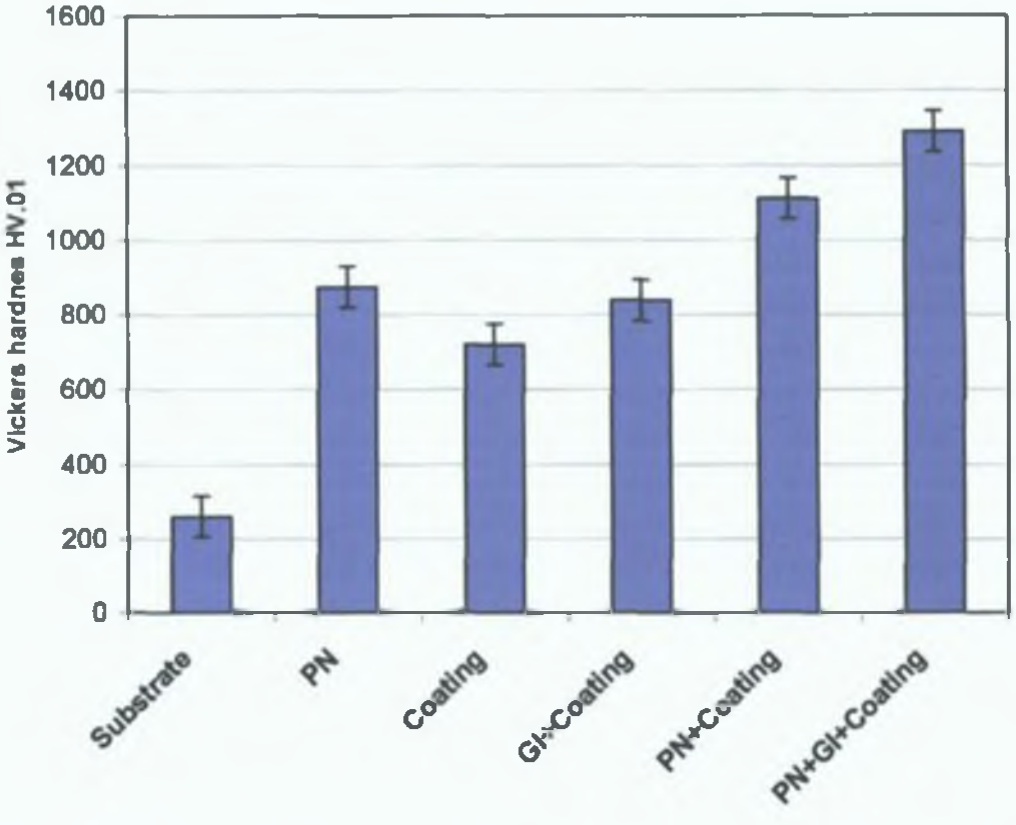

Figure 4.59: Vickers hardness of the substrate, the plasma nitrided (PN) substrate, the TiN+MoS_x coating on the non-nitrided substrate (Coating), the TiN+MoS_x coating with a graded interlayer on the non-nitrided substrate (GI+Coating), the TiN+MoS_x coating on the plasma nitrided substrate (PN+Coating) and the TiN+MoS_x coating with a graded interlayer on the plasma nitrided substrate (PN+GI+Coating).

Figure 4.59 shows that the plasma nitrided substrate had a higher hardness value than the non-nitrided substrate by at least a factor of three. Coatings on plasma nitrided substrates (that means, duplex coating systems) showed higher hardness values than the coatings on the non-nitrided substrates (that means, non-duplex coating system). These findings can be explained by the composite effect of hard nitrided surface underneath the coating [138]. However, TiN+MoS_x coatings with graded interlayer in both duplex and non-duplex cases showed higher hardness than coatings without a graded interlayer due to

the additional load supporting effect of the graded interlayer. Of all the coating systems, the coatings with a graded interlayer on the nitrided substrate exhibited the highest hardness due to the combined effect of the hard nitrided substrate and the graded interlayer.

Optical micrography of the Vickers indentation can be used for the qualitative measurement of coating toughness [340,341]. The optical images of the Vickers indentation performed at higher load (500 g) for all four coating-substrate systems, as shown in figure 4.60, support the microhardness results. Circumferential cracks around the Vickers indentation were found in all coating systems. However, coatings with a graded interlayer on the plasma nitrided substrate exhibited the fewest circumferential cracks with no radial cracks and a small indentation area compared to other coating systems (Figure 4.60d). The results indicated that this coating system had the highest toughness due to the higher load support and adhesion from the combined effect of the plasma nitrided substrate and the graded interlayer. Coating without the graded interlayer on the non-nitrided substrate (Figure 4.60a) showed the maximum number of circumferential cracks and radial cracks and also the largest indentation area. This indicates that these coating had the poorest toughness.

All the coating systems tested had Rockwell indentation values in the HF2 to HF5 range, indicating good to poor coating adhesion. The coatings with graded interlayers had better adhesion in both duplex and non-duplex cases due to the smooth compositional variation across the interlayer. However, the plasma nitriding effect in the duplex coating systems did not produce any significant improvement in adhesion, possibly due to the comparatively rougher nitrided surface. The plasma nitrided sample showed a lower co-efficient of friction compared to non-nitrided substrate. This was due to the lower contact area as a result of the hard nitrided surface when tested up to 9, 000 revolutions on the pin-on-disc machine [210]. As all coating systems had the same TiN+MoS_x composition, they all exhibited an average coefficient of friction between 0.35 and 0.45, in the steady-state period.

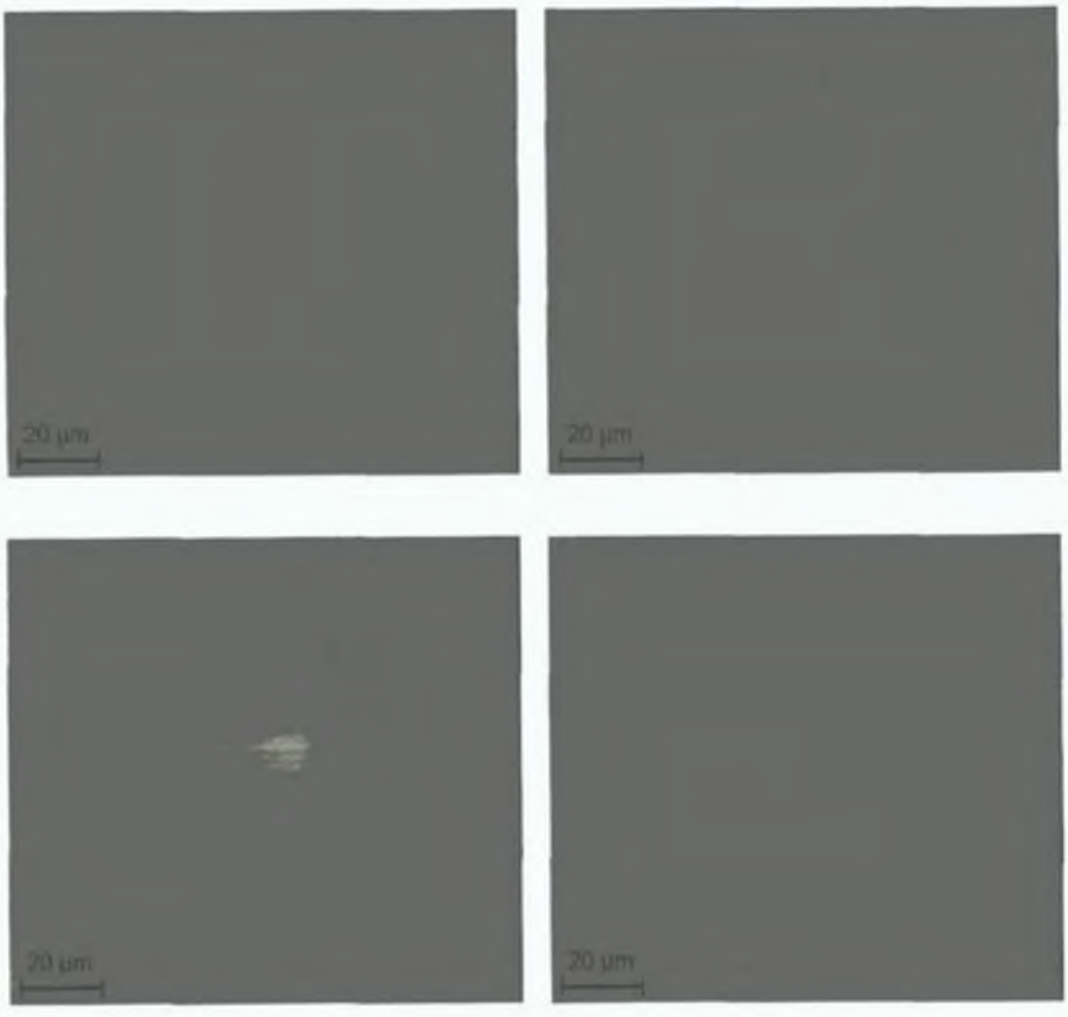

(c)

Figure 4.60: Optical micrograph of Vickers indentation for (a) the TiN+MoS_x coating on the non-nitrided substrate (Coating) (b) the TiN+MoS_x coating with graded interlayer on the non-nitrided substrate (GI+Coating) (c) the TiN+MoS_x coating on the plasma nitrided substrate (PN+Coating) and (d) the TiN+MoS_x coating with a graded interlayer on plasma nitrided substrate (PN+GI+Coating).

These values were lower than those of the nitrided and non-nitrided substrates as well as those of pure TiN. This fact can be explained by the lubrication effect from the MoS_x formed by combining Mo and S during the sliding operation [185,337]. However, the coefficient of friction on the coatings with graded interlayers on both nitrided and non-nitrided substrates, was smoother and more stable than for other coating systems, due to the better load bearing effect from graded interlayer and hard nitrided surface.

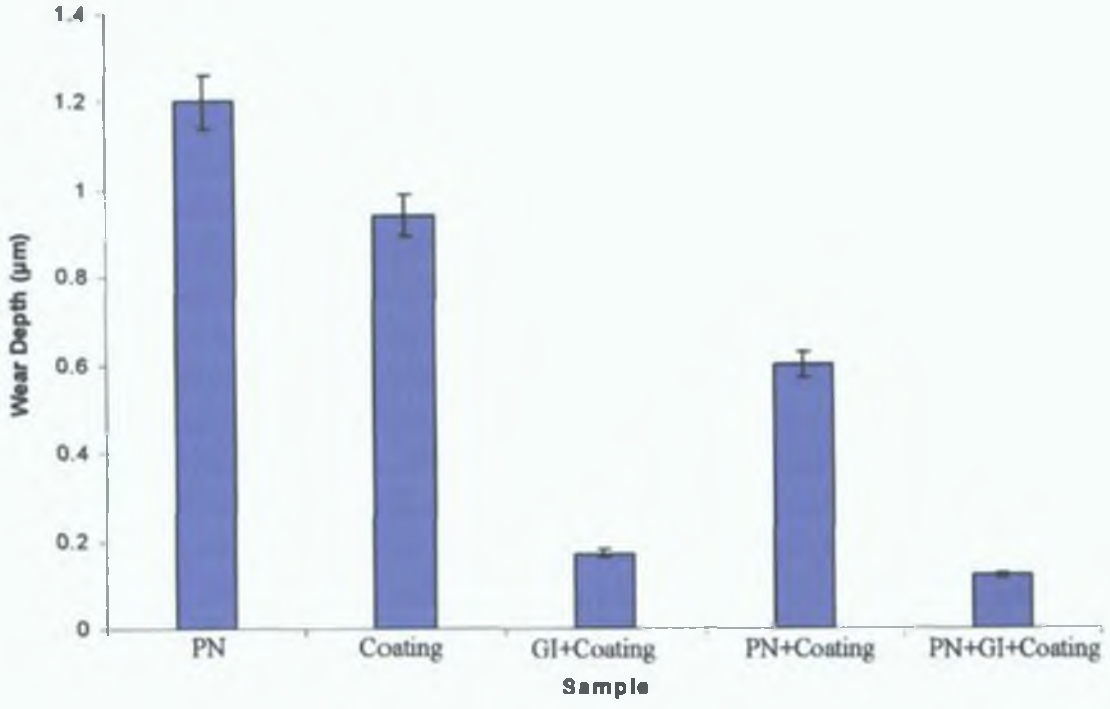

Figure 4.61: Wear depth of the plasma nitrided (PN) substrate, the TiN+MoS_x coating on the non-nitrided substrate (Coating), the TiN+MoS_x coating with a graded interlayer on the non-nitrided substrate (GI+Coating), the TiN+MoS_x coating on the plasma nitrided substrate (PN+Coating) and the TiN+MoS_x coating with a graded interlayer on plasma nitrided substrate (PN+GI+Coating).

Figure 4.61 shows the wear rate of different coating-substrate systems. Coatings on the plasma nitrided substrates (that means, duplex coating systems) showed lower wear rates than the coatings on the non-nitrided substrates (that means, non-duplex coating systems). Of all the coating-substrate systems, the coatings with the graded interlayer on the plasma nitrided surface showed the lowest wear rate due to the presence of the well-adhered graded interlayer [137] and the hard load supporting nitrided surface underneath the coating [138].

4.5. SUMMARY OF THE RESULT AND DISCUSSION

In this section, a summary of the results and discussion of the simulation work, plasma nitriding and duplex coating experimental work are presented in sub-subsection 4.4.3.1, 4.4.3.2 and 4.4.3.3 respectively. In the last sub-section, a table have been given for a comparative study of the tribological results of plasma nitrided and duplex coating all. The following is a summary of the results and discussion of this thesis:

4.5.1. SIMULATION WORK

a) Simulation of the gas flow and mixing pattern

Simulation of the gas flow and mixing pattern has been undertaken using the computational fluid dynamics software FLUENT. The pressure, velocity and mass fraction distribution have given the nature of flow of the gases inside the deposition chamber. It was also observed that the position of the substrate has an indirect influence on the coating composition. The results showed that placement of the substrate at the middle between Ar and N_2 inlets or infront of the N_2 inlet with optimum distance away from the chamber wall have been given more uniform gas composition distribution over the substrate surface than other locations in expense of mass concentration. This analysis provided an approximation of proper placement of the gas inlet, target and substrate inside the chamber before coating deposition test.

(b) Simulation of graded coating stress measurement

An analysis of the thermal stress developed in thin coating on stainless steel substrate has been performed using the finite element simulation package ANSYS and verified using appropriate analytical calculations. Significant reduction of thermal stresses was realised in the graded coating system compared to the single layer system. Increasing the number of graded layers was seen to decrease the stress components, particularly the shear stress (by around 36%). FEA provided detailed information about all the stress components and gave a better understanding of the thermal stress developed during cooling of the thin coating substrate system. This analysis proved to be very useful in the selection of the appropriate coating structure.

4.5.2. PLASMA NITRIDING

The plasma nitriding of a wide range of biomaterials such as 316 stainless steel, Ti-6Al-4V alloy and UHMWPE (Non-Conductive), was successfully conducted by a new process (saddle field fast atom beam source) in an existing Plasma Enhanced Chemical Vapor Deposition (PECVD) chamber. Conclusions are drawn from the results obtained for each material and are given below:

(a) Low temperature plasma nitriding of 316L Stainless steel

Low temperature nitriding experiments were carried out for the 316L stainless steel samples. The low temperature (420 ^{0}C) of the sample was controlled independent of the plasma beam. It was found that the nitriding time has a pronounced effect on the structural and mechanical properties of low temperature plasma nitrided samples. The following conclusions on the plasma nitriding of 316L samples have been made.

- A distinct surface morphology (twin structure), similar to that of the etched non-nitrided sample was observed on the nitrided surface. The number of twins and the sample surface roughness both increased as the nitriding time increased. A white nitrided layer was observed during the microstructural investigation and this confirmed the precipitation-free nitriding of stainless steel at low temperatures. The thickness of the nitrided layer increased as the nitriding time increased. However, the growth rate of nitrided layer was found to decrease after around 9 h.

- In the XRD study, the appearance of the peak at a lower angle and the broadening of the peak compared to the non-nitrided sample confirmed the formation of the S phase. The S peaks gradually moved to lower diffraction angles as the nitriding time increased. However, the maximum peak shift was found to occur for the 6 h nitrided samples. No further significant peak shifting was observed for nitriding time greater than this. It is believed that the formation of the S phase at lower temperatures allow the sample to retain the corrosion resistance of the stainless steel.

- The EDX spectra also showed the presence of nitrogen in the nitrided layer.

- A shallow hardened layer was observed and a four-fold increase in the surface hardness of the nitrided sample was achieved. The formation of a comparatively

higher thickness nitrided layer within a short processing time (8 h), possibly due to the energetic atom beam, proved the potential of this new nitriding process. The increase of hardness with nitriding time may be due to the formation of a thick nitrided layer. This thicker layer provides composite hardness and an increase in the surface concentration of nitrogen, which results in an additional solid solution strengthening effect.

- The plasma nitrided samples showed a lower, more stable and smoother co-efficient of friction compared to the non-nitrided substrate due to the hard nitrided surface leading to lower wear contact area and the prevention of asperities welding. A severe adhesive, abrasive and deformation wear mechanism usually was observed for untreated samples. Whereas, a modest polished type micro-abrasive wear mechanism was characterized for the nitrided samples. The wear depth value was seen to increase as the nitriding time increased. This may have been due to high stress generation in the sample which underwent nitriding for longer time periods. The wear depth values for all the nitrided samples were significantly lower than those for the untreated samples. The fact that the polished nitrided samples showed slightly better tribological properties compared to the as-received nitrided, perhaps due to the influence of the surface roughness.

- Finally, the Saddle field fast atom beam source proved to be a potential method for plasma nitriding, due to the formation of a comparatively thick precipitation-free nitrided layer within a short processing time.

(b) Low Pressure plasma nitriding of Ti-6Al-4V

Low pressure (0.1 Pa) plasma nitriding of the biomedical material, Ti-6Al-4V, was achieved using the above mentioned methods. In the microstructural investigation, a white, thick compound nitrided layer of TiN followed by a nitrogen enriched diffusion layer was observed and growth of this compound nitrided layer was found to increase as the nitriding temperature was increased. The XRD and XPS study confirmed the formation of the TiN on the top surface and the intensity of TiN peaks was found to increase as the nitriding temperature was increased. However, no X-ray spectrum lines of TiN phase were observed when nitriding was performed at temperatures below 700 ^{o}C. There is roughly a three-fold increase in hardness near to the nitrided surface (1578 $HV_{0.01S}$) compared to the untreated

samples (568 $HV_{0.015}$). Below this top layer hardness values were found to decrease gradually to nearly the same values as the untreated samples. The hardness values were found to increase as the nitriding temperature increased and a significant improvement in the hardness values were recorded when the sample was nitrided above 700 ^{0}C. A noticeable improvement in the tribological properties of the nitrided sample was found compared to the non-nitrided sample, due to the presence of a hard TiN phase in the thick nitrided layer. In addition, the samples nitrided at high temperatures exhibited a substantial decrease in the friction co-efficient value and the amount of wear that occurred compared to those for the untreated and low temperature nitrided samples.

(c) Low temperature and low pressure plasma nitriding of non-conductive UHMWPE material

Plasma nitriding of the non-conductive UHMWPE materials was also carried out and no problem with substrate charging experienced. No external heating was applied for polymer (UHMWPE) samples and the beam current was set sufficiently low to avoid any heating (temperature was maintained below 100 ^{o} C) and thus any degradation of the samples. It was observed by the naked eye that the surface colour of the nitrided polymer samples was changed from off-white to light yellowish. The surface morphology of the nitrided samples was featureless and more irregular (peaks and valleys) compared to that of the as-received samples. The surface roughness of the untreated samples was recorded to be 357 nm compared to the treated sample which had a value of 401 nm. The Raman study confirmed that changes in the surface structure and cross-linking had occurred in nitrided sample. The XPS results confirmed incorporation of nitrogen into the nitrided layer and bonding of nitrogen in the layer rather than unbound or precipitated nitrogen being present. Contact angle measurement confirmed the increase wettability of the plasma nitrided samples compared to un-treated samples and it is believed that the increased in wettability would increase the lubricity of the contact surface.

A dry sliding (un-lubricated) wear test confirmed the increase in the friction value of the nitrided sample compared to the untreated sample. Although wear testing confirmed the improvement of the overall tribological properties of the nitrided samples comparing to the non-nitrided samples.

4.5.3. CONTINUOUSLY DEPOSITED DUPLEX COATINGS

A continuous duplex process consisting of plasma nitriding followed by in-situ deposition of a DLC coating, has been successfully accomplished in a single process chamber (PECVD based Saddle field neutral fast atom beam source) without any interlayer or post nitriding treatment. Low temperature plasma nitriding of stainless steel produced precipitation and black-layer free, hard and thick load supporting nitrided layer, which was suitable for subsequent coating deposition in spite of having increased surface roughness. The amorphous and diamond nature of the deposited coating was confirmed by XRD, Raman and FTIR result. The coatings on low temperature plasma nitrided samples exhibited either less pinholes compared to the non-duplex sample or no pinholes at all. Rockwell C indentation result confirmed the improvement in the adhesion of the duplex treated coating samples compared to the non-duplex treated samples. Duplex treatment significantly increases the composite hardness and reduces the plastic deformation of the substrate. The pin-on-disk test result show that the duplex treatment increases the overall wear properties of the coating compared to the non-duplex coating.

4.5.4. DISCONTINUOUSLY DEPOSITED DUPLEX COATINGS

A discontinuous duplex process consists of plasma nitriding followed by the later deposition of a TiN+MoS_x coating, with or without graded interlayer, was developed by the PECVD based fast atom beam method and closed-field unbalanced magnetron sputtering respectively. Ball cratering and EDX line profile analysis results confirmed the formation of graded interlayer. TiN peak shifting to lower angles in the TiN+MoS_x coating indicated the inclusion of Mo and S atoms in the TiN phase. TiN+MoS_x coating reduced the coefficient of friction compared to pure TiN coating. Interlayer effect study confirmed that coatings with graded interlayer have shown better mechanical and tribological properties compared with soft or hard single interlayer.

The discontinuously deposited duplex coating study confirmed that, plasma nitriding in the coating-substrate system enhanced the composite hardness and load bearing capacity significantly. Of all the coating-substrate systems, the coatings with graded interlayers on the plasma nitrided surface showed the lowest wear rate compared to other combinations. However, no significant reduction in wear was found between the duplex and non-duplex coatings with graded interlayer. The graded interlayer in the coating-

substrate systems increased the adhesion and additional composite hardness and toughness as well as the solid lubricant effect of the top layer. The coatings with graded interlayers on the plasma nitrided substrate exhibited the best mechanical and tribological performances of all the coating systems.

4.5.5 OVERVIEW OF PLASMA NITRIDED AND DUPLEX COATING RESULTS

A summary of the plasma nitrited and duplex coating results have been given in table 4.3.

Table 4.3: A summary of the plasma nitrided and duplex coating results

	Plasma Nitriding						Coating on 316L Substrate				
	316L		Ti-alloy (Ti-6AL-4V)		Polymer (UHMWPE)		$TiN+MoS_2$			DLC	
	Untreated	*Treated*	*Untreated*	*Treated*	*Untreated*	*Treated*	*Coating**	*(GI+Coating)***	*(PN+GI+Coating)*** (Duplex[a])*	*Non-duplex*	*Duplex*
Hardness (HV)	230	515-855	455	580-1445	-		725	860	1280	1287	3209
Friction Co-efficient	0.76	0.49-0.64	0.57	0.51-0.32	0.05	0.24	0.4-0.5			0.35-0.65	
Wear depth (μm)	6.7	1.1-2.2	4.8	0.2-0.42	1.44	1.06	0.94	0.18	0.11	-	
Wear width μm)	503	240	560	88-140	312	230	-			230	90
Comments	Plasma nitriding enhanced the tribological properties of the soft substrate materials within sort processing time (1-10 hr) without losing the corrosion properties (black layer free) which will be appropriate for (a) many tribological applications (Engineering application where a surface is in contact motion with another surface) and (b) also deposition of thin coating on soft substrate such as 316L stainless steel, Ti-base alloy and so on, for improve the adhesion and load bearing capacity of the coating-substrate system.						Solid lubricant coating on plasma nitrided substrate with graded interlayer improves the load bearing capacity of the coating-substrate composite system which will be suitable under severe and long term contact conditions (such as piston, cutting tolls, forming and so on).			DLC coating on plasma nitrided substrate significantly increased hardness, wear resistance and adhesions properties of the deposited coating which will be suitable under severe and long term contact conditions (such as biomedical, piston, cutting tolls, forming and so on)	

* Coating = $TiN+MoS_x$ coating on the non-nitrided substrate, ** GI+Coating = $TiN+MoS_x$ coating with a graded interlayer (GI) on the non-nitrided substrate, *** PN+GI+Coating = $TiN+MoS_x$ coating with a graded interlayer (GI) on the plasma nitrided (PN) substrate, [a] Duplex = Coating on Plasma nitrided substrate,

CHAPTER 5: CONCLUDING REMARKS AND RECOMMENDATIONS FOR FUTURE WORK

5.1. INTRODUCTION

In this present work, a new method of plasma nitriding and duplex coating has been developed. The research work which was carried out included, the design and characterization of the treated samples and deposition systems, through the use of experimental and simulation works. This chapter provides concluding remarks, and an outline of the direction of the further research.

5.2. CONCLUDING REMARKS

The conclusions that were derived from the present study are given as follows:

- A new plasma nitriding process (PECVD based Saddle field neutral fast atom beam source) has been developed using an existing carbon based coating system to overcome the problems associated with the conventional plasma nitriding process. The results showed that this technique is a potential method for the plasma nitriding of a wide rage of materials, due to the formation of comparatively thicker nitrided layer within a short processing time. It has been observed that low temperature plasma nitriding of stainless steel produced a precipitation and black-layer free, hard and thick load supporting nitrided layer within a short processing time which was suitable for the subsequent coating deposition as well. Plasma nitriding has also been carried out on Ti-6Al-4V and non-conductive UHMWP biomaterials without electric charging problem. In both cases plasma nitriding treatment substantially increased the overall wear properties of the untreated substrate. As this method produced a thicker , wear and corrosion resistance nitrided layer which will be suitable for many biomedical (total hip, knee replacement, dental and so on) and engineering applications (such as aerospace, marine, sports equipment, chemical and automobile industries, pumps, turbine, combustion motor for racing car and so on).
- For further improvement of the frictional properties of the nitrided substrate for the severe and long-term wear resistance application, a continuous and discontinuous duplex coating process has been developed. Continuous duplex process consisting of plasma nitriding followed by in-situ deposition of the DLC coating, have been successfully carried out in a single process chamber (PECVD based Saddle field neutral fast atom beam source) without any interlayer or post nitriding treatment. Duplex

treatment significantly increased the composite hardness, reduced of the plastic deformation of the substrate, and increased the adhesion properties. DLC base duplex coating will be suitable for applications (mechanical and biomedical) involving surfaces in mutual contact and under load or relative motion in term. A discontinuous duplex treatment consisting of plasma nitriding followed by TiN+MoS_x coatings, with and without graded interlayers on the stainless steel substrate, was evolved by the PVD and PECVD method. The results showed that the overall tribological properties of this solid lubricant based (MoS_2) coating could be improved by the deposition of the coating with a graded interlayer on the plasma nitrided samples. TiN+MoS_x base duplex coating will be suitable for application in severe wear condition such as forming, die cast, piston, cutting tools and so on.

- Furthermore, a finite volume (using FLUENT) and finite element method (using ANSYS) have been developed to determine (i) the gas mixture pattern inside the sputtering chamber and (ii) the thermal stress inside the graded thin coating respectively. This method could be used in future research work for the primary approximation of the different process parameters.

5.3. FUTURE WORK

In this research work, PECVD based fast atom beam source has been used for the first time for the successful plasma nitriding of a wide range of engineering materials and for the in-situ deposition of duplex coatings. It can be recommended that this method and the materials treated using this method may have important applications in diverse tribological applications and should be the focus for future research. Although, a significant amount of work and results have been reported in this thesis regarding the mechanical, physical and structural properties of duplex coatings and nitrided samples, there is still scope for future work in this area. The following areas are recommended for future research focus:

- It is important to know the depth bonding structure of the nitrided layer to better understand the relationship between the structural and mechanical properties of the plasma nitrided sample. Depth bonding structure of the plasma nitrided and coating layer could be investigated using XPS with a high etching rate.
- A qualitative measurement of hardness in the polymer samples has been evaluated using the Vickers microhardness tester. As polymer materials are very soft and the plasma nitriding layer is very thin, the hardness values measured using the microhardness tester are thought to be substrate dependent. Therefore, the nanohardness of the polymer nitrided samples should be evaluated using a nanohardness tester.
- Simulation and Modeling could be carried out to give a better understanding of the relationship between different mechanical properties, such as load bearing capacity, hardness and indentation response of the plasma nitrided, duplex and graded coating layers.
- The exact nature of the corrosion of untreated, coated and plasma nitrided stainless samples at both high and low temperatures could be investigated. Post annealing treatment of nitrided samples could also be considered to see how it affects the structural and corrosion properties.
- In case of biomedical applications, testing of the biocompatibility properties of the treated sample might be carried out in order to determine how these materials would perform. As wettability has a great influence on the tribological properties of the polymer based materials, an elaborate study of the relationship between tribological properties and wettability is needed. Wear tests in wet conditions, such as human plasma or water, are suggested for future study.

- Experimental and characterization test could to be carried out on others shape (for example cylindrical in case piston application, curved surface in case of biomedical application) rather than flat substrate.

PUBLICATIONS ARISING FROM THIS RESEARCH

➢ PUBLICATIONS

The following publications/manuscripts resulted from this work present in this thesis.

Journal papers

1. **M. Rahman** and M. S. J. Hashmi, "Saddle field fast atom beam source: A low-pressure plasma nitriding method of Ti–6Al–4V alloy", Thin Solid Film, In press, 2006
2. **M. Rahman** and M. S. J. Hashmi, "Effect of treatment time on low temperature plasma nitriding of stainless steel by saddle filed neutral fast atom beam source", Thin Solid Film, In press, 2006
3. **M. Rahman**, J. Haider and M. S. J. Hashmi, "Low temperature plasma nitriding of 316 stainless steel by a saddle field fast atom beam source", Surface and Coatings Technology, Vol. 200, 2005, pp. 1645-1651
4. **M. Rahman**, J. Haider, D. P. Dowling, P. Duggan and M. S. J. Hashmi, "Investigation of mechanical properties of TiN+MoS_x coating on plasma nitrided substrate", Surface and Coatings Technology, Vol. 200, 2005, pp. 1451-1457
5. **M. Rahman**, J. Haider, P. Duggan, D. P. Dowling and M. S. J. Hashmi, "Deposition of magnetron sputtered TiN+MoS_x coating with Ti-TiN graded interlayer", Surface and Coatings Technology, Vol. 200, 2005, pp. 1071-1075

Manuscript submitted for publication in Journal

1. **M. Rahman**, I. Reid, P. Duggan, D. P. Dowling, G. Hughes and M. S. J. Hashmi, "Structural and tribological properties of the Plasma nitrided Ti-alloy biomaterials: Influence of the treatment temperature", Accepted for Publication in Surface and Coatings Technology, 2006
2. **M. Rahman**, P. Duggan, D. P. Dowling and M. S. J. Hashmi, "Continuously deposited duplex biomedical coatings", Accepted for publication in Surface and Coatings Technology, 2006
3. **M. Rahman**, P. Duggan, D. P. Dowling and M. S. J. Hashmi, "Tribological properties of low temperature plasma nitrided stainless steel", Surface and Coatings Technology (waiting for the decision of referees), 2005

Conference Proceeding papers

1. **M. Rahman**, J. Haider, B. Corcoran and M. S. J. Hashmi "Finite element modeling of thermal stresses in sputter deposited graded coating system", Proceedings of the 21st International Conference on Advanced Manufacturing Conference, IMC 21,1-3 September 2004, Limerick, Ireland, Page: 175-182

Poster Presentation

1. **M. Rahman**, and M. S. J. Hashmi, "Improvement of tribological properties of polymer materials", Presented (poster) at the Fifth Asian-European International Conference on Plasma Surface Engineering (AEPSE 2005), September 12 to Friday, September 16, 2005, in Qingdao city, China
2. **M. Rahman**, and M. S. J. Hashmi, "Continuously deposited duplex biomedical coatings", Presented (poster) at the Fifth Asian-European International Conference on Plasma Surface Engineering (AEPSE 2005), September 12 to Friday, September 16, 2005, in Qingdao city, China
3. **M. Rahman**, and M. S. J. Hashmi, "Tribological properties of low temperature plasma nitrided stainless steel", Presented (poster) at the Fifth Asian-European International Conference on Plasma Surface Engineering (AEPSE 2005), September 12 to Friday, September 16, 2005, in Qingdao city, China
4. **M. Rahman** and M. S. J. Hashmi," Saddle field fast atom beam source: A low pressure plasma nitriding method of biocompatible Ti–6Al–4V alloy", Presented (poster) at the International Conference on Surfaces, Coatings and Nanostructured Materials, nanoSMat2005, 7-9 September 2005, University of Aveiro, Portugal
5. **M. Rahman** and M. S. J. Hashmi, "Effect of treatment time on Low Temperature plasma nitriding of stainless steel by saddle field neutral fast atom beam source", Presented (poster) at the International Conference on Surfaces, Coatings and Nanostructured Materials, nanoSMat2005, 7-9 September 2005, University of Aveiro, Portugal
6. **M. Rahman**, J. Haider and M. S. J. Hashmi, "Low temperature plasma nitriding of 316 stainless steel by a saddle field fast atom beam source", Presented (poster) at the International Conference on Metallurgical coatings and Thin Films, May 2-6, 2005, Town and Country Hotel, San Diego, California, USA

REFERENCES

REFERENCES

[1] Thick Ceramic Coatings, Newsletter 7, http://www.euroceram.org/en/news/ news_7_1.cfm

[2] S. Carrera, O. Salas, J. J. Moore, A. Woolverton and E. Sutter, "Performance of CrN/MoS2, Ti, coatings for high wear low friction applications", Surface and Coatings Technology, Vol. 167, 2003, pp. 25-32

[3] D. G. Teer, "New solid lubricant coatings", Wear, Vol. 251, 2001, pp. 1068-1074

[4] V. Derflinger, H. Brändle and H. Zimmermann, "New hard/lubricant coating for dry machining", Surface and Coatings Technology, Vol. 113, 1999, pp. 286-292

[5] R. Gilmore, M. A. Baker, P. N. Gibson, W. Gissler, M. Stoiber, P. Losbichler and C. Mitterer, "Low-friction TiN–MoS2 coatings produced by dc magnetron co-deposition", Surface and Coatings Technology, Vol. 108-109, 1998, pp. 345-351

[6] N. J. Ianno, R. O. Dillon, A. Ali and A. Ahmad, "Deposition of diamond-like carbon on a titanium biomedical alloy", Thin Solid Films, Vol. 270, 1995, pp. 275-278

[7] D. P. Dowling, P. V. Kola, K. Donnelly, T. C. Kelly, K. Brumitt, L. Lloyd, R. Eloy, M. Therin and N. Weill, "Evaluation of diamond-like carbon-coated orthopaedic implants", Diamond and Related Materials, Vol. 6, 1997, pp. 390-393

[8] V. -M. Tiainen, "Amorphous carbon as a bio-mechanical coating — mechanical properties and biological applications", Diamond and Related Materials, Vol. 10, 2001, pp. 153-160

[9] A. Grill, "Diamond-like carbon coatings as biocompatible materials—an overview", Diamond and Related Materials, Vol. 12, 2003, pp. 166-170

[10] R. Hauert, "An overview on the tribological behavior of diamond-like carbon in technical and medical applications", Tribology International, Vol. 37, 2004, pp. 991-1003

[11] H. A. Jehn, "Multicomponent and multiphase hard coatings for tribological applications", Surface and Coatings Technology, Vol. 131, 2000, pp. 433-440

[12] C. Donnet and A. Erdemir, "Historical developments and new trends in tribological and solid lubricant coatings", Surface and Coatings Technology, Vol. 180-181, 2004, pp. 76-84

[13] K. Holmberg and A. Matthews, "Coatings tribology: properties, techniques and applications in surface engineering", Elsevier, Amsterdam, ISBN: 0444888705, 1994

[14] T. Burakowski and T. Wierzchon, "Surface engineering of metals: Principles, Equipment, technologies", Boca Raton, Fla. : CRC Press, ISBN: 0849382254, 1999

[15] K. N. Strafford, R. S. Smart, I. Sare and C. Subramanian, "Surface engineering: processes and applications", Technomic Publishing Co., Lancaster, Pennsylvania, ISBN: 1566761549, 1995

[16] M. Suzui, S. Tokito and Y. Taga, "Review of thin film technology in automobile industry", Materials Science and Engineering B, Vol. 51, 1998, pp. 66-71

[17] K. Seshan, "Handbook of Thin-Film Deposition Process and Techniques: Principles, Methods, Equipment and Applications", Second Edition, Noyes Publications, Norwich, New York, U.S.A, ISBN: 0-8155-1442-5, 2002

[18] R. F. Bunshah, "Handbook of Deposition technologies for Films and Coating: Science, Technology and Application", Second Edition, Noyes Publications, Park Ridge, New Jersey, ISBN: 0-8155-1337-2, 1994

[19] K. L. Choy, "Chemical vapor deposition of coatings", Progress in Materials Science, Vol. 48, 2003, pp. 57-170

[20] H. O. Pierson, "Handbook of Chemical Vapor Deposition (CVD): Principles, Technology and Applications", Noyes Publications, New York, U. S. A., ISBN: 0815513003, 1992

[21] LeMay and D. Sheriff, "A User's Guide to Accurate Gas Flow Calibration," Solid State Technology, 1996, pp. 83–96

[22] Drexel, C. F., "Digital Mass Flow Controller Come of Age," Solid State Technology, 1996, pp. 99–106

[23] R. F. Bunshah, "Hand book of Hard coating: Deposition Technologies, Properties and Applications", Noyes Publications, Park Ridge, New Jersey, U.S.A, ISBN: 0-8155-1438-7, 2001

[24] M. Amaral, F. Mohasseb, F.J. Oliveira, F. Bénédic, R.F. Silva and A. Gicquel, "Nanocrystalline diamond coating of silicon nitride ceramics by microwave plasma-assisted CVD", Thin Solid Films, Vol. 482, 2005, pp. 232-236

[25] S. Chowdhury, E. de Barra and M.T. Laugier,"Hardness measurement of CVD diamond coatings on SiC substrates", Surface and Coatings Technology, Vol. 193, 2005, pp.200-205

[26] B. Yan, N. L.Loh, Y.Fu, C. Q. Sun and P. Hing,"Surface and interface characterization of diamond coatings deposited on pure titanium", Surface and Coatings Technology, Vol. 115, 1999, pp. 256-265

[27] S. –T. Lee, Z. Lin and X. Jiang, "CVD diamond films: nucleation and growth", Materials Science and Engineering: R: Reports, Vol. 25, 1999, pp. 123-154

[28] K. L Choy. "Handbook of nanostructured materials and nanotechnology: synthesis and processing", Edited by H. S Nalwa , San Diego (CA), Academic Press, Vol. 1, 2000, pp. 533.

[29] B. Chapman, "Glow discharge processes: sputtering and plasma etching", John Wiley, New York, ISBN: 047107828x, 1980

[30] M. J. Rand, "Plasma-promoted deposition of thin inorganic films", Journal of vacuum science and technology, Vol. 16, 1979, pp. 420-427

[31] J. E. Greene and S. A. Barnett, "Ion–surface interactions during vapor phase crystal growth by sputtering, MBE and plasma-enhanced CVD: Applications to semiconductors", Journal of vacuum science and technology, Vol. 21, 1982, pp. 285-302

[32] T. Czerwiec, N. Renevier and H. Michel, "Low-temperature plasma-assisted nitriding", Surface and Coatings Technology, Vol. 131, 2000, pp. 267-277

[33] A. Bogaerts, E. Neyts, R. Gijbels and J. V. D. Mullen, "Gas discharge plasmas and their applications", Spectrochimica Acta Part B: Atomic Spectroscopy, Vol. 57, 2002, pp. 609-658

[34] T. Czerwiec, H. Michel and E. Bergmann, "Low-pressure, high-density plasma nitriding: mechanisms, technology and results", Surface and Coatings Technology, Vol. 108-109, 1998, pp. 182-190

[35] M. P. Fewell, J. M. Priest, M. J. Baldwin, G. A. Collins and K. T. Short, "Nitriding at low temperature", Surface and Coatings Technology, Vol. 131, 2000, pp. 284-290

[36] A. Anders, "Plasma and ion sources in large area coating", Surface and Coatings Technology, Vol. 200, 2005, pp. 1893-1906

[37] A. Bogaerts, E. Neyts, R. Gijbels and J. v. d. Mullen,"Gas discharge plasmas and their applications", Spectrochimica Acta Part B: Atomic Spectroscopy, Vol. 57, 2002, pp.609-658

[38] J. Takadoum, H. Houmid-Bennani, D. Mairey and Z. Zsiga, Adhesion Coatings and Wear Resistance of Thin Hard Coatings, Journal of the European Ceramic Society, Vol. 17, 1997, pp.1929-1932

[39] P. G. Schultz, X. Xiaodong, I. Goldwasser, G. Briceno, S. Xiao-Dong, W. Kai-An, "Preparation and screening of crystalline zeolite and hydrothermally-synthesized materials", United States Patent 6864201, 2005

[40] G. Kim, S. Lee and J. Hahn ,"Properties of TiAlN coatings synthesized by closed-field unbalanced magnetron sputtering", Surface and Coatings Technology, Vol. 193, 2005, pp. 213-218

[41] K. A. Gruss and R. F. Davis, "Adhesion measurement of zirconium nitride and amorphous silicon carbide coatings to nickel and titanium alloys", Surface and Coatings Technology, Vol. 114, 1999, pp. 156-168

[42] P. J. Kelly and R. D. Arnell, "Magnetron sputtering: a review of recent developments and applications", Vacuum, Vol. 56, 2000, pp.159-172

[43] W. D. Sproul and K. O. Legg, "Opportunities for innovation: Advanced Surface Engineering, Part-I", Technomic Publishing Co., Lancaster, ISBN: 1566762529, 1995

[44] P. D. Townsend, J. C. Kelly and N. E. W. Hartley, "Ion Implantation, Sputtering and their Applications", Academic Press, London, UK, ISBN: 0126969507, 1976
[45] R. Parsons, "Sputter Deposition process", In: Thin film Process II, Edited by J. L. Vossen and W. Kern, Academic press, Boston, ISBN: 0127282513, 1991
[46] J. Musil and S. Kadlec, "Reactive sputtering of TiN films at large substrate to target distances", Vacuum, Vol. 40, 1990, pp. 435-444
[47] P. J. Kelly , R. D. Arnell , W. Ahmed and A. Afzal, "Novel engineering coatings produced by closed-field unbalanced magnetron sputtering", Materials & Design, Vol. 17, 1996, pp. 215-219
[48] P. J. Kelly and R. D. Arnell, "The influence of magnetron configuration on ion current density and deposition rate in a dual unbalanced magnetron sputtering system", Surface and Coatings Technology, Vol. 108-109, 1998, pp. 317-322
[49] D. G. Teer, UK patent no. 2 258 343, USA patent No. 5 554 519, European patent No. 0 521 045
[50] W. D. Sproul, P. J. Rudnick, M. E. Graham and S. L. Rohde, "High rate reactive sputtering in an opposed cathode closed-field unbalanced magnetron sputtering system", Surface and Coatings Technology, Vol. 43-44, 1990, pp. 270-278
[51] W. D. Munz, F. J. M. Hauzer, D. Schulze and B. Buil, "A new concept for physical vapor deposition coating combining the methods of arc evaporation and unbalanced-magnetron sputtering", Surface and Coatings Technology, Vol. 49, 1991, pp. 161-167
[52] J. L. Vossen and W. Kern, "Thin Film Processes", Academic Press, Inc., ISBN 0-12-728251-3, 1991
[53] N. Pfeiffer, "Process Development for Fabrication of Silicon Semiconductor Devices in a Low Gravity, High Vacuum, Space Environment", Phd Thesis, University of British Columbia, 1988
[54] D. W. Sheel and M. E. Pemble,"Atmospheric Pressure CVD Coatings on Glass", Sheel and Pemble, Link: http://www.cvdtechnologies.com/ CVD%20on% 20 Glass.pdf CVD Coatings on glass, ICCG4, November 2002
[55] K. N. Strafford and C. Subramanian, "Surface engineering: an enabling technology for manufacturing industry", Journal of Materials Processing Technology, Vol. 53, 1995, pp. 393-403
[56] Heat Treating of Malleable Irons, Source: http://www.key-to-steel.com/ ViewArticle.asp ?ID=121
[57] R. A. Ganeev, "Low-power laser hardening of steels", Journal of Materials Processing Technology, Vol.121, 2002, pp.414-419
[58] Ion-Nitriding, Laser Hardening, & Electron-Beam (EB) Hardening, Source: http://tristate.apogee.net/et/eetdion.asp
[59] S. H. Avner, "Introduction to Physical Metallurgy", Glencoe /Mcgraw-Hill, 2nd edition, ISBN: 0070024995 ,1974
[60] J. R. Davis, Surface Engineering for corrosion and wear resistance, ASM International, Materials Park, OH 44073-0002, 2001,ISBN: 0-87170-700-4
[61] Surface Engineering Processes - A Review of Their Suitability for Space Vacuum Applications, Source: http://www.poeton.co.uk/w1/space/review.htm
[62] T. Bell, "Surface engineering: its current and I future impact on tribology, "Journal of Physics D: Applied Physics, Vol. 25, 1992, pp. A297-A306
[63] P. J. Wilbur and B. W. Buchholtz, "Engineering tribological surfaces by ion implantation", Surface and Coatings Technology, Vol. 79, 1996, pp. 1-8
[64] R. Wei, P. J. Wilbur, O. Ozturk and D. L. Williamson, "Tribological studies of ultrahigh dose nitrogen-implanted iron and stainless steel", Nuclear Instruments and Methods in Physics Research B, Vol. 59-60, 1991, pp. 731-736

[65] D. L. Williamson, O. Ozturk, S. G. Wei and P. J. Wilbur, "Microstructure of ultrahigh dose nitrogen-implanted iron and stainless steel", Nuclear Instruments and Methods in Physics Research B, Vol. 59-60, 1991, pp. 737-741
[66] R. Hutchings, G. A. Collins and J. Tendys, "Plasma immersion ion implantation: duplex layers from a single process", Surface and Coatings Technology, Vol. 51, 1992, pp. 489-494
[67] J. R. Conrad, J. L. Radtke, R. A. Dodd, F. J. Worzala and N. C. Tran, "Plasma source ion-implantation technique for surface modification of materials", Journal of Applied Physics, Vol. 62, 1987, pp. 4591-4596
[68] R. Grun and H. J. Gunther, "Plasma nitriding in industry-problems, new solutions and limits", Materials Science and Engineering A, Vol. 140, 1991, pp. 435-441
[69] H. Michel, T. Czerwiec, M. Gantois, D. Ablitzer and A. Ricard, "Progress in the analysis of the mechanisms of ion nitriding", Surface and Coatings Technology, Vol. 72, 1995, pp. 103-111
[70] E. I. Meletis and S. Yan, "Low-pressure ion nitriding of AISI 304 austenitic stainless steel with an intensified glow discharge", Journal of vacuum science and technology A, Vol. 11, 1993, pp. 25-33
[71] M. Berg, C. V. Budtz-Jørgensen, H. Reitz, K. O. Schweitz, J. Chevallier, P. Kringhøj and J. Bøttiger, "On plasma nitriding of steels", Surface and Coatings Technology, Vol. 124, 2000, pp. 25-31
[72] T. Jung, "Kinetics and mechanism of plasma nitridation of thin Aluminium films", Physica Status Solidi, 93, 1986, pp. 479-485
[73] M. Benda, J. Vlek and J. Musil, "Anodic plasma nitriding with a molybdenum cathode", Vacuum, Vol. 46, 1995, pp. 43-47
[74] Z. L. Zhang and T. Bell, "Structure and corrosion resistance of plasma nitrided stainless steel", Surface Engineering, Vol. 1, 1985, pp. 131-136
[75] G. A. Collins, R. Hutchings, K. T. Short, J. Tendys, X. Li and M. Samandi, "Nitriding of austenitic stainless steel by plasma immersion ion implantation", Surface and Coatings Technology, Vol. 74-75, 1995, pp. 417-424.
[76] C. Blawert, A. Weisheit, B. L. Mordike and F. M. Knoop, "Plasma immersion ion implantation of stainless steel: Austenitic stainless steel in comparison to austenitic-ferritic stainless steel", Surface and Coatings Technology, Vol. 85, 1996, pp. 15-27
[77] J. Musil, J. Vlcek and M. Ruzicka, "Recent progress in plasma nitriding", Vacuum, Vol. 59, 2000, pp. 940-951
[78] S. Mandl, R. Gunzel, E. Richter and W. Moller, "Nitriding of austenitic stainless steels using plasma immersion ion implantation", Surface and Coatings Technology, Vol. 100-101, 1998, pp. 372-376
[79] C. F. M. Borges, S. Hennecke and E. Pfender, "Decreasing chromium precipitation in AISI 304 stainless steel during the plasma-nitriding process", Surface and Coatings Technology, Vol. 123, 2000, pp. 112-121
[80] A. S. Korhonen and E. H. Sirvio, "A new low pressure plasma nitriding method", Thin Solid Films, Vol. 96, 1982, pp. 103-108
[81] A. S. Korhonen, E. H. Sirvio and M. S. Sulonen, "Plasma nitriding and ion plating with an intensified glow discharge", Thin Solid Films, Vol. 107, 1983, pp. 387-394
[82] A. S. Korhonen and E. H. Sirvio, "A new low pressure plasma nitriding method", Thin Solid Films, Vol. 96, 1982, pp.103-108
[83] A. S. Korhonen, E. H. Sirvio and M. S. Sulonen, "Metallurgical and protective coatings: Plasma nitriding and ion plating with an intensified glow discharge", Thin Solid Films, Vol. 107, 1983, pp. 387-394
[84] A. Leyland, K. S. Fancey, A. S. James and A. Matthews, "Enhanced plasma nitriding at low pressures: A comparative study of d. c. and r. f. techniques", Surface and Coatings Technology, Vol. 41, 1990, pp. 295-304

[85] A. Leyland, K. S. Fancey and A. Matthews, "Plasma nitriding in a low pressure triode discharge to provide improvements in adhesion and load support for wear resistant coatings", Surface Engineering, Vol. 7, 1991, pp. 207-215
[86] A. Leyland, D. B. Lewis, P. R. Stevenson and A. Matthews, "Low temperature plasma diffusion treatment of stainless steels for improved wear resistance", Surface and Coatings Technology, Vol. 62, 1993, pp. 608-617
[87] K. S. Fancey, A. Leyland, D. Egerton, D. Torres and A. Matthews, "The influence of process gas characteristics on the properties of plasma nitrided steel", Surface and Coatings Technology, Vol. 76-77, 1995, pp. 694-699
[88] J. C. Avelar-Batista, E. Spain, J. Housden, A. Matthews and G. G. Fuentes, "Plasma nitriding of Ti6Al4V alloy and AISI M2 steel substrates using D.C. glow discharges under a triode configuration,Surface and Coatings Technology", Vol. 200,2005, pp. 1954-1961
[89] A. A. Adjaottor, E. Ma and E. I. Meletis, "On the mechanism of intensified plasma-assisted processing", Surface and Coatings Technology, Vol. 89, 1997, pp. 197-203
[90] G. A. Collins, R. Hutchings and J. Tendys, "Plasma immersion ion implantation of steels", Material Science and Engineering A, Vol. 139, 1991, pp. 171-178
[91] G. A. Collins, R. Hutchings, K. T. Short, J. Tendys and C. H. Van-Der-Valk, "Development of a plasma immersion ion implanter for the surface treatment of metal components", Surface and Coatings Technology, Vol. 84, 1996, pp. 537-543
[92] B. Y. Tang, R. P. Fetherston, M. Shamim, R. A. Breun, A. Chen and J. R. Conrad, "Measurement of ion species ratio in the plasma source ion implantation process", Journal of Applied Physics, Vol. 73, 1993, pp. 4176-4180
[93] S. Leigh, M. Samandi, G. A. Collins, K. T. Short, P. Martin and L. Wielunski, "The influence of ion energy on the nitriding behaviour of austenitic stainless steel", Surface and Coatings Technology, Vol. 85, 1996, pp. 37-43
[94] J. Tendys, I.J. Donnelly, M.J. Kenny and J.T.A. Pollock, "Plasma immersion ion implantation using plasmas generated by radio frequency techniques", Applied Physic Letter, Vol. 53, 1988, pp.2143.
[95] G. A. Collins, R. Hutchings and J. Tendys, "Plasma immersion ion implantation of steels ", Materials Science and Engineering A, Vol. 139, 1991, pp. 171.
[96] M. K. Lei and Z. L. Zhang, "Plasma source ion nitriding of pure iron: Formation of an iron nitride Layer and hardened diffusion layer at low temperature", Surface and Coatings Technology, Vol. 91, 1997, pp. 25-31...
[97] M. K. Lei and Z. L. Zhang, "Plasma source ion nitriding: A new low temperature low-pressure nitriding approach", Journal of Vacuum Science and Technology A, Vol. 13, 1995, pp. 2986-2990
[98] J. Musil, M. Ruzicka, J. Vlcek and J. G. Han, "Low-pressure nitriding in gas activated by a discharge", 7th International Conference on Plasma Surface Engineering, Garmisch-Partenkirchen, Germany, Paper No. P 18:15, 2000
[99] D. Hovorka, J. Vlcek, R. Cerstvy, J. Musil, P Belsky and M. Ruzicka, "Microwave plasma nitriding of a low-alloy steel", Journal of vacuum science and technology A, Vol. 18, 2000, pp. 2715-2721
[100] J. D'Haen, C. Quaeyhaegens, G. Knuyt, L. De Schepper, L. M. Stals and M. Van Stappen, "An interface study of various PVD TiN coatings on plasma-nitrided austenitic stainless steel AISI 304", Surface and Coatings Technology, Vol. 60, 1993, pp. 468-473
[101] B. Xu and Y. Zhang, "Collision Dissociation Model in Ion Nitriding", Surface Engineering, Vol. 3, 1987, pp. 226-232
[102] M. Hudis, "Study of ion-nitriding", Journal of Applied Physics, Vol. 44, 1973, pp. 1489-1496
[103] K. Pawlak and W. Zymicki, "Spectroscopic investigations into plasma used for nitriding processes of steel and titanium", Thin solid films, Vol. 230, 1993, pp. 115-120

[104] Y. Sun, A. Bloyce and T. Bell. "Finite element analysis of plastic deformation of various TiN coating/ substrate systems under normal contact with a rigid sphere", Thin Solid Films, Vol. 271, 1995, pp. 122-131
[105] B. Podgornik and J. Vizintin, "Tribology of thin films and their use in the field of machine elements", Vacuum, Vol. 68, 2002, pp. 39-47
[106] C. Weaver, "Adhesion of thin films", Journal of vacuum science and technology, Vol. 12, 1975, pp. 18-25
[107] F. S. Shieu, L. H. Cheng, Y. C. Sung, J. H. Huang and G. P. Yu, "Microstructure and coating properties of ion-plated TiN on type 304 stainless steel", Thin Solid Films, Vol. 334, 1998, pp. 125-132
[108] E. Kusano, M. Kitagawa, Y. Kuroda, H.Nanto and A. Kinbara, "Adhesion and hardness of compositionally gradient TiO2/Ti/TiN, ZrO2/Zr/ZrN, and TiO2/Ti/Zr/ZrN coatings", Thin Solid Films, Vol. 334,1998, pp. 151-155
[109] J.-Y. Chen, G. -P. Yu and J.-H. Huang,"Corrosion behavior and adhesion of ion-plated TiN films on AISI 304 steel", Materials Chemistry and Physics, Vol. 65, 2000, pp. 310-315
[110] Wuu-Ling Pan, Ge-Ping Yu and Jia-Hong Huang, "Mechanical properties of ion-plated TiN films on AISI D2 steel", Surface and Coatings Technology, Vol. 110,1998, pp. 111-119
[111] J. A. Thornton and D. W. Hofman, "The influence of discharge current on the intrinsic stress in Mo films deposited using cylindrical and planar magnetron sputtering sources", Journal of Vacuum Science Technology, Vol. A 3, 1985, pp. 576-579
[112] Z. Xianting, S. Zhang and J. Hsieh, "Development of graded Cr–Ti–N coatings", Surface and Coatings Technology, Vol. 102, 1998, pp. 108-112
[113] C. Fernández-Ramos, J. C. Sánchez-López, A. Justo, T. C. Rojas, I. Papst, F. Hofer and A. Fernández, "Microstructural characterization of Ti–TiN/CNx gradient-multilayered coatings", Surface and Coatings Technology, Vol. 180-181, 2004, pp. 526-532
[114] J. A. Imery, H. B. McShane and R. D. Rawlings, "A Two-Dimensional Finite Element Analysis of a Double Layer Functionally Gradient Material", Proceedings of 1994 ANSYS Conference, ANSYS Inc., 1994
[115] J. E. Sundgren and H. T. G. Hentzell, "A review of the present state of art in hard coatings grown from the vapor phase", Journal of Vacuum Science Technology, Vol. A 4, 1986, pp. 2259-2279
[116] K. –L. Choy and E. Felix, "Functionally graded diamond-like carbon coatings on metallic substrates", Materials Science and Engineering A, Vol. 278, 1999, pp. 162-169
[117] J. Deng and M. Braun, "DLC multilayer coatings for wear protection", Diamond and Related Materials, Vol. 4, 1995, pp. 936-943
[118] H. -J. Spies, B. Larisch, K. Höck, E. Broszeit and H. -J. Schröder, "Adhesion and wear resistance of nitrided and TiN coated low alloy steels", Surface and Coatings Technology, Vol. 74-75, 1995, pp. 178-182
[119] M. D. Zlatanovic, A. M. Kunosic, R. B. Beloševac and N. V. Popovic, "Plasma Deposition of Hard Coatings - Duplex Treatment", Material Science Forum: Advanced Materials for High Technology Applications, Vol. 214, 1996, pp. 179–188
[120] H. Dong, Y. Sun and T. Bell, "Enhanced corrosion resistance of duplex coatings", Surface and Coatings Technology, Vol. 90, 1997, pp. 91-101
[121] T. Bell, H. Dong and Y. Sun, "Realizing the potential of duplex surface engineering", Tribology International, Vol. 31, 1998, pp. 127-137
[122] K. -T. Rie and E. Broszeit, "Plasma diffusion treatment and duplex treatment - recent development and new applications", Surface and Coatings Technology, Vol. 76-77, 1995, pp. 425-436
[123] M. Yasuo, Z. Yang and Y. –W. Chung, "Optimization of properties of carbon nitride and CNx/TiN coatings prepared by single-cathode magnetron sputtering", Surface and Coatings Technology, Vol. 86-87, 1996, pp. 586-591

[124] S. Hogmark, S. Jacobson and M. Larsson, "Design and evaluation of tribological coatings", Wear, Vol. 246, 2000, pp. 20-33
[125] F. Jamarani, M. Korotkin and R. V. Lang, "Compositionally graded thermal barrier coatings for high temperature aero gas turbine components", Surface and Coatings Technology, Vol. 54-55, 1992, pp. 58-63
[126] E. Kusano, A. Kinbara and I. Kondo, "Formation of compositionally graded multilayer films by discharge gas flow modulation in magnetron sputtering", Journal of Non-Crystalline Solids, Vol. 218, 1997, pp. 58-61
[127] X. Qiao, Y. Hou, Y. Wu and J. Chen, "Study on functionally gradient coatings of Ti-Al-N", Surface and Coatings Technology, Vol. 131, 2000, pp. 462-464
[128] X. M. He, L. Shu and Z. W. Xie, "Effects of the Ti/Al atomic ratio on the properties of gradient, Ti, Al, N films synthesized by ion beam assisted deposition", Journal of Vacuum Science and Technology B, Vol. 17, 1999, pp. 845-850
[129] M. Pinkas, J. Pelleg and M. P. Dariel, "Structural analysis of, Ti1-xAlx, N graded coatings deposited by reactive magnetron sputtering", Thin Solid Films, Vol. 355-356, 1999, pp. 380-384
[130] A. Raveh, M. Weiss, M. Pinkas, D. Z. Rosen and G. Kimmel, "Graded Al-AlN, TiN and TiAlN multilayers deposited by radio-frequency reactive magnetron sputtering", Surface and Coatings Technology, Vol. 114, 1999, pp. 269-277
[131] A. Inoue, T. Yamaguchi, B. G. Kim, K. Nosaki and T. Masumoto, "Production of compositionally gradient Al-AlN films by reactive sputtering and their mechanical and electrical properties", Journal of Applied Physics, Vol. 71, 1992, pp. 3278-3282
[132] A. A. Voevodin, M. A. Capano, S. J. P. Laube, M. S. Donley and J. S. Zabinski, "Design of a Ti/TiC/DLC functionally gradient coating based on studies of structural transitions in Ti-C thin films", Thin Solid Films, Vol. 298, 1997, pp. 107-115
[133] A. A. Voevodin, J. M. Schneider, C. Rebholz and A. Matthews, "Multilayer composite ceramic-metal-DLC coatings for sliding wear applications", Tribology International, Vol. 29, 1996, pp. 559-570
[134] N. Dingremont, E. Bergmann, P. Collignon and H. Michel, "Optimization of duplex coatings built from nitriding and ion plating with continuous and discontinuous operation for construction and hot working steels", Surface and Coatings Technology, Vol. 72,1995, pp. 163-168
[135] N. Dingremont, P. Collignon, H. Michel and E. Bergmann, "Optimisation of duplex coatings built from nitriding and ion plating with continuous and discontinuous operation for construction and hot-working steels", Surface and Coatings Technology, Vol. 72, 1995, pp. 163-168
[136] O. H. Kessler, F. T. Hoffmann and P. Mayr, "Combinations of coating and heat treating processes: establishing a system for combined processes and examples", Surface and Coatings Technology, Vol. 108-109, 1998, pp. 211-216
[137] K. Höck, H. -J. Spies, B. Larisch, G. Leonhardt and B. Buecken, "Wear resistance of prenitrided hardcoated steels for tools and machine components", Surface and Coatings Technology, Vol. 88, 1997, pp. 44-49
[138] B. Podgornik, S. Hogmark, O. Sandberg and V. Leskovsek, "Wear resistance and anti-sticking properties of duplex treated forming tool steel", Wear, Vol. 254, 2003, pp. 1113-1121
[139] Y. Sun and T. Bell, "Plasma surface engineering of low alloy steel", Materials Science and Engineering A, Vol. 140, 1991, pp. 419-434
[140] M. Zlatanovic and W. D. Munz, "Wear resistance of plasma-nitrided and sputter-ion-plated hobs", Surface and Coatings Technology, Vol. 41, 1990, pp. 17-30
[141] J. Musil, J. Vlcek, V. Jezek and M. Benda, "Protection of aluminium by duplex coatings", Surface and Coatings Technology, Vol. 76-77, 1995, pp. 341-347

[142] M. Bader, H. J. Spies, K. Hock, E. Broszeit and H. J. Schroder, "Properties of duplex treated (gas-nitriding and PVD -TiN, -Cr2N) low alloy steel", Surface and Coatings Technology, Vol. 98, 1998, pp. 891-896
[143] N. Dingremont, E. Bergmann, M. Hans and P. Collignon, "Comparison of the corrosion resistance of different steel grades nitrided, coated and duplex treated", Surface and Coatings Technology, Vol. 76-77, 1995, pp. 218-224
[144] B. Buecken, G. Leonhardt, R. Wilberg, K. Hoeck and H. J. Spies, "Direct combination of plasma nitriding and PVD hard coating by a continuous process", Surface and Coatings Technology, Vol. 68-69, 1994, pp. 244-248
[145] J. C. A. Batista, C. Godoy, A. Matthews and A. Leyland, "Process Developments Towards Producing Well Adherent Duplex PAPVD Coatings", Surface Engineering, Vol. 19, 2003, pp. 37-44
[146] H. J. Spies, B. Larisch and K. Hoeck, "Optimisation of TiN hard coatings on prenitrided low alloy steels", Surface Engineering, Vol. 11, 1995, pp. 319-323
[147] T. Bjork, R. Westergard, S. Hogmark, J. Bergstrom and P. Hedenqvist, "Physical vapour deposition duplex coatings for aluminium extrusion dies", Wear, Vol. 225-229, 1999, pp. 1123-1130
[148] J. C. A. Batista, A. Matthews and C. Godoy, "Micro-abrasive wear of PVD duplex and single-layered coatings", Surface and Coatings Technology, Vol. 142-144, 2001, pp. 1137-1143
[149] S. Rudenja, C. Leygraf, J. Pan, P. Kulu, E. Talimets and V. Mikli, "Duplex TiN coatings deposited by arc plating for increased corrosion resistance of stainless steel substrates", Surface and Coatings Technology, Vol. 114, 1999, pp. 129-136

[150] I. Efeoglu and A. Celik, "Mechanical and structural properties of AISI 8620 steel TiN coated, nitrided and TiN coated + nitrided", Materials Characterization, Vol. 46, 2001, pp. 311-316
[151] B. Skoric, D. Kakas and T. Gredic, "Influence of plasma nitriding on mechanical and tribological properties of steel with subsequent PVD surface treatments", Thin Solid Films, Vol. 317, 1998, pp. 486-489
[152] B. Podgornik, J. Vizintin, O. Wanstrand, M. Larsson, S. Hogmark, H. Ronkainen and K. Holmberg, "Tribological properties of plasma nitrided and hard coated AISI 4140 steel", Wear, Vol. 249, 2001, pp. 254-259
[153] E. I. Meletis, A. Erdemir and G. R. Fenske, "Tribological characteristics of DLC films and duplex plasma nitriding/DLC coating treatments", Surface and Coatings Technology, Vol. 73, 1995, pp. 39-45
[154] P. Kaestner, J. Olfe, J. W. He and K. T. Rie, "Improvement in the load-bearing capacity and adhesion of TiC coatings on TiAl6V4 by duplex treatment", Surface and Coatings Technology, Vol. 142-144, 2001, pp. 928-933
[155] G. H. Jeong, M. S. Hwang, B. Y. Jeong, M. H. Kim and C. Lee, "Effects of the duty factor on the surface characteristics of the plasma nitrided and diamond-like carbon coated high-speed steels", Surface and Coatings Technology, Vol. 124, 2000, pp. 222-227
[156] B. S. Yilbas, M. S. J. Hashmi and S. Z. Shuja, "Laser treatment and PVD TiN coating of Ti-6Al-4V alloy" Surface and Coatings Technology, Vol. 140, 2001, pp. 244-250
[157] M. Zlatanovic, "Deposition of, (Ti, Al) N coatings on plasma nitrided steel", Surface and Coatings Technology, Vol. 48, 1991, pp. 19-24
[158] N. Dingremont, A. Pianelli and E. Bergmann, "Analysis of the compatibility of plasma-nitrided steels with ceramic coatings deposited by the ion-plating technique", Surface and Coatings Technology, Vol. 61, 1993, pp. 187-193
[159] J. Dhaen, C. Quaeyhaegens, L. M. Stals and M. Van Stappen, "Interface study of physical vapor-deposition TiN coatings on plasma-nitrided steels", Surface and Coatings Technology, Vol. 61, 1993, pp. 194-200

[160] B. Larisch, U. Brusky and H. -J. Spies, "Plasma nitriding of stainless steels at low temperatures", Surface and Coatings Technology, Vol. 116-119, 1999, pp. 205-211
[161] M. Zlatanovic, D. Kakas, L. Mezibrada, A. Kunosic and W. D. Munz, "Influence of plasma nitriding on wear performance of TiN coating", Surface and Coatings Technology, Vol. 64, 1994, pp. 173-181
[162] A. Matthews, A. Leyland "Hybrid techniques in surface engineering", Surface and Coatings Technology, Vol. 71, 1995, pp. 88-92
[163] W. Liang, G. Yuzhou and X. Bin, "Plasma vapour deposition hard coating on pre-nitrided low alloy steel", Surface and Coatings Technology", Vol. 131, 2000, pp. 452-456
[164] B. Podgornik, J. Vizintin, O. Wanstrand M. Larsson and S. Hogmark, "Wear and friction behaviour of duplex-treated AISI 4140 steel". Surface and Coatings Technology, Vol. 120-121, 1999, pp. 502-508
[165] C. A. Straede, V. Mikli, E. Tallimets, S. Rudenja and P. Kulu, "Corrosion performance of duplex TiN coatings deposited by arc plating", Surface and Coatings Technology, Vol. 100-101, 1998, pp. 247-250
[166] J. Michalski, L. Ellina, T. Wierzchon and S. AlGhanem, "Wear and corrosion properties of TiN layers deposited on nitrided high-speed steel", Surface and Coatings Technology, Vol. 72, 1995, pp. 189-195
[167] B. Navinsek, P. Panjan and F. Gorenjak, "Improvement of hot forging manufacturing with PVD and Duplex coatings". Surface and Coatings Technology, Vol. 137, 2001, pp. 255-264
[168] D. T. Quinto, "Technology Perspective on CVD and PVD Coated Metal-Cutting Tools", International Journal of Refractory Metals and Hard Materials, Vol. 14, 1996, pp. 7-20
[169] M. Pancielejko, W. Precht and A. Czyzniewski, "Tribological properties of PVD titanium carbides", Vacuum, Vol. 53, 1999, pp. 57-60
[170] H. Holleck, "Material selection for hard coatings", Journal of Vacuum Science and Technology A, Vol. 4, 1986, pp. 2661-2669
[171] P. Engel, G. Schwarz and G. K. Wolf, "Characterisation of chromium nitride films prepared by ion-beam-assisted deposition", Surface and Coatings Technology, Vol. 112, 1999, pp. 286-290
[172] L. Cunha and M. Andritschky, "Residual stress, surface defects and corrosion resistance of CrN hard coatings", Surface and Coatings Technology, Vol. 111, 1999, pp. 158-162
[173] H. Randhawa, "Cathodic arc plasma deposition of TiC and TiCxN1-x films", Thin Solid Films, Vol. 153, 1987, pp. 209-218
[174] O. Knotek, E. Elsing, M. Atzor and H. G. Prengel, "The influence of the composition and coating parameters of PVD Ti-Al-V, C, N, films on abrasive and adhesive wear of coated cemented carbides", Wear, Vol. 133, 1989, pp. 189-198
[175] T. Spalvins, "A review of recent advances in solid film lubrication", Journal of vacuum science and technology", Vol. 5, 1987, pp. 212-219
[176] N. J. Mikkelsen and G. Sorensen, "Ion beam modification of MoSx films on metals", Materials Science and Engineering A, Vol. A 115, 1989, pp 343-347
[177] T. Spalvins, NASA TN D-7169, 1973
[178] R. Messier, A. R. Badzian, T. Badzian, K. Spear, P. Bachmann and R. Roy, "From diamond-like carbon to diamond coatings", Thin Solid Films, Vol. 153, 1987, pp. 1-9
[179] L. D. Marks, M. R. Hiltonand and G. Jayaram, "Nanostructure of Au--20%Pd layers in MoS2 multilayer solid lubricant", Surface and Coatings Technology, Vol. 76-77, 1995, pp. 393-399
[180] G. Weise, A. Teresiak, I bacher, P. Markchlager and G. Kampschulte, "Influence of magnetron sputtering process parameters on wear properties of steel/Cr3Si or Cr/MoSx", Surface and coating technology, Vol. 76-77, 1995, pp. 383-392

[181] T. L. Mogne, C. Donnet, J. M. Martin, A. Tonck and N. M. Pinard,, "Nature of super-lubricating MoS2 physical vapor deposition coatings", Journal of Vacuum Science technology: A, Vol. 12, 1994, pp. 1998-2004
[182] T. Spalvins, ASLE transactions, Vol. 17, 1973, pp. 1
[183] D. -Y. Wang, C. -L. Chang, Z. -Y. Chen and W. -Y. Ho, "Microstructural and tribological characterization of MoS2–Ti composite solid lubricating films", Surface and coating technology, Vol. 120–121, 1999, pp. 629–635
[184] H. Chermette, F. Rogemond, O. El Beqqali, J. F. Paul, C. Donnet, J. M. Martin and T. Le Mogne, "Lubricating properties of molybdenum disulphur: a density functional theory study", Surface Science, Vol. 472, 2001, pp. 97-110
[185] R. Goller, P. Torri, M. A. Baker, R. Gilmore and W. Gissler, "The deposition of low-friction TiN–MoSx hard coatings by a combined arc evaporation and magnetron sputter process", Surface and Coatings Technology, Vol. 120-121, 1999, pp. 453-457
[186] G. Xu, Z. Zhou, J. Liu and X. Ma, "An investigation of fretting behavior of ion-plated TiN, magnetron-sputtered MoS2 and their composite coatings", Wear, Vol. 225-229, 1999, pp. 46-52
[187] Y. W. Bae, W. Y. Lee, T. M. Besmann, C. S. Yust and P. J. Blau, "Preparation and friction characteristics of self-lubricating TiN-MoS2 composite coatings", Materials Science and Engineering A, Vol. 209, 1996, pp. 372-376
[188] A. Savan, E. Pflüger, R. Goller and W. Gissler, "Use of nanoscaled multilayer and compound films to realize a soft lubrication phase within a hard, wear-resistant matrix", Surface and Coatings Technology, Vol. 126, 2000, pp. 159-165
[189] H. W. S. Jaffee and K. Y. L. Lawrence, "An investigation of the effect of surface roughness and coating thickness on the friction and wear behaviour of a commercial MoS2–metal coating on AISI 400C steel", Wear, Vol. 237, 2000, pp. 283-287
[190] H. Tsai and D. B. Bogy, "Characterization of diamondlike carbon films and their application as overcoats on thin-film media for magnetic recording", Journal of vacuum science and technology A, Vol. 5, 1987, pp. 3287-3312
[191] J. C. Angus and F. Jansen, "Dense ``Diamondlike'' hydrocarbons as random covalent networks", Journal of vacuum science and technology A, Vol. 6, 1988, pp. 1778-1782
[192] A. Singh, G. Ehteshami, S. Massia, J. He, R. G. Storer and G. Raupp, "Glial cell and fibroblast cytotoxicity study on plasma-deposited diamond-like carbon coatings", Biomaterials, Vol. 24, 2003, pp. 5083-5089
[193] G. Reisel, A. Dorner-Reisel and B. Wielage, "Silicon doped diamond like carbon as substitute for lubrication in spin-extrusion", Diamond and Related Materials, Vol. 14, 2005, pp. 1810-1814
[194] C. Donnet, M. Belin, J. C. Augé, J. M. Martin, A. Grill and V. Patel, "Tribochemistry of diamond-like carbon coatings in various environments", Surface and Coatings Technology, Vol. 68-69, 1994, pp. 626-631
[195] T. L Huu, H. Zaïdi and D. Paulmier, "Lubricating properties of diamond-like coating", Wear, Vol. 181-183, 1995, pp. 766-770
[196] R. Hauert, "A review of modified DLC coatings for biological applications", Diamond and Related Materials, Vol. 12, 2003, pp. 583-589
[197] Y. Liu, A. Erdemir and E. I. Meletis, "An investigation of the relationship between graphitization and frictional behavior of DLC coatings", Surface and Coatings Technology, Vol. 86-87, 1996, pp. 564-568
[198] Y. Aoki and N. Ohtake, "Tribological properties of segment-structured diamond-like carbon films", Tribology International, Vol. 37, 2004, pp. 941-947
[199] D. –H. Kim, H. -E. Kim, K. –R. Lee, C. –N. Whang and I. -S. Lee, "Characterization of diamond-like carbon films deposited on commercially pure Ti and Ti–6Al–4V", Materials Science and Engineering: C, Vol. 22, 2002, pp. 9-14

[200] C. Kwietniewski, H. Dong, T. Strohaecker, X. Y. Li and T. Bell, "Duplex surface treatment of high strength Timetal 550 alloy towards high load-bearing capacity", Surface and Coatings Technology, Vol. 139, 2001, pp. 284-292
[201] Y. Lifshitz, G. D. Lempert, E. Grossman, I. Avigal, C. Uzansaguy, R. Kalish, J. Kulik, D. Marton and J. W. Rabalais, "Growth mechanisms of DLC films from C+ ions: experimental studies", Diamond and Related Materials, Vol. 4, 1995, pp. 318-323
[202] K. Bewilogua, C. V. Cooper, C. Specht, J. Schröder, R. Wittorf and M. Grischke, "Effect of target material on deposition and properties of metal-containing DLC, Me-DLC, coatings", Surface and coating technology, Vol. 127, 2000, pp. 224–232
[203] G. F. Yin, J. M. Luo, C. Q. Zheng, H. H. Tong, Y. F. Huo and L. L. Mu, "Preparation of DLC gradient biomaterials by means of plasma source ion implant-ion beam enhanced deposition", Thin Solid Films, Vol. 345, 1999, pp. 67-70
[204] B. -Y. Jeong and M. -H. Kim,"Effects of pulse frequency and temperature on the nitride layer and surface characteristics of plasma nitrided stainless steel", Surface and Coatings Technology, Vol. 137,2001, pp. 249-254
[205] The APP Annual Conference & Exposition May 2-6, 2004, The Riviera Hotel & Casino, Las Vegas, The Official Newsletter of The Association of Professional Piercers, Spring, Issue 28, 2004,Source: http://www.safepiercing.org/PDFs/Point28.pdf
[206] A. Fossati, F. Borgioli, E. Galvanetto and T. Bacci, "Glow-discharge nitriding of AISI 316L austenitic stainless steel: influence of treatment time", Surface and Coatings Technology, In Press, 2004
[207] X. L. Xu, L. Wang, Z. W. Yu and Z. K. Hei, "Microstructural characterization of plasma nitrided austenitic stainless steel", Surface and Coatings Technology, Vol. 132, 2000, pp. 270-274
[208] Y. Sun and T. Bell, "Low Temperature Plasma Nitriding Characteristics of Precipitation Hardening Stainless Steel", Surface Engineering, Vol. 19, 2003, pp. 331-336
[209] X. Y. Li, "Low Temperature Plasma Nitriding of 316 Stainless Steel – Nature of S Phase and Its Thermal Stability", Surface Engineering, Vol. 17, 2001, pp. 147-152
[210] V. Singh, K. Marchev, C. V. Cooper and E. I. Meletis, "Intensified plasma-assisted nitriding of AISI 316L stainless steel", Surface and Coatings Technology, Vol. 160, 2002, pp. 249-258
[211] E. Menthe, A. Bulak, J. Olfe, A. Zimmermann and K. -T. Rie, "Improvement of the mechanical properties of austenitic stainless steel after plasma nitriding", Surface and Coatings Technology, Vol. 133-134, 2000, pp. 259-263
[212] M. P. Fewell, D. R. G. Mitchell, J. M. Priest, K. T. Short and G. A. Collins, "The nature of expanded austenite", Surface and Coatings Technology, Vol. 131, 2000, pp. 300-306
[213] N. X. Randall, N. Renevier, H. Michel and P. Collignon, "Correlation between processing parameters and mechanical properties as a function of substrate polarization and depth in a nitrided 316 L stainless steel using nanoindentation and scanning force microscopy", Vacuum, Vol. 48, 1997, pp. 849-855
[214] T. Bell, "Surface engineering of austenitic stainless steel", Surface Engineering, Vol. 18, 2002, pp. 415-422
[215] K. Marchev, M. Landis, R. Vallerio, C. V. Cooper and B. C. Giessen, "The m phase layer on ion nitrided austenitic stainless steel (III): an epitaxial relationship between the m phase and the γ parent phase and a review of structural identifications of this phase", Surface and Coatings Technology, Vol. 116-119, 1999, pp. 184-188
[216] A Short History of Titanium, Vulcanium, Bulletin 1.2, 2005, http://www.vulcanium.com/uploadedFiles/VMI-ShortHistoryOfTitanium-Medical.pdf
[217] Titanium Information; Source: http://www.titaniumart.com/titanium-info.html
[218] Titanium come to age, Source: http://www.businessweek.com/magazine/content/02_48/b3810116.htm

[219] R. Boyer, G. Welsch, E. W. Collings, "Titanium Data sheets", In: Materials Properties Handbook: Titanium Alloys, eidited by R. Boyer, G. Welsch, Materials Park, OH: ASM Intl, 1994, ISBN: 0-87170-481-1
[220] Properties and Apllications of Titanium, Source: http://www.titaniumart.com/ titanium-info-cp. Html
[221] K. Matsuura and M. Kudoh, Surface modification of titanium by a diffusional carbo-nitriding method, Acta Materialia, Vol. 50, , 2002, pp. 2693-2700
[222] H. L. Freese, M. G. Volas and J. R. Wood, "Metallurgy and technological properties of titanium and titanium alloys", In: Titanium in Medicine, eidited by D. M. Brunette, P. Tengvall, M. Textor and P. Thomsen, Springer-Verlag, Berlin, ISBN: 3-540-66936-1, 2001
[223] M. Long and H. J. Rack, "Titanium alloys in total joint replacement—a materials science perspective", Biomaterials, Vol. 19, 1998, pp. 1621-1639
[224] H. -J. Spies, B. Reinhold and K. Wilsdorf, "Gas nitriding – process control and nitriding non-ferrous alloys", Surface Engineering, Vol. 17, 2001, pp. 41-54
[225] C. S. Javorsky, T. R. Strohaecker, J. A. T. Borges da Costa and M. A. Z. Vasconcellos, "Ion beam analysis of plasma nitrided Ti6Al4V-ELI", Nuclear Instruments and Methods in Physics Research Section B, Vol. 175-177, 2001, pp. 726-731
[226] A. Zhecheva, W. Sha, S. Malinov and A. Long, "Enhancing the microstructure and properties of titanium alloys through nitriding and other surface engineering methods", Surface and Coatings Technology, Vol. 200, 2005, pp. 2192-2207
[227] H. C. Man, Z. D. Cui and X. J. Yang, "Analysis of laser gas nitrided titanium by X-ray photoelectron spectroscopy", Applied Surface Science, Vol. 199, 2002, pp. 293-302
[228] V. Fouquet, L. Pichon, M. Drouet and A. Straboni, "Plasma assisted nitridation of Ti-6Al-4V", Applied Surface Science, Vol. 221, 2004, pp. 248-258
[229] S. Y. Wang, P. K. Chu, B. Y. Tang, X. C. Zeng, Y. B. Chen and X. F. Wang, "Radio-frequency plasma nitriding and nitrogen plasma immersion ion implantation of Ti-6Al-4V alloy", Surface and Coatings Technology, Vol. 93, 1997, pp. 309-313
[230] C. E. Pinedo, W. A. Monteiro, "Surface hardening by plasma nitriding on high chromium alloy steel", Journal of Materials Science Letters, Vol. 20, 2001, pp. 147-149
[231] R. Wei, T. Booker, C. Rincon and J. Arps, "High-intensity plasma ion nitriding of orthopedic materials: Part I. Tribological study", Surface and Coatings Technology, Vol. 186, 2004, pp. 305-313
[232] D. Ikeda, M. Ogawa, Y. Hara, Y. Nishimura, O. Odusanya, K. Azuma, S. Matsuda, M. Yatsuzuka and A. Murakami, "Effect of nitrogen plasma-based ion implantation on joint prosthetic material", Surface and Coatings Technology, Vol. 156, 2002, pp. 301-305
[233] J. M. Brian, "Alternative bearing surfaces in hip replacement surgery", Maine Joint Replacement Institute, Portland ME, Source: http://www. orthoassociates. com/Totalhip2. htm, 2001
[234] H. Dong and T. Bell, "State-of-the-art overview: ion beam surface modification of polymers towards improving tribological properties", Surface and Coatings Technology, Vol. 111, 1999, pp. 29-40
[235] C. X. Li and T. Bell, "Potential of plasma nitriding of polymer for improved hardness and wear resistance", Journal of Materials Processing Technology, Vol. 168, 2005, pp. 219-224
[236] F. F. Shi, "Recent advances in polymer thin films prepared by plasma polymerization: Synthesis, structural characterization, properties and applications", Surface and Coatings Technology, Vol. 82, 1996, pp. 1-15
[237] C. -M. Chan, T. -M. Ko and H. Hiraoka, "Polymer surface modification by plasmas and photons", Surface Science Reports, Vol. 24, 1996, pp. 1-54
[238] F. Z. Cui and Z. S. Luo, "Biomaterials modification by ion-beam processing", Surface and Coatings Technology, Vol. 112, 1999, pp. 278-285

[239] J. S. Chen, S. P. Lau, Z. Sun, B. K. Tay, G. Q. Yu, F. Y. Zhu, D. Z. Zhu and H. J. Xu, "Structural and mechanical properties of nitrogen ion implanted ultra high molecular weight polyethylene", Surface and Coatings Technology, Vol. 138, 2001, pp. 33-38
[240] C. Allen, A. Bloyce and T. Bell, "Sliding wear behaviour of ion implanted ultra high molecular weight polyethylene against a surface modified titanium alloy Ti-6Al-4V", Tribology International, Vol. 29, 1996, pp. 527-534
[241] W. Shi, X. Y. Li and H. Dong, "Improved wear resistance of ultra-high molecular weight polyethylene by plasma immersion ion implantation", Wear, Vol. 250, 2001, pp. 544-552
[242] J. N. Matossian and R. Wei, "Challenges and progress toward a 250 kV, 100 kW plasma ion implantation facility", Surface and coating technology, Vol. 85, 1996, pp. 111–119
[243] T. W. H. Oates, D. R. McKenzie and M. M. M. Bilek, "Plasma immersion ion implantation using polymeric substrates with a sacrificial conductive surface layer", Surface and coating technology, Vol. 156, 2002, pp. 332–337
[244] K. Y. F. Ricky, I. T. L. Cheung, Y. F. Mei, C. H. Shek, G. G. Siu, Paul K. Chu, W. M. Yang, Y. X. Leng, Y. X. Huang, X. B. Tian and S. Q. Yang, "Surface modification of polymeric materials by plasma immersion ion implantation", Nuclear Instruments and Methods in Physics Research Section B: Beam Interactions with Materials and Atoms, Vol. 237, 2005, pp. 417-421
[245] S. Desa, S. Ghosal, R. L. Kosut, J. L. Ebert, T. E. Abrahamson, A. Kozak, D. W. Zou, X. Zhou, J. F. Groves and H. N. G. Wadley, "Reactor-scale models for rf diode sputtering of metal thin films", Journal of Vacuum Science and Technology A, Vol. 17, 1999, pp. 1926-1933
[246] D. E. Koteck, S. Barbee, J. D. C. Sokol, T. D. Cacouris, R. A. Conti, R. J. Eschbach, D. L. Wilson, J. Wong and S. P. Zuhoski, "Applications of computational fluid dynamics for improved performance in chemical-vapor-deposition reactors", Journal of Vacuum Science and Technology B, Vol. 12, 1994, pp. 2752-2757
[247] P. V. Kola, "Magnetron sputtering of thin Nitride Films", PhD thesis, School of MME, DCU, Ireland, 1995
[248] FLUENT CFD solver 6. 0: documentation, fluent inc., http://www. fluent. com, 2001
[249] M. Gad-el-Hak, "Flow physics in MEMS", Mécanique & Industries, Vol. 2-4, 2001, pp. 313-341
[250] G. Scherer, "On the numerical modeling of the transitional flow in rarefied gases", Journal of Computational and Applied Mathematics, Vol. 103, 1999, pp. 165-173
[251] Yu. E. Egorov and A. I. Zhmakin, "Numerical simulation of low-Mach number gas mixture flows with heat and mass transfer using unstructured grids", Computational Materials Science, Vol. 11, 1998, pp. 204-220
[252] R. Iwatsu, Computational Fluid Dynamics, http://www.fml.m.dendai.ac.jp/iwatsu/profiwatsu/Computational%20Fluid%20Dynamics.pdf
[253] Design-centered introduction to acrospace enginineering, Source: http://www.adl.gatech.edu/classes/dci/hispd/dci09.html
[254] FLUENT CFD solver 6. 0: data base of software, fluent inc., http://www. fluent. com, 2001
[255] GAMBIT CFD Preprocessor 2. 0. 4 documentation, fluent inc., http://www. fluent. com. 2001
[256] CFD Online discussion fourm, http://www. cfd-online. com/Forum/, 1994-2005
[257] M. Sitges, M. Jones,T. Shiota etl., "Interaliasing Distance of the Flow Convergence Surface for Determining Mitral Regurgitant" , Journal of the American College of Cardiology, Vol. 38, 2001, pp. 1195-1202
[258] M. Buchmann, R. Gadow and J. Tabellion, "Experimental and numerical residual stress analysis of layer coated composites", Materials Science and Engineering: A, Vol. 288, 2000, pp. 154-159

[259] A. Khor and Y. W. Gu, "Effects of residual stress on the performance of plasma sprayed functionally graded ZrO2/NiCoCrAlY coatings", Materials Science and Engineering: A, Vol. 277, 2000, pp. 64-76
[260] Y. Islamoglu, E. Celik, C. Parmaksizoglu and Y. S. Hascicek, "Effects on residual stresses of annealing parameters in high-temperature ZrO2 insulation coatings on Ag/Bi-2212 superconducting tapes using finite element method", Materials and Design, Vol. 23, 2002, pp. 531-536
[261] V. Teixeira, M. Andritschky, W. Fischer, H. P. Buchkremer and D. Stöver, "Analysis of residual stresses in thermal barrier coatings", Journal of Materials Processing and Technology, Vol. 92-93, 1999, pp. 209-216
[262] B. A. Boley and J. H. Weiner, "Theory of thermal stresses", Dover Publications, Mineola, NY, ISBN: 0486695794, 1997
[263] J. E. Greene and J. L. Zilko, "The nature of the transition region formed between dc-bases rf sputtered TiC films and steel substrates", Surface Science, Vol. 1, 1978, pp. 109-124.
[264] Y. C. Tsui and T. W. Clyne, "An analytical model for predicting residual stresses in progressively deposited coatings, Part 1: Planar geometry", Thin Solid Films, Vol. 306, 1997, pp. 23-33
[265] J. -h. Jeong, S. -Y. Lee, W. -S. Lee, Y. -J. Baik and D. Kwon, "Mechanical analysis for crack-free release of chemical-vapor-deposited diamond wafers", Diamond and Related Materials, Vol. 11, 2002, pp. 1597-1605
[266] A. Mimaroglu, A. Ozel and S. Genc, "Influence of interlayer material and geometry on stress levels in MgO. ZrO2-GG coatings subjected to thermal shock", Materials and Design, Vol. 18, 1997, pp. 73-76
[267] S. Widjaja, A. M. Limarga and T. H. Yip, "Modeling of residual stresses in a plasma-sprayed zirconia/alumina functionally graded-thermal barrier coating", Thin Solid Films, Vol. 434, 2003, pp. 216-227
[268] X. J. Sheng, J. Liu, X. Zhou and J. Li, "Thermal stress analysis of Ceramic/metal gradient thermal barrier coating by ANSYS", Paper of Ninth International ANSYS Conference and Exhibition, Pittsburgh, USA, 2000
[269] A. F. Okyar and M. Gosz, "Finite element modeling of a microelectronic structure under uniform thermal loading", Finite Elements in Analysis and Design, Vol. 37, 2001, pp. 961-977
[270] J. K. Wright, R. L. Williamson and K. J. Maggs, "Finite element analysis of the effectivness of interlayers in reducing thermal residual stresses in diamond films", Materials Science and Engineering: A, Vol. 187, 1994, pp. 87-96
[271] U. Wiklund, J. Gunnars and S. Hogmark, "Influence of residual stresses on fracture and delamination of thin hard coatings", Wear, Vol. 232, 1999, pp. 262-269
[272] J. Gunnars and A. Alahelisten, "Thermal stresses in diamond coatings and their influence on coating wear and failure", Surface and Coatings Technology, Vol. 80, 1996, pp. 303-312
[273] J. K. Wright, R. L. Williamson, D. Renusch, B. Veal, M. Grimsditch, P. Y. Hou and R. M. Cannon, "Residual stresses in convoluted oxide scales", Materials Science and Engineering: A, Vol. 262, 1999, pp. 246-255
[274] R. O. E. Vijgen and J. H. Dautzenberg, "Mechanical measurement of the residual stress in thin PVD films", Thin Solid Films, Vol. 270, 1995, pp. 264-269
[275] S. Haque and K. L. Choy, "Finite element modeling of the effect of a functionally graded protective coating for SiC monofilaments on Ti-based composite behaviour", Materials Science and Engineering A, Vol. 291, 2000, pp. 97–109
[276] F. Vaz, J. Ferreira, E. Ribeiro, L. Rebouta, S. Lanceros-Mendez, J. A. Mendes, E. Alves, Ph. Goudeau, J. P. Riviere, F. Ribeiro, I. Moutinho, K. Pischow and J. de Rijk, "Influence of nitrogen content on the structural, mechanical and electrical properties of TiN thin films", Surface and Coatings Technology, In press, 2004

[277] A. Rouzaud, E. Barbier, J. Ernoult and E. Quesnel, "A method for elastic modulus measurements of magnetron sputtered thin films dedicated to mechanical applications", Thin Solid Films, Vol. 270, 1995, pp. 270-274
[278] ANSYS software manual: the general-purpose finite element software, version 7. 0, 2003
[279] Y. Park and I. Jeon, "Mechanical stress evolution in metal interconnects for various line aspect ratios and passivation dielectrics", Microelectronic Engineering, Vol. 69, 2003, pp. 26-36
[280] F. Shimokawa, "High-power fast-atom beam source and its application to dry etching", Journal of Vacuum Science and Technology A, Vol. 10, 1992, pp. 1352-1357
[281] A. H. McIlraith, "A Charged Particle Oscillator", Journal of Vacuum Science and Technology A, Vol. 9, 1972, pp. 209-212
[282] A. Voevodin, J. M. Schneider, C. Caperaa, P. Stevenson and A. Matthews, "Studies of atom beams produced by a saddle field source used for depositing diamond-like carbon films on glass", Vacuum, Vol. 46, 1995, pp. 299-303
[283] R. V. Kruzelecky and S. Zukotynski, "Plasma properties deposition and etching", Materials Science Forum, Vol. 89, 1993, pp. 140-142
[284] S. L. Rohde, W. D. Sproul and J. R. Rohde, "Correlations of plasma properties and magnetic field characteristics to TiN film properties formed using a dual unbalanced magnetron system", Journal of Vacuum Science and Technology A, Vol. 9, 1991, pp. 1178-1183
[285] R. D. Arnell, "Control of mechanical and structural properties of coatings deposited using unbalanced magnetrons", Surface and Coatings Technology, Vol. 59, 1993, pp. 105-109
[286] B. D. Cullity, "Elements of X-ray diffraction", Addison-Wesley, Massachusetts, ISBN: 0201011743, 1978
[287] E. F. Kaelble, "Handbook of X-rays", McGraw-Hill, New York, 1967
[288] G. K. Williamson and W. H. Hall. "X-ray line broadening from filed aluminium and wolfram", Acta Metallurgical, Vol. 1, 1953, pp. 22-31
[289] M. Ohring, "The Material Science of Thin Films", Academic Press, New York, ISBN: 0-12-524975-6, 1991
[290] J. H. Scofield, "Hartree-Slater subshell photoionization cross-sections at 1254 and 1487 eV", Journal of Electron Spectroscopic Relation Phenomena, Vol. 8, 1976, pp. 129-137
[291] C. R. Brundle, C. A. Evans and S. Wilson, "Encyclopedia of Materials Characterization - surfaces, interfaces, thin films", Manning, Boston, ISBN: 0750691689, 1992
[292] V. Fox and Teer, "BC-2: Ball crater device, a specification and user guide", Worcestershire, UK, 2004
[293] D. Camino, A. H. S. Jones, D. Mercs and D. G. Teer, "High performance sputtered carbon coatings for wear resistant applications", Vacuum, Vol. 52, 1999, pp. 125-131
[294] J. F. Paddy, "Surface Tension", Surface Colloid Science, Vol. 1, 1969, pp. 39-149
[295] G. F. Voort and G. M. Lucas, "Microindentation Hardness Testing", Advanced Materials and Processes, Vol. 154, 1998, pp. 21-25
[296] B. Jonsson and S. Hogmark, "Hardness measurements of thin films", Thin Solid Films, Vol. 114, 1984, pp. 257-269
[297] P. J. Burnett and D. S. Rickerby, "The mechanical properties of wear-resistant coatings", Thin Solid Films, Vol. 148, 1987, pp. 41-50
[298] D. Chicot and J. Lesage, "Absolute hardness of films and coatings", Thin Solid Films, Vol. 254, 1995, pp. 123-130
[299] S. Prawer, K. W. Nugent, Y. Lifshitz, G. D. Lempert, E. Grossman, J. Kulik, I. Avigal and R. Kalish, "Systematic variation of the Raman spectra of DLC films as a function of sp2:sp3 composition", Diamond and Related Materials, Vol. 5, 1996, pp. 433-438
[300] H. Ollendorf and D. Schneider, "A comparative study of adhesion test methods for hard coatings", Surface and Coatings Technology, Vol. 113, 1999, pp. 86-102

[301] W. Heinke, A. Leyland, A. Matthews, G. Berg, C. Friedrich and E. Broszeit, "Evaluation of PVD nitride coatings, using impact, scratch and Rockwell-C adhesion tests", Thin Solid Films, Vol. 270, 1995, pp. 431-438
[302] H. Jehn, G. Reiners and N. Siegel, "Characterisierung diinner Schichren", DIN Fachbericht 39, Beuth Verlag, Berlin, 1993
[303] D. J. Ward and A. F. Williams, "Finite element simulation of the development of residual stress in IAPVD films", Thin Solid Films, Vol. 355-356, 1999, pp. 311-315
[304] F. Borgioli, A. Fossati, E. Galvanetto and T. Bacci, "Glow-discharge nitriding of AISI 316L austenitic stainless steel: influence of treatment temperature ", Surface and Coatings Technology, Vol. 200, 2005, pp. 2474-2480
[305] M. Rahman, J. Haider and M. S. J. Hashmi, "Low temperature plasma nitriding of 316 stainless steel by a saddle field fast atom beam source", Surface and Coatings Technology, Vol. 200, 2005, pp. 1645-1651
[306] S. Thaiwatthana, X. Y. Li, H. Dong and T. Bell, "Mechanical and chemical properties of low temperature plasma surface alloyed 316 austenite stainless steel", Surface Engineering, Vol. 18, 2002, pp. 140-144
[307] T. Bacci, F. Borgioli, E. Galvanetto and G. Pradelli, "Glow-discharge nitriding of sintered stainless steels", Surface and Coatings Technology, Vol. 139, 2001, pp. 251-256
[308] L. Wang, S. Ji and J. Sun, "Effect of nitriding time on the nitrided layer of AISI 304 austenitic stainless steel", Surface and Coatings Technology, In Press, 2005
[309] M. K. Lei, L. J. Yuan, Z. L. Zhang, P. Wang, Y. Huang and Z. W. Yu, "Tribological studies of plasma source ion nitrided low alloy tool steel", Wear, Vol. 209, 1997, pp. 301-307
[310] C. X. Li and T. Bell, "Sliding wear properties of active screen plasma nitrided 316 austenitic stainless steel", Wear, Vol. 256, 2004, pp. 1144-1152
[311] T. F. J. Quinn, "Oxidation wear", in: ASM Handbook -Friction, Lubrication and Wear technology", ASM International, Metals Park, Ohio, ISBN: 0871703807, Vol. 18, 1992, pp. 280–289
[312] K. C. Chen and G. J. Jaung, "DC diode ion nitriding behavior of titanium and Ti-6Al-4V", Thin Solid Films, Vol. 303, 1997, pp. 226-231
[313] L. Thair, U. K. Mudali, R. Asokamani and B. Raj, "Corrosion Properties of Surface Modified Ti-6Al-7Nb Alloy Under Pulsed Plasma Nitriding and Nitrogen Ion Implantation Conditions", Surface Engineering, Vol. 20, 2004, pp. 11-16
[314] T. –S. Kim, Y. –G. Park and M. –Y. Wey, "Characterization of Ti–6Al–4V alloy modified by plasma carburizing process", Materials Science and Engineering A, Vol. 361, 2003, pp. 275-280
[315] S. G. Lakshami, D. Arivuoli and B. Ganguli, "Surface modification and characterisation of Ti–Al–V alloys", Materials Chemistry and Physics, Vol. 76, 2002, pp. 187-190
[316] M. Rahman and M. S. J. Hashmi, "Structural and tribological properties of the plasma nitrided Ti-alloy Biomaterials: Influence of the treatment temperature", Thin Solid Films, To be published, 2005
[317] E. Rollinski, "Surface properties of plasma-nitrided titanium alloys", Materials Science and Engineering A, Vol. A 108, 1989, pp. 37-44
[318] S. L. R. da Silva, L. O. Kerber, L. Amaral and C. A. dos Santos, "X-ray diffraction measurements of plasma-nitrided Ti–6Al–4V", Surface and Coatings Technology, Vol. 116-119, 1999, pp. 342-346
[319] B. S. Yilbas, A. Z. Sahin, A. Z. Al-Garni, S. A. M. Said, Z. Ahmed, B. J. Abdulaleem and M. Sami, "Plasma nitriding of Ti---6Al---4V alloy to improve some tribological properties", Surface and Coatings Technology, Vol. 80, 1996, pp. 287-292
[320] Y. Itoh, A. Itoh, H. Azuma and T. Hioki, "Improving the tribological properties of Ti–6Al–4V alloy by nitrogen-ion implantation", Surface and Coatings Technology, Vol. 111, 1999, pp. 172-176

[321] M. Veres, M. Füle, S. Tóth, I. Pócsik, M. Koós, A. Tóth, M. Mohai and I. Bertóti, "Raman scattering of ultra-high molecular weight polyethylene treated by plasma-based ion implantation", Thin Solid Films, Vol. 482, 2005, pp. 211-215
[322] A. Tóth, T. Bell, I. Bertóti, M. Mohai and B. Zelei, "Surface modification of polyethylene by low keV ion beams", Nuclear Instruments and Methods in Physics Research Section B, Vol. 148, 1999, pp. 1131-1135
[323] D. Marton, K. J. Boyd and J. W. Rabalais, "Synthesis of carbon nitride", Journal of Modern Physics B, Vol. 9, 1995, pp. 3527-3558
[324] Y. Taki, T. Kitagawa and O. Takai, "Shielded arc ion plating and structural characterization of amorphous carbon nitride thin films", Thin Solid Films, Vol. 304, 1997, pp. 183-190
[325] T. Ujvári, A. Tóth, M. Mohai, J. Szépvölgyi and I. Bertóti, "Composition and chemical structure characteristics of CNx layers prepared by different plasma assisted techniques", Solid State Ionics, Vol. 141-142, 2001, pp. 63-69
[326] S. Ge, Q. Wang, D. Zhang, H. Zhu, D. Xiong, C. Huang and X. Huang, "Friction and wear behavior of nitrogen ion implanted UHMWPE against ZrO2 ceramic", Wear, Vol. 255, 2003, pp. 1069-1075
[327] W. S. Jung, H. Y. Lee, K. H. Nam and J. G. Han, "The synthesis of W–Ti–C films with a control of element composition by hybrid system", Surface and Coatings Technology, Vol. 200, 2005, pp. 721-725
[328] M. A. Tamor and W. C. Vassell, "Raman ``fingerprinting" of amorphous carbon films", Journal of Applied Physics, Vol. 76, 1994, pp. 3823-3830
[329] T. Heitz, B. Drevillon, C. Godet and J. E. Bouree, "Quantitative study of C—H bonding in polymerlike amorphous carbon films using in situ infrared ellipsometry", Physical review B, Vol. 58, 1998, pp. 13957-13973
[330] C. Thomsen and S. Reich, "Double Resonant Raman Scattering in Graphite", Physical Review Letter, Vol. 85, 2000, pp. 5214-5217
[331] Y. Liu and E. I. Meletis, "Tribological behavior of DLC coatings with functionally gradient interfaces", Surface and Coatings Technology, Vol. 153, 2002, pp. 178-183
[332] C. Donnet and A. Grill, "Friction control of diamond-like carbon coatings", Surface and Coatings Technology, Vol. 94-95, 1997, pp. 456-462
[333] K. Y. Li, Z. F. Zhou, I. Bello, C. S. Lee and S. T. Lee, "Study of tribological performance of ECR–CVD diamond-like carbon coatings on steel substrates: Part 1. The effect of processing parameters and operating conditions", Wear, Vol. 258, 2005, pp. 1577-1588
[334] Z. M. Zeng, T. Zhang, X. B. Tian, B. Y. Tang, T. K. Kwok and P. K. Chu, "Surface modification of 9Cr18 bearing steels by a metal and carbon co-plasma immersion ion implantation", Surface and Coatings Technology, Vol. 128-129, 2000, pp. 236-239
[335] Y. X. Leng, J. Y. Chen, P. Yang, H. Sun, G. J. Wan and N. Huang, "Mechanical properties and thermomechanical stability of diamond-like carbon films synthesized by pulsed vacuum arc plasma deposition", Surface and Coatings Technology, Vol. 173, 2003, pp. 67-73
[336] C. Tsotsos, A. L. Yerokhin, A. D. Wilson, A. Leyland and A. Matthews, "Tribological evaluation of AISI 304 stainless steel duplex treated by plasma electrolytic nitrocarburising and diamond-like carbon coating", Wear, Vol. 253, 2002, pp. 986-993
[337] P. Cosemans, X. Zhu, J. P. Celis and M. Van Stappen, "Development of low friction wear-resistant coatings", Surface and Coatings Technology, Vol. 174-175, 2003, pp. 416-420
[338] M. Bromark, P. Hedenqvist and S. Hogmark, "The influence of substrate material on the erosion resistance of TiN coated tool steels", Wear, Vol. 186-187, 1995, p. 189-194
[339] J. S. Zabinski, J. Tanga and L. Fenga, The effects of metal interlayer insertion on the friction, wear and adhesion of TiC coatings, Surface and Coatings Technology, Vol. 99, 1998, pp. 242-247.
[340] W. Feng, D. Yan, J. He, G. Zhang, G. Chen, W. Gu and S. Yang, "Microhardness and toughness of the TiN coating prepared by reactive plasma spraying", Applied Surface Science, Vol. 243, 2005, pp. 204-213

[341] M. Llusar, C. Rodrigues, J. Labrincha, M. Flores and G. Monrós, "Reinforcement of single-firing ceramic glazes with the addition of polycrystalline tetragonal zirconia, 3Y–TZP, or zircon", Journal of the European Ceramic Society, Vol. 22, 2002, pp. 639-652
[342] T. W. Clyne, "Residual Stresses in Thick and Thin Surface Coatings", Source:http://www.msm.cam.ac.uk/mmc/publications/journal/twc010.pdf
[343] S. J. Howard, Y. C. Tsui and T. W. Clyne, "The effect of residual stresses on the debonding of coatings—I. A model for delamination at a bimaterial interface", Acta Metallurgical Materialia, 42, 1994, pp. 2561.
[344] G. G. Stoney, "The tension of metallic films deposited by electrolysis", Proc. R. Soc. London, Ser. A, 82 ,1909, pp. 172.
[345] P. K. Chu, J. Y. Chen, L. P. Wang and N. Huang, "Plasma-surface modification of biomaterials", Materials Science and Engineering: R, Vol. 36, 2002, pp. 143-206.
[346] X. Liu, P. K. Chu and C. Ding, "Surface modification of titanium, titanium alloys and related materials for biomedical applications", Materials Science and Engineering: R, Vol. 47, 2004, pp. 49-121.
[347] G. D Winter, "Tissue reactions to metallic wear and corrosion products in human patients", Journal of Biomedical Material Research, Vol. 5, 1974, pp. 11-26.
[348] W. H. Harris, "Osteolysis and particle disease in hip replacement", Acta Orthopædica Scandinavica, Vol. 65, 1994, pp. 113-123.
[349] T. M. Wright and S. B. Goodman, "Implant Wear: The Future of Total Joint Replacement", American Academy of Orthopaedic Surgeons, Rosement, New York, 1996.

APPENDICES

APPENDIX A

A.1 SIMULATION EQUATION FOR THE GAS FLOW MODEL

The following are the overall mass, momentum and individual species mass conservation equations used by the CFD software for the solution of this problem after considering all the assumptions and conditions.

The Mass Conservation Equation for laminar flow

The equation for conservation of mass, or the continuity equation, can be written as follows:

$$\frac{\partial \rho}{\partial t} + \Delta.(\rho \vec{v}) = S_m \quad \text{..... (A.1)}$$

Equation A.1 is the general form of the mass conservation equation and it is valid for incompressible as well as compressible flows. Where p is the static pressure, υ is velocity and t is time. The source S_m is the mass added to the continuous phase from the dispersed second phase (that means, due to vaporization of liquid droplets) and any user-defined sources. In this work, such types of mass have not been used, therefore, it can be placed $S_m = 0$ in equation A.1,

$$\frac{\partial \rho}{\partial t} + \Delta.(\rho \vec{v}) = 0 \quad \text{..... (A.2)}$$

Momentum Conservation Equations for laminar flow

The conservation of momentum in an inertial (non-accelerating) reference frame is described by:

$$\frac{\partial}{\partial t}(\rho \vec{v}) + \nabla.(\rho \vec{v}\vec{v}) = -\nabla p + \nabla.(\bar{\bar{\tau}}) + \rho \vec{g} + \vec{F} \quad \text{..... (A.3)}$$

Where $\bar{\bar{\tau}}$ is the viscous stress tensor, ρg and $\vec{F}$ are the gravitational body force and external body forces (that means, that arise from interaction with the dispersed phase), respectively. $\vec{F}$ also contains other model-dependent source terms such as porous-media and user-defined sources. Gravitational and body forces of gases do not have any influence on the momentum calculation. So, ρg and $\vec{F}$ terms can be neglected from equation A.3,

$$\frac{\partial}{\partial t}(\rho \vec{v}) + \nabla.(\rho \vec{v}\vec{v}) = -\nabla p + \nabla.(\bar{\bar{\tau}}) \quad \text{..... (A.4)}$$

The stress tensor $\bar{\bar{\tau}}$ is given by:

$$\bar{\bar{\tau}} = \mu[(\nabla \vec{v} + \nabla \vec{v}^T) - \frac{2}{3}\nabla.\vec{v}I] \quad \text{..... (A.5)}$$

Where μ is the molecular viscosity, I is the unit tensor, and the second term on the right hand side of the equation A.5, is the effect of volume dilation.

Species Transport Equations

The mixing and transport of the chemical species can be modelled by solving the conservation equations describing convection, diffusion, and reaction sources for each component species. The species transport modelling can be carried out both with and without reactions. By predicting the local mass fraction of each species, Y_i, through the solution of a convection-diffusion equation for the i^{th} species, the conservation equations can be solved. This conservation equation takes the following general form:

$$\frac{\partial}{\partial t}(\rho Y_i) + \nabla.(\rho \vec{v} Y_i) = -\nabla \vec{J}_i + R_i + S_i \quad \text{..... (A.6)}$$

Where R_i is the net rate of production by chemical reaction and S_i is the rate of creation by addition from the dispersed phase plus any user-defined sources. As in this work, the species transport model has been considered without any chemical reaction, therefore, $R_i = 0$ and $S_i = 0$ (because there is no such phase) can be putted in equation A.6.

$$\frac{\partial}{\partial t}(\rho Y_i) + \nabla.(\rho \vec{v} Y_i) = -\nabla \vec{J}_i \quad \text{..... (A.7)}$$

An equation of this form will be solved for N-1 species where N is the total number of fluid phase chemical species present in the system. Since the mass fraction of the species must sum to unity, the n^{th} mass fraction is determined as one minus the sum of the N-1 solved mass fractions. To minimize numerical error, the n^{th} species should be selected as it is the species with the overall largest mass fraction.

Mass Diffusion in Laminar Flows

In Equation A.7, $\vec{J}_i$ is the diffusion flux of species i, which arises due to concentration gradients. In the case of dilute approximation, the diffusion flux can be written as,

$$\vec{J}_i = -\rho D_{i,m} \nabla Y_i \quad \text{..... (A.8)}$$

Here $D_{i,m}$ is the diffusion coefficient for species i in the mixture. For certain laminar flows, the dilute approximation may not be acceptable, and full multicomponent diffusion is required. In such cases, the Maxwell-Stefan equations can be solved. In this case dilute approximation has been considered

A.2 THERMAL STRESS EQUATION FOR THE COATING

Combining the analytical model of the thermal stress in the progressively deposited coating for a simple planar geometry with the well-known Stoney's equation, the following equation (A.9) for the thermal stress in a thin coating can be derived [264,342-344].

$$\sigma_f = \left[-E_{ef} \int_{T_r}^{T_d} (\alpha_s - \alpha_f)\, dT \right] \Big/ \left[1 + 4\left(\frac{E_{ef}}{E_{es}}\right)\left(\frac{h}{H}\right) \right] \quad \text{..... (A.9)}$$

Where E_{ef} [$= E_f/(1- \nu_f)$], E_{es} [$= E_s/(1- \nu_s)$], ν_f, h, H, T_d, T_r, α_s, and α_f are effective Young's modulus of the coating, effective Young's modulus of the substrate, Poisson ratio of the coating, coating thickness, substrate thickness, deposition temperature, room temperature, thermal expansion coefficients of the substrate and the coating respectively. The whole coating substrate system is considered to be a composite beam, where the coating is very thin compared to the substrate. The biaxial stress ($\sigma_x = \sigma_z = \sigma$ and $\sigma_y = 0$) state can thus be assumed.

A.3 SURFACE MODIFICATION OF BIOMATERIALS

Biomaterials and biomedical devices are used throughout the human body. When a material is placed into the body, a number of important factors need to be considered such as it's bio-compability (that means, material must not degrade in its properties within the environment of the body and must not cause any adverse reactions within the host's body), and mechanical properties, manufacturing cost and so on (Figure A.3.1).

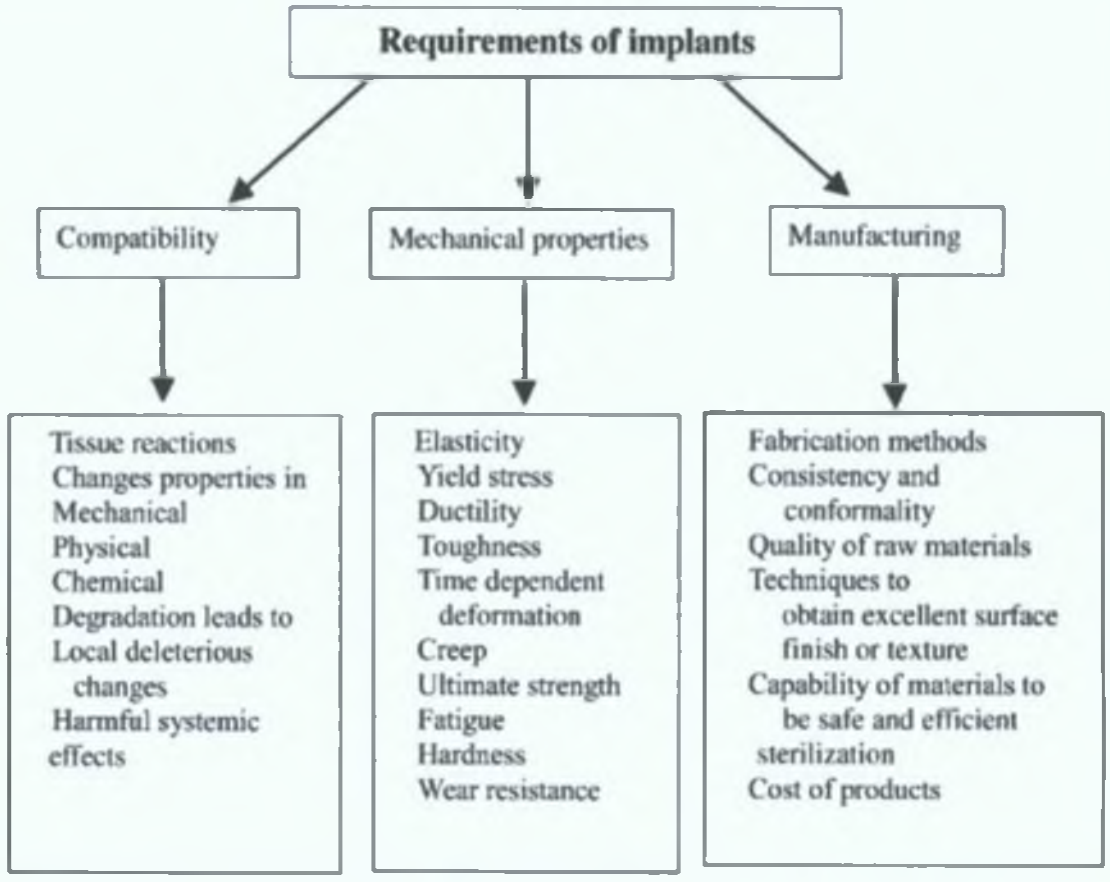

Figure A.3.1: Basic requirement for orthopedic application [345]

The use of synthetic bulk materials in hard-tissue implants applications (such as joint implant) has increased dramatically during the past few decades. Biomaterials used in joint replacement require not only biocompability but also mechanical strength. Wear may occur on any implant that undergoes dynamic loading. All implants are somehow fixed in the body and may articulate against natural tissue or another synthetic material

(a metal head of an artificial hip joint articulating against a polyethylene cup). The severeness of the wear depends on the implant and counterface material, its surface properties, the presence of particles of a third-body material causing wear , the medium around the implant, and the mechanical conditions (load, amplitude and so on). An example of a fixed implant in which virtually no movement occurs, is a bone plate, which is fixed to the bone with screws. Small movements on the micrometer scale may occur between the screw heads and the walls of the holes in the bone plate, while the movement of ball and cup of a hip joint is in the range of centimeters.

Polymer base material, titanium based alloy, stainless steel and hydroxyapatite all represent individual classes of materials which have attracted much attention within biomaterials research field. A typical used of these material in total hip replacement application shown in figure A.3.2 The implant consists of three main parts: (1) the stem (2) the ball or head, and (3) the acetabular shell and accompanying liner. Currently, most artificial joints consist of a metallic component (titanium alloy) articulating against a polymer (typically ultrahigh molecular weight polyethylene, UHMWPE).

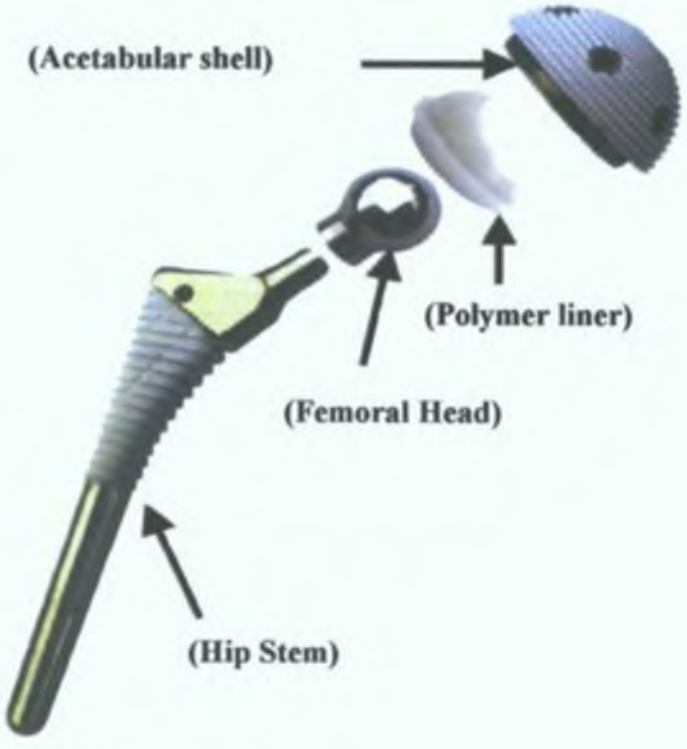

Figure A.3.2: Materials used in total hip replacement [346].

The use of many of these material is limited in orthopedic applications by the need of attaining specific tribological (low friction and wear rate) and mechanical (high hardness, high load-bearing capacity) properties [347]. This is because wear debris

produced by different wear mechanism can cause a harmful biological reaction with the tissue inside the body and can ultimately breakdown the implant system. The breakdown of the implant by wear processes is currently the limiting factor in the long-term outcome of the total joint replacement [348,349] and for this reason much research is being carried out in this area in order to reduce the incidence of wear.

It is hard to find a material that meets all the requirements of a given application and biomaterials are no exception. Changing the bulk material severely limits options in materials selections, and often is not economically or technologically viable. Hence, among the options available for evaluating the performance of a biomaterial, the enhancement of the surface phenomenon holds the key. Modifying the surface of a material can improve its surface properties without changing its bulk properties. Typically, modifications can either alter the atoms, compounds, or molecules on the existing surface chemically or physically. Several methodologies have been considered and developed for improve properties of biomaterials, plasma surface modification (such as plasma nitriding or ion nitriding) is one of these methodologies. Plasma surface modification can improve biocompatibility, biofunctionality and mechanical properties of the surface of the bulk materials.